THESIS

This is to certify that the

dissertation entitled
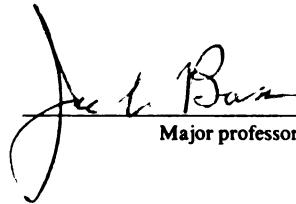
The Electrical Resistivity and the Thermoelectric Ratio
of Potassium, Sodium, Lithium, Rubidium, and Potassium-
Rubidium Alloys from 0.07K to 4.2K

presented by

Zhao-Zhi Yu

has been accepted towards fulfillment
of the requirements for

_____Ph.D._____ degree in __Physics__

_____
Major professor

Date__10/5/84_____

O-12771

THE ELECTRICAL RESISTIVITY AND THE THERMOELECTRIC RATIO OF POTASSIUM, SODIUM, LITHIUM, RUBIDIUM, AND POTASSIUM-RUBIDIUM ALLOYS FROM 0.07K TO 4.2K

By

Zhao-Zhi Yu

A DISSERTATION

Submitted to
Michigan State University
in partial fulfillment of the requirements
for the degree of

DOCTOR OF PHILOSOPHY

Department of Physics and Astronomy

1984

THE ELECTRICAL RESISTIVITY AND THE THERMOELECTRIC RATIO OF POTASSIUM, SODIUM, LITHIUM, RUBIDIUM, AND POTASSIUM-RUBIDIUM ALLOYS FROM 0.07K TO 4.2K

By

Zhao-Zhi Yu

AN ABSTRACT OF A DISSERTATION

Submitted to
Michigan State University
in partial fulfillment of the requirements
for the degree of

DOCTOR OF PHILOSOPHY

Department of Physics and Astronomy

1984

ABSTRACT

THE ELECTRICAL RESISTIVITY AND THE THERMOELECTRIC RATIO OF POTASSIUM, SODIUM, LITHIUM, RUBIDIUM, AND POTASSIUM-RUBIDIUM ALLOYS FROM 0.07K TO 4.2K

By

Zhao-Zhi Yu

The electrical resistivities (ρ) of thick (diam. = 1.0 - 3.0 mm) samples of K, Na, Li, and Rb; of thin (diam. = 0.09 - 0.5 mm) samples of K and Na; of samples of K and Na encased in polyethylene and teflon tubes; and of samples of K-Rb alloys were measured from 4.2K down to 0.07K with a precision of 0.1-0.01 ppm. The thermoelectric ratios (G) of the same samples were measured over the same temperature range.

In free-hanging, bare, high-purity thick samples, we found a T^2 variation of the electrical resistivity for K, from about 1.1K down to about 0.3K; for Li, from 4.2K down to about 1.6K; and, perhaps, for Na from 1.9K down to 1.2K. No temperature range over which a T^2 variation was dominant was found for thick Rb samples. Clear deviations from a T^2 variation for K, Na, and Li below the temperature ranges just listed were also found.

In thin samples of K cooled in He gas, we found a size effect pattern in ρ leading to a negative $d\rho/dT$ when the

diameter became smaller than electron mean-fee-path. The only model we know which might explain the negative $d\rho/dT$ we observed is an interaction between surface scattering and normal electron-electron scattering first proposed by Gurzhi and then calculated by a Monte Carlo method by Black.

A Kondo-type anomaly was observed in the electrical resistivity below 1K for K samples encased in polyethylene tubes. The data can be well fitted by $\rho = \rho_o + AT^2 - B\ln T$, where $-B\ln T$ is a typical Kondo effect term.

The resistivity of 9.4 at.% Rb alloy samples evidenced a strong deviation from the expected T^2 behavior for $T \leq 1K$. The reasons for this deviation are not yet clear.

All G data of thick samples of pure K, Na, Li, and Rb and K-Rb dilute alloy could be well fitted by $G = G_o + B*T^2 + (C*/T)Exp(-\theta*/T)$, where the third term is negligible for Na and Li. Both the normal and Umklapp phonon drag terms were quenched by increased surface and impurity scattering. G data of K samples encased in polyethylene tubes were well fitted by $G = G_o + B*T^2 + D*/T$, $(D*<0)$ where the last term is attributed to the Kondo effect.

TO MY WIFE

ACKNOWLEDGEMENTS

It is a great pleasure to thank my thesis advisor, Professor Jack Bass, for his supervision, support, criticism, and invaluable aid in all aspects of this research. I would also like to thank Professors Pratt and Schroeder for their precious advice, discussions, and help at many stages of this study.

Thanks also are due to Professor Spence for his help in testing the single-crystal potassium, and to Professor J. C. Garland of Ohio State University for providing high-purity sodium.

I wold like to extend thanks to Dr. Mark Haerle and Dr. Vernon Heinen for their unselfish aid in various stages of this research, to Mr. John Zwart for his help in design and construction of the sample can, and to Zhao Jing and Qian Yao-Jin for their help in taking some data. I wish also to thank the good humored fellows in the machine shop for their help in constructing the sample can, the presses and other apparatus.

Finally, the financial support of the National Science Foundation is gratefully acknowledged.

TABLE OF CONTENTS

v

LIST OF TABLES

LIST OF FIGURES

CHAPTER 1

Introduction

This dissertation is a report of experimental studies of electrical transport properties such as electrical resistivity and thermo-electric ratio in the alkali metals K, Li, Na, Rb, and in K-Rb alloys. One of the main purposes of this study is to try to find the concealed reasons for disagreements between experimental results from different groups (see section 1.2.1). Particular attention is concentrated on: 1) a size effect in pure K samples at temperatures below 1K; 2) a contact effect of polyethylene and oil on K at temperatures from above 1K down to 0.1K; 3) anomalous deviations from the simple T^2 variation expected for electron-electron scattering in thick, pure, free hanging K, Li, Na, and Rb samples when the temperature is lower than a certain limit for each; and 4) a deviation from the expected T^2 behavior in the resistivity of K-Rb alloys at temperatures below 1K.

In this introduction, we first explain why people are interested in measurements on the alkali metals, especially potassium, and then review previous work on K, Li, Na, Rb, and K-Rb and discuss some disagreements among work done previously by different groups. In Chapter 2 we introduce

1

all related theories. In Chapter 3, the experimental techniques of the present study are described. The experimental results and interpretations are presented in Chapter 4. Summary and conclusions are given in Chapter 5.

1.1 ALKALI METALS AND BASIC ELECTRON TRANSPORT PROPERTIES

The alkali metals have been attracting renewed theoretical and experimental interest in the past few decades. These metals are simple monovalent metals which have b.c.c. lattice structures at room temperature, so that they have nearly spherical Fermi surfaces (to within 0.1% for K according to dHvA measurements). They have no unfilled d- or f- shells to complicate calculations. No superconducting phenomena and Kondo effects at low temperatures have been previously seen in the alkali metals. Potassium has been studied most often among the alkali metals. The reasons are:

1) Unlike lithium and sodium, potassium does not undergo a martensitic phase transformation at low temperatures. It thus keeps its b.c.c. structure and spherical Fermi surface.

2) Potassium is less reactive than rubidium and cesium and thus easier to work with.

3) Potassium is softer than lithium and sodium, and can be easily extruded through small dies into thin wires.

4) Overhauser has claimed that potassium is the best material for testing the existence of charge density waves (CDW) (ref. 1) in simple metals. If found to exist in K, CDW theory would change our basic understanding of electronic transport in metals.

In all studies of electronic transport, the fundamental bases are the microscopic transport equations,

$$\vec{j} = \overset{\leftrightarrow}{L}_{11}\vec{E} + \overset{\leftrightarrow}{L}_{12}\vec{\nabla}T \tag{1-1}$$

$$\vec{q} = \overset{\leftrightarrow}{L}_{21}\vec{E} + \overset{\leftrightarrow}{L}_{22}\vec{\nabla}T \tag{1-2}$$

where $\vec{j}$ is the electrical current density, $\vec{q}$ is the heat flow current density, $\vec{E}$ is the electric field, and $\vec{\nabla}T$ is the temperature gradient. In general, all four $\overset{\leftrightarrow}{L}$ coefficients are tensors, but in cubic metals, such as alkali metals under zero magnetic field, the $\overset{\leftrightarrow}{L}$'s are scalars. Then we can rewrite (1-1) and (1-2) as

$$\vec{E} = \rho\vec{j} + S\vec{\nabla}T \tag{1-1'}$$

$$\vec{q} = \frac{TS}{\rho}\vec{E} - \kappa\vec{\nabla}T \tag{1-2'}$$

The electrical resistivity is defined as

$$\rho = \left.\frac{\vec{E}}{\vec{j}}\right|_{\vec{\nabla}T = 0} \tag{1-3}$$

where $\vec{E}$ and $\vec{j}$ are in the same direction.

Considering electron-phonon, electron-electron, and electron-defect scattering, the electrical resistivity at

temperatures well below the Debye temperature is expected to
have the form (ref. 2)

$$\rho(T) = \rho_o + \rho_{e-e} + \rho_{e-ph}^N + \rho_{e-ph}^U \qquad (1-4)$$

Here ρ_o is the residual resistivity caused by elastic scat-
tering of electrons by impurities or lattice defects in the
metal and is temperature independent in the first approxima-
tion; ρ_{e-e} is attributed to electron-electron scattering and
is expected to have a temperature dependence of the form
AT^2, where A is basically independent of ρ_o; ρ_{e-ph}^N is due to
electron-phonon scattering normal processes and, according
to Bloch-Gruneisen theory, is expected to have the form
$\rho_{e-ph}^N = BT^5$; and the last term ρ_{e-ph}^U, comes from electron-
phonon Umklapp scattering processes which, in a metal with a
spherical Fermi surface completely within the first
Brillioun zone, are expected to lead to the form (ref. 3,4)

$$\rho_{e-ph}^U = CT^n e^{-\theta^*/T} \qquad (1-5)$$

The thermal conductivity κ is defined as

$$\kappa = -\left.\frac{\dot{q}}{\nabla T}\right|_{E=0.} \qquad (1-6)$$

We have the Wiedemann-Franz law (ref. 2)

$$\frac{\kappa \rho}{T} = L(T) \qquad (1-7)$$

When elastic scattering of electrons is dominant,

$$L(T) = L_O = \frac{\pi^2}{3} \frac{k^2}{e^2} = 2.45 \times 10^{-8} V^2 K^{-2} \qquad (1-8)$$

where L_O is the ideal Lorentz number.

The thermopower S is defined as

$$S = \frac{E}{\nabla T} \bigg|_{\vec{j}=0} \qquad (1-9)$$

The thermoelectric ratio G is defined as

$$G = \frac{\dot{j}}{\dot{q}} \bigg|_{\vec{E}=0} \qquad (1-10)$$

In general,

$$S = GLT \qquad i.e., \quad \frac{S}{G} = LT = \kappa\rho \qquad (1-11)$$

Where L is usually temperature dependent.

When elastic scattering is dominant, $L(T) = L_O$ and

$$S = GL_O T \qquad (1-12)$$

In pure potassium this is true only when the temperature is below 1K (according to our present data).

At low temperatures, when elastic scattering is dominant, G is expected to have the form (ref. 5,6,7,8)

$$G = G_O + AT^2 + \frac{Be^{-\theta^*/T}}{T} \qquad (1-13)$$

Where G_O is attributed to electron diffusion, the second term is due to normal phonon drag, and the last term is an

Umklapp phonon drag term appropriate to the alkali metals with b.c.c. lattice structure.

1.2 PREVIOUS WORK

1.2.1 Previous Work on Resistivities

Earlier resistivity measurements on the alkali metals have made the electron-phonon scattering contribution to the electrical resistivities of the alkali metals, including the contribution of normal and Umklapp processes, well understood (ref. 9,10,11,12,13).

Since van Kempen et al. developed high-precision (1 ppm) measurements of the electrical resistivity at low temperatures (1K and above) in 1976, (ref. 14) the electron-electron scattering contribution to the electrical resistivity of simple metals, and deviations from this contribution under various conditions, have been a subject of interest.

Four groups in the world have made high precision measurements of the electrical resistivities of alkali metals in the last few years. They are the Wyder, van Kempen group in the Netherlands, the Greenfield group in Israel, the Woods and Rowlands group in Canada, and our group at Michigan State University (MSU). This previous work is briefly described as follows:

1.2.1.1 Previous work on the resistivity of potassium at low T

In 1976 van Kempen et al. measured the resistivity of high-purity potassium (purity 99.97%) samples each clad in a 1-m-long polyethylene tube with an inner diameter of 0.9 mm. They reported that from 1.75K down to 1.1K, their data could be fit to the formula

$$\rho = \rho_0 + AT^s + BT^n e^{-\Theta^*/T} \qquad (1-14)$$

with $n = 1$, $\Theta^* = 19.9 \pm 0.2K$, and s = between 1 and 2. Using s = 2, as expected for electron-electron scattering, their coefficients, A varied from sample to sample by a factor of as much as 3.6, in contradiction to the standard theory. They also reported that the residual resistance ratio [RRR = R(300K)/R(OK)] of the samples changed after annealing the samples at room temperature. One of their samples originally had RRR = 3000, then changed to 6300 after two days annealing at room temperature in a He atmosphere, and finally changed to 8100 after 80 days annealing at room temperature in vacuum. The coefficient A decreased as the RRR increased (ref. 14).

Following on the heels of the results of van Kempen et al., a theory of electron-electron scattering in the presence of anisotropic scatterers such as dislocations was proposed by M. Kaveh and N. Wiser (ref. 15) to explain the sample-dependence of A in $\rho(T) = AT^2$.

In 1978, Rowlands et al. (ref. 16) measured the resistivity of bare, high-purity potassium samples, 1.8 m

long with diameter of 0.79 mm, which were wrapped into a helical groove on a 3-cm-diam Teflon cylinder under a helium atmosphere. They reported that the RRR of their samples increased upon annealing at room temperature (e.g., from 1300 to 4800 in 3 weeks), and that the best fit of their data from 0.5K to 1.3K was $\rho(T) = BT^{3/2}$ with $B = (86 \pm 10)$ x $10^{-6} \rho_o K^{-3/2}$. However, $\rho(T) \propto T^2$ could not be ruled out because of the uncertainty in the measurements. They proposed an explanation involving a size effect associated with Knudsen flow of electrons. Alternatively, Bishop and Overhauser (ref. 17) proposed a mechanism of electron-phason scattering (according to CDW theory), to explain the $T^{3/2}$ behavior.

In 1979, Greenfield et al. (ref. 18) measured high purity potassium samples inside polyethylene tubes with diameters of 1.0 mm. They reported that by heating and cold working their samples, they sharply increased the impurity content in their samples, and brought the RRR down (e.g., from 14000 to 2000). They plotted their data as $(\rho-\rho_o)/T^2$ versus T with an adjustable parameter ρ_o, and claimed that a term $AT^{2.0\pm0.1}$, attributed to electron-electron scattering, was found from 1.4K down to 1.1K. They also reported their coefficient A was sample-dependent, and decreased as RRR decreased. They plotted A versus $(\rho_d/\rho_o)^2$, for a given sample, leaving ρ_d as a constant parameter, and claimed their $A \propto (\rho_d/\rho_o)^2$, consistent with the theory of

Kaveh and Wiser mentioned above. Here ρ_d was an assumed anisotropic resistivity due to dislocations.

In 1982, C. W. Lee et al. (MSU group) (ref. 19) reported 0.1 ppm precision measurements of $d\rho/dT$ for free-hanging, bare, high-purity potassium samples, with diameters ranging from 0.9 mm to 3.0 mm, down to 70 mK under Ar atmosphere. They reported that $d\rho/dT$ varied closely as T, (i.e., $\rho(T) = AT^2$), from 1.3K to 0.35K. The RRR of their samples did not change much upon annealing or contaminating when left at room temperature, (e.g., the RRR of one of their samples changed from 5100 to 4100 in 83 days, and another one changed from 3600 to 3700 in 11 days). They found that the coefficient A did not change much from sample to sample, with a mean value of 0.24 ± 0.02 pΩcm/K^2 consistent with simple electron-electron scattering (ref. 20,21). They also reported a deviation form T^2 behavior below 0.35K.

The main disagreements among these various sets of results and their different experimental conditions are summarized in Table 1-1.

More recently, M. Haerle (ref. 22) reported that deformation in K samples brought the coefficient A up, enhanced the anomalous turn-up at low temperatures found by Lee et al. (ref. 19), and enhanced the electron-phonon scattering term from 4.2K to about 1K. For the anomalous turn-up at the low T end, he suggested an explanation based on low energy excitations associated with dislocations (or conceivably some other product of deformation) which would

Table 1-1. Previous work on potassium.

	van Kempen et al.	Greenfield et al.	Woods and Rowlands	Lee et al. (MSU Group)
precision	0.1 ppm	1.0 ppm	1.0 ppm	0.1 ppm
T region	above 1K	above 1K	0.5K and up	70mK and up
Sample diameter	d = 0.9 mm	d = 1.0 mm	d = 0.8 mm	d = 1.5 or 3.0 mm
RRR	390 – 8200	~12000	1300 – 4800	3600 – 5100
ρ_0 ($\rho_{4.2K}$)	0.88 – 18.6 nΩcm	0.5 – 3.6 nΩcm	1.5 – 5.6 nΩcm	(1.4 – 2.0 nΩcm)
Circumstance	in polyethylene tube	in polyethylene tube	bare in He	bare in He and Ar
Result	for T=1K to 1.4K $\rho(T) = AT^2$ ($A_{max}/A_{min}=3.6$) Note: $\rho(T)=\rho-\rho_0$	for T=1K to 1.4K $\rho(T) = AT^2$ $A \propto (\rho_d/\rho_0)^2$ Note: $\rho(T)=\rho-\rho_0$	for T=0.5K to 1.4K the best fit is $\rho(T)=BT^{3/2}$ ($\rho(T) \propto T^2$ cannot be ruled out)	for T=0.35 to 1.3K dρ/dT=2AT i.e., $\rho(T)=AT^2$ ($\Delta A=15\%A$) ——— for T<0.35K down to 70 mK deviations from $\rho(T)=AT^2$
Proposed Explanations	electron-electron scattering in the presence of anisotropic scatterers such as dislocations	electron-electron scattering in the presence of anisotropic scatterers such as dislocations	electron-phason scattering according to CDW theory ——— a size effect associated with Knudsen flow of electrons.	standard electron-electron scattering ——— not yet clear.

cause inelastic scattering of electrons. His deformed K samples showed complete recovery upon annealing at temperatures above 165K.

1.2.1.2 Previous work on resistivity of K-Rb alloys

In 1980, C. W. Lee et al. (ref. 23) reported resistivity measurements of bare, free-hanging K-Rb alloy samples with nominal concentrations of 2.24, 0.83, 0.32, 0.13, and 0.05 At.% Rb from 180mK to 4K. The samples were about 4cm long with d = 3.0 mm. They claimed that below 1K, $d\rho/\rho dT = (2A_o/\rho_o + 2A_i)T$, (i.e., $\rho = \rho_o + (A_o + A_i\rho_o)T^2$, with $A_i = (8.5 \pm 0.3) \times 10^{-6}/K^2$ and $A_o = (2.2 \pm 0.31) \times 10^{-13}$ $\Omega cm/K^2$. The A_o was consistent with the A they found in pure K, and the A_i was comparable to the theoretical values of $13.7 \times 10^{-6}/K^2$ from P. L. Taylor (ref. 24) and $12.5 \times 10^{-6}/K^2$ from Kus and D. W. Taylor (ref. 25).

1.2.1.3 Previous work on the resistivity of Na

In 1979, Greenfield et al. (ref. 18) reported resistivity measurements of high-purity Na samples clad in polyethylene tubes with d = 1.0 mm. As they did for their K samples, they plotted their Na data as $(\rho-\rho_o)/T^2$ versus T with an adjustable parameter ρ_o, and claimed $\rho(T) = AT^2$ was found from 1.1K to 2.1K. The RRR of their samples increased slightly with sample annealing time at room temperature; in 9 days ρ_o changed from 0.916 n cm to 0.787 nΩcm, while the coefficient A changed form 0.195 to 0.180 pΩcm/K^2. They claimed that A was a linear function of $(\rho_d/\rho_o)^2$, in accord

with the theory of Kaveh and Wiser (ref. 15). The lowest temperature they reached was 1.1K; the sensitivity they achieved was one to few ppm.

1.2.1.4 Previous work on resistivity of Li

In 1971, G. Krill (ref. 26) reported electrical resistivity measurements of a high-purity Li sample with RRR = 7000 and ρ_o = 7.30 nΩcm from 40K down to 1.3K. His sample was 50 cm long with d = 0.5 mm. He found $\rho(T) \propto T^4$ at 10K<T<40K, and $\rho(T) = AT^2$ with A = 3.3 pΩcm/K^2 at 4.5K<T<10K. In 1981, Greenfield et al. (ref. 27) reported $d\rho/dT$ measurements on a bare high-purity Li sample of 4.3 m long with d = 3 mm and ρ_o = 12.1 nΩcm. They got $d\rho/dT$ = 2AT, (i.e., $\rho(T) = AT^2$), throughout the temperature range of the experiment, 1.2 – 4.2 K, with A = 3.0 ± 0.1 pΩcm K^{-2} consistent with data from Krill, but an order of magnitude larger than that predicted by MacDonald et al. (ref. 20). They proposed that this anomalously large value for A was due to the anisotropy of the electron relaxation time for Li, in accord with the theory of Kaveh and Wiser.

1.2.1.5 Previous work on resistivity of high-purity Rb at low temperatures

No high precision resistivity measurements on high-purity Rb at low temperatures have been previously reported.

1.2.2 Previous Work on Thermopower S and Thermoelectric Ratio G

More than twenty years ago, MacDonald et al. (ref. 5,6,7) measured the thermal e.m.f. E of pure K and reported that their deduced thermopower $S = dE/dT$ could be fitted, from 3K down to 0.1K, to the formula

$$S = A'T + B'T^3 + C'e^{-\Theta^*/T} \qquad (1-15)$$

The first term, $A'T$, was attributed to electron diffusion thermopower; $B'T^3$ was attributed to normal phonon drag thermopower, and the exponential term was attributed to electron-phonon Umklapp processes with $\Theta^* = 21K$, where C' could be T-dependent.

In 1980, C. W. Lee (ref. 8) reported G measurements on pure K and K-Rb alloys from 4.2K down to 80 mK. Their samples were the same as the ones for electrical resistivity measurements described above. They claimed that for pure K, G had the form $G = G_0 + B^*T^2 + (C^*/T)e^{-\Theta^*/T}$, with $G_0 = -0.03 \pm 0.03$ V^{-1}, $B^* = -0.30 \pm 0.01$ $V^{-1}K^{-2}$, and $\Theta^* = 23 \pm 2K$. These results were consistent with the results of MacDonald et al., (i.e., G_0 was the diffusion term, B^*T^2 was the normal phonon drag term, and the last one was the Umklapp phonon drag term). For K-Rb alloys, they found roughly the same three terms as above. The normal and Umklapp phonon drag terms were quenched more and more as the impurity concentration increased. They also found that the diffusion term G_0 is positive and roughly obeys the Gorter-Nordheim rule: $G_0 = G_i + (\rho_p/\rho_0)(G_p - G_i)$ with $G_i = +0.48 \pm 0.01V^{-1}$,

where ρ_p = the residual resistivity of pure K, ρ_o = the residual resistivity of K-Rb sample, G_p = the diffusion term of G for pure K, and G_i = the diffusion term of G due to impurity scattering.

In 1983, M. L. Haerle et al. (ref. 22) reported G measurements on deformed pure K samples from 4.2K to 0.08K. They claimed that $G = G_o + B^*T^2 + (C/T)^*e^{-\theta^*/T}$ could fit their data for $T \geq 0.2K$, with $\theta^* \sim 18 \pm 2K$, $G_o < 0$, $B^* < 0$, and $C^* > 0$. But below 0.2K, their data start turning down from the fit, and can be fitted better by $G = G_o + B^*T^2 + A^*T$, with $G_o < 0$, $B^* < 0$, and $A^* > 0$.

1.3 PRESENT THESIS

1.3.1 Electrical Resistivity

As noted in the introduction above, at low enough temperatures, the electrical resistivity $\rho(T)$ in metals is predicted to vary as T^2 due to electron-electron scattering. It is predicted (ref. 21) that such behavior would be seen in alkali metals such as K when the temperature is lower than about 1-2K. However, experimental results on potassium below 1.5K by various groups showed discrepancies with this simple theory, as well as disagreements with each other, as described above in section 1.2.1. In order to find the reasons for these discrepancies and disagreements, in this thesis more than 100 measurements of $d\rho/dT$ were made on alkali metals such as K, Na, Li, Rb, and on K-Rb alloys, from 4.2K to about 0.07K with 0.1 ppm - 0.01 ppm precision.

1. To study the deviation from T^2 behavior found by Lee et al. below 0.35K for pure, thick K samples cooled in Ar gas, as described above in section 1.2.1, we used improved techniques to measure 14 free-hanging, bare, pure K samples, with d = 1.5 and 2.0 mm, under Ar gas, He gas, or partial vacuum, respectively. The improved techniques included a better glove box, an improved sample can with an external thermal radiation shield, and a computer averaging technique for data taking.

2. To investigate the approximately $T^{3/2}$ behavior reported by Rowlands et al. for pure K samples of d = 0.79 mm cooled in the gas and measured from 1.4K to 0.5K, as described in section 1.2.1, sets of pure samples with d ranging from 1.5 down to 0.09 mm were cooled in He gas, Ar gas, or partial vacuum and measured from 1.8K down to 0.07K. An unusual size-effect was found, which lead to a negative $d\rho/dT$ in very thin samples. To test whether the electron mean-free-path was an important parameter in this size-effect, measurements of $d\rho/dT$ were made on two K-0.08% Rb samples with d = 0.25 mm, which had a much smaller electron mean-free-path ($\lambda \approx 0.04$ mm) than the pure bulk K samples ($\lambda \approx 0.2$ mm). In an attempt to get a longer electron mean-free-path, so as to see whether the size-effect could be observed in a thicker sample, we tried to make and measure a single crystal K sample with d = 1.5 mm. To test for effects of surface corrosion, two different thicknesses of

samples were allowed to thin by means of such corrosion, which occurs naturally inside the sample can.

3. To investigate further the variations in magnitude of the T^2 coefficient reported by van Kempen et al. and Levy et al. for pure thick K samples clad in polyethylene tubes and measured down to about 1K, and described in section 1.2.1., we measured 4 pure K samples clad in polyethylene tubes with d = 1.6 or 0.9 mm down to 0.07K. To test for annealing effects, after each measurement, each sample was allowed to anneal for varying periods of time at room temperature under Ar gas, He gas, or partial vacuum, respectively. Samples were remeasured after being annealed for a few days, a few weeks, and a few months. Anomalous behavior in $d\rho/dT$ which might be due to a Kondo effect was seen. To test whether the contact with polyethylene is an important condition for this anomalous behavior, we measured pure K samples in contact with other materials such as Teflon, Kel-F, and paraffin oil.

4. To investigate further the resistivity ρ of K-Rb alloys, with improved techniques, we made and measured K - 0.08 at.% Rb and K - 9.4 at.% Rb samples from 4.2K down to about 0.07K.

5. Previous work on Li and Na at temperatures down to about 1K by Greenfield group, as described in section 1.2.1, showed T^2 behavior in $\rho(T)$ from 4.2K down to 1.1K for Li, and from 2.1K down to 1.1K for Na. No previous work on $\rho(T)$ of Rb has been reported. In order to see whether there are,

as in K, anomalous deviations from T^2 behavior of ρ at lower temperatures in Li, Na, and Rb, we extended resistivity measurements of all these three pure metals down to about 0.07K. We measured thin high-purity Na samples and high-purity Na samples encased in polyethylene tubes to test whether the size-effects and polyethylene effects seen in pure K can also be seen in pure Na.

1.3.2   Thermoelectric Ratio G and Thermopower S

About twenty years ago, MacDonald et al. (ref. 5,6,7) measured the thermal e.m.f. of pure K from 3K down to 0.1K and deduced the thermopower S from their data. More recently, Lee et al. made G measurements on pure K and K-Rb alloys from 4.2K down to 0.07K, and M. Haerle et al. made G measurement on deformed pure K samples from 4.2K down to 0.07K, as described in section 1.2.2. We measured G for most of the samples mentioned above concurrently with $d\rho/dT$; (i.e., we extended G measurements to thin samples of K, Na, and K-Rb, thick K samples in contact with plastic and oil, and thick samples of Li, Rb, and Na from 4.2K down to 0.07K). In order to find the low temperature limit of L(T) = L_O (equation 1-8) and thus $S = GL_OT$ (equation 1-12), and to find the form of L(T) in K, the thermopower S was concurrently measured with G in one pure K sample with d = 0.5 mm.

CHAPTER 2

Theory

In this chapter the theory of electronic transport, especially for alkali metals, is reviewed.

First, the basic "standard model" of the electrical resistivity for alkali metals is described.

Second, since many measurements on many different topics have been done, and various deviations from the standard model have been seen, it is necessary to review quite a few models which might be candidates for explaining our data. Some of these models were proposed to explain previous work on the resistivities of alkali metals. Some were previously used for other metals. Some are candidates for only one topic, some for more than one. The candidates for explaining deviations from the standard theory in our bulk pure samples are: 1) anisotropic electron-electron scattering; 2) electron-phason scattering based on CDW theory; 3) inelastic scattering of electrons due to low energy excitations associated with dislocations; and 4) inelastic scattering of electrons by impurities. The candidates for explaining deviations in our thin samples are: 1) the Knudsen flow model; 2) electron-phason

scattering; 3) size-dependent DMR; and 4) the Gurzhi theory.
The candidates for explaining deviations in alloys and in
pure samples in contact with hydrocarbons are: 1) the Kondo
effect; 2) inelastic scattering of electrons by impurities;
3) localization effect; and 4) electron-electron interaction
effects. These models are introduced and discussed
separately.

Third, the theory of thermopower S and thermoelectric
ratio G is introduced and discussed.

2.1 STANDARD THEORY OF ELECTRICAL RESISTIVITY FOR ALKALI METALS

When an electric potential is applied across a piece of
metal, the conduction electrons in the metal will drift in
a definite direction to form a current. Any mechanism of
electron scattering that reduces the total crystal momentum
of the electrons will cause resistance. The standard theory
considers electron and phonon systems inside a crystal with
impurities and defects. So the mechanisms contributing to
the resistivity include: electron-phonon scattering,
electron-electron scattering, electron-impurity scattering,
and electron-defect (including electron-surface) scattering.

2.1.1 Electron-Phonon Scattering (ref. 2,28)

There are two different kinds of collisions between
electrons and phonons: normal and Umklapp. It is helpful
to understand these two processes first. When an electron
is in the periodic potential of a lattice, the free electron

model can no longer be used; $\hbar\vec{k}$, where $\vec{k}$ is the wave vector
(w.v.) of the electron wave function, is not a real
momentum. $\hbar\vec{k}$ acts, however, rather like a real momentum,
and is thus called the crystal momentum of the electron.
Strictly speaking, phonons do not carry momenta, because
they are associated with the vibrations of whole lattice.
But when a phonon interacts with another kind of particle,
such as a photon, a neutron, or an electron, it acts like it
possesses a momentum $\hbar\vec{q}$, called the crystal momentum of the
phonon. Here, $\vec{q}$ is the w.v. of the phonon. When an
electron is scattered from a phonon, the total crystal
momentum is conserved to within a reciprocal lattice vector
G, (i.e., $\hbar\vec{k} + \hbar\vec{q} + \hbar\vec{G} = \hbar\vec{k}'$ or $\vec{k}' = \vec{k} + \vec{q} + \vec{G}$ where $\vec{k}$ is
the wave vector of the incoming electron and $\vec{k}'$ the w.v. of
the scattered electron). This process is called phonon anni-
hilation. In phonon creation we have $\hbar\vec{k} + \hbar\vec{G} = \hbar\vec{k}' + \hbar\vec{q}$ or
$\vec{k} + \vec{G} = \vec{k}' + \vec{q}$. For a normal process, $\vec{G}$ is zero, and there
is no crystal momentum exchange between the lattice and the
electron. When $\vec{G}$ is not zero, it is called an Umklapp
process, and there is crystal momentum exchange between the
electron and the lattice. The alkali metals in the bcc
structure have nearly spherical Fermi surfaces, completely
inside the first Brillouin zone. Figure 2.1 shows schemati-
cally the normal and Umklapp processes of phonon annihila-
tion and creation in the alkali metals with bcc structure,
where the Brillouin zone has been simplified. Clearly, for
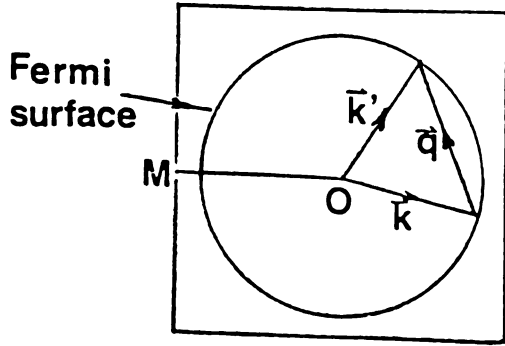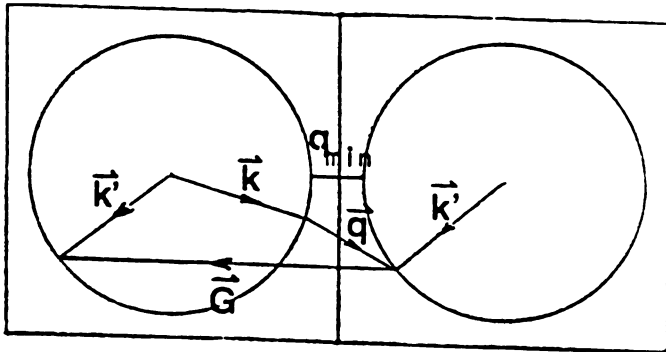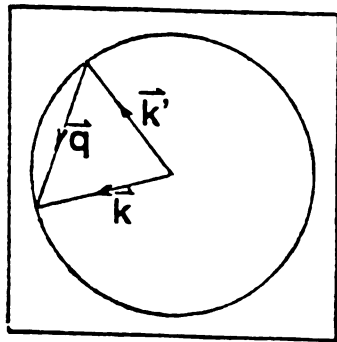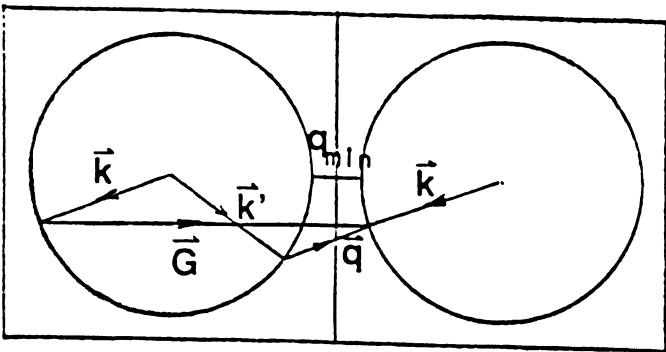
Fig. 2-1. Normal and Umklapp processes of e-ph scattering.

an Umklapp process to take place, a minimum value of phonon w.v. (q_{min}) is required.

For electron-phonon scattering, assuming: 1) thermal equilibrium phonon distribution; 2) the relaxation time approximation; 3) only normal processes; and 4) the Debye model of phonons, Bloch (ref. 28) predicted that,

$$\rho_{e-ph} = \text{const } (T/\theta_d)^5 \ j_5(\theta_d/T), \qquad (2-1)$$

where:

$$j_n = \int_0^{\theta_D/T} z^n \ (e^z-1)^{-1} \ (1-e^{-z})^{-1} dz \qquad (2-2)$$

and θ_D is the Debye temperature. At high temperatures, $T \gg \theta_D$, $j_5 \sim (\theta_D/T)^4$, so $\rho_{e-ph} \propto (T/\theta_D)$; at low temperatures, $T \ll \theta_D$, j_5 is constant, so $\rho_{e-ph} \propto (T/\theta_D)^5$.

When the phonons are not in thermal equilibrium, a phenomenon called phonon drag can occur. Consider the system of all electrons and phonons. If there are only collisions among themselves and none of these collisions are Umklapp, (i.e., this system has no crystal momentum exchange with the whole lattice or anything else such as impurities or defects), then the total crystal momentum of this system should be conserved. The only effect of the collisions between electrons and phonons is then to drag each other along so that they drift together. This is called phonon drag for electrons, or electron drag for phonons. Phonon drag reduces the resistivity by reducing the Bloch T^5 term. When phonon drag occurs, the electron-phonon scattering can

contribute to electrical resistivity only through Umklapp processes.

For electron-phonon Umklapp processes in the alkali metals with bcc structure, we have already mentioned that a minimum value of phonon w.v. q_{min} is required. The minimum w.v. is associated with a minimum energy $\hbar\omega_{min}$. When $k_B T$ is well below $\hbar\omega_{min}$, the number of phonons available for such events should become proportional to $\exp(-\hbar\omega_{min}/k_B T)$, i.e., $\exp(-\theta*/T)$. That is why Ziman (ref. 2) concluded that the Umklapp process contribution to the resistivity is

$$\rho_{e-ph} \propto e^{-\theta*/T} \tag{2-3}$$

For the resistivity of potassium at low temperature, Kaveh, Leavens and Wiser (ref. 3) proposed an empirical expression,

$$\rho_{e-ph} = CT^n \exp(-\theta*/T) \tag{2-4}$$

where the value of n was related to that of $\theta*$; increasing n by one would reduce $\theta*$ by about 2.8K.

2.1.2 Electron-Electron Scattering (ref. 4)

As in electron-phonon scattering, the total crystal momentum in electron-electron scattering is conserved to within a reciprocal lattice vector $\vec{G}$, (i.e., $\vec{k}_1 + \vec{k}_2 = \vec{k}_1' + \vec{k}_2' + \vec{G}$ where $\vec{k}_1$ and $\vec{k}_2$ are the w.v.s of the incoming electrons, $\vec{k}_1'$ and $\vec{k}_2'$ are the w.v.s of the scattering electrons). Since electrons obey the Pauli exclusion principle, $\vec{k}_1$, $\vec{k}_2$, $\vec{k}_1'$, and $\vec{k}_2'$ are all within $k_B T$ of the

Fermi Surface. So, the numbers of possible w.v.s $\vec{k}_1$ and $\vec{k}_2$ are both proportional to T. Thus, the scattering rate, $1/\tau_{e-e}$, is proportional to T^2. But, not all electron-electron scattering events contribute to electrical resistivity. For normal processes, $\vec{G} = 0$, the total crystal momentum of the electrons is strictly conserved. Such scattering thus makes no contribution to the resistivity, assuming an isotropic relaxation time. For Umklapp processes, $\vec{G} \neq 0$, crystal momentum is exchanged between the electrons and the lattice, thus there is a contribution to the resistivity, $\rho_{e-e} = (m/ne^2) (1/\tau_{e-e}) \propto T^2$. Lawrence and Wilkins (ref. 21) developed a theory of screened Coulomb interaction between electrons for potassium. MacDonald et al. (ref. 20) refined this theory. They found that the contribution of screened Coulomb interaction was much smaller than that calculated by Lawrence and Wilkins, and proposed a dominant term due to phonon-exchange scattering instead. Both theories predicted an AT^2 term which accidentally had the same values A = 0.17 pΩcm/K^2.

2.1.3 The Residual Resistivity

In the first order, the scattering of electrons by static imperfections in the lattice, such as impurities, vacancies, dislocations, surface and so on is elastic, and makes a temperature-independent contribution to the resistivity, called the residual resistivity ρ_0.

However, inelastic scattering of electrons by lattice imperfections can also cause a temperature-dependent resistivity, as will be discussed in section 2.2.8.

According to Matthiessen's rule (ref. 2), the standard theory for the alkali metals described above should give

$$\rho = \rho_o + AT^2 + BT^5 + CT^n e^{-\Theta*/T} \qquad (2-5)$$

At a very low temperature, when the last two terms become negligible, we expect

$$\rho = \rho_o + AT^2 \qquad (2-6)$$

and

$$d\rho/dT = 2AT, \text{ or } (\frac{1}{T}) \; d\rho/dT = 2A \qquad (2-7)$$

If $d\rho/dT$ is plotted versus T, a straight line with slope = 2A should result. If $(1/T)(d\rho/dT)$ is plotted versus T, a horizontal straight line should result.

2.2   BEYOND THE STANDARD MODEL OF ELECTRICAL RESISTIVITY FOR ALKALI METALS

2.2.1   Electron-Electron Scattering in the Presence of Anisotropic Scatterers such as Dislocations (ref. 15)

As mentioned in section 1.2.1, Kaveh and Wiser proposed an anisotropic electron-electron scattering model to explain the variations in magnitude of the T^2 coefficient reported by van Kempen et al. for pure K sample clad in polyethylene

tubes. Their model was also used to explain some later
experimental results from others. In this section, the
details of this model are described in what follows.

Under the following conditions: a) steady state, b) no
temperature gradient, c) no magnetic field, and d) relaxation
time approximation, the Boltzmann equation, which lies at
the heart of the theory of electronic transport in metals,
is of the form

$$-\frac{e}{h}\vec{E} \cdot \vec{\nabla}_k f(\vec{k}) = \frac{-f(\vec{k}) - f_o(\vec{k})}{\tau(\vec{k})} \quad .$$

Since, $\quad \vec{\nabla}_k f(\vec{k}) = [\vec{\nabla}_k \epsilon(\vec{k})] [\frac{\partial f(\vec{k})}{\partial \epsilon}] = \hbar v(\vec{k}) [\frac{\partial f(\vec{k})}{\partial \epsilon}]$,

thus, $\quad f(\vec{k}) - f_o(\vec{k}) = e\tau(\vec{k}) \vec{V}(\vec{k}) \cdot \vec{E} (\frac{\partial f(\vec{k})}{\partial \epsilon})$ $\qquad$ (2-7)

where $\vec{E}$ is the external electric field, $f(\vec{k})$ is the
electronic distribution function, $f_o(\vec{k})$ is the equilibrium
distribution function, and $\tau(\vec{k})$ is the relaxation time.

Kaveh and Wiser defined $\phi(\vec{k})$ as $f(\vec{k}) - f_o(\vec{k}) = -\phi(\vec{k})(\frac{\partial f(\vec{k})}{\partial \epsilon})$, and argued that in terms of $\phi(\vec{k})$, the inte-
grand of the multiple integral for $\rho_{e-e}(T)$ contains the
product (Ziman 1960) (ref. 2)

$$[f(\vec{k}_1) + f(\vec{k}_2) - f(\vec{k}_3) - f(\vec{k}_4)]^2 [\vec{k}_1 + \vec{k}_2 - \vec{k}_3 - \vec{k}_4]$$
$$\propto [\phi(\vec{k}_1) + \phi(\vec{k}_2) - \phi(\vec{k}_3) - \phi(\vec{k}_4)]^2 [\vec{k}_1 + \vec{k}_2 - \vec{k}_3 - \vec{k}_4]$$

$\qquad$ (2-8)

where $\vec{k}_1$ and $\vec{k}_2$ are the initial states, $\vec{k}_3$ and $\vec{k}_4$ final
states. They argued that for one-OPW electron wavefunctions

(which are primarily appropriate for alkali metals) $\phi(\vec{k}) \propto \tau(\vec{k})\vec{k}\cdot\vec{E}$. Thus,

$$[\phi(\vec{k}_1) + \phi(\vec{k}_2) - \phi(\vec{k}_3) - \phi(\vec{k}_4)]^2 \; \delta[\vec{k}_1 + \vec{k}_2 - \vec{k}_3 - \vec{k}_4]$$
$$\propto [(\tau(\vec{k}_1)\vec{k}_1 + \tau(\vec{k}_2)\vec{k}_2 - \tau(\vec{k}_3)\vec{k}_3 - \tau(\vec{k}_4)\,\vec{k}_4)\cdot\vec{E}]^2$$
$$\delta[\vec{k}_1 + \vec{k}_2 - \vec{k}_3 - \vec{k}_4]$$

$$(2\text{-}9)$$

The δ function in equations (2-8) and (2-9) implies that there is no contribution from Umklapp scattering. So, only normal scattering needs to be considered. Moreover, they pointed out that the $\tau(\vec{k})$ is determined by all electron scattering mechanisms, not only by electron-electron scattering. At low enough temperatures, electron-impurity and electron-dislocation scattering are dominant. There are thus two different limits for the determination of $\tau(\vec{k})$. In the first limit, the dominant scattering mechanism is electron-impurity scattering. They argued that electron-impurity scattering is approximately isotropic [$\tau(\vec{k})$ is constant]. This is termed the 'isotropic limit.' In this limit, integrand (2-9) is equal to zero, so $\rho_{e-e}^{N}(T)$ vanishes. In the other limit, the dominant scattering mechanism is electron-dislocation scattering. They argued that electron-dislocation scattering is highly anisotropic, so that the resulting relaxation time $\tau(\vec{k})$ will be anisotropic over the Fermi surface, (i.e., not equal for different directions). This is called the anisotropic limit. In this limit, the $\tau(\vec{k})$s in equation (3) are

different for $\vec{k}_1$, $\vec{k}_2$, $\vec{k}_3$, and $\vec{k}_4$, $\rho^N_{e-e}(T)$ does not vanish, and can assume a relatively large value.

Next, they generalized the discussion to include multiple-OPW electron wavefunctions, and argued that the Umklapp scattering term $\rho^U_{e-e}(T)$ no longer vanishes but is still considerably smaller than $\rho^N_{e-e}(T)$ in the anisotropic limit for alkali metals, because the wavefunctions for the alkali metals have primarily one-OPW character.

In summary, they had:

$$\rho_{e-e}(T) \longrightarrow \rho^U_{e-e}(T) = A^U T^2 \qquad \text{isotropic limit} \tag{2-10}$$

$$\rho_{e-e}(T) \longrightarrow \rho^{N,ani}_{e-e}(T) + \rho^U_{e-e}(T) \qquad \text{anisotropic limit}$$
$$\approx \rho^{N,ani}_{e-e}(T) = A^N T^2 \tag{2-11}$$

Finally, they predicted the coefficient of the e-e T^2 term to be $A = A^U + A^N$ with

$$A^N \propto (\rho_{od}/\rho_0)^2 = (1 + \rho_{oi}/\rho_{od})^{-2} \tag{2-12}$$

where ρ_{oi} and ρ_{od} are the residual resistivity contributions due to impurities and dislocations, respectively.

This model was able to describe the sample dependence of the coefficient A for K data of van Kempen et al. of Levy et al., and of Rowlands et al.

The main difficulty with this model is that the required number of dislocations in the K samples are at least two orders of magnitude more than is believed could easily exist in strain free K samples. Moreover, there was no way to determine ρ_{oi}, ρ_{od}, and their ratio, so that one

adjustable parameter was needed to make each set of data fit the theory.

2.2.2 Inelastic Scattering of Electrons Due to Low Energy Excitations Associated With Dislocations

As mentioned in section 1.2.1, M. Haerle (ref. 22) used theories of inelastic scattering of electrons due to low energy excitations associated with dislocations to explain anomalous deviations at the low T end in bulk potassium samples. In this section, this model is introduced. Two kinds of low energy excitations are discussed; one is associated with local electronic states, the other with local phonon modes.

Theoretical and experimental work on understanding the contribution of dislocations and grain boundaries to the residual resistivity in metals was summarized by Brown in 1981 (ref. 29). He suggested that additional bound states for electrons with energy slightly larger than the Fermi energy exist near the cores of dislocations. He estimated the energy of these additional levels to be above the Fermi level by ϵ which is a few meV for common metals such as copper, gold, aluminum, silver, molybdenum, tungsten and zinc, and about 0.1 meV for potassium. Earlier, Gantmakher and Kulesko (ref. 30) had derived an equation for the additional resistivity due to changes in the elastic scattering cross-section because of filling of electron levels localized at dislocations as

$$\rho_{e-dis} = \alpha[1 + \beta \exp(\epsilon/kT)]^{-1} \qquad (2-13)$$

where β is the spin degeneracy of the additional level and α is a proportionality constant. Fulde and Peschel (ref. 31) calculated the resistivity contribution of inelastic scattering of electrons off of a localized energy level. Their theory could be applied to scattering off local electronic states caused by dislocations such as the ones predicted by Brown. They obtained

$$\sigma(T) = \sigma_0[1 - \frac{\gamma^2\delta/T}{Sinh(\delta/T)}] \qquad (2\text{-}14)$$

They compared the above result with the corresponding expression one would obtain by applying Matthiessen's rule,

$$\sigma_M(T) = \sigma_0[1 + \frac{\gamma^2}{1 + 2/3\ Sinh^2\ \delta/2T}]^{-1} \qquad (2\text{-}15)$$

where σ_0 is the residual conductivity, δ is the energy separation between the associated two states, and γ is a constant. These two functions have the same limiting values for $T \ll \delta$ and $T \gg \delta$.

In another mechanism, inelastic scattering of electrons off of dislocations is associated with local phonon modes. Anderson and O'Hara worked on the lattice thermal conductivity in undeformed superconducting Al and deformed superconducting Pb and Ta, and claimed that their data showed resonant phonon absorption at certain energies. Their results were in good agreement with calculations based on the elastic-string model of localized phonon modes associated with dislocations (ref. 32). The elastic-string

model of dislocations considers a dislocation which is anchored at both ends. Since there is an elastic energy associated with unit length of dislocation, there will always be a tendency for a dislocation to make itself as short as possible so as to minimize this energy, like an elastic string does. In this model, additional local phonon modes can come from the oscillation of the elastic disloca- tion string; the longest wave length, and thus the lowest energy state, are associated with the length of the disloca- tion. The anchoring sources can be impurities, nodes in a dislocation network, or some other crystal defect. Adding more impurities and dislocations will shorten the length of dislocations, and thus increase the. lowest energy of this system. The random placement of the dislocations and im- purities would give a random distribution of lengths of the anchored dislocations.

The scattering of electrons from these local modes should be inelastic. Approximating the local modes by a single frequency oscillator, Gantmakher and Kulesko (ref. 30) calculated the contribution of such inelastic scattering to the resistivity as of the form

$$\rho_{e\text{-dis}} = (C/4T) \; \text{Sinh}^{-2}(\hbar\omega/2kT) \qquad (2\text{-}16)$$

where ω is the frequency of the ground state and C is a constant.

2.2.3 CDW Theory and Electron-Phason Scattering

An electron-phason scattering mechanism from CDW theory, first proposed by Boriack and Overhauser (ref. 33) and later improved by Bishop and Overhauser (ref. 34), was proposed to explain the $T^{3/2}$ variation in the resistivity of potassium, reported by Rowlands et al. (ref 16).

According to Overhauser (ref. 1), in a metal for which the positive-ion lattice closely approximates the deformable jellium model, the electronic ground state is a charge density wave (CDW) state. The spatial density of conductive electrons is not uniform throughout the crystal, but is of the form

$$\rho(\vec{r}) = -en[1-P \cos(\vec{Q}\cdot\vec{r} + \phi)] \qquad (2-17)$$

where n is the density of the electron gas, and P, $\vec{Q}$, and ϕ are the amplitude, wave vector, and phase of the electronic CDW. In potassium Q is claimed to be slightly greater than $2k_F$ (ref. 1).

In order to neutralize this charge modulation, the lattice tends to be deformed. Potassium might undergo this deformation easily because of its softness. This deformation of the ionic lattice is given by

$$\vec{U}(\vec{L}) = \vec{A} \sin(\vec{Q}\cdot\vec{L} + \phi) \qquad (2-18)$$

with parameters defined above, and $|\vec{A}| = P/|\vec{Q}|$.

In general, the CDW wave vector $\vec{Q}$ is incommensurate with the reciprocal lattice vector $\vec{G}$. Thus the lattice

should have an extra one dimensional periodicity along the direction of $\vec{Q}$. This extra periodicity introduces additional Bragg planes, and thus, extra Brillouin zone boundaries. In potassium, Q is presumed to be slightly greater than $2k_F$, so the first extra zone boundary is very close to the Fermi surface, and the spherical Fermi surface of potassium is changed to a lemon shaped surface that just touches the extra zone boundary (Figure 2-2).

One of the consequences of this modification is that in the region of contact points between two Fermi surfaces in neighboring new Brillouin zones, the minimum wave vector of phonons joining electron-phonon Umklapp scattering is reduced (Figure 2-3), thus the scattering is enhanced, and its contribution to the electrical resistivity increases. In addition, electron-electron Umklapp scattering can occur not only through $\vec{k}_1 + \vec{k}_2 = \vec{k}_1' + \vec{k}_2' + \vec{G}$, but also through $\vec{k}_1 + \vec{k}_2 = \vec{k}_1' + \vec{k}_2' + \vec{Q}$, (i.e., the CDW enhances this scattering and its contribution to the resistivity).

According to Overhauser, a CDW crystal is typically divided into $\vec{Q}$ domains. The direction of $\vec{Q}$, along with the domain boundaries, is very unstable at high temperature, but is frozen at low temperatures. Overhauser predicted that the enhanced electron-phonon Umklapp scattering along the direction of $\vec{Q}$ would cause an anisotropy of the electrical resistivity of potassium at low temperature as large as four to one (ref. 34). For wire samples, the orientation of the $\vec{Q}$ domains is sample-dependent, so the electron-electron
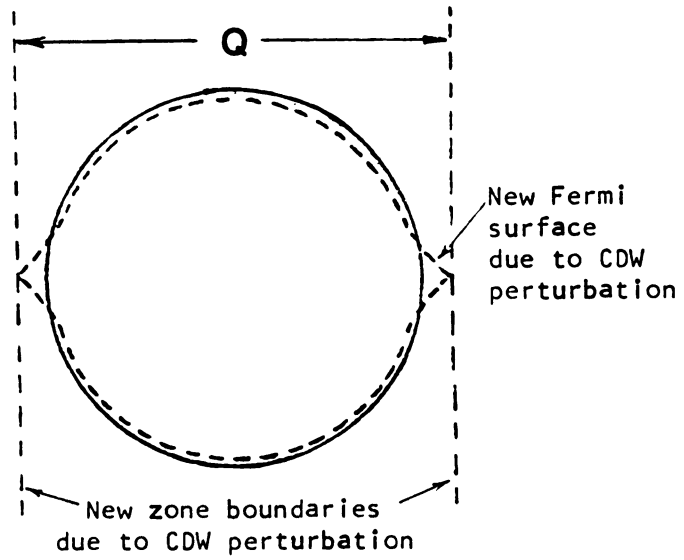
Fig. 2-2. The effect of a CDW perturbation on the Fermi

surface. The sphere is distored to a lemon shape.

(After Overhauser (ref.1))
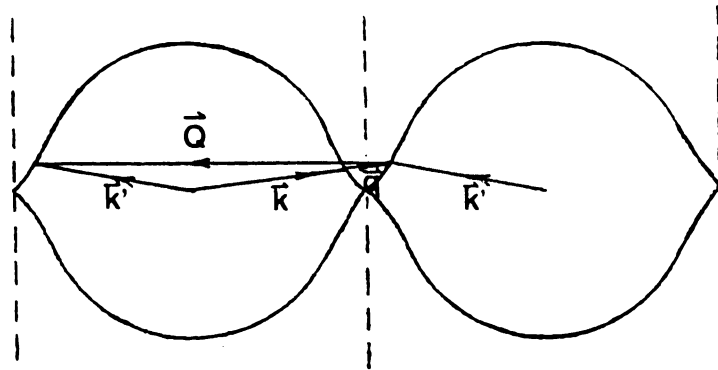
Fig. 2-3. The Umklapp scattering for a distored Fermi

surface. (After Overhauser (ref.1))

scattering contribution to the resistivity should also be sample dependent. This can be used to explain the sample dependencies of ρ_0 and of A, the coefficient of the T^2 term in the resistivity of potassium, reported by van Kempen et al., Levy et al. and Rowlands et al.

Another consequence of a CDW, is phonon-like excitations, called phasons. Without a CDW, phonons arise from thermal vibration of the lattice ions because of the lattice periodicity. Similarly, phasons arise from the new ionic periodicity of CDW, since $\vec{Q}$ is incommensurate with $\vec{G}$.

Boriack and Overhauser (ref. 33) suggested an electron-phason interaction of the form

$$V_{e\phi} = 1/2 \, G \sum_{\vec{q}} \phi_{\vec{q}} \{\cos[(\vec{Q} + \vec{q}) \cdot \vec{r} - \omega_{\vec{q}} t] -$$
$$\cos[(\vec{Q} - \vec{q}) \cdot \vec{r} - \omega_{\vec{q}} t]\} \qquad (2\text{-}19)$$

where $G \cos(\vec{Q} \cdot \vec{r})$ is the total self-consistent potential, and $\phi_{\vec{q}}$, $\omega_{\vec{q}}$, $\vec{q}$ are magnitude, frequency, and wave vector of the phason, respectively. With this potential, and assuming the Fermi surface to be rigidly displaced in k-space by the external electric field, Bishop and Overhauser (ref. 34) obtained the electrical resistivity by using the variational method as

$$\rho_{e\phi}(T) = A(\sqrt{2} \, T/\theta_\phi)^5 \, J_5(\theta_\phi/\sqrt{2} \, T) + B(T/\theta_\phi)^4$$
$$J_4(\theta_\phi/T) + C(T/\theta_\phi)^2 \, J_2(\theta_\phi/T)$$

$$(2\text{-}20)$$

where

$$J_n(x) = \int_0^x \frac{z^n dz}{(e^z-1)(1-e^{-z})}$$

is the Bloch-Gruneisen function. Each one of the three terms given above can fit well to Rowlands' data with different parameters Θ_ϕ, but their extensions below 0.5K differ from each other (Figure 2-4).

It is important to note that this model cannot lead to a negative $d\rho/dT$, since all three terms given above increase monotonically with temperature. This means that this model of electron-phason scattering cannot explain the appearance of a negative $d\rho/dT$ in our thinnest K samples, which will be analyzed in Chapter 4.

2.2.4 The Knudsen Flow Model

By analogy with the Knudsen flow (ref. 35) of rarefied gases in a cylindrical tube, Rowlands et al. (ref. 16) proposed a size effect model associated with the Knudsen flow of electrons to explain their experimental results for K (section 1.2.1).

They noted that the relaxation time (τ) for electron-electron normal scattering in potassium at 1K from Lawrence and Wilkins' calculation (ref. 21) is about 1.09×10^{-7} sec, and the Fermi velocity (V_F) of potassium is about 8.6×10^5 m/sec. Thus, the mean free path (λ) of this scattering is about 9 cm. Comparing λ with the radius (r) of their samples (r = 0.4 mm), they argued that most collisions of
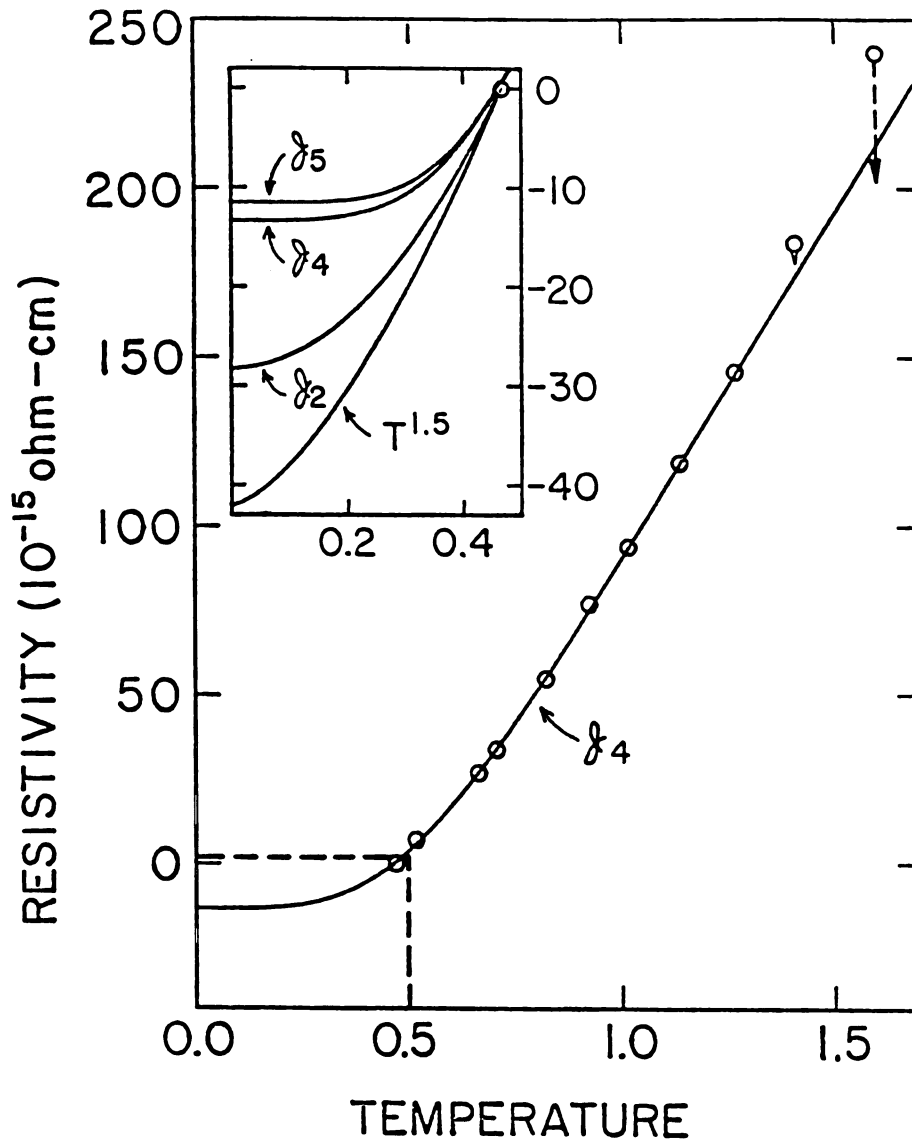
Fig. 2-4. Plot of resistivity vs T for the data of sample K2C of Rowlands et al. (ref.13). The fitting curve with J_4 is shown. In the inset, extrapolations of $T^{1.5}$, J_2, J_4, J_5 fits to lower temperatures are shown. (After Bishop and Overhauser (ref.17))

electrons below 1K were with boundaries, and thus the Knudsen flow model can be used. Assuming diffusely scattering walls they proposed an appropriate formula for the resistance to the electron "Knudsen flow" as

$$\rho = \rho_O \ (1 + kr/\lambda) \tag{2-21}$$

where k is about 1 for gasses (found by Dushman) (ref. 36), for phonons in liquid helium (found by Whitworth) (ref. 37), and for electrons (found later by Black in a Monte Carlo calculation (ref. 38)).

For electron-electron scattering, $\lambda \propto T^{-2}$, so the temperature-dependent resistivity should be

$$\rho_T = \rho - \rho_O = BT^2 \tag{2-22}$$

with

$$B \propto \rho_O r$$

Black (ref. 38) pointed out later that in the Knudsen case, ρ_O is proportional to $1/r$, and hence, the coefficient B is independent of the residual resistivity ρ_O. Black also argued that if ρ_O is something other than the size-limited resistivity, as suggested by Rowlands et al., then $B \propto \rho_O r$ could be valid.

We noticed that $r/\lambda = 0.005$ at 1K in Rowlands case, and if $k \sim 1$, as calculated by Black, the $\rho_T(1K)/\rho_O$ is about 5 x 10^{-3}. But the data of van Kempen et al., of C. W. Lee et al., and even of Rowlands et al. themselves, showed

$\rho_T(1K)/\rho_0$ to be about 2×10^{-4}. Even considering a possible smaller effective radius due to additional scattering from other scatterers, as suggested by Rowlands et al. for their data, the predicted ratio $\rho_T(1K)/\rho_0$ is still about an order of magnitude too big.

Alternatively, according to Kukkonen and Smith (ref. 39) τ could be an order of magnitude smaller. In such a case, Rowlands et al. proposed that a term in $(r/\lambda)^2$ ought to be taken into account to give

$$\rho_T = BT^2 - CT^4 \qquad (2-23)$$

In this case, the ratio $\rho_T(1K)/\rho_0$ is even two orders of magnitude too big compared to experimental results.

Starting from a force-force correlation function formula for the residual resistivity, March and Woods provided a possible alternative justification for equation (2-21) above (ref. 40). In their form

$$\rho = \rho_0 \left(1 + \frac{\lambda^*}{\lambda} + \ldots \right) \qquad (2-24)$$

where λ^* is found to reflect long-range correlations in the electronic motions and not necessarily to be size limited. λ is electron-electron scattering mean-free-path in low temperature resistivity study of potassium. In explaining data of the potassium wire samples from Rowlands et al., they suggested $\lambda^* \sim 1/2$ mm. So, the $\rho_T(1K)/\rho_0$ in their model is still an order of magnitude too big.

As mentioned above, we need a model to explain the negative $d\rho/dT$ in our thinnest K samples. In the two models described in this section, only the second term in equation (2-23) seems to be able to generate a negative $d\rho/dT$. But when sample radius r is smaller, $(r/\lambda)^2$ is less important, so $-CT^4$ term is less important. So if for bigger r we do not see a negative $d\rho/dT$, (i.e., with our thick samples), then for thinner samples this equation cannot lead to a negative $d\rho/dT$.

2.2.5 Size-Dependent DMR

In this section we first describe two size-dependent DMR models, which were previously used for explaining size-effects in other metals. The possibility for using each of these models to explain the negative $d\rho/dT$ found in our thinnest K samples is discussed.

The well known Matthiessen's rule (MR) can be written in the form

$$\rho_a(c,T) = \rho_p(T) + \rho_o(c) \tag{2-25}$$

where $\rho_a(c,T)$ is the resistivity of a dilute alloy containing a concentration c of impurity, $\rho_p(T)$ is the resistivity of an ideally pure metal, and $\rho_o(c)$ is the impurity produced resistivity at zero K.

In fact, there are always deviations from MR. $\rho_a(c,T)$ can be written exactly as

$$\rho_a(c,T) = \rho_p(T) + \rho_o(c) + \Delta(c,T) \tag{2-26}$$

For 'normal' size dependent DMR, induced by a spatial variation in the distribution function $f_k(\vec{r})$ due to the existence of boundaries, Dingle (1950) (ref. 41) developed a theory for metal wires of circular cross section. Dingle assumed that the electrons in the metal were free-electron-like with a spherical Fermi surface and that the surface scattering might be characterized by a single specularity parameter, p (defined as the probability that an electron incident upon the surface is reflected specularly as though from a mirror) which was assumed to be independent of the incident angle. A few years later, Ziman (ref. 2) (1960) formulated an angle-dependent specularity parameter $P_s(\theta) = \exp[-(4\pi h/\lambda_e)^2 \cos^2\theta]$, by assuming that all electrons have the same wavelength λ_e and that the surface can be characterized by a root mean square surface roughness h. More recently this $p_s(\theta)$ was incorporated into Dingle's model by Sambles et al. (ref. 42), obtaining an expression for the ratio of bulk to thin wire resistivity,

$$\frac{\rho_\infty}{\rho} = 1 - \frac{12}{\pi k} \int_0^{\pi/2} \cos^2\theta \sin^2\theta \, d\theta \int_0^{\pi/2} \sin\psi \, d\psi$$

$$\frac{(1-p)[1-\exp(-k\sin\psi/\sin\theta)]}{1-p \cdot \exp(-k\sin\psi/\sin\theta)} \qquad (2-27)$$

where $k = d/\lambda_\infty$ and $p = \exp[-(4\pi h/\lambda_e)^2 \sin^2\theta \sin^2\psi]$. Since ρ_∞/ρ is a function of only k, Sambles defined $f(k) = (\rho - \rho_\infty)k/\rho_\infty = (\rho/\rho_\infty - 1)k$. Thus $\rho - \rho_\infty = f(k)\rho_\infty/k = f(k) \cdot \rho_\infty\lambda_\infty/d$. To determine the sign of $\partial\rho/\partial T$, Sambles (ref. 43)

argued that

$$\frac{\partial \rho}{\partial T} = \frac{\partial}{\partial T} \; (\rho - \rho_\infty) \; + \; \frac{\partial \rho_\infty}{\partial T}$$

$$= \frac{\rho_\infty \lambda_\infty}{d} \frac{\partial f(k)}{\partial T} + \frac{\partial \rho_\infty}{\partial T} \qquad \text{(since } \frac{\rho_\infty \lambda_\infty}{d} \text{ is a constant)}$$

$$= \frac{\rho_\infty \lambda_\infty}{d} \frac{\partial f(k)}{\partial k} \cdot \frac{\partial k}{\partial T} + \frac{\partial \rho_\infty}{\partial T} \qquad \text{(since } f(k) \text{ is a function of only } k)$$

$$= (1 + \frac{\partial f}{\partial k}) \; \frac{\partial \rho_\infty}{\partial T} \qquad \text{(since } k = \frac{d}{\lambda_\infty} = \frac{d\rho_\infty}{\rho_\infty \lambda_\infty} \text{ thus}$$

$$\partial k / \partial T = (d/\rho_\infty \lambda_\infty)(\partial \rho_\infty / \partial T)$$

$$(2\text{-}28)$$

Finally, Sambles argued that in their model, $\partial f/\partial k$ cannot be smaller than -1, $\partial \rho/\partial T$ cannot be negative unless $\partial \rho_\infty/\partial T$ is negative (ref. 43).

Boughton and Neighbor (1972) (ref. 44) calculated size-dependent DMR under several different situations. For wires of circular cross section, their calculation led to two different results: a) For metals with cylindrical Fermi surface, they obtained the ratio of thin wire to bulk resistivity

$$\frac{\rho}{\rho_\infty} = \frac{3\pi^2}{16k} \; [0.590 - \ln\frac{8k}{3\pi}]^{-1} \qquad (2\text{-}29)$$

as a function of only k, with $k = d/\lambda_\infty$. This gave

$$f(k) = (\frac{\rho}{\rho_\infty} - 1) \; k$$

$$= \frac{3\pi^2}{16} \; [0.590 - \ln\frac{8k}{3\pi}]^{-1} - k \qquad (2\text{-}30)$$

and

$$\frac{\partial f}{\partial k} > -1$$

with the same argument for equation (2-28), one can conclude that $\partial P/\partial T$ cannot be negative unless $\partial P_\infty/\partial T$ is negative. b) For metals with spherical Fermi surface, they obtained

$$\frac{\rho}{\rho_\infty} = \frac{1}{k} + \frac{3}{8} \, [\ln\frac{3\pi}{8} - \ln k - \Gamma_s] \tag{2-31}$$

where Γ_s is a constant, for wires of circular cross-section $\Gamma_s < -1$ can be obtained from an equation given by them (ref. 44). This gave

$$f(k) = 1 + \frac{3k}{8} \, [\ln\frac{3\pi}{8} - \ln k - \Gamma_s] - k \tag{2-32}$$

Thus,

$$\frac{\partial f(k)}{\partial k} > -1,$$

and,

$$\frac{\partial P}{\partial T} > 0 \qquad (\text{as long as } \frac{\partial P_\infty}{\partial T} > 0).$$

2.2.6 The Gurzhi Theory (ref. 45)

None of the theories associated with size-effect discussed above can provide an explanation of negative dP/dT in our data of thinnest potassium. In this section, the only published candidate which might provide such an explanation is introduced.

In 1962, Gurzhi predicted that normal electron-electron scattering (NEES) should affect the path length between two sequential electron-surface collisions in impurity-free conductors and thus cause a negative temperature derivative of resistivity ($d\rho/dT < 0$).

Gurzhi argued that a) The frequency of electron-electron scattering decreases with temperature more slowly than the frequency of the electron-phonon scattering and will be dominant at low temperatures. b) In a bulk conductor, electron-electron scattering gives rise by itself to electrical resistivity only through Umklapp processes, NEES makes no contribution. c) When $l_V \gg d$, where l_V is the mean free path connected with the scattering by the inhomogeneities such as phonons, impurities and internal defects, and d is the sample diameter, the effective mean free path with diffusely scattering walls should be of the form $l_{eff} \sim d$ if the effect of NEES is not taken into account. But, when $d \gg l_{e-e}$ (l_{e-e} = the mean free path of NEES), before an electron situated deep in the sample reaches the walls, it would be scattered by other electrons many times and thus would move like a Brownian particle. According to the formula of Brownian motion, the length of the path length between two collisions with the wall is of order d^2/l_{e-e}, i.e., $l_{eff} \sim d^2/l_{e-e}$. But $1/l_{e-e} \propto 1/\tau_{e-e} \propto T^2$, so $\rho \propto 1/l_{eff} \propto l_{e-e}/d^2 \propto T^{-2}$. This gives us $d\rho/dT \propto -T^{-3}$, a negative derivative!

According to the Gurzhi theory, a negative temperature

derivative of resistivity would be expected in a high-purity thin sample with $l_{e-e} \ll d$.

2.2.7 The Kondo Effect (ref 4,46,47)

In the standard theory (section 1.3.1) nonmagnetic scatterers, such as impurities and lattice imperfections, led to a temperature-independent term toward which the resistivity monotonically drops with decreasing temperature. But if magnetic impurities are the predominant type of scatterers, the scattering from them will be the primary source of electrical resistance at low enough temperature. Then, instead of dropping monotonically, the resistivity can rise with decreasing temperature (ref. 4,47).

In 1963, Kondo (ref. 46) argued that when the scattering center has a magnetic moment, the exchange interaction between the conduction electrons and the local moment leads to flipping of the electronic spin with a compensating change of spin on the local moment. Kondo discovered that in all higher orders of perturbation theory the magnetic scattering cross-section is divergent, yielding an infinite resistivity as in a term of $-\log T$. The balancing of this term against the electron-phonon scattering term results in a resistivity minimum.

According to subsequent analysis by Kondo and others, the thermal rounding of the electron distribution removes the divergence. Experiments showed that the logarithmic Kondo behavior is followed by the resistivity only down to a certain temperature known as Kondo temperature, below

which the resistivity becomes approximately constant (ref. 47).

No Kondo effect in the alkali metals has been reported in previous work. In section 4.4 we will report a possible Kondo effect in the present study.

2.2.8 Inelastic Scattering of Electrons by Impurities and Defects

Considering inelastic scattering of electrons by the thermal motion of impurity ions, Koshino (ref. 48) in 1960 first obtained a T^2 behavior of the resistivity at low temperature of the form

$$\rho_{inel} \propto J_2 Z^2 T^2 \qquad (2-33)$$

where

$$J_2 = \left\{ \begin{array}{ll} 2.4 & \text{for } T \rightarrow 0 \\ \Theta_D/T & \text{for } T >> \Theta_D \end{array} \right.$$

and Z is the excess charge of the impurity ion.

Considering that the displacement of the impurity potential induced by the thermal motion of the impurity ion leads to a reduction of elastic as well as inelastic scattering of electrons, Taylor (ref. 24) pointed out that this reduced the additional resistivity due to inelastic scattering. In 1963, Koshino (ref. 48) argued that this reduction cancels out the additional resistivity due to inelastic scattering at high temperatures, but brings no essential change in the additional resistivity at low temperatures. Taylor (1964) (ref. 24) recalculated the

additional resistivity at low temperatures and obtained an

expression without Z as

$$\rho_{inel} = \frac{\pi^2 \hbar^2 K_{av}^2}{2Mk_B \Theta_D^3} \rho_o T^2 = 1.37 \times 10^{-5} \rho_o T^2 \qquad (2-34)$$

where K_{av} is an averaged wave vector close to $2k_F$ (k_F =

Fermi wave vector), M the host ionic mass, Θ_D the Debye

temperature, and k_B the Boltzmann's constant.

Kus and Taylor (ref. 25) obtained for K-Rb

$$\rho_{inel} = 1.25 \times 10^{-5} \rho_o T^2 \qquad (2-35)$$

Froböse and Jackle (ref. 49) derived the same formula

as equation (2-34) for structure defect inelastic

scattering, and calculated ρ_{inel} for K and obtained

$$\rho_{inel} = 1.8 \times 10^{-5} \rho_o T^2 \qquad (2-36)$$

C. W. Lee et al. (ref. 23) reported that in K-Rb

alloy resistivity measurements they obtained

$$\rho = \rho_o + (8.5 \pm 0.3) \times 10^{-6} \rho_o T^2 + (2.2 \pm 0.3) \times 10^{-13} T^2,$$

and claimed the second term, $(8.5 \pm 0.3) \times 10^{-6} \rho_o T^2$, as an

unambiguous Koshino-Taylor term.

2.2.9 Electron-Electron Interaction and Localization Effects

In this section, two different theories of the

temperature dependence of the resistivity in impure metals

with nonmagnetic impurities are given.

The first is the theory of electron-electron interaction effects.

A square-root temperature dependence of resistivity due to the electron-electron interaction effects was first obtained by Altshuler et al. (ref 50). They argued that electron-electron interaction accompanied by the impurity scattering leads to a singularity in the density of states near the Fermi surface, and thus leads to a zero bias anomaly in the tunneling current-voltage characteristic. They showed that at low temperatures, the resistivity decreases as $-\sqrt{T}$ with increasing T.

In 1980, Fleurov et al. (ref. 51) obtained a more clear picture. They argued that when $T < c\Theta_D$, (where c denotes the concentration of the impurities, Θ_D denotes Debye temperature), the electron-phonon interaction is negligibly small compared with Coulomb interaction, thus resistivity decreases with increasing temperature according to $\Delta\rho(T) \sim -c^{5/2}(T/\epsilon_F)^{1/2}$, due to the Coulomb interaction between the electrons scattered by the static impurities. Moreover, they argued that the quasiclassical mechanism of the scattering from vibrating defects compensates the electron-phonon contribution over all this temperature region. At $T \sim c\Theta_D$ only this quasiclassical mechanism remains, giving an increase in the resistivity term of about $cT^2/\Theta_D\epsilon_F$, which exceeds the Coulomb term at $T \sim c\Theta(\Theta/\epsilon_F)^{1/3}$. The temperature of a resistivity minimum lies near this value.

The second theory given in this section is localization theory.

Scaling theories of localization have been discussed by Thouless et al. (ref. 52), by Wegner (ref. 53), by Schuster (ref. 54), and by Abrahams et al. (ref. 55). Abrahams et al. (1979) (ref. 55) using a scaling approach to localization, have obtained a correction of the conductivity to the Boltzmann result in three-dimensional disordered metallic state:

$$\delta\sigma \simeq \frac{e^2}{2^{3/2}\,\pi^2\hbar}\,(\frac{1}{L} - \frac{1}{L_o}) \qquad (2\text{-}37)$$

where L is the length of a cubic system, or, at finite temperatures, the inelastic diffusion length, L_i : $L_i^2 = 1/2\, l_e l_i$; $1/L_o$ is a constant of integration. l_e is the elastic mean free path and L_i is the inelastic mean free path. Using this result along with that of electron-electron interaction model, Howson (ref. 56) recently analyzed the temperature-dependent part of the scaling result of conductivity in the form

$$\sigma(T) \simeq \frac{1}{\pi^2}\frac{e^2}{\hbar}\,(\frac{1}{L_i(T)} - \frac{(k_F l_e)^2}{3}\frac{1}{l_i(T)}) \qquad (2\text{-}38)$$

where the first term will always give a non-metallic positive contribution to $d\sigma/dT$ while the second term will give a metallic negative contribution. Howson argued that in high-resistivity metallic glasses (>150 $\mu\Omega$cm), for which l_e may be as small as an atomic spacing, the second term in Eqn.

(2-38) can be neglected, then,

$$\sigma(T) \simeq \frac{1}{\pi^2} \frac{e^2}{\hbar} \frac{1}{L_i(T)} \qquad (2-39)$$

At low temperature,

$$l_i(T) \propto T^{-2} \qquad T < \theta_D$$

for both electron-electron and electron-phonon inelastic

scattering. At high temperature, the electron-phonon

scattering leads to

$$l_i(T) \propto T^{-1} \qquad T > \theta_D$$

but

$$L_i^2(T) = 1/2 \; l_e l_i(T)$$

Thus, Howson obtained

$$\sigma(T) \propto T \qquad T < \theta_D$$
$$\text{and} \quad \sigma(T) \propto \sqrt{T} \qquad T > \theta_D \qquad (2-40)$$

when $\sigma_O \gg \sigma(T)$, where σ_O is temperature-independent part of

conductivity, then one has

$$\rho = \rho_O - CT \qquad T < \theta_D$$
$$\text{and} \quad \rho = \rho_O - C\sqrt{T} \qquad T > \theta_D \qquad (2-41)$$

in first approximations, where $C \propto \rho_O^3$.

2.3   Thermoelectric Power S and Thermoelectric Ratio G

As described in section 1.1, generally there are three terms in S (or G) at low temperatures. The first is the diffusion term. The other two terms are due to normal and Umklapp phonon drag, respectively. In normal phonon drag (described in section 2.1.1), electrons tend to flow along with phonons from the hot to the cold end, and thus contribute a negative term in S (or G). In Umklapp phonon drag, electrons tend to flow opposite to the phonon flow, and thus contribute a positive term to S and G.

Details of the theory of S and G for Alkali metals have been described by C. W. Lee (ref. 8) and M. Haerle (ref. 22) in their theses. Only the main points of this theory are briefly reviewed in this section.

2.3.1   Thermoelectric Power S

At low temperatures, the thermopower S of alkali metals with b.c.c. lattice structure, can be written in the general form

$$S = A'T + B'T^3 + C'(T) \exp(-\theta^*/T). \qquad (2\text{-}42)$$

The first term (A'T) is the diffusion term, where A' can be written as the generally used Mott's expression (ref. 2):

$$A' = - \frac{\pi^2 k^2}{3e} \left. \frac{\partial \ln \sigma(E)}{\partial E} \right|_{E=E_f}. \qquad (2\text{-}43)$$

Here E_f = the Fermi energy, $\sigma(E)$ = energy dependent conductivity. Simplifying this general form, Guenault and MacDonald (ref. 5) obtained

$$A' = - \frac{\pi^2 k^2}{3eE_f} \left(\frac{\partial \ln[n(E)v^2(E)]}{\partial \ln E} + \frac{\partial \ln \tau(E)}{\partial \ln E} \right) \Bigg|_{E=E_f} \qquad (2\text{-}44)$$

where $\tau(E)$ = the relaxation time, $n(E)$ = the density of states, and $V(E)$ = the average electron velocity at energy E. When temperature independent mechanisms such as impurity scattering, dislocation scattering, etc. dominate, a temperature-independent A' is expected from either equation (2-43) or (2-44). And for spherical Fermi surface, as in alkali metals with b.c.c. structure, we expect to have a negative A' (ref. 8).

Applying Matthiessen's rule $\rho = \rho_i + \rho_d$ to Mott's formula, one gets the Gorter-Nordheim relation

$$S = (\rho_i S_i + \rho_d S_d)/\rho \qquad (2\text{-}45)$$

where ρ_i and S_i are the electrical resistivity and thermopower, respectively, due to impurity scattering, and ρ_d and S_d are the electrical resistivity and thermopower, respectively, due to another temperature independent scattering (such as dislocation or surface scattering).

A slight change in the concentration of impurities, or in the density of dislocations, can easily change the dominant scattering mechanism and thus change the magnitude of A'.

The second term $B'T^3$ is the normal phonon drag term, where B' is a simple constant. At very low temperatures in a sufficiently pure metal, the boundary scattering of phonons will dominate, the contribution of normal phonon drag to S will then go roughly as the lattice specific heat, which has T^3 temperature dependence (ref. 8).

The third term $(C'(T)\exp(-\Theta^*/T))$ is the Umklapp phonon drag term. For Umklapp scattering, as described in section 2.1.1, a minimum phonon wave vector (q_{min}) is needed, and thus the number of phonons available for such events should be proportional to exp $(-\Theta^*/T)$.

Guenault and MacDonald (ref. 7) obtained an approximation for $C'(T)$ at low temperatures as

$$C'(T) = [\frac{1/\tau_{ph-e}}{1/\tau_{ph-e} + 1/\tau_{ph-i}}] \ (0.200) \ [\frac{k}{e}] \ [\frac{\Theta^*}{\Theta_D}]$$

$$[\frac{\Theta^*}{T} + 3 + 6\frac{T}{\Theta^*}] \hspace{3cm} (2-46)$$

where τ_{ph-e} = phonon-electron scattering relaxation time, τ_{ph-i} = phonon-impurity scattering relaxatin time, Θ_D = Debye temperature, and Θ^* = a constant.

Ziman (ref. 57) and Bailyn (ref. 58) developed more detailed theories, but so far only the simplest forms for the Umklapp scattering have been used for fitting experimental data.

Guenault and MacDonald (ref. 7) claimed that their potassium data could be fitted by

$$S = A'T + B'T^3 + C'\exp(-\Theta^*/T)$$

with C' = a constant and $\Theta^* \sim 21K$. They found, as expected, that A' and B' were negative while C' was positive.

2.3.2 Thermoelectric Ratio G

Very little theory has been worked out for G. But, as described in section 1.1, G may be related to S by

$$S = GL(T)T \qquad (1-11)$$

and when elastic scattering of electrons is dominant

$$L(T) = L_0 = 2.45 \times 10^{-8} V^2 K^{-2} \qquad (1-8)$$

According to our present data, $L/L_0 \sim 0.96$ in K at 1K, the ratio L/L_0 becoming closer to 1 at lower temperatures.

At very low T, G is thus expected to be

$$G = G_0 + B'T^2 + \frac{C'}{T}\exp(-\Theta^*/T) \qquad (1-13)$$

or even

$$G = G_0 + B'T^2 \qquad (2-47)$$

where $G_0 = A'$ is the diffusion term, $B'T^2$ is the normal phonon drag term, and $C'/T \exp(-\Theta^*/T)$ is the Umklapp phonon drag term.

CHAPTER 3

Experimental Techniques

3.1 INTRODUCTION

In this chapter the basic experimental techniques and equipment, and our samples, are briefly described. Since most of the techniques and equipment have already been described elsewhere (ref. 8,22), only some modifications are given in detail.

As mentioned above, one of the main purposes of this study is to try to find the concealed reasons for disagreements between experimental results from different groups (section 1.2.1), and to study various deviations from electron-electron scattering when according to standard theory electron-electron scattering should dominate over electron-phonon scattering at low enough temperature. Thus, it was necessary to get the temperature below 1K. Second, there are two ways to study the temperature dependence of resistivity at low temperature. One is to measure ρ directly. But $\rho = \rho_0 + \rho(T)$, and at 1K, $\rho(T)/\rho_0$ is about 200 ppm for pure potassium of typical RRR~5000 (ref. 14,59). Since ρ_0 cannot be directly measured, it must then be left as an adjustable parameter, which produces an inevitable uncertainty in $\rho(T)$. The other way, used in this study, is to

measure dP/dT. Since P_0 is a constant, this must be exactly equal to $dP(T)/dT$ with no adjustable parameters. To determine the measured quantity $\Delta P/P\Delta T$ with a precision of 1%, extremely high precision ($\leq$ 0.1 ppm) of $\Delta C/C$ ($=\Delta P/P$) was needed, because for our highest purity potassium $\Delta P/P \approx 10^{-5}$ with a $\Delta T = 0.1K$ near 1K.

3.1.1 The Main Equipment Used for measurements

1) A locally built dilution refrigerator with good vibration isolation, giving a temperature range from 4.2K to 60 mK. The whole system could be cooled down to liquid nitrogen temperature ($\sim$77.4K) in about 12 hours by adding liquid nitrogen to the outer dewar with appropriate exchange gasses, and then cooling further to liquid helium temperature (4.2K) by transferring liquid helium into the inner dewar. This transfer took about 2 hours. 1.3K could be obtained at the 1K pot by pumping on the liquid helium. The lowest temperature of 70 mK was reached at the mixing chamber and the attached sample can about 3~5 hours after circulation of the dilution refrigerator was started. That means that all of our samples were cooled slowly. See C. W. Lee's thesis (ref. 8) for details.

2) A high precision ($\leq$0.1ppm) resistance bridge consisting of a commercial direct-current comparator modified by D. Edmunds et al. (ref. 60) and a very sensitive SQUID (Superconducting Quantum Interference Device) null-detector, capable of detecting voltages less than 10^{-15}V, or current less than 10^{-9}A. The ratio of two currents (slave

current to master current) could be read with a precision of
0.1 ppm using a set of eight decade-dials. Nearly 0.01 ppm
could be achieved by interpolating beyond the last dial
using a computer averaging technique.

3) A screened room for screening out radio frequency
noise that affects the operation of the SQUID. 1) and 2)
were enclosed in the screen room, and all the pumps were
kept outside (ref. 8).

3.1.2 Thermometers

Temperature measurements were very important in this
study. Three germanium resistance thermometers GRT2, GRT4,
and GRT5 were used.

The calibration of these three thermometers was done by
C. W. Lee and M. L. Haerle (ref. 8,22). GRT4 and GRT5 were
calibrated simply by carefully comparing them to GRT2. GRT2
itself was calibrated in three steps. First, it was
carefully compared to a Cryocal CR50 thermometer, calibrated
by J. L. Imes (ref. 61) and G. L. Neiheisel (ref. 62) from
0.065K to 4.2K by using the He^3 vapor pressure and a
susceptibility thermometer. A fit of the data with the
equation,

$$\ln R = \sum_{i=0}^{9} A_i \, (\ln T)^i \tag{3-1}$$

was used for calculating the temperature from 1.3K to 4.2K.
Below 1.3K, this fit was not accurate enough for the
present study. Second, using a set of Superconducting Fixed
Point Devices SRM 767 and SRM 768 from the National Bureau

of Standards (ref. 63) to get 6 absolute temperature points
from 0.099K to 1.17K and using a susceptibility thermometer
to interpolate between these six points. The fit of this
set of data, from 0.059K ot 1.24K, with the above equation
(3-1) has been used for measurements below 0.5K. Third, for
0.5K to 1.3K calibration, a large powdered sample of cerous
magnesium nitrate and four of the fixed points between
0.519K to 3.414K were used to again fit Eqn. (3-1).

The accuracy of these calibrations was tested by using
the Wiedemann-Franz law and a Ag-0.1 at% Au Alloy. One end
of this alloy was attached to the mixing chamber at a fixed
temperature, and GRT2 was mounted to the other end for
measuring the temperature there. The calibration gave the
product TΔT to within an average value of 0.47% with a
standard deviation of 1.2%. The maximum deviation from the
Wiedemann-Franz law was 2.6% (ref. 22).

To ensure that there were no problems with temperature
measurements while taking the data, the Wiedemann Franz law
was also used to double check the thermometry for every run
(see section 3.4).

The resistances of GRT2 and GRT4 were measured with two
SHE conductance bridges in the 4-terminal mode. The
bridges, using low excitation voltage (10 to 100 μV), were
accurate to better than 0.5%. They were self-balancing and
had a differential output, which was also used for regulat-
ing the mixing chamber temperature (section 3.5.1).

3.1.3 The Main Equipment for Sample Preparation

The alkali metals are all very reactive. They react rapidly with air and water vapor. Secondly, in this study, samples were measured under different circumstances: under Ar, He, or vacuum, and either bare, or encased in, or touched by, plastic. Therefore, some special equipment was needed for sample preparation.

The main equipment included: a) two glove boxes supplied by Vacuum Atmospheres Company; b) two different kinds of stainless steel presses used for making wire samples and potential leads; c) two sample cans, used to protect the samples from reacting with air; d) a high vacuum system, with all metal parts, capable of getting a 10^{-9} torr vacuum, used to pump out the sample can and clean some plastic tubings and pieces, glass tubings and molecular sieves, all needed for sample preparation.

The details of the glove boxes, presses, sample cans, sample preparation, measurement method, and uncertainty analysis will be given in what follows.

3.2 THE GLOVE BOXES AND PRESSES

Two glove boxes supplied by Vacuum Atmospheres Company were used for sample preparation. One had a built-in Pedatrol pressure control, Dri-train Mo 40-1 inert gas purifier with circulation rate of 50 cfm for He, and AO 316-C Oxygen analyzer. It was used under He atmosphere with an oxygen contamination level less than 0.5 ppm. Fresh

potassium exposed inside this glove box stayed shiny for at least 2 hours. The other glove box was evacuable and had only a built-in Pedatrol pressure control and locally built inert gas purifier with circulation rate of about 1 cfm. It was used under Ar atmosphere. Fresh potassium exposed inside of it stayed shiny for at least 2 hours also. All the samples were made inside these two glove boxes.

Two kinds of stainless steel presses were used. Figure 3-1 shows the structure of these presses. The big one, which is threaded, was much more powerful than the other and was used for making samples which could not easily be extruded, such as Li or thin Na samples. When the big one was used, it was stabilized in a big vice, and a long wrench was used to screw the piston in.

There were two ways to put the material into the press. For K, Rb, or Na, which were originally in ampoules, the material was melted in the glove box with a hot-plate and then poured into the press. For Li or Na, which were not originally in ampoules, the surface was first cleaned with a stainless steel knife, and the metal was then cut to reasonable size and put into the press. After the material was poured or put into the press, it was melted and allowed to solidify into one piece.

Different sample thicknesses were produced by using stainless steel dies with different hole diameters.
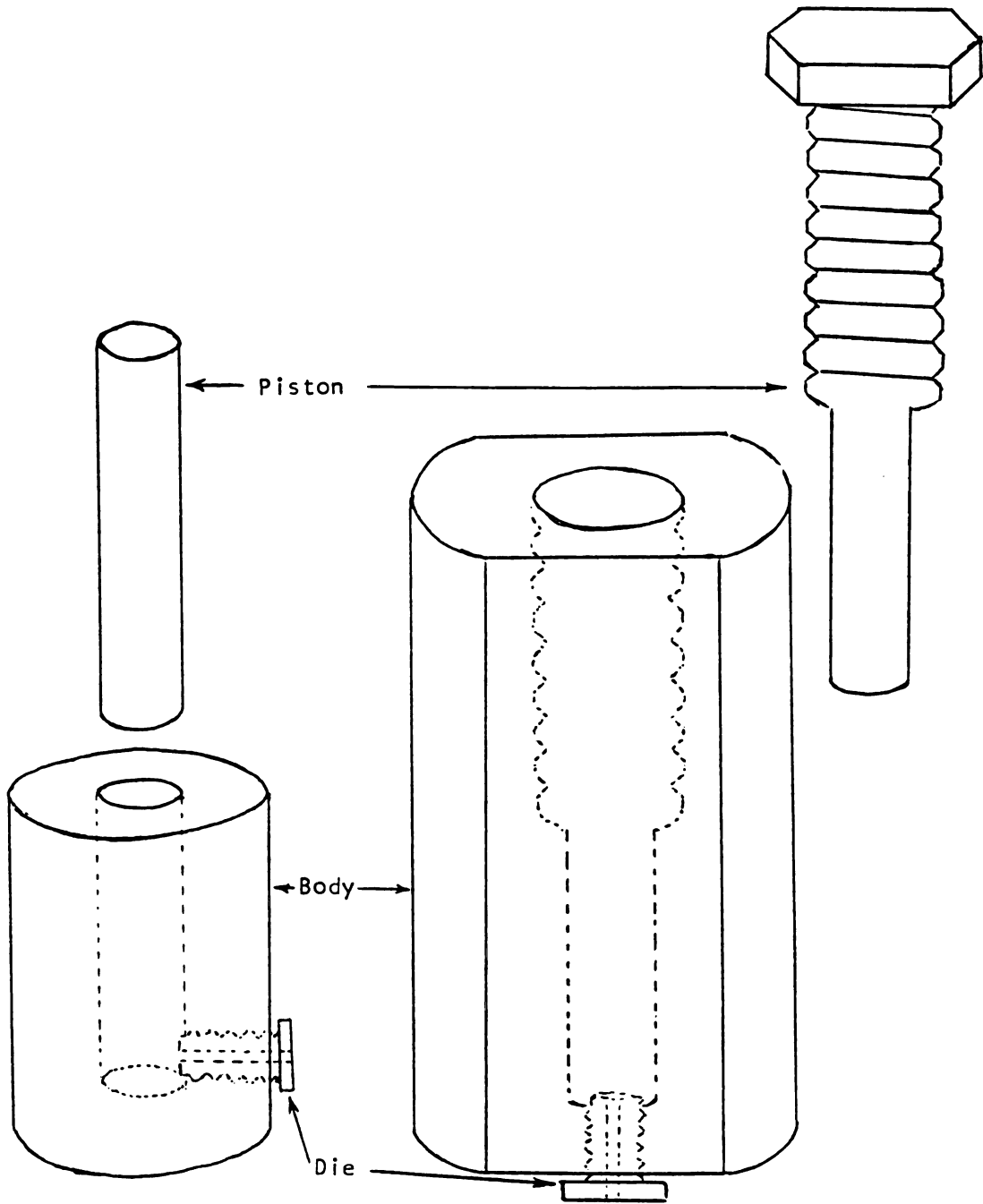
Fig. 3-1. Two kinds of stainless steel presses.

3.3 SAMPLE CAN

Two sample cans were used. Figures 3-2 and 3-3 show the structure of sample can number 1, used for K, Rb, and Na samples. Its sample holder has two separated sides, each with two copper supports for current leads, and two more for voltage leads. Sample can number 2, used for Li, is a modified version of sample can number 1. The main difference is that sample can number 2 has 8 copper clamps instead of 8 copper supports, because Li is not soft and thus not easily cold welded to copper. All eight copper supports or clamps were carefully cleaned with alcohol and filed just before being brought into the glove box, and then filed again inside the glove box.

Before the samples were made, a little material was extruded out to clean the stainless steel die. Then more material was squeezed out and smeared (cold welded) onto all copper supports or clamps. After a sample was made, it could be mounted onto either side of the sample holder in three different ways (Figure 3-4). In method (a), the sample was first cold welded onto the current supports. Then two potential probes of the same material with the same diameter were extruded and cold welded first to the sample, typically 5 cm apart, and then onto the voltage supports. In method (b), used for mounting thin samples, two thick (d=1.0 or 1.5 mm) leads were made from the same material, and each was cold welded onto a current support and the neighboring voltage support. Then a thin sample (d$\leq$0.25 mm),
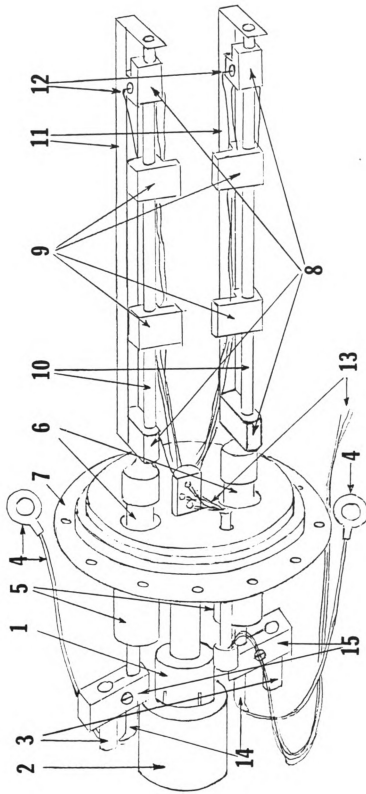
Fig. 3-2. Sample holder 1: 1,2. Copper well and teflon ring for attachment to the mixing chamber, 3. Thermometers, 4. Ag thermal link, 5. Copper tubes, 6. Stainless steel tubes, 7. Brass flange, 8. Copper supports for current leads, 9. Copper supports for potential leads, 10. Nylon props, 11. Copper props, 12. G heater, 13. Superconducting leads, 14. Copper thermal feedthrough, 15. Copper clamps for holding the thermometers.
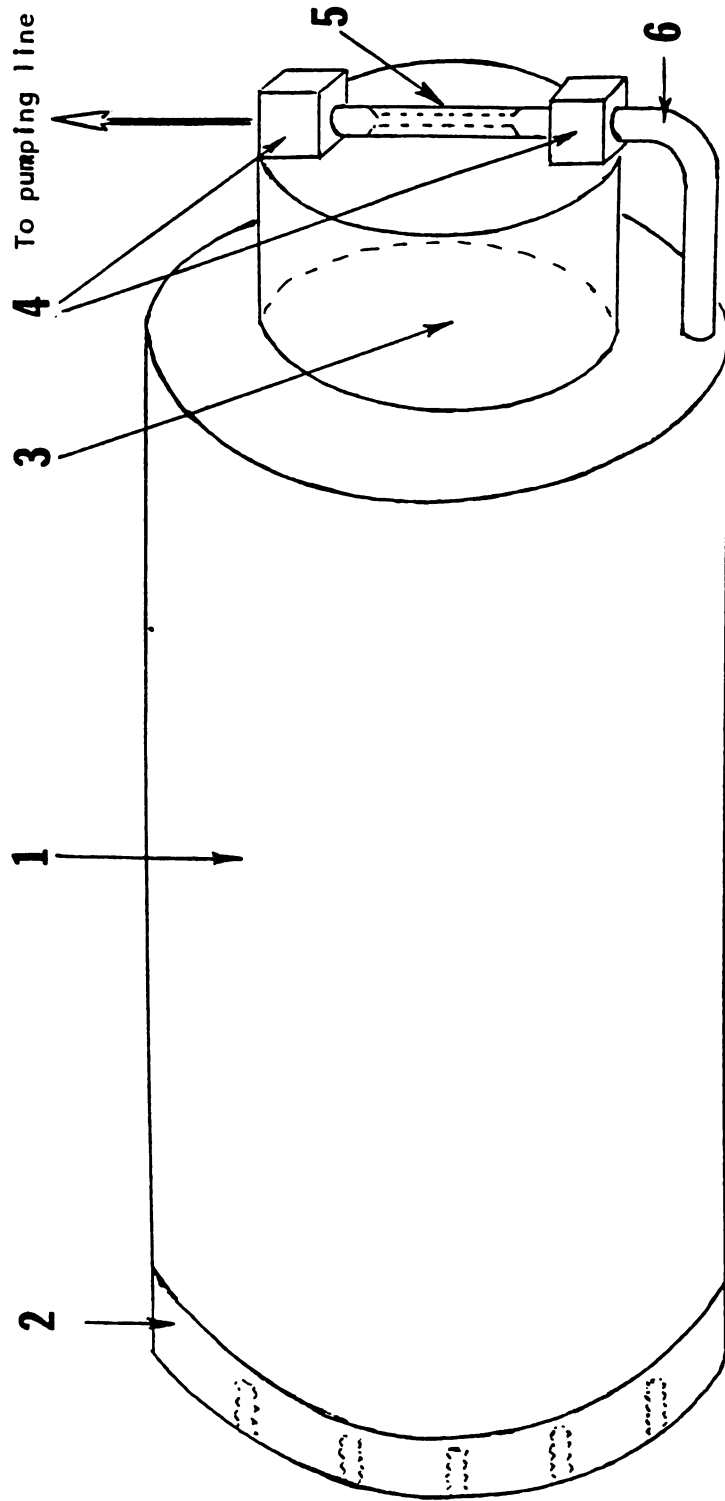
Fig. 3-3. Cover of the sample holder: 1. Copper can, 2. Brass ring, 3. Cu molecular sieve chamber, 4. Brass pipe casing, 5. Indium filled brass tube, 6. Copper tube.

(a)

For thick samples of
K, Rb, and Na.

(b)

For thin samples of
K, and Na.

(c)

For LI samples.
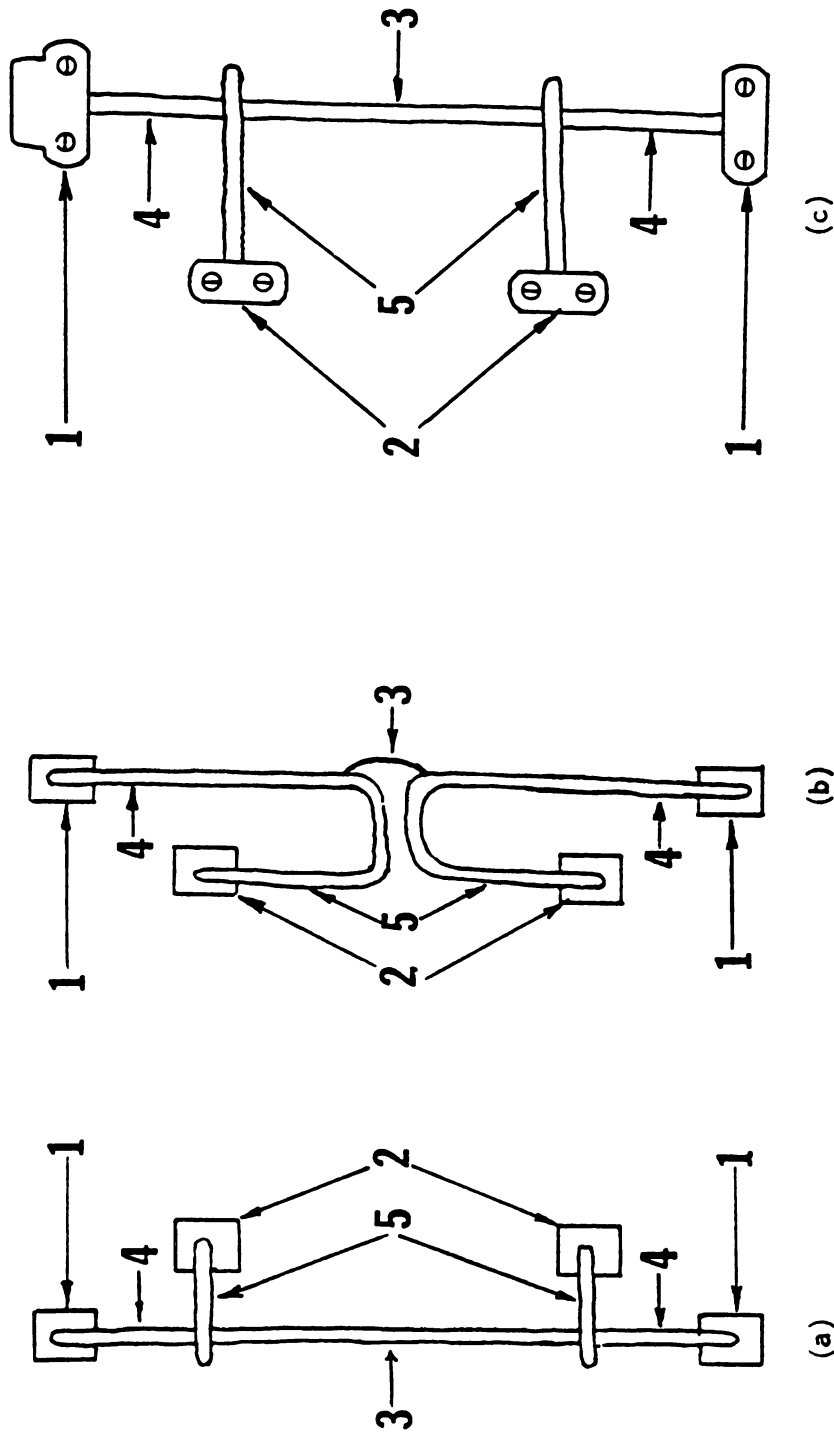
Fig. 3-4. Three different ways of mounting samples: 1. Copper support or clamp for current
leads, 2. Copper support or clamp for potential leads, 3. Samples, 4. Current
lead, 5. Potential leads.

typically 0.5-1.0 cm long, was cold welded onto those two thick leads. As described later, for 0.25 mm K samples, the data were same by methods (a) and (b). In method (c), used for Li, the sample and potential leads were first clamped by the copper clamps. The sample was then cold welded to the potential leads by pinching them together with a stainless steel tweezer.

Our samples were cooled in one of three different atmospheres: Ar atm., He atm., and partial vacuum ($\sim 10\mu$Hg of He).

Under Ar atmosphere, the sample can was simply closed with an indium "O" ring.

Under He atmosphere, some cleaned Linde Molecular Sieve Type 13X pellets were left inside the can to adsorb the He gas at low temperature, so as to prevent heat exchange between the samples and the can. The molecular sieve was cleaned by pumping it down to a vacuum of less than 10^{-6} torr in an Erlenmeyer flask with a stopcock, and then heated to about 200°C under vacuum for two days. The flask was then allowed to cool to room temperature, sealed by closing the stopcock, moved into the glove box, and opened just before closing the sample can. After the pellets were poured into the sieve chamber, a piece of stainless steel screen was pressed in to hold the pellets in place.

To evacuate the sample can down to 10 μHg, and then seal it properly, a piece of indium-filled brass tube was needed. In making these tubes, first the brass tube was

filled with molten indium. After the indium solidified, a hole was drilled through it and the tube was soldered onto the sample can as shown in Figure 3-3. [See M. L. Haerle's thesis for details (ref. 22).] An extension tube with a valve was soldered to the indium tube before the can was moved into the glove box. The sample can was sealed at room temperature by closing the valve, and then was taken out of the glove box and hooked onto a high vacuum system. In order to prevent the diffusion of the air through the pump to the can, the vacuum system was first completely evacuated, then the input valve of the pump was closed and the valve on the can was opened, this procedure was repeated until the sample can was evacuated properly; typically, about 10 μ-Hg helium gas at room temperature was left inside the can as exchange gas for the cooling process. The indium tube was then pinched to seal the can. The indium cold-welded to itself, providing a leak-tight seal at the lowest temperature in this study. Finally, the valve was removed from the sample can, and the can was attached to the mixing chamber of the dilution refrigerator through a copper well and teflon ring (Fig. 3-2).

As noted above, temperature measurements were critical to the results of this study. The two thermometers, GRT2 and GRT4, used for measuring the temperatures of the samples, were clamped with copper clamps onto two copper thermal feedthroughs outside the sample can. To ensure that each of the thermometers was at the same temperature as the

sample it was measuring: 1) The thermal resistance between the sample and the thermometer was minimized by using a well annealed copper rod, 8 cm long and 3 mm in diameter, as the thermal feedthrough; 2) Each feedthrough was sealed onto a thin wall stainless steel tube using stycast 3850 GT epoxy, and the stainless steel tube was then soldered onto the sample can (Fig. 3-2). The samples were thus thermally isolated from the sample can, because both epoxy and stainless steel are very effective thermal insulators at very low temperatures; 3) The sample can and dilution refrigerator were both thermally isolated from liquid He by enclosing them inside a vacuum can. To cut down thermal radiation from the vacuum can to the thermometer sitting on the sample can, the sample can was shielded by a thin copper can, which was attached to the mixing chamber.

3.4 SAMPLE PREPARATION

All of our high-purity potassium (99.95%), rubidium (99.95%) and some of the high-purity sodium (99.95%) were obtained from the Callery Chemical Company, sealed in glass ampoules under Ar gas. Some high-purity sodium was kindly supplied by Prof. J. C. Garland of Ohio State University, packed under paraffin oil in a plastic bottle. Our high-purity lithium (99.99%) was obtained from Atomergic Chemetals Corp. in a low sodium dry pack.

In order to keep the glove box clean, the oil bottle of Na was first moved into a glove bag filled with Ar gas, the

Na pieces were taken out of the oil with a clean stainless steel tweezer, soaked in a beaker of petroleum ether for a few minutes to dissolve the oil, dried, sealed in a glass container, and then transferred into the glove box.

The common way of preparing bare pure K, Rb, Li, and Na samples was already described in section 3.1. In this section, the details of each sample are given in Table 3-1 (for K), Table 3-2 (for Rb), Table 3-3 (for Li), and Table 3-4 (for Na). The details of making pure K samples encased in plastic tubings, coated by oil, or touched by various kinds of plastic pieces, and the details of attempting to grow a single crystal K sample and of making some K-Rb alloy samples will be given next.

In order to make a K sample inside a polyethylene, teflon, or glass tube, an ampoule of K was opened inside a glove box, heated with a hot plate until the potassium melted, and then the molten potassium was sucked up into the tube using a syringe (Figure 3-5). The tubes had been freshly cleaned by placing them in a flask, pumping the flask down to less than 10^{-6} torr, and heating the tubes with a heat lamp to above 100°C for two days. In order to determine effects of different plastics, each ampoule of potassium was allowed to come into contact with only one kind of plastic. And, after a tool touched one kind of plastic, it was cleaned by alcohol before being used for dealing with another kind of plastic. The surface of a K sample touching polyethylene was always shiny during all the

Table 3-1. Characteristics of bare free hanging pure K samples.

$$(RRR = \frac{R(295K)}{R(4.2K)})$$

Samples	Ampoule No.	Circumstance at R.T.	d (mm)	$\rho(4.2K)$ $[\rho_o]$ ($n\Omega cm$)	RRR	Mount method	Other
K-7	# 1	Ar atm.	1.50	1.41 [1.13]	5100	(a)	
K-8	# 1	Ar atm.	1.50	1.50 [1.22]^	4790	(a)	
K-9	# 2	Ar atm.	1.50	1.72 [1.44]^	4180	(a)	
K-10	# 2	Ar atm.	1.50	1.47 [1.19]^	4890	(a)	
K-11	#11	Ar atm.	2.00	1.26 [1.01]	5710	(a)	
K-H1a	# 3	He atm.	1.50	1.70 [1.42]^	4230	(a)	
K-H1b	# 3	He atm.	1.50	1.65 [1.37]^	4360	(a)	Second run of K-H1a
K-H2	# 4	He atm.	1.50	1.27 [0.99]^	5660	(a)	
K-H3	# 5	He atm.	1.50	1.97 [1.69]^	3650	(a)	
K-H4	# 5	He atm.	1.50	1.22 [0.94]^	5890	(a)	Annealed at 50°C for 30 min.
K-H5a	# 8	10 μHg He	1.50	1.27 [1.02]	5660	(a)	
K-H5b	# 8	10 μHg He	1.50	1.39	5170	(a)	Second run of K-H5a
K-H6a	# 8	He atm.	1.50	1.23 [0.95]^	5850	(a)	

Table 3-1. (Continued)

Samples	Ampoule No.	Circumstance at R.T.	d (mm)	$\rho(4.2K)$ $[\rho_o]$ (nΩcm)	RRR	Mount method	Other
K-H6b	# 8	10 μHg He	1.50	1.32 [1.05]^	5406	(a)	Second run of K-H6a
K-H6C	# 8	100 μHg He	1.50	1.35 [1.10]	5330	(a)	Third run of K-H6a
K-0.9H6a	# 5	He atm.	0.90	1.29 [1.01]^	5570	(a)	Done by M. Haerle
K-0.9H6b	# 4	He atm.	0.90	1.37 [1.05]^	5250	(a)	Second run of K-0.9H6a
K-0.5H	# 5	He atm	0.50	1.79 [1.51]^	4020	(a)	
K-.25H1a	# 6	He atm.	0.25·	2.37 [2.05]^	3030	(a)	
K-.25H2a	# 6	He atm.	0.25	2.36 [2.08]^	3050	(a)	
K-.25H1b	# 6	He atm.	0.16*	3.13 [2.85]^	2300	(a)	Second run of K-.25H1a
K-.25H2b	# 6	He atm.	0.16*	3.27	2200	(a)	Second run of K-.25H2a
K-.25H3	# 6	He atm.	0.25	2.25 [1.98]	3200	(b)	
K-.25H4	# 6	He atm.	0.25	2.23 [1.96]	3220	(b)	
K-.10H1a	# 9	He atm.	0.10	11.60 [11.30]	620	(b)	
K-.10H2a	# 9	He atm.	0.10	13.80 [13.40]	520	(b)	
K-.10H1b	# 9	He atm.	0.09*	11.60 [11.30]	620	(b)	Second run of K-.10H1a
K-.10H2b	# 9	He atm.	0.09*	13.00 [12.70]	550	(b)	Second run of K-.10H2a

Table 3-1. (Continued)

Samples	Ampoule No.	Circumstance at R.T.	d (mm)	ρ(4.2K) [ρ_0] (nΩcm)	RRR	Mount method	Other
K-.25V1	# 7	~10 μHg He	0.25	2.11 [1.86]	3410	(b)	
K-.25V2	# 7	~10 μHg He	0.25	2.25 [1.99]	3200	(b)	
K-.10V1	# 7	~10 μHg He	0.10	7.70 [7.42]^	930	(b)	
K-.10V2	# 7	~10 μHg He	0.10	7.16 [6.88]^	1000	(b)	
K-.10V3	# 7	~10 μHg He	0.10	8.83 [8.49]	810	(b)	
K-.10V4	# 7	~10 μHg He	0.10	7.83 [7.49]	920	(b)	
K-.10A1	#10	Ar atm.	0.10	6.22 [5.91]	1160	(b)	Without molecular sieve
K-.10A2	#10	Ar atm.	0.10	8.31 [7.99]	870	(b)	Without molecular sieve
K-.10A3	#11	Ar atm.	0.10	3.67 [3.37]	1960	(b)	With molecular sieve
K-.10A4	#11	Ar atm.	0.10	5.00 [4.69]	1440	(b)	with molecular sieve

*Diameters of corroded versions were estimated by the change of room temperature resistances.

^Values are determined by $\rho_0 = \rho$(4.2K) - 0.28 nΩ-cm. all other values are determined by $\rho_0 \approx \rho$(~1K).

Table 3-2. Characteristics of bare free hanging pure Rb
           samples (from one ampoule)

Samples	Ampoule No.	Circumstance at Rm. Temp.	d (mm)	$P(4.2K)$ $[\rho_o]$ $(n\Omega cm)$	RRR	Mount method
Rb-H1	#1	He atm.	1.50	41.8 [35.6]^	300	(a)
Rb-H2	#1	He atm.	1.50	44.8 [38.6]^	280	(a)
Rb-V1	#1	~10 μHg He	1.50	31.0 [24.7]	403	(a)
Rb-V2	#1	~10 μHg He	1.50	31.0 [24.9]	403	(a)

^Values determined by $\rho_o = P(4.2K) - 6.2\Omega n$ cm, all others
determined by $\rho_o \approx P(-1K)$.

Table 3-3. Characteristics of bare free hanging pure Li samples
           (from same batch)

Samples	Circumstance at Rm. Temp.	d (mm)	$P(4.2K)$ $(n\Omega cm)$	RRR	Mount method	Other
Li-H1a	He atm.	3.0	9.0	1030	(c)	
Li-H2a	He atm.	3.0	10.8	860	(c)	
Li-H1b	He atm.	3.0	8.3	1120	(c)	Second run of Li-1a
Li-H2b	He atm.	3.0	10.4	900	(c)	Second run of Li-2a

Table 3-4. Characteristics of bare free hanging pure Na samples.

Samples	Source	Circumstance at Rm. Temp.	d (mm)	$\rho(4.2K)$ [ρ_0] ($n\Omega cm$)	RRR	Mount method
Na-H1	Callery Chemical Company	He atm.	1.0	12.40	380	(a)
Na-H2	Callery Chemical Company	He atm.	1.0	13.00	360	(a)
Na-H3	J. C. Garland	He atm.	1.0	1.02 [1.01]	4660	(a)
Na-H4	J. C. Garland	He atm.	1.0	1.00 [1.00]	4720	(a)
Na-.25A1	J. C. Garland	Ar atm.	0.25	1.18 [1.18]	4010	(b)
Na-.25A2	J. C. Garland	Ar atm.	0.25	1.14 [1.14]	4160	(b)
Na-.25H1	J. C. Garland	He atm.	0.25	1.42 [1.42]	3350	(b)
Na-.25H2	J. C. Garland	He atm.	0.25	1.47 [1.49]	3230	(b)
Na-.10H1	J. C. Garland	He atm.	0.10	2.08 [2.08]	2270	(b)
Na-.10H2	J. C. Garland	He atm.	0.10	2.57 [2.57]	1850	(b)
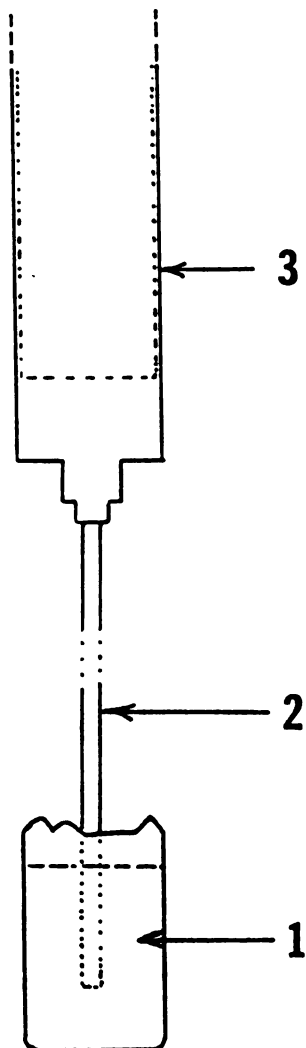
Fig. 3-5. The way of sucking potassium into a tube: 1. Melting potassium, 2. Tube, 3. Syringe.

experiments. The surface of K samples touching teflon turned black right away, but the rest of the sample below the very thin surface remained shiny during all the experiments.

Two Na samples encased in polyethylene tubes were made in the way described above.

One K sample was coated by cleaned paraffin oil and several were measured while in contact with plastic.

To try to grow a single crystal K sample, a beaker of 0-122 White Heavy Paraffin Oil from Fisher Scientific Company was carefully cleaned in the system shown in Fig. 3-6. The oil was heated to about 150°C while it was being pumped by a mechanical pump for about 3 days until no more bubbles came out. Then the input of the mechanical pump was closed and liquid nitrogen was poured into the thermos and the input valve of the cold trap was opened to better evaluate the system. Some crumbs of clean potassium were put into the oil to clean out left over dissolved air or other impurities. This cleaned paraffin oil was used separately also for coating a K sample, (sample K-0). A piece of precision bore pyrex capillary, with internal diameter d=1.5 mm from Wilmad Glass Co., Inc., was carefully cleaned in the same manner as the plastic tubing described above. The cleaned oil and pyrex capillary were moved into the Ar filled glove box. First, a little cleaned paraffin oil was sucked into and pushed out of the capillary with a syringe to lubricate the internal wall of the capillary. Second,
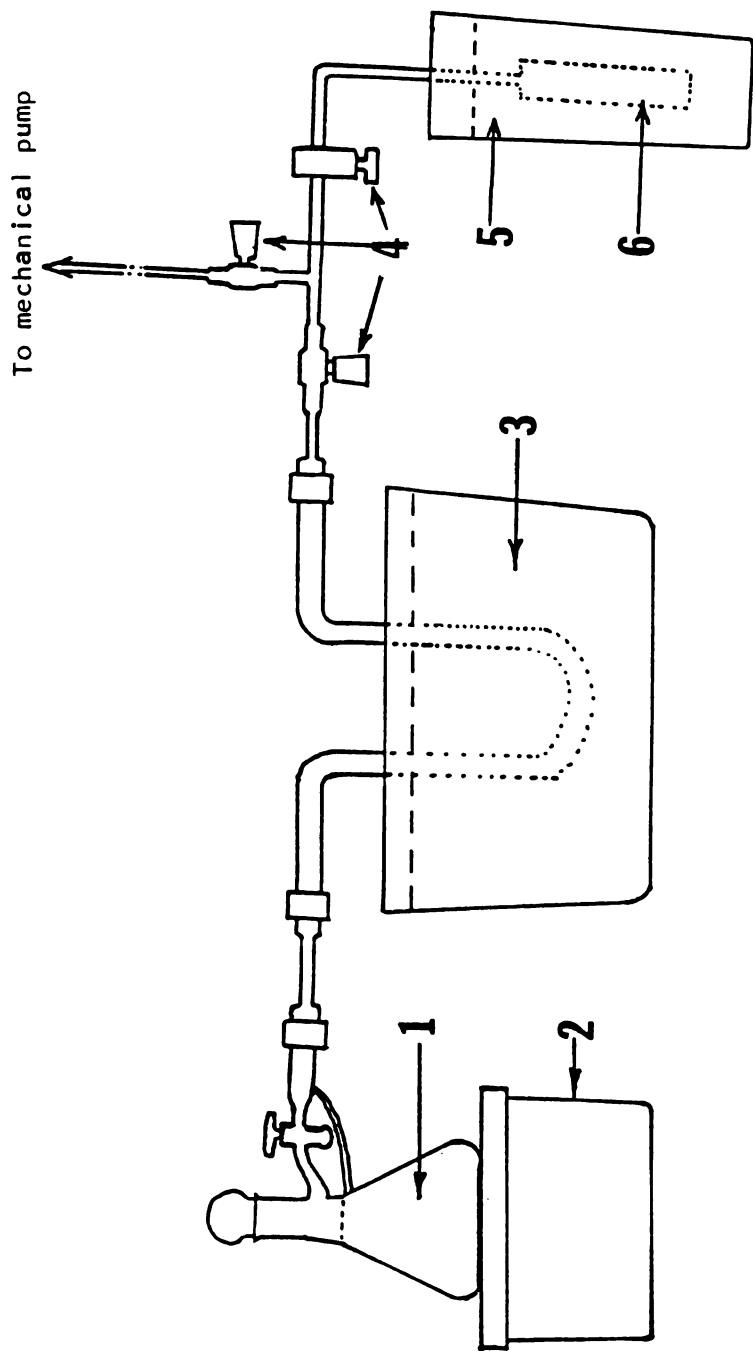
Fig. 3-6. The system for purifying paraffin oil: 1. Paraffin oil, 2. Hot-plate, 3. Ice bath, 4. Valve, 5. Liquid nitrogen, 6. Cold trap filled with cleaned Linde Molecular Sieve Type 13X Pellets.

molten potassium was sucked into the capillary and allowed to solidify. Third, the cleaned paraffin oil was poured into a clean hot-beaker, the part of the capillary with potassium in it was submerged in the oil, and the oil was heated to about 70°C, a few degrees above the melting point of potassium. The capillary was then slowly pulled out of the hot oil at the rate of 0.5 cm per half an hour (see Fig. 3-7). After growth, the sample was pushed out of the capillary with a syringe. Its ends were carefully scraped with a cleaned surgical knife to clean off the oil and were cold welded to the current and potential leads as in method (b) of Fig. 2-4. After the measurements were completed, a 1 cm long piece of this sample was cut out and put into a thin wall glass tube filled with cleaned paraffin oil to protect the sample from reacting with air. Then it was tested on GE. XRD-5 x-ray machine with $\bar{\lambda} = 0.7107$ Å and beam diameter $d = 0.4$ mm. The result showed a sharp peak at $2\theta = 15.6°$. From Bragg equation $n\lambda = 2d\sin\theta$, $d = 5.2$ Å was obtained for $n = 2$, thus, at least, within the spot of x-ray beam, a single crystal part with $d = 0.4$ mm was found. Unfortunately, since only one spot of the sample was tested, the verification of the whole piece as a single crystal K sample was not established, but Dr. P. A. Schroeder (ref. 64) and his collaborators did grow some single crystal K samples in the Netherlands using the same technique with even faster pulling speeds. Their samples were tested with x-ray diffraction at three different spots along each sample.
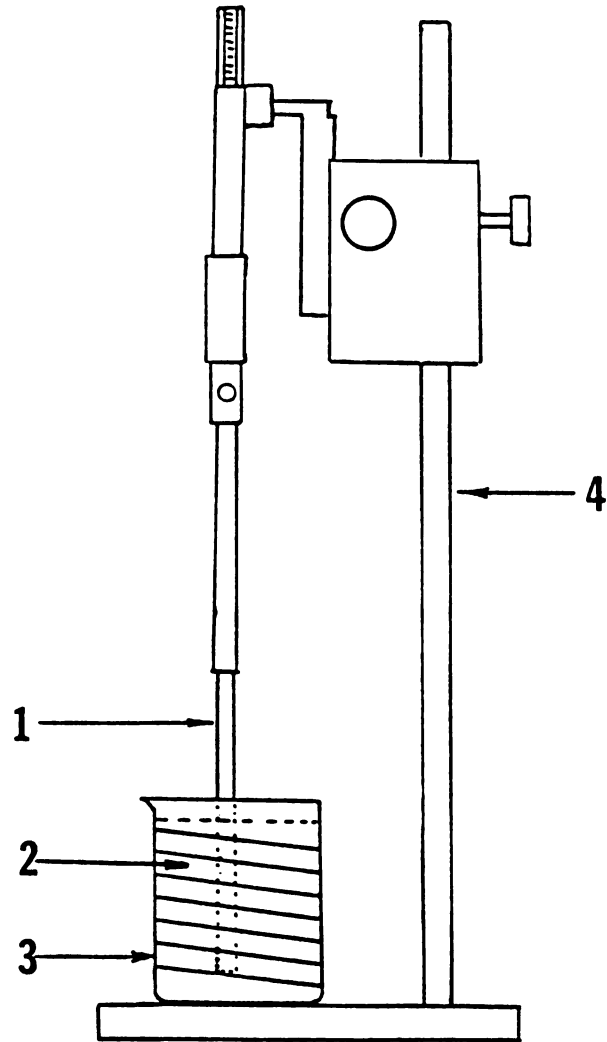
Fig. 3-7. The system for pulling single crystal potassium
           sample: 1. Precision bored PX capillary,
           2. Cleaned paraffin oil, 3. Hot-beaker.
           4. Manipulator with adjustment in two perpendicular
           directions.

The K(0.077 at% Rb) alloy was obtained by first making a K(1.3 at% Rb) mixture and then adding some of this mixture to pure potassium to form a K(0.077 at% Rb) alloy. The K(9.40 at% Rb) alloy was obtained by adding Rb directly to pure potassium. The percentages above were calculated from the weights of each material, which were weighed on a precision scale inside the glove box (ref. 22).

The samples of the alloys were extruded through a die and mounted in the same way as the pure K samples described earlier. For the K(9.40 at% Rb) alloy, the resistivity was high. Since a high resistance sample would cause big heating effects at low temperature when a current passes through it, the samples and potential leads were thick (d = 3.0 mm) and short (potential leads were ~1.8 cm apart, each sample was ~4 cm long.) to keep the resistance low. The sample holders were shortened for holding those short samples.

The characteristics of the possible single crystal K sample, of the K samples coated by clean paraffin oil, and those enclosed in polyethylene or teflon tubes, are given in Table 3-5. The characteristics of the K-Rb alloy samples are given in Table 3-6. The characteristics of the Na samples encased in polyethylene tubes are given in Table 3-7.

Table 3-5. Characteristics of K samples in contact with oil or plastics

Samples	Ampoule No.	Circumstance at Rm. Temp.	d (mm)	$\rho(4.2K)$ [ρ_o] (nΩcm)	RRR	Mount method	Days @ Rm. Temp.	Other
K-S .	#12	a. Try to be grown as a single-crystal sample b. Ar atm.	1.5	1.17 [0.91]	5150	(b)	13.0	
K-0	#15	a. coated by cleaned paraffin oil b. Ar atm.	1.5	1.32 [1.07]	5450	(a)		
K-Ph1a	#8	a. in a polyethylene tube b. 10 μHg He	1.6	2.97 [2.70]	2420	(a)	0.5	
K-Ph1b	#8	a. in a polyethylene tube b. 10 μHg He	1.6	1.68 [1.42]	4280	(a)	11.0	Second run of K-Ph1a
K-Ph1c	#8	a. in a polyethylene tube b. He atm.	1.6	1.18	6090	(a)	24.5	Third run of K-Ph1a
K-Ph1d	#8	a. in a polyethylene tube b. 10 μHg He	1.6	1.20	5990	(a)	26.0	Fourth run of K-Ph1a
K-Ph1e	#8	a. in a polyethylene tube b. 100 μHg He	1.6	1.20 [0.95]	5990	(a)	27.0	Fifth run of K-Ph1a
K-Ph2a	#15	a. in a polyethylene tube b. He atm.	.9	3.30 [3.02]	2180	(b)	0.5	

Table 3-5. (Continued)

Samples	Ampoule No.	Circumstance at Rm. Temp.	d (mm)	$\rho(4.2K)$ [ρ_0] (nΩcm)	RRR	Mount method	Days @ Rm. Temp.	Other
K-Ph2b	#15	a. in a polyethylene tube b. He atm.	.9	1.35 [3.02]	5330	(b)	2.5	Second run of K-PH2a
K-Ph2c	#15	a. in a polyethylene tube b. He atm.	.9	1.42 [1.17]	5060	(b)	13.0	Third run of K-PH2a
K-Ph2d	#15	a. in a polyethylene tube b. He atm.	.9	1.28 [1.04]	5620	(b)	73.5	Fourth run of K-PH2a
K-TH1a	#16	a. in teflon tube b. He atm.	1.5	8.41 [8.10]	855	(b)	0.5	
K-TH1b	#16	a. in teflon tube b. He atm.	1.5	5.17 [4.87]	1390	(b)	2.5	Second run of K-TH1a
K-TH1c	#16	a. in teflon tube b. He atm.	1.5	1.62 [1.34]	5370	(b)	13.0	Third run of K-TH1a
K-TH1d	#16	a. in teflon tube b. He atm.	1.5	1.20 [0.94]	5990	(b)	73.5	Fourth run of K-TH1a
K-PA1a	#14	a. in a polyethylene tube b. Ar atm.	.9	5.46 [3.02]	1320	(b)	0.5	
K-PA1b	#14	a. in a polyethylene tube b. Ar atm.	.9	1.45 [1.20]	4960	(b)	4.5	Second run of K-PA1a

Table 3-5. (Continued)

Samples	Ampoule No.	Circumstance at Rm. Temp.	d (mm)	$\rho(4.2K)$ [ρ_o] (nΩcm)	RRR	Mount method	Days @ Rm. Temp.	Other
K-PA1c	#14	a. in a polyethylene tube b. Ar atm.	.9	1.39 [1.14]	5170	(b)	16.0	Third run of K-PA1a
K-PA1d	#14	a. in a polyethylene tube b. Ar atm.	.9	1.57	4580	(b)	19.0	Fourth run of K-PA1a
K-PA1e	#14	a. in a polyethylene tube b. Ar atm.	.9	1.36 [1.12]	5290	(b)	97.0	Fifth run of K-PA1a
K-PA2a	#14	a. in a polyethylene tube b. Ar atm.	1.6	5.48 [5.20]	1310	(a)	0.5	
K-PA2b	#14	a. in a polyethylene tube b. Ar atm.	1.6	1.22 [0.97]	5890	(a)	4.5	Second run of K-PA2a
K-PA2c	#14	a. in a polyethylene tube b. Ar atm.	1.6	1.38 [1.12]	5210	(a)	16.0	Third run of K-PA1a
K-PA2d	#14	a. in a polyethylene tube b. Ar atm.	1.6	1.23	5850	(a)	19.0	Fourth run of K-PA1a
K-PA2e	#14	a. in a polyethylene tube b. Ar atm.	1.6	0.95 [0.73]	7570	(a)	97.0	Fifth run of K-PA1a

Table 3-5. (Continued)

Samples	Ampoule No.	Circumstance at Rm. Temp.	d (mm)	$\rho(4.2K)$ [ρ_o] ($n\Omega cm$)	RRR	Mount method	Days @ Rm. Temp.	Other
K-KA	#17	a. In contact with two pieces of Kel-F b. Ar atm.	1.5	1.28 [1.03]	5620	(a)		
K-PPA		a. Bare sample with potential leads in polyentylene tube b. Ar atm.	1.5	1.22 [0.96]	5890	(a)		

85

Table 3-6. Characteristics of bare free hanging K-Rb samples

Samples	Ampoule No.	Circumstance at Rm. Temp.	At % Rb	d (mm)	$\rho(4.2K)$ [ρ_0] (nΩcm)	RRR(4.2) [RRR_0]	Mount method
K-Rb1	K: #58 #6 Rb: #2	He atm.	0.077%	0.25	--- [11.2]	--- [640]	(b)
K-Rb2	K: #58 #6 Rb: #2	He atm.	0.077%	0.25	--- [11.6]	--- [620]	(b)
K-Rb3	K: #13 Rb: #3	Ar atm.	9.400%	3.20	1010 [1010]	8.30 [8.30]	(a)
K-Rb4	K: #13 Kb: #3	Ar atm.	9.400%	3.20	1040 [1040]	8.10 [8.10]	(a)

Table 3-7. Characteristics of Na samples encased in polyethylene tubes

Samples	Source	Circumstance at Rm. Temp.	d (mm)	$\rho(4.2K)$ [ρ_o] (nΩcm)	RRR	Mount method	Days @ Rm. Temp.	Other
Na-PA1a	J. C. Garland	Ar gas	1.6	2.27		(a)	12.0	
Na-PA2a	J. C. Garland	Ar gas	1.6	2.52		(a)	12.0	
Na-PA1b	J. C. Garland	Ar gas	1.6	2.29 [2.29]		(a)	33.0	Second run of Na-PA1a
Na-PA2b	J. C. Garland	Ar gas	1.6	2.40 [2.39]		(a)	33.0	Second run of Na-PA2a

3.5 MEASUREMENT METHOD

3.5.1 Resistivity

More than fifty runs were made in this study. In each, we measured $\rho(4.2K)$, ρ_0 (usually), and both $d\rho/dT$ and G from 0.07K to 4.2K. In each run, two twin samples or similar samples were measured.

3.5.1.1 R(295K)

First, the room temperature resistance of sample was measured using a constant current supply and a Keithley digital nanovoltmeter. The room temperature T was also measured. Then the room temperature resistance was converted to 295K resistance R(295K) by assuming a linear temperature dependence, i.e.,

$$\frac{R(295K)}{R(T)} = \frac{\dfrac{\rho(295K) \times L(295K)}{A(295K)}}{\dfrac{\rho(T) \times L(T)}{A(T)}} = \frac{\rho(295K)}{\rho(T)} \qquad (3-2)$$

where L and A are the length and cross-section area of sample respectively, and $L(295k)/A(295K) = L(T)/A(T)$ to a precision better than 0.1% at room temperature. Hence,

$$R(295K) = R(T) \times \frac{\rho(295K)}{\rho(T)}$$

$$= R(T) \frac{1 + 21.8\alpha}{1 + \alpha(T - 273.2)} \qquad (3-3)$$

assuming

$$\rho(T) = \rho(273.2K) [1 + \alpha(T - 273.2)] \qquad (3-4)$$

Actually, we happened to use the approximation R(295K) = R(T) x 295/T for some measurements of potassium, this made R(295K) not more than 0.5% too big in our room temperature range.

The α and ρ(295K) used for K, Li, Rb, and Na were those as listed in Table 3-8 (from Landolt-Bornstein Numerical Data and Functional Relationships in Science and technology, Group III, Volume 15).

3.5.1.2 Circuit for Measuring ρ(4.2K), ρ_0, and $\overline{d\rho/dT}$.

When the samples were cooled to 4.2K or lower, the circuit in Fig. 3-8 was used. This circuit consisted of a SQUID (Superconducting Quantum Interference Device) null detector and three resistors wired in series. These three resistors were the samples, R1 and R2, and a standard resistor R_{st} = 1.134 $\mu\Omega$ made of a tin-indium alloy, chosen to be superconducting at about 3.8K. For thin pure samples and thick alloys with high resistances at low temperature, an inductor ($L_t \approx$ 50 μH) was inserted in series with the three resistors to keep the relaxation time of the circuit long enough to have the SQUID lock properly. The inductor and all the wires in this circuit were made of Niomax CN, a multifilament Nb-Ti superconducting (T_c > 4.2K) wire with Cu-Ni cladding made by Imperial Metal Industries (ref. 22).

To keep the noise introduced by stray magnetic fields as low as possible: 1) R_{st} and most of the wiring except

Table 3-8. The electrical resistivities of some alkali metals

Metals	(273.2K)	α	ρ(295K) (calculated)
K	6.45	.0050	7.19*
Li	8.50	.00445	9.32
Rb	11.25	.0051	12.50
Na	4.29	.00485	4.74

* This number should be 7.15 from the calculation, but we used ρ(295) = 7.19 for K to be consistent with van Kempen et al. (ref. 14).
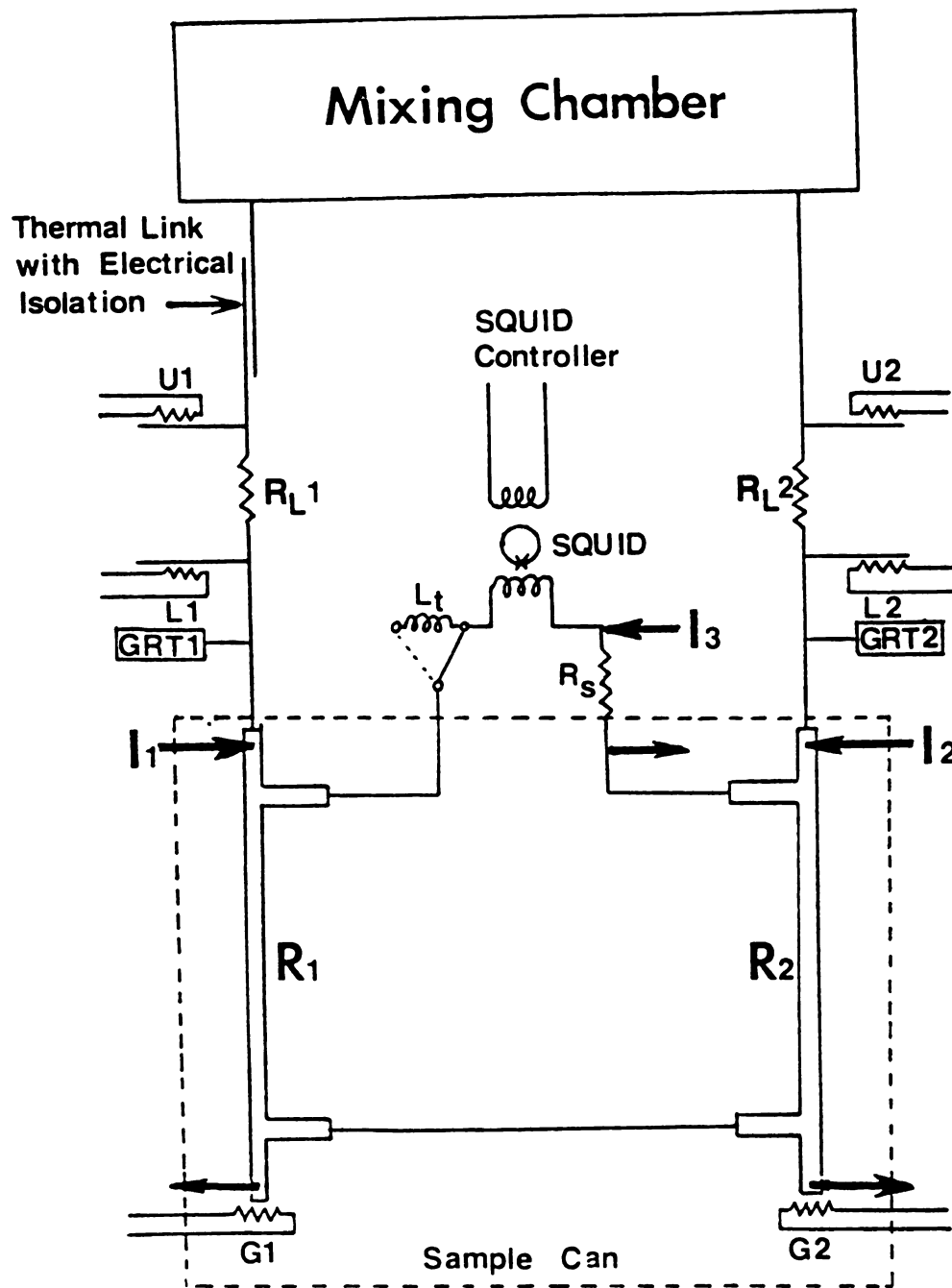
Fig. 3-8. The low temperature circuit. The components inside the broken line are inside the sample can.

that near the samples were shielded in superconducting lead (Pb)(T_c = 7K) tubing. 2) All the wires leading to the samples were carefully tied or varnished down to reduce vibration and thus reduce magnetically induced currents. 3) The vacuum can, with the sample can inside, was shielded by one Nb can, and the whole refrigerator was surrounded with another μ-metal can. Both the Nb can and the μ-metal can had openings only at the tops.

The wires were drawn out of the can through a special electrical feedthrough. This feedthrough was made by running several pieces of insulated Niomax wire through a clean 1/8" diameter stainless steel tube, which was then inverted in a small cup of liquid Stycast 1266 epoxy that was then allowed to harden.

The ratio of the resistances for any two of the three resistors in this low temperature circuit could be measured by using the current comparator (mentioned in section 3.1). Let R_m and R_s represent the resistances of these two resistors respectively. When the current comparator was used to compare them, the master current I_m was passed through R_m while the slave current I_s was passed through R_s. Here, I_s = CI_m, where C was the switch setting of the current comparator. A standard current reversal technique was used to eliminate thermal EMFs generated in this circuit as follows. For currents going one way (the directions of currents through two resistors in this circuit should be opposite to each other), the SQUID voltage is

$$V^{+} = I_m R_m - I_s R_s + V_T$$
$$= I_m R_m - C I_m R_s + V_T \qquad (3-5)$$

where V_T represents the stray voltage due to any thermal EMF. After the currents on the two sides are reversed, the SQUID voltage is

$$V^{-} = -I_m R_m + I_s R_s + V_T$$
$$= -I_m R_m + C I_m R_s + V_T \qquad (3-6)$$

C was adjusted to make $V^{+} = V^{-}$. Then,

$$I_m R_m - C I_m R_s = -I_m R_m + C I_m R_s \qquad (3-7)$$

and hence, $R_m/R_s = C$ independent of V_T.

At 4.2K, the resistances of two samples, R_1 and R_2 in Figure 2-8, were measured by using the current comparator to compare each of them with R_{st}. Then the ratio of the 4.2K resistances to the 295K resistances were calculated. neglecting the change of L/A between 4.2K and 295K (the error caused by this neglecting will be discussed in section 3-5), one has

$$\rho(4.2K)/\rho(295K) = R(4.2K)/R(295K) = 1/RRR.$$

For pure samples,

$$\rho(295K) = \rho_{pure}(295K), \text{ and}$$
$$\rho(4.2K) = \rho(295K)/RRR.$$

For K-Rb alloys, assuming Matthiessen's Rule (MR) as a first approximation,

$$\rho(295K) \cong \rho(4.2K) + \rho_{pureK}(295K).$$

Therefore,

$$\rho(4.2K) \cong \rho_{pureK}(295K)/(RRR-1).$$

The impurity-dependent deviation from MR might cause an error as large as 1-3% when RRR is as small as 8 for a 9.4% K-Rb alloy (ref. 65).

The $\rho_{pure}(295K)$s for K, Li, Rb, and Na are listed in Table 3-8.

As described in section 3.1, there are two ways to study the temperature dependence of resistivity at low temperature. One is to measure ρ directly, the better one is to measure $d\rho/dT$. We measured $d\rho/dT$ in this study.

To obtain $d\rho/dT$ of a sample, (e.g., R_2), the current comparator was used again to compare R_2 (as R_m) to R_1 (as R_s). The reference R_1 was kept at a constant temperature T_1 by regulating the mixing chamber temperature with a temperature controller monitored by GRT4. The temperature of the sample R_2 was changed from T_2 to ($T_2 + \Delta T$) either by using heaters U_2 and L_2 alternately with the same power input into each or only L_2 with two different powers. (These two methods were tested several times in each run, to make sure both of them gave consistent results.) When the sample was at temperature T_2, the ratio of its resistance to the reference resistance $R(T_1)$ was measured as $C(T_2) = R_2(T_2)/R(T_1)$. When it was at $T_2 + \Delta T$, the ratio was measured as $C(T + \Delta T) = R_2(T + \Delta T)/R_1(T_1)$. Then,

$$\frac{\Delta C}{C} = \frac{C(T_2 + \Delta T) - C(T_2)}{C(T_2)}$$

$$= \frac{R_2(T_2 + \Delta T) - R_2(T_2)}{R_2(T_2)} = \frac{\Delta R_2}{R_2} = \frac{\Delta \rho_2}{\rho_2} \qquad (3-8)$$

since the change of L/A in ΔT, typically 0.1K, was less than 10^{-7}%, which is negligible. Hence,

$$\frac{d\rho}{\rho dT} = \lim_{\Delta T \to 0} \frac{\Delta \rho}{\rho \Delta T} = \frac{\Delta C}{C \Delta T} \qquad (3-9)$$

and,

$$\frac{d\rho}{dT} = \frac{\rho \Delta C}{C \Delta T}$$

The current through the sample was usually 50 mA, or occasionally, to test for current dependence, 20 mA. There was never any measurable current dependence in $d\rho/dT$.

In order to get optimal precision, the noise caused by the reference resistor must not be worse than that of the sample. For this reason, the two samples were normally made as similar as possible, and each of them was the reference for the other. Even so, the Johnson noise ($\sqrt{4kTR\Delta f}$) in the reference would be larger than that in the sample if the temperature of the reference was higher than that of the sample. To minimize this noise, the reference was cooled down together with the sample to a given temperature, and then kept at this temperature while the sample was heated to higher temperatures for taking data. The Johnson noise in

the reference resistor was thus always smaller than that in the sample.

At the ends of most runs, ρ_os of the samples were measured by stopping the 1K pot pump and the circulation of the dilution refrigerator when the temperature of the sample was below 1K. When the standard resistor R_{st}, which was attached to the 1K pot, became normal ($T_c = 3.8K$), while the temperature of the samples was still around 1K, the ratio of resistance of each sample to the resistance of the standard was measured using the current comparator. The resistivity at about 1K was then calculated as $\rho(4.2K)$ was done above. According to van Kempen et al. (ref. 14), W.P. Pratt, Jr. (ref. 59), and our new results, when the temperature is below 1K, the electron-phonon scattering contribution to the resistivity was negligible and the electron-electron scattering contribution was at least 3 orders of magnitude smaller than ρ_o in K, Li and Na. Thus, $\rho(1K)$ was chosen as ρ_o.

As already mentioned, temperature measurements were critical in this study. Even though the thermometers were already well calibrated (ref. 22), the Wiedemann-Franz (W-F) Law was used for in-situ checking to be sure that no systematic errors crept into the temperature measurements. The procedure was as follows. In Fig. 3-8, R_L1 and R_L2, both A_g-0.1 at% Au alloys, were used for weak thermal links between the mixing chamber and the samples. For each link, the U-heater was placed at one end (called the U end), which

was connected to the mixing chamber. Another identical heater, the L-heater, was placed at the other end (called the L end). The reference resistor and the mixing chamber were kept at a constant temperature. The sample was first heated to a temperature T by running a current through the U heater. In thermal equilibrium there should not be any heat flowing through R_L (see Fig. 3-8). There should thus not be any temperature difference between the U and L ends. Then the sample was heated to $T + \Delta T$ by running the same current through the L heater, this time there was a continuous heat flow from the L heater through R_L to the mixing chamber, which caused a temperature difference between the U and L ends. In these two cases, the temperature of the U end should not change since the heating power in these two cases were the same, so that the heat current flowing from the U end to the mixing chamber did not change. Thus, we can say that the temperature difference between U and L ends in the second case was equal to ΔT. Applying the W-F Law, $\kappa/\sigma T = L_0$, to R_L, one has:

$$R_L = L_0 T \, \Delta T / \dot{Q} = L_0 T \, \Delta T / R_h I^2 \tag{3-10}$$

where R_h was the resistance of the heater, I was the current through the heater, and $T_{ave} = T + \Delta T/2$ was taken as T. The resistance of the alloy R_L was dominated by its residual resistance R_0 at low temperatures, so $T_{ave} \Delta T / R_h I^2$ should not change for every datum we got. This was used for in-situ checking the product $T \cdot \Delta T$ and thus $\Delta C/CT \cdot \Delta T$. The

uncertainty in T is estimated much less than 1% except near

0.1K where the uncertainty is closer to 1% (ref. 59).

3.5.2 Thermoelectric Ratio G and Thermopower S

The thermoelectric ratio G of each sample was also

standardly measured in each run, since it was easily

obtained. The only additional requirement was a G heater

at the hot end of each sample (Fig. 3-8).

As mentioned in section 1.1,

$$G = \frac{j}{q} \bigg|_{\vec{E}=0} \quad , \quad \text{i.e.,} \quad G = \frac{I}{\dot{Q}} \bigg|_{\vec{E}=0} \quad (3-11)$$

G was measured by sending a current I_G to the G heater

to heat the sample from one end, and then sending another

current I through the sample to cancel out the resulting

thermal voltage. This voltage was detected by the SQUID.

The master current was normally set to be 50 x 0.1 mA, the

cancelling current was supplied by the slave side of the

current comparator, (i.e., the cancelling current was C x

5 mA. The resistance of the G heater, a Dale resistor, was

measured at liquid helium temperature, and stayed constant

(change less that 0.1%) below 4.2K. The heating power was

calculated from

$$\dot{Q} = R_G I_G^2 \qquad (3-12)$$

thus

$$G = C \times 5 \text{ mA}/R_G I_G^2 \qquad (3-13)$$

The thermopower S of only one K sample (K - 1/2 H) was measured in this study. The G heater mentioned above was still needed. In order to measure the temperature difference across the sample, two Germanium Resistance Thermometers GRT4 and GRT5 were placed on the copper supports of potential leads (section 3-3).

As mentioned in section 1.1,

$$S = \frac{E}{\nabla T} \Big|_{j=0} \quad , \quad \text{i.e., } S = \frac{V}{\Delta T} \Big|_{j=0}$$

S was measured by sending a current I_G to the G heater to heat the sample from one end, and then sending another current I through the reference to cancel out the resulting thermal voltage. This thermal voltage was detected by the SQUID. The cancelling current was the same as in the G measurements mentioned above, i.e., I = C x 5 mA. So the cancelling IR drop was C x 5 mA x R_r. The different temperatures of the two ends of sample were measured by GRT4 and GRT5. Then ΔT was obtained. Thus,

$$S = \frac{C \times 5 \text{ mA} \times R_r}{\Delta T} \tag{3-14}$$

To determine S, it is thus necessary to determine R_r (T). R_r was measured only at 4.2K. Since $[R_r (4.2K) - R_r (0K)]/R_r (4.2K) = [\rho_r(4.2K) - \rho_r(0K)]/\rho_r(4.2K)$, where $\rho_r(4.2K) - \rho_r(0K) = 0.28$ nΩcm for potassium (ref. 12,59). $R_r(0K)$ was then obtained as $R_r(0K) = R_r(4.2K) [1 - 0.28$ nΩcm$/\rho_r(4.2K)]$. Furthermore, assuming R(T) = R(0K) +

$Ce^{-\Theta*/T}$ with $\Theta* = 20K$, where C could be obtained from $R(4.2K) = R(0K) + Ce^{-20/4.2}$, R(T) was calculated for temperatures between 0K and 4.2K. The uncertainty of this calculated R(T) is estimated as 3%.

3.6 UNCERTAINTIES

3.6.1 Uncertainties in G and S Measurements

In G and S measurements, our attention was focused on the temperature dependence of G or S.

As mentioned in section 3.5.2, G was calculated by $G = C \times 5$ mA$/R_G I_G^2$. The 0.1×50 mA current setting of the current comparator had 0.16% uncertainty. The uncertainty in the resistance of the heater R_G was 0.1%. The error in measuring I_G was due mainly to the digital round-off of the DVM used to measure it; this could cause 0.5% error at the worst. Finally, the uncertainty of the resistance used to measure this current was 0.05%. Taken together, these uncertainties sum to, at worst 1%.

The major source of uncertainty in G was in the determination of C, due to thermal EMF noise and Johnson noise. This uncertainty was less than 1% when the temperature was above 1K, but the percentage error got worse as the magnitude of C and the heat input got smaller at lower temperatures. At the lowest temperatures, the uncertainty in C could be as large as 5%.

The major uncertainty in T measurement was random error due to thermal fluctuations and thermal drifts in the

system. The worst case was when T was around 3K, since the dilution refrigerator had not been completely started, the cooling power was varying with time, thus temperature regulation could not be used. This uncertainty in T is estimated as only 0.5% in the worst case.

As mentioned in section 3.5.2, S was calculated by $S = (C \times 5 \text{ mA} \times R_r)/\Delta T$. The uncertainty in 0.1 x 50 mA current setting was 0.16% (see above). The uncertainty in C was less than 1% in whole temperature region for this S measurement. The uncertainty in ΔT is estimated as 1% (section 3.5.1, ref. 59) in the worst case. The major uncertainty in S was in determination of R_r. This uncertainty is estimated as 3% (see section 3.5.2).

3.6.2 Uncertainties in $P(4.2K)$, P_o, and dP/TdT Measurements

$P(4.2K)$ was determined from $P(4.2K) = P(295K) \times R(4.2K)/R(295K)$, where R(295K) was measured by $R(295K) = R(T) (1 + 26.8 \times \alpha)/(1 + \alpha(T - 273.2))$ or $R(295K) = R(T) \times 295/T$ (see section 2.4.1). P_o was determined similarly. So, the uncertainties in $P(4.2K)$ and P_o were dependent on three main factors: a) The uncertainty of R(295K) was mainly due to the uncertainty of the room temperature resistance R(T) which was always measured with better than 1% precision. b) R(4.2K) or R_o were measured against R_{st} within 2%, due to the temperature dependence of R_{st} near 4.2K (ref. 22). R(4.2K) was also affected, in lesser degree, by the small temperature variation of the liquid He bath due to changes

in atmospheric pressure. c) The main error was the systematic error due to ignoring the change of L/A when the sample underwent thermal contraction from room temperature to 4.2K or 1K. The room temperature linear thermal expansion coefficients of the samples (in units of 10^{-6} K^{-1}) were 83 for K, 71 for Na, 66 for Rb, and 45 for Li. These coefficients would stay constant from room T to about their Debye temperatures Θ_Ds (330K for Li, 160K for Na, 114K for K, and 65K for Rb), then start turning down, at about $0.1\Theta_D$ they would decrease as fast as T^3. Calculations showed this caused about 2% errors in $\rho(4.2K)$ and ρ_o. The 0.5% opposite systematic error from using R(295K) = R(T) x 295/T as an approximation is negligible. In summary, the error in $\rho(4.2K)$ and ρ_o measurements could be as high as 4%, including a correctable systematic error of 2% due to c). But, any error in $\rho(4.2K)$ and ρ_o would not affect the form of plots of the final quantity $d\rho/dT$ versus T either as $\rho(4.2K)$ $\Delta C/C$ ΔT or ρ_o $\Delta C/C$ ΔT. The only effect of this error would be to multiply $d\rho/dT$ by a constant close to 1.

In the calculation of the quantity $\rho\Delta C/C_{ave}$ ΔT, C was shown to have precision better than 0.1 ppm earlier, so the main uncertainties came from ρ, ΔC, and ΔT. a) $\rho(1K)$ was chosen to be ρ_o in this calculation. As already mentioned, our attention was focused on the temperature region where electron-electron scattering was dominant, in this temperature region the temperature dependent part of ρ was at least 3 orders of magnitude smaller than ρ_o or $\rho(1K)$ (see section

3.5.1). So this caused less than 0.1% random error. Sometimes $P(4.2K)$ was used instead of ρ_o; and $P(4.2K)$ could be 20% bigger than ρ_o. This, however, represents only a different renormalization of the quantity of interest. The systematic errors in $P(4.2K)$ and ρ_o measurements were already discussed above. b) In many cases of this study, ΔC could be very small or even zero, so the percentage uncertainty of ΔC could be very large. To reduce the uncertainty in ΔC when ΔC was small, a micro-computer averaging technique was used to measure C to within 0.01 ppm. Typically, except at the lowest temperature, the uncertainty in ΔC was less than 1%. c) The uncertainty in ΔT, which was estimated using W-F law in-situ checking was within 1-2% (ref. 59).

CHAPTER 4

Experimental Results and Analysis

4.1 FREE HANGING, BARE, THICK (d = 1.5-2.0 mm) HIGH-PURITY K SAMPLES

As mentioned in section 1.2.1, C. W. Lee et al. (ref. 8) used the same technique as described above to measure free hanging, bare, high-purity, thick (d = 0.9-3.0 mm) K samples under Ar gas. Their $d\rho/dT$ data varied closely as T, (i.e., $\rho(T) = AT^2$, from 1.3K to 0.35K. "A" did not change much from sample to sample, having a mean value of 0.24 ± 0.02 pΩcm/K^2. This value is consistent with that expected for electron-electron scattering, 0.17 pΩcm/K^2 (ref. 7,21). Below 0.35K, their data showed deviations from T^2. Their G data had the approximate form $G = G_0 + B*T^2 + (C*/T) \times \exp(-\theta*/T)$, with $G_0 = -0.03 \pm 0.03V^{-1}$, $B* = -0.30 \pm 0.01V^{-1}K^{-2}$, and $\theta* = 23 \pm 2K$.

Using a better glove box, an improved sample can (see section 2.3), and a thin copper can attached to the mixing chamber to shield the sample can and the thermometers on it from heat radiation (see section 2.3), we measured 14 free hanging bare K samples with d = 1.5-2.0 mm; 4 were still measured under Ar atm.; 6 under He atm. (one among these was sample K-H4 annealed at 50°C for 30 minutes); and 4 under partial vacuum.

4.1.1 The Resistivity

The results of resistivity measurements on these thick samples are shown in Fig. 4-1. Again, $\rho(T)$ varied closely as AT^2 from 1.1K to 0.2K → 0.4K (for different samples), with $A = 0.24 \pm 0.02$ pΩcm/K^2 for Ar gas (the same as C. W. Lee found), $A = 0.25 \pm 0.02$ pΩcm/K^2 for He gas without annealing at 50°C, and $A = 0.22 \pm 0.01$ pΩcm/K^2 for partial vacuum. The sample annealed at 50°C showed the smallest $\rho(4.2K) = 1.22 \times 10^{-9}$ Ωcm and the smallest $A = 0.19$ pΩcm/K^2. Below 0.2K → 0.4K, all the samples showed an anomalous turn-up similar to that found by Lee. The parameters of the samples are given in Tables 3-1 and 4-1.

In the data of our 6 samples cooled in He gas, the higher coefficient A corresponded to higher residual resistivity ρ_0. But our samples cooled in Ar gas and partial vacuum did not show any simple relation between A and ρ_0. We plot A versus ρ_0 [$\rho_0 = \rho(4.2K) - 0.28$ pΩcm/K^2] for 5 of our samples cooled in He (Fig. 4-2). These samples are consistent with the constant value 0.25 ± 0.02 pΩcm/K^2. However, they also fit $A = A_0 + c\rho_0$ (the solid line in Fig. 4-2) with $A_0 \approx 0.175$ pΩcm/K^2 and $c \approx 5.7 \times 10^{-5}$K^{-2}. This latter fit would imply a ρ_0-dependent part in A of about $A(\rho_0) = A - A_0 = 5.7 \pm 0.5 \times 10^{-5}\rho_0$. This is somewhat larger than that expected for electron-defect inelastic scattering (section 2.2.8). With either fit, A has a dominant component A_0 due to electron-electron scattering. The linear fit in ρ_0 would suggest an additional component due
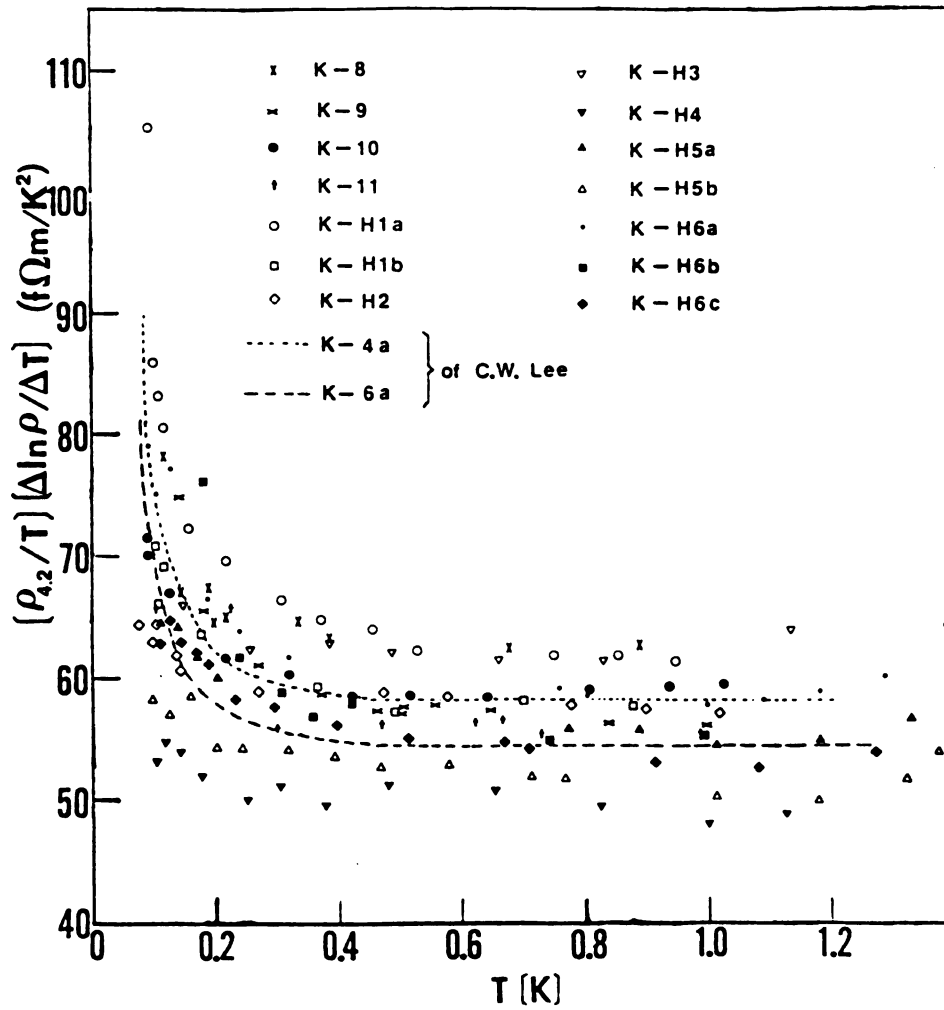
Fig. 4-1.. $(\rho(4.2K)/\rho T)(\Delta\rho/\Delta T)$ versus T for free hanging bare high-purity thick K samples.

Table 4-1. Coefficient A and other parameters of thick K samples. To
determine A, we assume ρ_0 = $\rho(4.2K)$ - 0.28 nΩcm. t = time at
room temperature.

Sample	Diam (mm)	t (days)	$\rho(4.2K)$ (nΩcm)	A (pΩcm/K^2)	Circumstance at room T.
K-8	1.5	0.5	1.50	0.25	Ar atm.
K-9	1.5	0.5	1.72	0.24	Ar atm.
K-10	1.5	0.5	1.47	0.24	Ar atm.
K-11	2.0	0.5	1.26	0.22	Ar atm.
K-H1a	1.5	0.5	1.70	0.26	He atm.
K-H1b	1.5	26.0	1.65	0.25	He atm.
K-H2	1.5	0.5	1.27	0.23	He atm.
K-H3	1.5	0.5	1.97	0.27	He atm.
K-H4	1.5	0.5	1.22	0.19	He atm. annealed at 50°C for 30 min.
K-H5a	1.5	0.5	1.27	0.22	10 μHg He
K-H5b	1.5	11.0	1.39	0.21	10 μHg He
K-H6a	1.5	0.5	1.23	0.23	He atm.
K-H6b	1.5	2.0	1.33	0.22	10 μHg He
K-H6c	1.5	3.0	1.35	0.22	100 μHg He + molecular seive

to electron-defect or electron-impurity inelastic scattering. However, in view of the small number of data points in Fig. 4-2 and the lack of any correlation of A with ρ_0 in samples cooled in Ar or vacuum, we cannot rule out the possibility that the observed variation with ρ_0 shown in Fig. 4-2 is just apparent, in that a large number of data points might end up randomly fluctuating the dashed line.

The anomalous turn-up below 0.35K might be associated with defects in the samples. Comparing K-H1a (the first run of sample K-H1) and K-H1b (the second run of sample K-H1 after annealing at room temperature for 26 days), we see that K-H1b has a much smaller turn-up than K-H1a. Similarly, sample K-H5b has a smaller turn-up than K-H5a. This result is consistent with what M. L. Haerle (ref. 22) found; deformation in pure K samples not only brought the coefficient A up, but also enhanced the anomalous turn-up at low temperatures.

More discussions of the anomalous turn-up will be given in section 4.6, together with the similar anomalous turn-up in Na, Li, and Rb.

4.1.2 The Thermoelectric Ratio G

G measurements were made for samples K-11, K-H5a, K-H5b, K-H6a, K-H6b, and K-H6c from about 4.2K down to about 70 mK, and for samples K-10, K-H1a, and K-H2 from about 1K down to about 70 mK. All the data are shown in Fig. 4-3. They have the same form as C. W. Lee's data, except the data of K-H5a and K-H6b, which have small bumps at temperatures
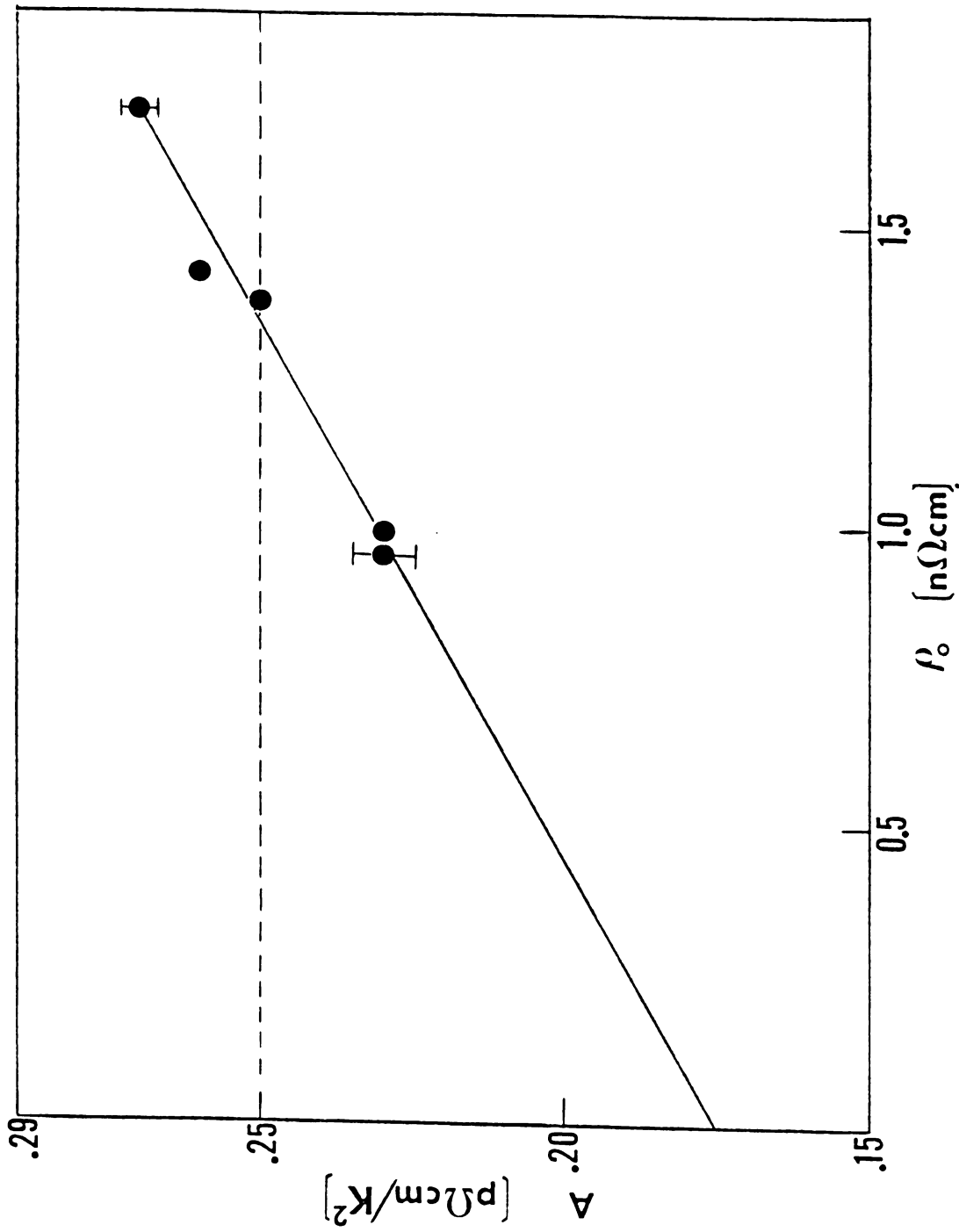
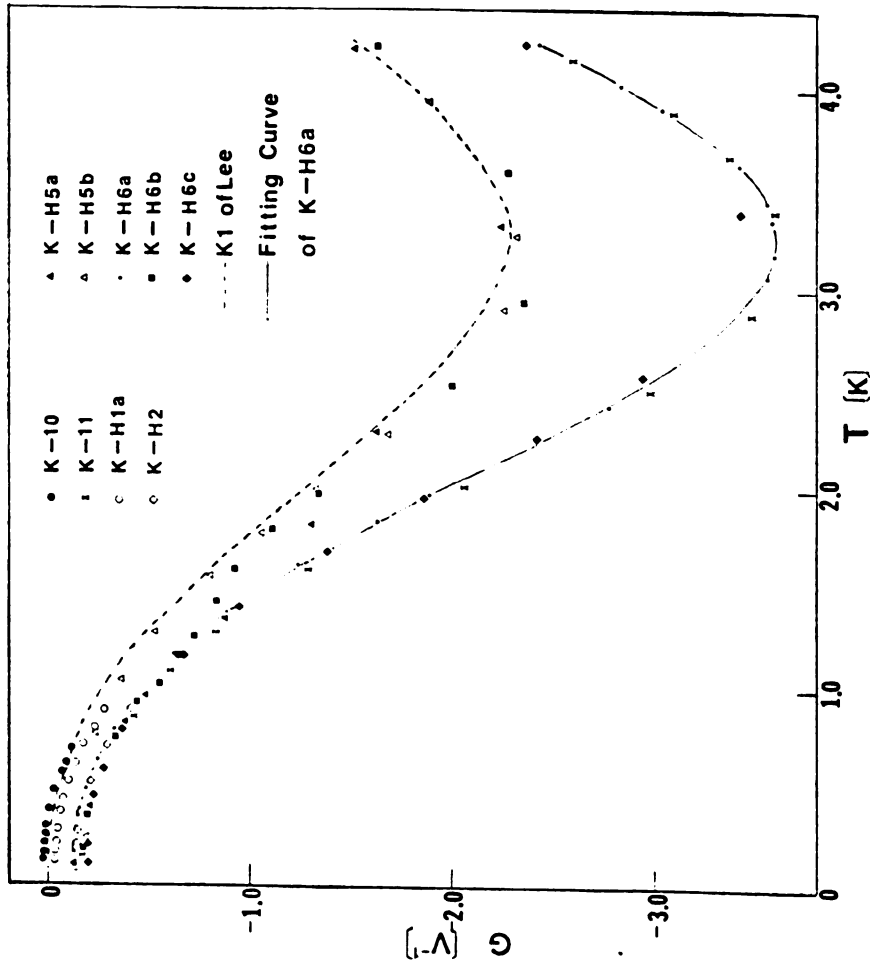Fig. 4-2. A vs ρ_o for 5 thick K samples cooled in He.

Fig. 4-3.   G vs T for free hanging bare high-purity thick K samples.

around 1.5-2.0K. At T < 1K, the data of all the samples almost overlap. Above 1K, the data diverge from sample to sample, but can be divided into two groups. In the first group, data of samples K-H5a, K-H5b, K-H6b almost overlap and are close to sample K-1 of Lee from 2.0-4.2K. These data stay less negative than the others. These three samples were under 10 μHg He gas without molecular sieve before being cooled down. The second group of samples, K-11 (under Ar atm. at room temperature), K-H6a (under He atm. with molecular sieve at room temperature), and K-H6c (under 100 μHg He with molecular sieve at room temperature) almost overlap each other over the whole temperature range, and are more negative at T > 1K than the other data. Both groups have the general form $G = G_o + B*T^2 + (C*/T) \, Exp \, (-\theta*/T)$ (see section 2.3). Assuming $\theta* = 23K$, for the first group we got $G_o^* = -0.17 \pm 0.01V^{-1}$, $B* = -0.314 \pm 0.0004V^{-1}K^{-2}$ and $C* = 4100 \pm 100V^{-1}K$ for the second group $G_o = -0.075 \pm 0.015V^{-1}$, $B* = -0.484 \pm 0.005V^{-1}K^{-2}$, and $C* = 6200 \pm 140V^{-1}K$. These two fits are given in Fig. 4-3 by the dashed and solid line, respectively.

The reason for the difference between these two groups might be explained as follows. Without the molecular sieve, the little amount of He gas (10 μHg at room temperature) could be incompletely adsorbed, the heat current from the G heater only partly passed through the sample, and part of it through the left-over He gas. But in the calculation, we still assumed that all the heat current passed through the

sample, (i.e., we divided the electric current I by too big
a heat current, so we got a smaller absolute value of G).
The small bumps could be explained as a kind of condensation
of left-over He gas occurred from 2K down to 1.5K, so the
data fell back to the position where they should be, and
overlapped with the second group.

The heat current passed through the left-over He gas
mentioned above could be roughly calculated as follows:
first we assume all the surface exposed to the 10 μHe gas
inside the sample can can only adsorb one layer of He atoms
at 4K. The total surface area is roughly calculated as: S
= 25 cm x 10 cm x 2 (the height of the sample can $\approx$ 10 cm,
the perimeter of the sample can $\approx$ 25 cm, the areas of two
bottoms, sample holders, and samples are all included in the
factor 2). The atom spacing of liquid He is about 7.5Å.
So, the number of He atoms that could be adsorbed is:

$$n = \frac{S}{(7.5A)^2} \approx 9 \times 10^{16}$$

The total number of He atoms inside the sample can is

$$n = \frac{6.023 \times 10^{23}}{22.4 \times 10^3 \text{ cm}^3} \times \frac{10 \times 10^{-3} \text{ mm}}{760 \text{ mm}} \times 500 \text{ cm}^3$$

$$\approx 18 \times 10^{16}. \qquad \text{(where V} \approx 500 \text{ cm}^3)$$

So, the left-over He gas would be half as much as at room
temperature. To find the thermal conductivity (κ =
1/3 $C_v \ell v$) of the left-over He gas, we need to calculate ,

C_V, and V:

ℓ = 8 cm (the diameter of the sample can)

C_V = n x 1/2k

$$= .5 \text{ x } \frac{6.023 \text{ x } 10^{23}}{22.4 \text{ x } 10^3 \text{ cm}^3} \text{ x } \frac{10 \text{ x } 10^{-3} \text{ mm}}{760 \text{ mm}} \text{ x } .5 \text{ x}$$

$1.38 \text{ x } 10^{-16}$ erg/K

$= 1.2 \text{ x } 10^{-9}$ J/Kcm^3

Using the velocity formula of ideal gas,

$$V = 1.6 \sqrt{RT/\mu} = 1.60 \sqrt{8.3128 \text{ x } 4 \text{ x } 10^7 \text{ erg/4g}}$$

$= 15 \text{ x } 10^3$ cm/s.

Thus,

$$\kappa = 1/3 \text{ } C_V\ell V \approx 4.7 \text{ x } 10^{-5} \text{ watt/cm-K}.$$

So the heat current passed through the assumed left-over He gas would be approximately

$$\dot{Q} = \kappa S\Delta T/\Delta X \approx 4.7 \text{ x } 10^{-5} \text{ watt/cm-K x 3 cm}^2 \text{ x 0.1 K/4 cm}$$

$\approx 3.5 \text{ x } 10^{-6}$ watt.

This is comparable to the heating power of the G heater:

$$\dot{Q}_G = I^2R = (40 \text{ } \mu A)^2 \text{ x } 4000\Omega = 6.4 \text{ x } 10^{-6} \text{ watt}.$$

4.2 FREE HANGING, BARE, THIN (d = 0.09-0.5MM) HIGH-PURITY K SAMPLES

4.2.1 The Resistivity

As mentioned in section 1.2.1, Rowlands et al., unlike other investigators, found that below 1.3K, their $\rho(T)$ data of pure K samples were better fitted by $\rho(T) \propto T^{3/2}$ than by $\rho(T) \propto T^2$. Subsequently, their data were interpreted as evidence for electron-phason scattering (section 2.2.3). We noticed that their samples were thinner than ours, with d = 0.79 mm. After reviewing the old data of our group, we found that the plotting of $d\rho/dT$ versus T for two pure K samples (d = 0.9 mm) of M. Haerle cooled in He gas also showed deviations from a straight line, i.e. deviations from T^2 behavior. In hopes of discovering the reason for the difference between the data of Rowlands et al. and our thick sample data, we set out to measure a set of thin samples with d = 0.5, 0.25, 0.16, 0.1, and 0.09 mm in three different circumstances, Ar atm., He atm., and partial vacuum.

We found that data for wires cooled in He gas displayed a clear pattern of unusual behavior which is consistent with that reported by Rowlands et al. in the region of overlap, but more complex in form. The characteristics of all these samples are shown in Table 3-1.

Fig. 4-4 shows a normalized $d\rho/dT$ (ref. 59) plotted versus T from 0.07 to 1.8 K for selected samples with $0.09 \leq d \leq 1.5$ mm, prepared in He gas and cooled down with

molecular sieve. They were, in sequence from top to bottom in Figure 4-4: samples K-H1a with d = 1.5 mm (+), K-1/2H with d = 0.5 mm (■), K-1/4H3 with d = 0.25 mm (x), K-1/4H2a with d = 0.25 mm (●), K-1/4H2b with calculated d = 0.16 mm (o), K-1/10H2a with d = 0.1 mm (♦), K-1/10H1b with calculated d = 0.09 mm (☆), and K-1/10H2b with calculated d = 0.09 mm (◊). The characteristics of these samples are given in Table 3-1. Two samples of each diameter were measured concurrently. The data for such sample pairs always agreed quite well with each other; one of the largest disparities is indicated by the different symbols (☆ and ◊) for the two thinnest (d = 0.09 mm) samples.

For comparison with data of K-H1a with d = 1.5 mm, the dotted and dashed line indicate C. W. Lee's data for 3.0 mm and 0.9 mm samples, respectively, in Ar gas (ref. 8). Together with data of K-H1a, these data lines indicate the range of variation for all "thick" samples of our group (including old data (ref. 8) and new data in this study) in both Ar (d = 0.9-3 mm) and He (d = 1.5 mm). Two solid lines indicate data for two independent d = 0.9 mm samples in He, measured by M. Haerle. Samples K-1/4H2a and K-1/4H3 both had d = 0.25 mm but were mounted in different ways. K-1/4H2a was mounted using method (a), while K-1/4H3 with method (b) (section 3-2 and Fig. 3-4). Data for our other d = 0.25 mm samples approximately spanned the range between these two sets of data.
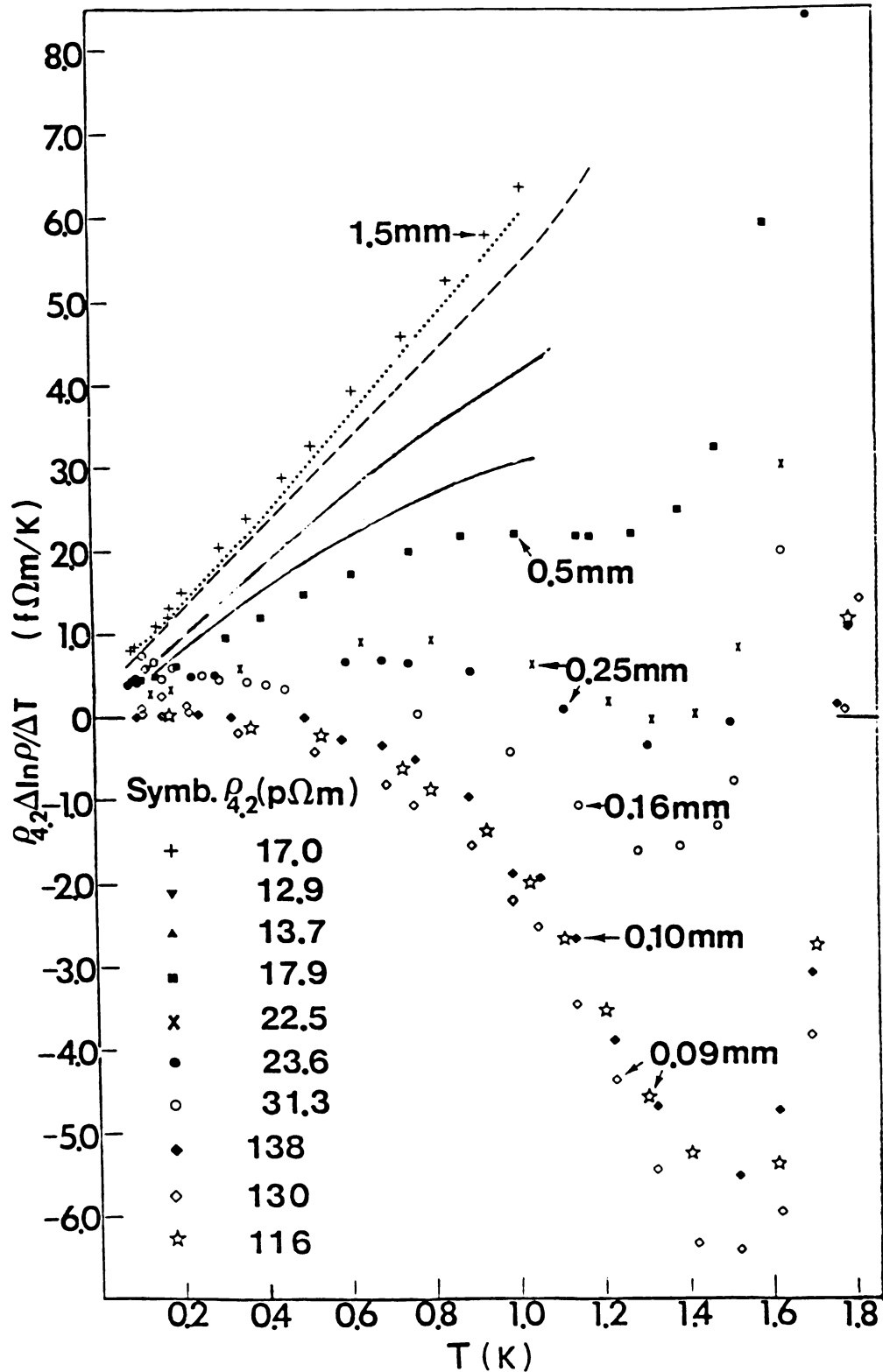
Fig. 4-4. $P(4.2K)(\Delta \ln P/\Delta T)$ vs T for thin wires of K cooled in a He atmosphere.

Fig. 4-5 compares data of Rowlands et al. with the data of Fig. 4-4. The samples of Rowlands et al. had d = 0.8 mm and comparable purity (residual resistivity ratio (RRR) = [R(295K)/R(4.2K)] ≈ 6000) to ours. Both the form and magnitude of their data are consistent with what we expect for samples of d = 0.8 mm in He gas, sitting right between d = 0.9 mm data and d = 0.5 mm data. However, the more complex form of our data rules out the simple $T^{3/2}$ form for $\rho(T)$ that they originally proposed.

To calculate the mean-free-path of electron-impurity scattering (l_{ei}), we used the equation

$$l_{ei} = (r_s/a)^2 \times 92 \, \overset{\circ}{A}/\rho_\mu \qquad (4-1)$$

(ref. 4), where r_s is the radius of a sphere whose volume is equal to the volume per conduction electron, a = 0.529 x 10^{-8} cm, ρ_μ is the resistivity in microhm centimeters. Our thickest samples had RRR's of about 6000 and ρ_μ of about 1.2 x 10^{-3} at temperatures lower than 4.2K. From equation (4-1) we find a corresponding lei of about 0.2 mm at temperatures lower than 4.2K. Samples with d ≤ 0.25 mm, comparable to or smaller than l_{ei}, displayed negative values of dρ/dT in the vicinity of 1K, followed by a rapidly increasing dρ/dT above 1.3K due to electron-phonon scattering. The changes in sign of dρ/dT from negative to positive shown in Fig. 4-4 indicate resistivity minima in these very thin samples. At lower temperatures, dρ/dT increases more slowly with decreasing temperature. The
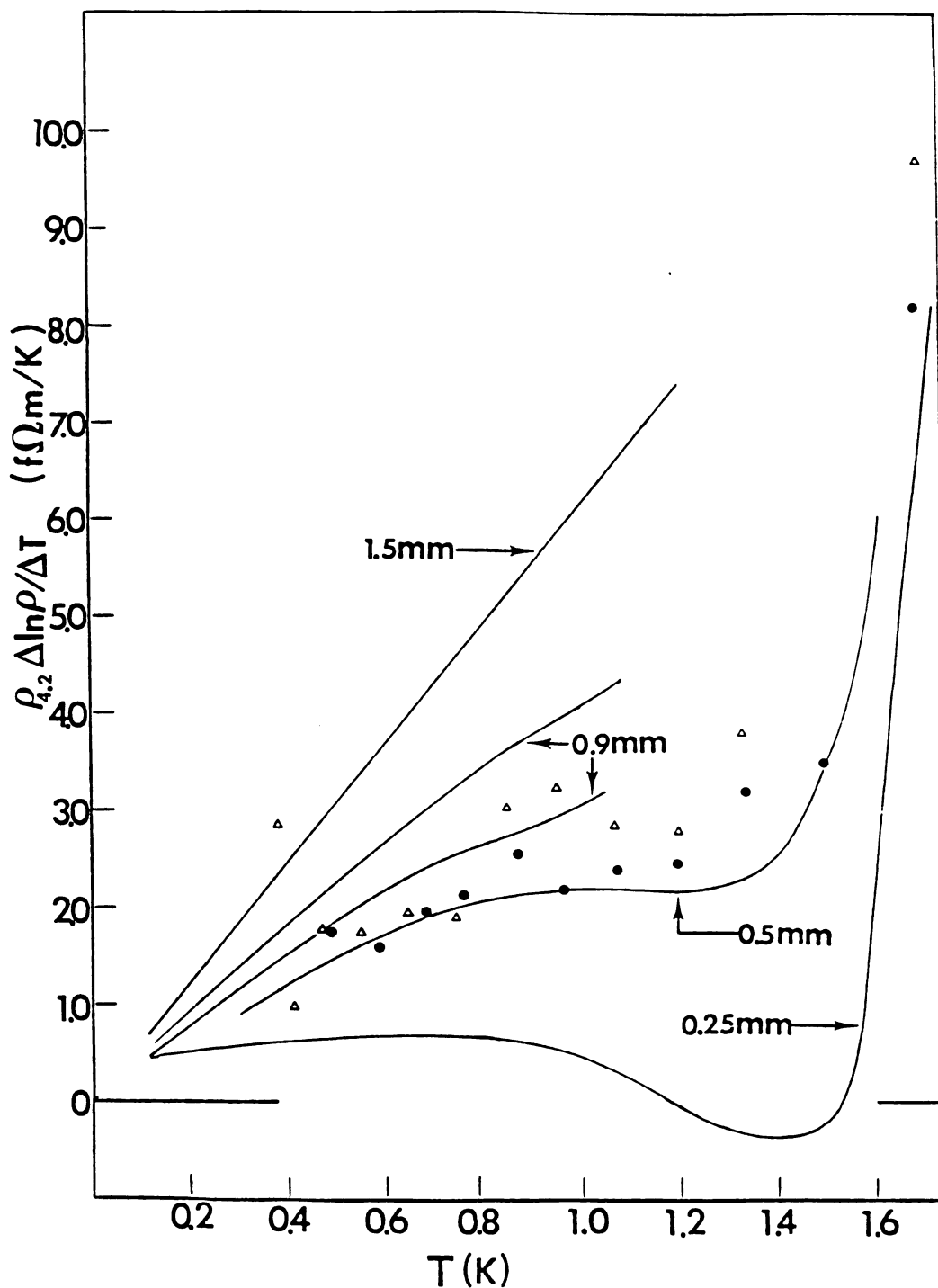
Fig. 4-5. P(4.2K)($\Delta\ln P/\Delta T$) vs T for two K samples of Rowlands et al. (ref.13) with d = 0.08 mm cooled in a He atmosphere. For comparison, the solid lines represent data from Fig. 4-4 for K samples having the diameters indicated.

other changes in sign of $d\rho/dT$ at the low temperature end indicate local resistivity maxima in these samples.

The variations with sample diameter shown in Fig. 4-4 cannot be due to plastic deformation during either fabrication or cooling of these thin samples. According to M. Haerle (ref. 22) and the discussion in section 4.1, plastic deformation makes $d\rho/dT$ more positive, exactly the opposite of what is seen here.

To test for effects of surface corrosion, two different thicknesses of samples were allowed to thin by means of such corrosion, which occurred naturally inside the sample can. In Fig. 4-4, the two samples with d = 0.16 mm (K-1/4H2b:o) and d = 0.09 mm (K-1/10H2b:◊) were corroded versions of the two samples with d = 0.25 mm (K-1/4H2a:●) and d = 0.10 mm (K-1/10 H2a:♦), respectively. The reduced diameters of these corroded samples were inferred from their increased room-temperature resistances. The changes seen with decreasing thickness due to corrosion are similar to those seen with decreasing thickness in freshly extruded samples. The important quantity must thus be the size of the uncorroded portion of the sample.

To test whether the electron mean free path, l_{ei}, is also an important parameter, measurements of $d\rho/dT$ were made on d = 0.25 mm samples of K-0.08%-Rb alloys in He gas. These alloys have $l_{ei} \approx 0.04$ mm, obtained from the equation (4-1) used above. Fig. 4-6 shows the results of these samples, the solid line indicates sample KRbhc of M. Haerle,
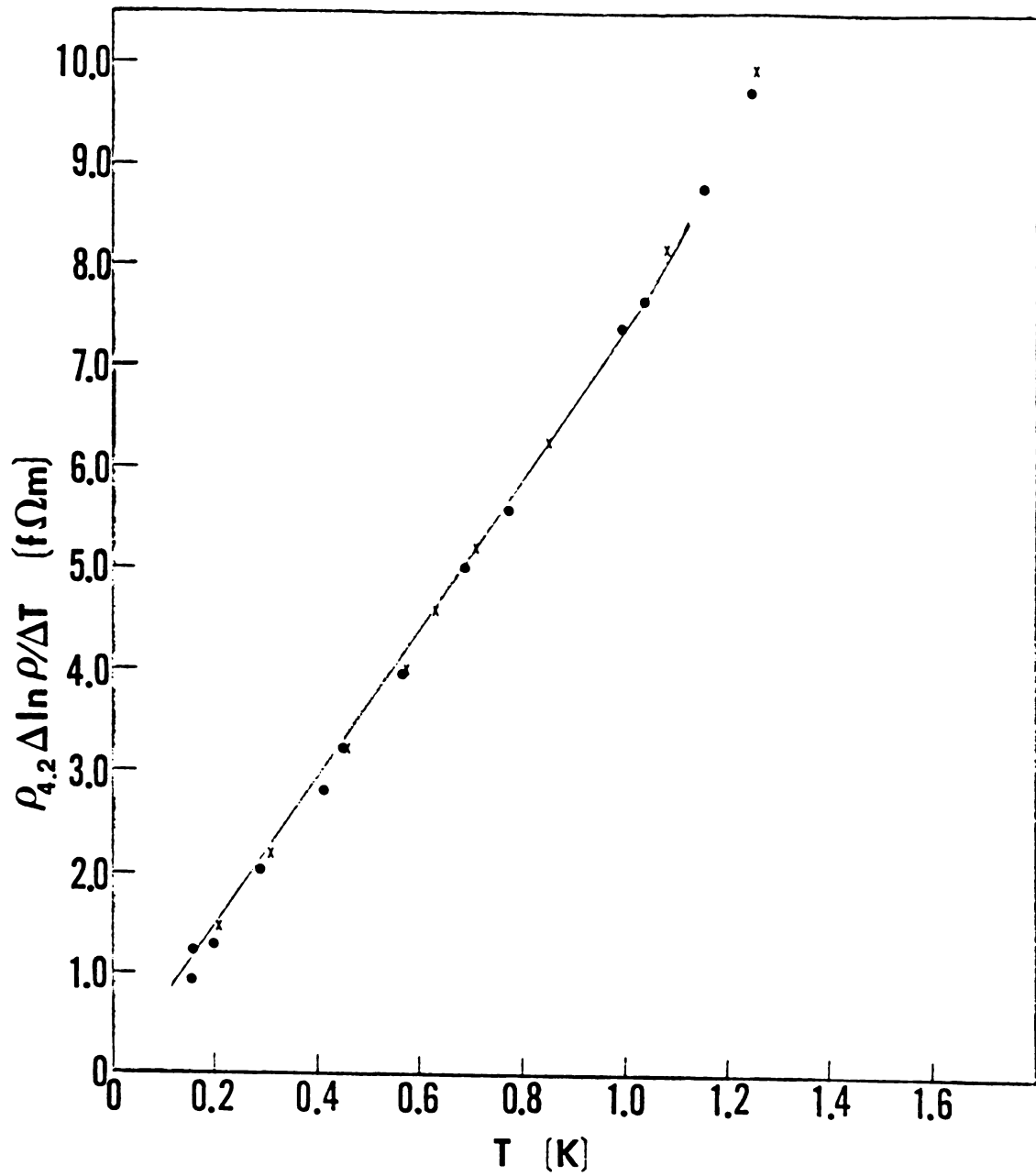
Fig. 4-6. $P(4.2K)(\Delta \ln P/\Delta T)$ vs T for two K-0.08at%Rb alloy samples with d = 0.25 mm.

which had the same composition but with d = 0.9 mm. No size effect was seen; $d\rho/dT$ increased linearly with T and had the same magnitude as data of thicker samples with the same composition. It can thus be concluded that the size effects described above only occur in samples with diameters comparable to l_{ei}.

The complex form of the data in Fig. 4-4 and Fig. 4-5, and especially the negative $d\rho/dT$ for $d \leq 0.25$ mm samples, are incompatible with most of the models proposed to explain either previous data on K below 1K or "size effects" in other metals. The standard model (section 2.1) cannot explain either the general form of our data or the appearance of a negative $d\rho/dT$. The anisotropic electron-electron scattering model of Kaveh and Wiser (section 2.2.1) requires a simple T^2 variation, and has no way to explain the negative $d\rho/dT$. It was mentioned in section 2.2.3 that the electron phason scattering model, which was used to explain the $T^{3/2}$ behavior reported by Rowlands et al., cannot describe either the appearance of a negative $d\rho/dT$ in our thinnest samples, or the general form of our data. The Knudsen model of Rowlands et al. cannot give an explanation either. At first glance, the formula $\rho(T) = BT^2 - CT^4$, suggested by Rowlands et al., seems able to provide a negative term for $d\rho/dT$. But, Rowlands et al. proposed this two term formula only for large r/λ ratio, where r = sample radius and $\lambda =$ the mean-free-path of electron-electron scattering (section 2.2.4). They argued that for small r/λ

ratio, the contribution of a term in $(r/\lambda)^2$ or high order could be neglected. This led to $\rho(T) = BT^2$ and thus to a positive $d\rho(T)/dT$. Only when r/λ is large should the term in $(r/\lambda)^2$ to be taken into account to give $\rho(T) = BT^2 - CT^4$ (see section 2.2.4 for details). In our case, thick samples had $d\rho/dT > 0$. Thin samples had smaller r (i.e., smaller $\frac{r}{\lambda}$ ratio) and thus less contribution from any $(r/\lambda)^2$ term. According to the Rowlands et al. model, our thin samples should have had a more positive $d\rho/dT$, exactly the opposite of what is seen. Finally, none of the models of deviations from Matthiessen's rule used to describe size effects in other metals can generate a negative $d\rho/dT$ (see section 2.2.5 for details).

The only model we know, which might explain what we see, involves the combination of contributions from (a) UEES, giving a positive term, $2AT$, in $d\rho/dT$; and (b) NEES plus surface scattering, giving a negative term in $d\rho/dT$, [suggested by Gurzhi] (section 2.2.6), which at low enough temperatures increases in magnitude with increasing temperature [as calculated by Black (ref. 38)].

The main difficulty in directly comparing our data with this model is that the best estimates of l^N_{ee} (Normal electron-electron scattering mean free path) for K yield l^N_{ee} ~10-100 mm at 1K (ref. 39). The diameters of our samples which show size effects were d = 0.09-0.9 mm. This means that we are not in the Gurzhi limit $l^N_{ee} \ll d$, but rather in the opposite limit $l^N_{ee} \gg d$. A Monte Carlo calculation by

Black (ref. 38) can be used to estimate behavior in this
limits. Table 4-2 shows some of the results from Black.
Since l_{ei} (mean free path of electron-impurity scattering)
is temperature-independent in first approximation, and d
changes only 2% from room T to lowest T, $l_{ei}/(d/2)$ is roughly
constant. Unlike l_{ei}, l_{ee}^N is temperature-dependent, l_{ee}^N
T^{-2}. Thus, $l_{ee}^N/(d/2)$ decreases with increasing temperature.
This means that in Table 4-2, the direction of decreasing
$l_{ee}/(d/2)$ (to the right in Table 4-2) is the direction of
increasing temperature. Since $\rho \propto 1/l_{eff}$, then $d\rho/dT \propto$
$-(1/l_{eff})^2 dl_{eff}/dT$, where l_{eff} is the effective mean-free-
path of electrons. This means that an increase of l_{eff}
with increasing temperature gives a decrease in ρ and thus,
a negative $d\rho/dT$. In Table 4-2, when $l_{ei} \sim d$, which is the
situation for our thinnest samples, negative values of $d\rho$
/dT persist to at least $l_{ee}^N/(d/2) \gtrsim 10$. When $l_{ei}/(d/2) = 5$,
Table 4-2 shows a reduction in the total resistivity ρ of
about 1% (the limit of accuracy of Black's calculations)
from $l_{ee}^N/(d/2) = \infty$ to $l_{ee}^N/(d/2) = 10$. In the case of our
thinnest samples, $l_{ei}/(d/2) \approx 4.4$, (d = 0.09 mm and $l_{ei} =$
0.2 mm calculated above), $l_{ee}^N/(d/2) \sim$ 200-2000 at 1K, and the
reduction of ρ from T = 0K to T = 1K (i.e., from $l_{ee}^N/(d/2) =$
∞ to $l_{ee}^N/(d/2) \approx$ 200-2000) is only 0.003%. So, the
calculation of Black could be consistent with our data.

The fundamental theoretical questions are whether for
$l_{ei} \sim d$ the Gurzhi effect dominates the Knudsen-flow effect
at such large values of $l_{ee}^N/(d/2)$ and, if so, whether the

Table 4-2. l_{eff} for isotropic scattering (after Black (ref. 38))

$2\,l_{ei}/d$	$2\,l_{ee}/d$									
	10^5	10	5	2	1	0.5	0.2	0.1	0.05	0.025
10^5	1.33	1.30	1.31	1.37	1.53	1.86	2.97	4.7*	8.5*	16.1*
10	1.15	1.15	1.17	1.23	1.34	1.58	2.22	3.1*	4.2*	
5	1.03	1.04	1.06	1.11	1.19	1.37	1.80	2.28*	2.8*	3.3*
2	0.80	0.82	0.82	0.85	0.89	0.97	1.14	1.30	1.43*	
1	0.59	0.59	0.60	0.61	0.63	0.66	0.71	0.76	0.80	
0.5	0.38	0.38	0.39	0.39	0.39	0.39	0.41	0.42	0.43	0.44*
0.2	0.178	0.180	0.178	0.179	0.180	0.179	0.180	0.182	0.183	
0.1	0.094	0.094	0.094	0.093	0.094	0.094	0.094	0.094	0.094	
0.05	0.047	0.048	0.048	0.048	0.048	0.048	0.047	0.047	0.048	0.047*

* Values are accurate to ±2%, all other values are accurate to ±1%.

Gurzhi effect is large enough to be seen. A much more accurate Monte Carlo calculation will be needed to answer these questions. If the Gurzhi effect is not the source of the behavior we see, then there currently exists no satisfactory explanation for what we see.

As mentioned above, since we are not in the Gurzhi limit $l_{ee}^N \ll d$, there is no guidance for finding a closed form to fit our data.

Assuming electron-phonon scattering is negligible for $T \leq 1.1K$ (ref. 6,16), and since there are no anomalous low temperature deviations (described in section 4.1.1) for $T \geq 0.4K$, we tried to fit our data from 0.4K to 1.1K. First, we tried a fit which has an electron-electron scattering term plus an additional term, as in the form

$$\frac{\rho_{4.2}}{\rho} \frac{d\rho}{dT} = 2A'T - CT^n. \tag{4-2}$$

with $2A' \approx 0.61$ pΩcm/K^2 deduced from the data of thick sample K-H1a, and C, n as two adjustable parameters. The computer results showed $n \approx 4/3$ and $C \sim 1/\sqrt{d}$ for all our samples.

Considering that A varies a little from sample to sample, even for our thick samples, we then tried

$$\frac{\rho_{4.2}}{\rho} \frac{d\rho}{dT} = 2A'T - \frac{55}{\sqrt{d/1 \text{ mm}}} T^{4/3} \tag{4-2*}$$

and left only A' as an adjustable parameter. The computer results showed that Eqn. (4-2*) is a good fit for all our data from 0.4K to 1.1K (see Fig. 4-7) and that A' varies not much from sample to sample (see Table 4-3).

Table 4-3. Coefficient A' deduced from the fitting of Equation (4-2*)

Samples	K-1/2H	K-1/4H2a	K-1/4H2b	K-1/10H2a	K-1/10H2b
$2A'$ $(p\Omega cm/K^2)$	0.61	0.59	0.64	0.70	0.70

So far, data discussed in this section are all for K samples cooled in He gas. To test whether these observed size-effects are unique for samples cooled in He gas, measurements of $d\rho/dT$ were also made on thin samples cooled in Ar gas or in partial vacuum.

Four thin K samples with d = 0.1 mm cooled in Ar were measured in this study. They were samples K-1/10A1, K-1/10 A2, K-1/10A3, and K-1/10A4. Six other thin K samples cooled in ~10 μHg He were measured. Two of them with d = 0.25 mm were samples K-1/4V1 and K-1/4V2. Four of them with d = 0.1 mm were samples K-1/10V1, K-1/10V2, K-1/10V3 and K-1/10V4. The characteristics of these samples are given in Table 3-1.

Fig. 4-8 compares data of 8 of these samples with the data of K wires cooled in the He from Fig. 4-4. The solid lines in this figure denote the data of K wires cooled in
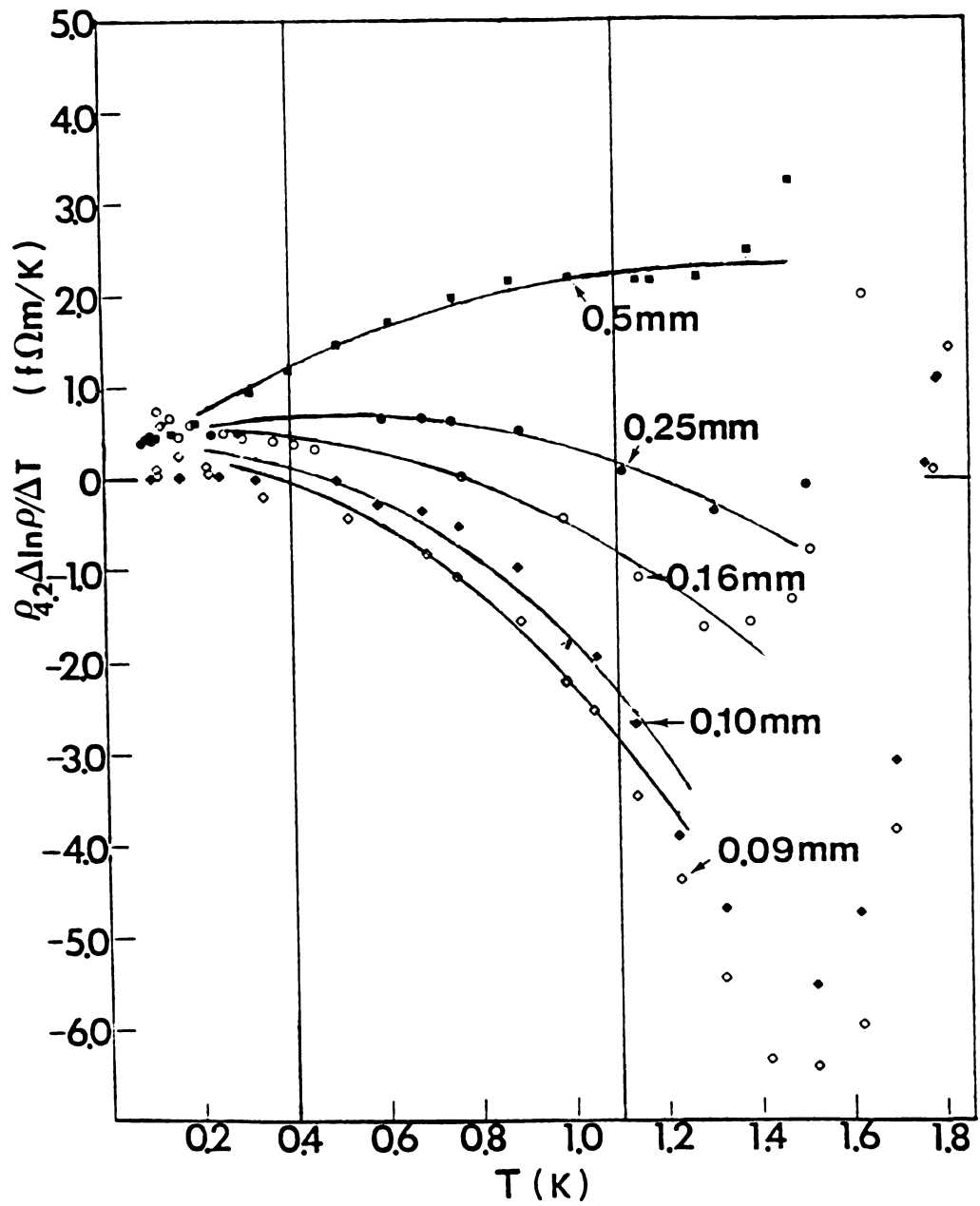
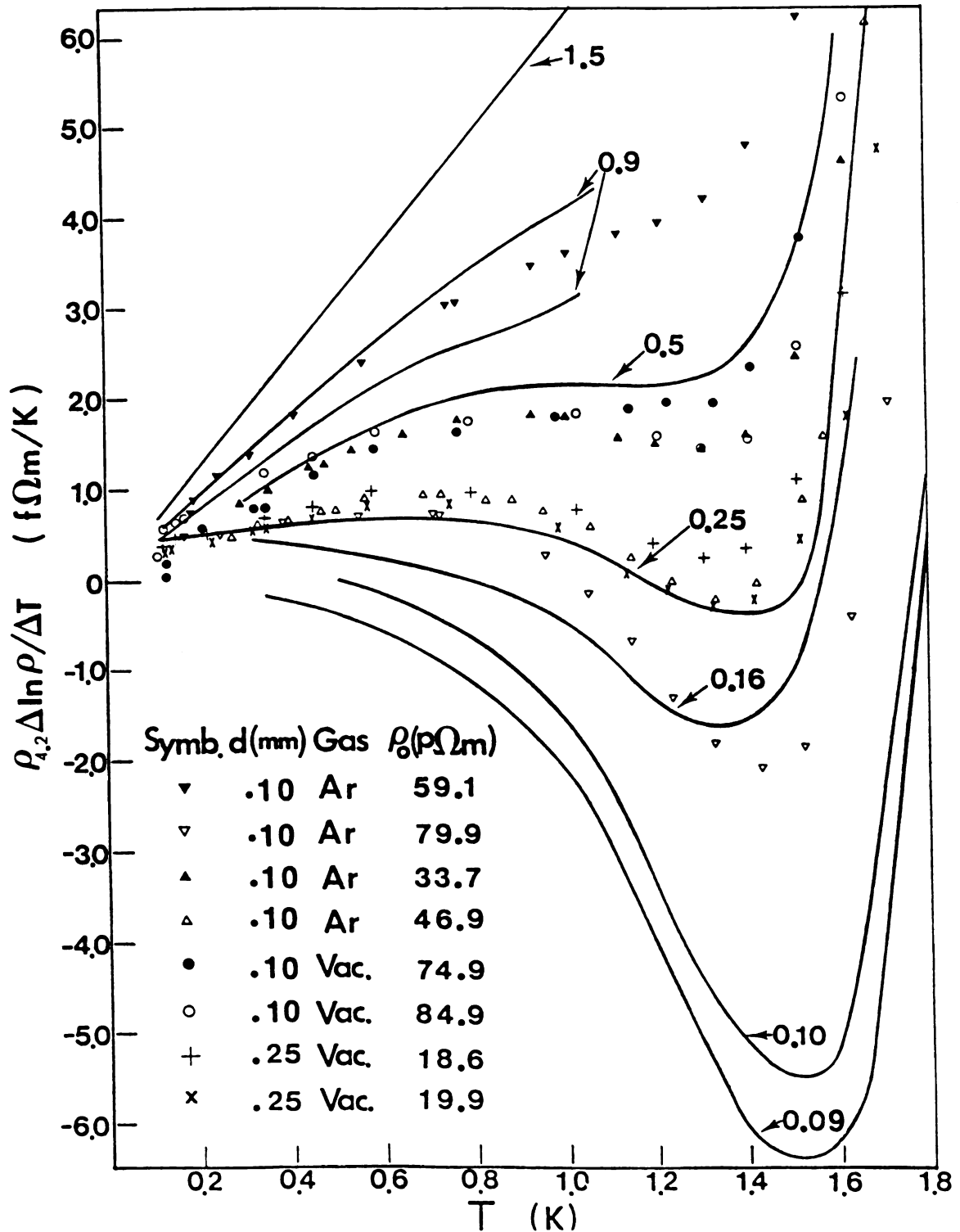Fig. 4-7. $P(4.2K)(\Delta \ln P/\Delta T)$ vs T for samples indicated in Fig. 4-4 with fitting curves of Eqn. 4.2.

Fig. 4-8. $\rho(4.2K)(\Delta\ln\rho/\Delta T)$ vs T for thin wires of K cooled in a Ar atmosphere or a partial vacuum. For comparison, the solid lines represent data from Fig. 4-4 for K samples having the diameters indicated.

He. (▼)s indicate sample K-1/10A1, (▽)s indicate sample K-1/10A2. These two samples, both with d = 0.1 mm, were measured in a same run. Each of them was used as the reference for the other. These two sets of data are quite different. The data of sample K-1/10A1 are close to those of typical d = 0.9 mm samples cooled in He; while the data of sample K-1/10A2 are close to those of d = 0.16 mm samples cooled in He. Data of another pair of samples with d = 0.1 mm cooled together in Ar are indicated by (▲)s and (△)s. The data of K-1/10A3 (▲) are close to data of d = 0.5 mm samples cooled in He; the data of K-1/10A4 (△) are close to data of d = 0.25 mm samples cooled in He. The plusses and crosses individually indicate data of a pair of samples, K-1/4V1 and K-1/4V2, with d = 0.25 mm cooled together in partial vacuum. Both of them are close to data of the same diameter samples cooled in He. But data of samples K-1/10V3 and K-1/10V4 with d = 0.1 mm cooled in partial vacuum, indicated by filled and open circles individually, are close to data of d = 0.5 mm samples cooled in He.

It can be seen in Fig. 4-8 that 1) The form of all these data is similar to that of data for thin K wires cooled in He. 2) The data of some of these samples: samples K-1/10A2, K-1/10A4 cooled in Ar and sample K-1/4V2 cooled in partial vacuum, show negative $d\rho/dT$ in the vicinity of 1K like those seen for samples cooled in He. 3) Data of 6 samples with d = 0.1 mm cooled in Ar gas or

partial vacuum tend to behave like data for samples in He of larger diameter and to show greater variability for fixed d.

The reasons for point 3) above are not yet clear. Possible contributions to an explanation include:

1) Since the contribution of electron-surface scattering to electrical resistivity is only from diffuse surface scattering, less diffuse scattering would make $d\rho/dT$ behave like that in a sample of larger diameter, and make ρ_0 smaller. He gas might somehow make the ratio of diffuse surface scattering to specular surface scattering large and stable, while Ar and partial vacuum might make this ratio smaller and less stable. One possibility is that small He atoms could diffuse into the surface layer of K samples and then provide a good condition for diffuse scattering; without He atoms, the surface would not provide a good and stable condition for diffuse scattering. This model could be used to explain a) that the 6 samples with d = 0.1 mm cooled in Ar or partial vacuum had smaller ρ_0 and behaved like thicker samples in $d\rho/dT$ than what would be expected when they were cooled in He gas. b) Sample K-1/10A1 had smaller ρ_0 than sample K-1/10A2, and behaved like a thicker sample than k-1/10A2 in $d\rho/dT$.

2) The influence of impurity concentration could also not be ruled out, since more impurity concentration tends to quench these size effects, as shown in K-Rb dilute alloy samples with d = 0.25 mm described above. Impurity input from the sample surface could occur during extrusion or

during surface corrosion. This will cause sample-dependence of impurity concentration. This source might contribute to why samples K-1/10V3 and K-1/10V4 had larger ρ_0 than samples K-1/4V1 and K-1/4V2, and behave like thicker samples than K-1/4V1 and K-1/4V2 in $d\rho/dT$.

In order to see a size effect in the residual resistivity ρ_0, ρ_0 is plotted versus 1/d for selected samples in Fig. 4-9. Data of other samples with particular values of d spanned the range bounded by the plotted data for samples with the same d. In Fig. 4-9, ($\bullet$)s indicate data of samples cooled in He gas; (x)s indicate data of samples cooled in Ar; and ($\triangle$)s indicate data of samples cooled in partial vacuum.

The residual resistivity is expected to have two components: one due to electron-impurity and electron-defect scattering, called the bulk residual resistivity ρ_∞, and the other due to electron-surface scattering, called $\rho_0(d)$. In the first approximation, $\rho_0(d) \propto 1/d$, so

$$\rho_0 = \rho_\infty + \frac{c}{d}$$

In a plot of ρ_0 versus 1/d, a straight line with slope c and intercept ρ_∞ is expected. Woods (ref. 66) suggested $c \approx 5 \times 10^{-11}$ Ωcm^2, which is indicated by the dashed line in Fig. 4-9. For data of our samples with $d \geq 0.16$ mm, a smaller c: $c \approx 3.4 \times 10^{-11}$ Ωcm^2 is obtained (see the solid line in Fig. 4-9); this is comparable to $c = 2.9 \times 10^{-11}$ Ωcm^2 (ref. 67) found in another study. For reasons

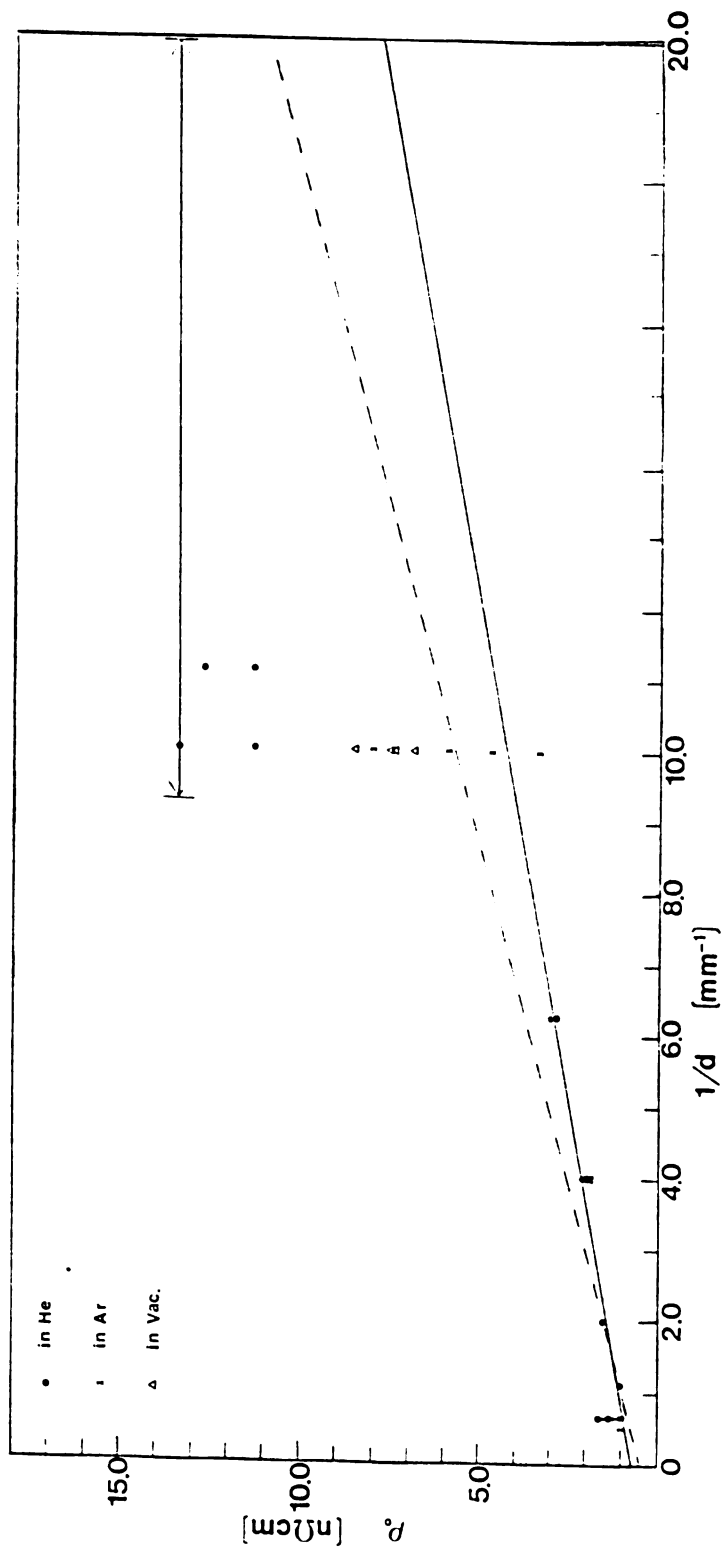Fig. 4-9. ρ_0 vs 1/d for thin K samples.

not yet clear, the ρ_o's of our thinnest samples (d $\leq$ 0.1 mm) showed a lot of scatter, with most of the ρ_o's much larger than expected. Possible explanations include: (1) Uncertainty in determining the diameters of these thinnest samples. The diameters were determined by the hole size of the dies. The smallest die (d = 0.1 mm) could easily get partially blocked or slightly damaged, which would reduce its hole size and make the extruded samples thinner. The ρ_o's of these samples would thus be higher. (2) Corrosion of sample surfaces. This would thin the samples. For the thinnest samples, the thinning due to corrosion would be significant. [(1) and (2) together could make the real d half as small as the hole size of 0.1 mm die.] (3) Impurity input from the sample surface during extrusion. This would give the thinnest samples the largest fractional concentration of impurities, which would increase their ρ_o's.

4.2.2 The Thermoelectric Ratio G

G measurements were made for each thin K sample from about 4.2K down to about 70 mK. Fig. 4-10 shows G data for the same samples shown in Fig. 4-4, which were cooled in He gas. For K-H1a (d = 1.5 mm), G measurements were made only for T $\leq$ 1K, so data of another thick sample, K-H6a (d = 1.5 mm), are added to Fig. 4-10. All these data have similar form, and can be well fitted by

$$G = G_o + B*T^2 + (C*/T) \, \mathrm{Exp}(-\Theta*/T).$$
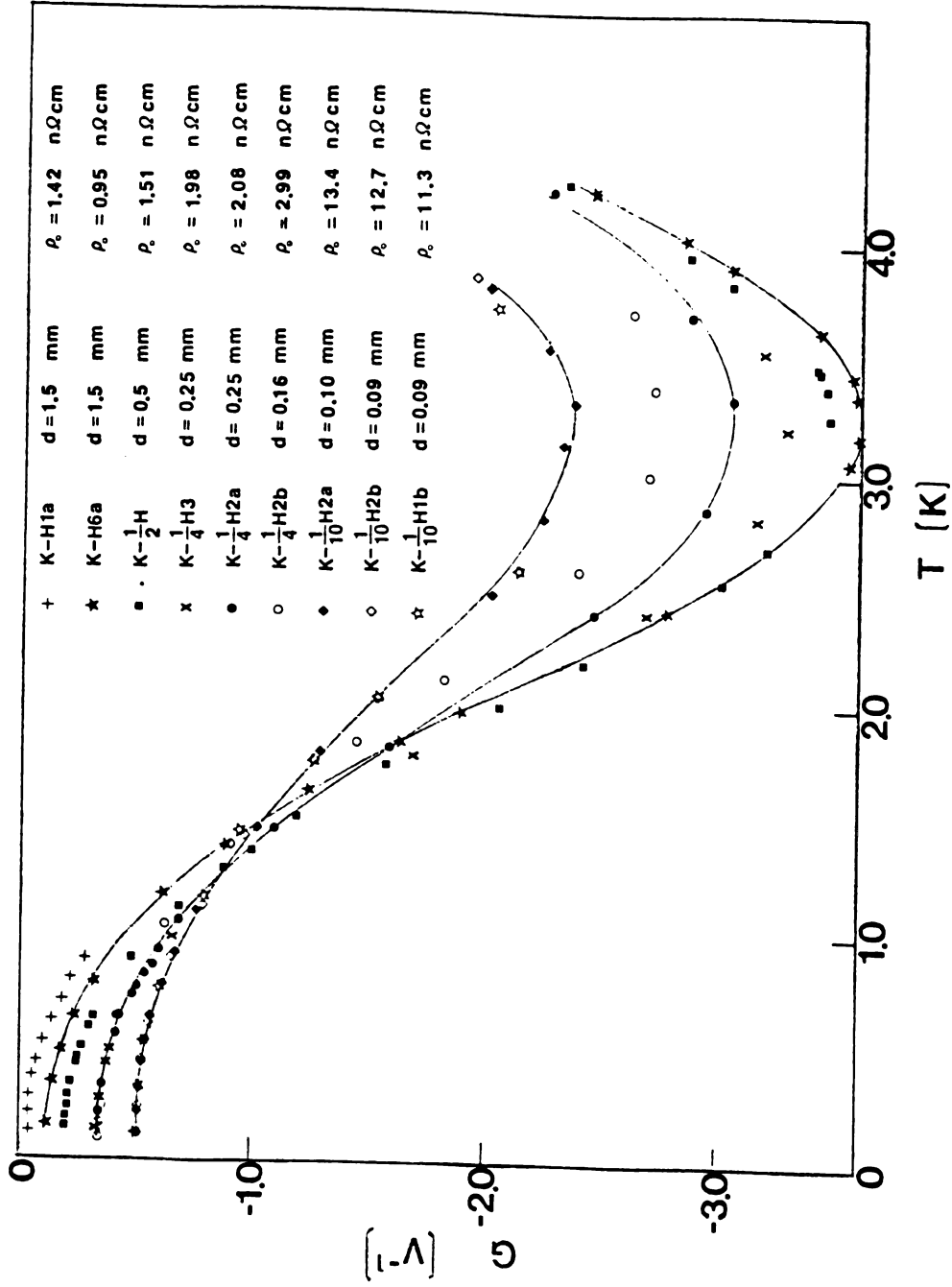
Fig. 4-10. G vs T for thin wires of K cooled in a He atmosphere.

But, the thicker samples show larger magnitudes of G at high temperatures and smaller magnitudes at lower temperatures than do the thinner samples. Table 4-4 shows the coefficients of the fits G_o, B*, C* for each sample with Θ* fixed as 23K, lines in Fig. 4-10 show the fits for three samples: K-1/10H2a, K-1/4H2a, and K-H6a. The fit for sample K-H6a was already shown in Fig. 4-3 (section 4.1.2).

Table 4-4 shows that as the diameter of a sample decreases: 1) the magnitude of G_o gets larger, and 2) the magnitudes of B* and C* get smaller. "1" can be explained by the Gorter-Nordheim rule (Eqn. 2-45) $S = (\rho_i S_i + \rho_d S_d)/\rho$ (see section 2.3.1), where S is only the diffusion term of the thermoelectric power, S_i = thermopower due to impurity scattering, ρ_i = electric resistivity due to impurity scattering, S_d = thermopower due to another temperature-independent scattering (here considering only surface scattering) $\rho = \rho_d + \rho_i$ = total residual resistivity. When d decreases, ρ_d increases. If S_d does not change in magnitude and always has the same sign as S_i, then S would increase in magnitude. But, since $S = G_o T$, this means that G_o would also increase in magnitude. "2" can be explained as follows. When a sample is thin, electrons and phonons are scattered from the surface more often, phonon drag (both normal and Umklapp) gets weaker, and the magnitudes of B* and C* get smaller.

Fig. 4-11 shows G data of four K samples with d = 0.1 mm cooled in Ar gas, (ρ data for these samples were

Table 4-4. The coefficients from fits to the G data of thin K samples cooled in He gas

Sample	d(mm)	$G_o(V^{-1})$	$B*(V^{-1}K^{-2})$	$C*(V^{-1}K)$
K-H6a	1.5	-0.075 ± 0.015	-0.484 ± 0.005	6200 ± 140
K-1/2H	0.5	-0.166 ± 0.010	-0.465 ± 0.004	6090 ± 120
K-1/4H3	0.25	-0.301 ± 0.013	-0.418 ± 0.006	5360 ± 160
K-1/4H2a	0.25	-0.302 ± 0.008	-0.382 ± 0.004	4840 ± 110
K-1/4H2b	0.16	-0.322 ± 0.010	-0.329 ± 0.004	4020 ± 100
K-1/10H2a	0.10	-0.488 ± 0.014	-0.257 ± 0.004	3280 ± 100
K-1/10H2b	0.09	-0.483 ± 0.023	-0.251 ± 0.011	3190 ± 220
K-1/10H1b	0.09	-0.487 ± 0.022	-0.255 ± 0.011	3260 ± 210
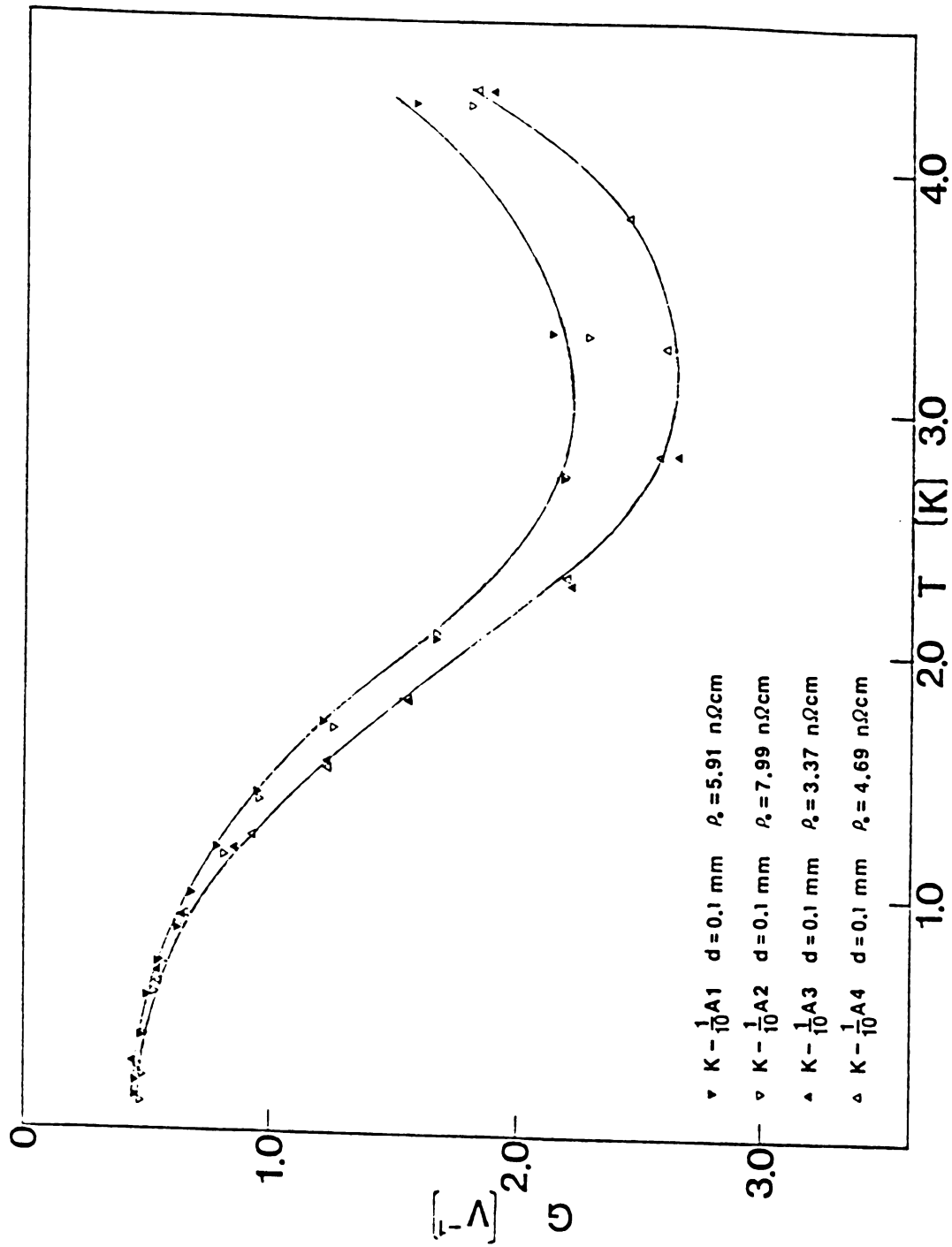
Fig. 4-11. G vs T for thin wires of K cooled in a Ar atmosphere.

▼ K-$\frac{1}{10}$A1 d=0,1 mm ρ_s=5,91 nΩcm

▽ K-$\frac{1}{10}$A2 d=0,1 mm ρ_s=7,99 nΩcm

▲ K-$\frac{1}{10}$A3 d=0,1 mm ρ_s=3,37 nΩcm

△ K-$\frac{1}{10}$A4 d=0,1 mm ρ_s=4,69 nΩcm

shown in Fig. 4-8). These data show similar form to the data shown in Fig 4-10, and can also be well fitted by

$$G = G_o + B*T^2 + (C*/T) \exp(-\Theta*/T).$$

The fits of samples K-1/10A1 and K-1/10A4 are indicated by two solid lines in Fig. 4-11. Table 4-5 shows the coefficients of the fits of each samples with $\Theta* = 23K$ fixed again.

Table 4-5 shows that for four thin samples with d = 0.1 mm cooled in Ar gas, (1) unlike $d\rho/dT$, G_o is almost sample-independent, and is close to the G_o of samples with the same size cooled in He gas; (2) B* and C* show sample-dependence, and tend to behave like data for samples in He of slightly larger diameter. The reasons for (1) and (2) are not yet clear. A trial explanation is as follows. As described in section 4.2.1, for $d\rho/dT$, more impurity scattering and less diffuse surface scattering of electrons would make the samples behave like one with thicker size. For G_o, things are different: from the Gorter-Nordheim rule (Eqn. 2-45)

$$S = \frac{1}{\rho_o} (\rho_i S_i + \rho_d S_d).$$

More impurity scattering will bring ρ_i and ρ_o up, and less diffuse surface scattering will bring ρ_d and ρ_o down. Both together could keep S unchanged, and thus G_o unchanged. For phonon drag, more impurity scattering of both electrons and

Table 4-5. The coefficients from fits to the G data of thin K samples cooled in Ar gas

Sample	d(mm)	$G_o(V^{-1})$	$B*(V^{-1}K^{-2})$	$C*(V^{-1}K)$
K-1/10A1	0.10	-0.445 ± 0.027	-0.259 ± 0.010	3500 ± 240
K-1/10A2	0.10	-0.466 ± 0.019	-0.261 ± 0.007	3280 ± 150
K-1/10A3	0.10	-0.419 ± 0.034	-0.341 ± 0.011	4490 ± 220
K-1/10A4	0.10	-0.465 ± 0.041	-0.312 ± 0.011	4070 ± 250

phonons will make phonon drag weaker, and less diffuse surface scattering of electrons will enhance phonon drag, these two factors coming together could explain why B* and C* were unstable, but less unstable than $d\rho/dT$.

Fig. 4-12 shows G data of four K samples with d = 0.10, 0.25 mm cooled in partial vacuum (10 μHg He), (ρ data of these samples were shown in Fig. 4-8). Each set of these data shows a "bump" in the vicinity of 1K. A possible explanation for these bumps was already given in section 4.1.2. For thinner samples the heat conductance is smaller, so a smaller part of the heat generated by the G heater passes through the samples; thus the error in the G calculation (discussed in section 4.1.2) is bigger and brings the data further down in magnitude. Except for the bumps, the shape of these data is similar to that of the data in Fig. 4-10 and Fig. 4-11.

4.2.3 The Thermoelectric Power S

The thermoelectric power S of one K sample (K-1/2H) was measured in this study to find the form of L(T) and the low temperature limit of L(T) = L_o (Eqn. 1.8) in K. The reason for choosing a sample with d = 0.5 mm is as follows. Since S is calculated from $S = V/\Delta T|_{I=0}$, the sample must be thin enough so that its heat conductance is small enough to give an accurately measurable ΔT across the sample with a small enough heat input to keep the sample cold. But if the
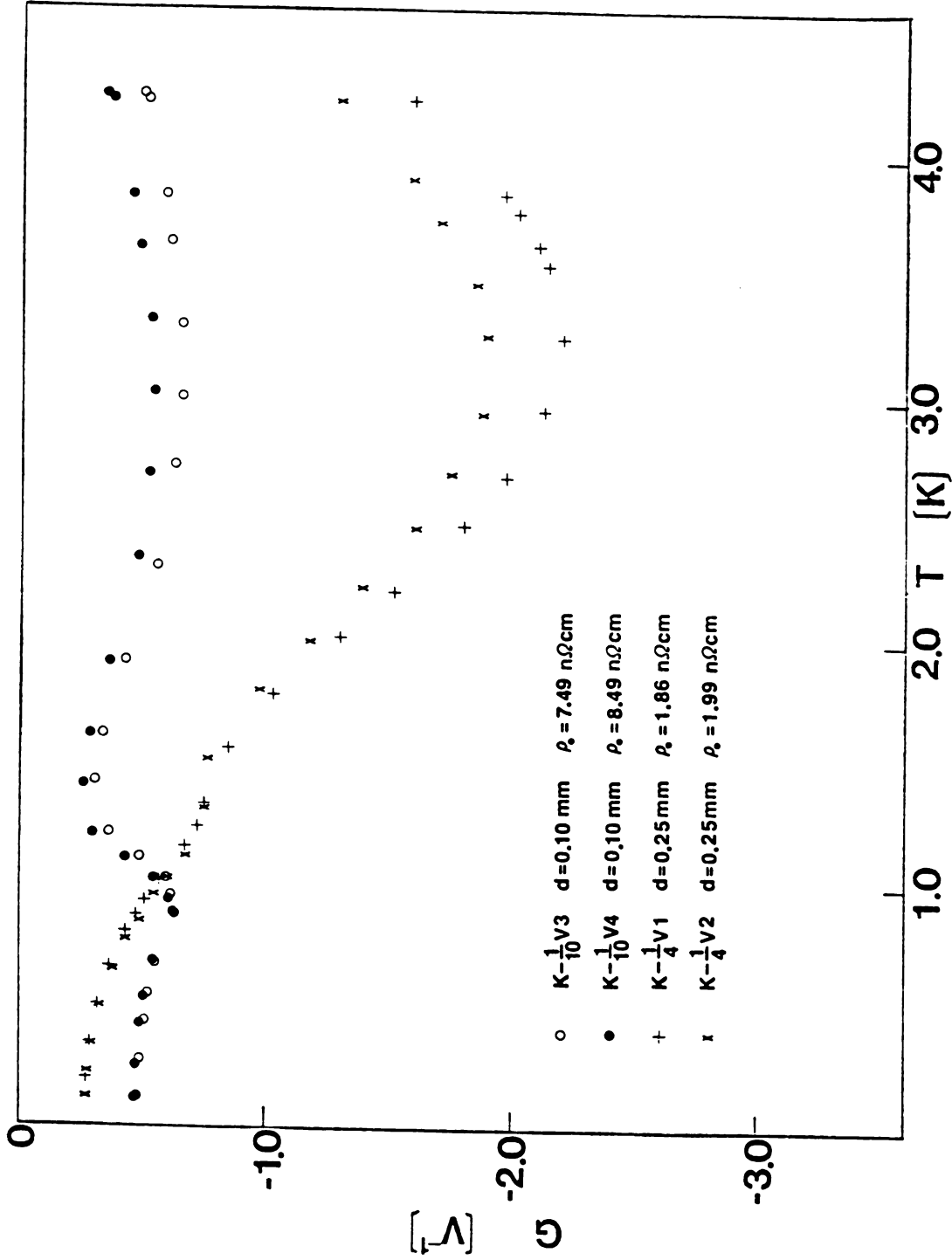
Fig. 4-12. G vs T for thin wires of K cooled in a partial vacuum.

sample is too thin, it would show a strong size-effect. d = 0.5 mm was thin enough, but not too thin.

Fig. 4-13 shows a plot of S versus T. The dashed line in Fig. 4-13 indicates a fit of $S = A'T + B'T^3 + C'e^{-\Theta^*/T}$ (section 2.3.1) with Θ^* fixed as 23K, as used for G data analysis above; the coefficients obtained were: $A' = -0.78 \pm 0.15 \times 10^{-8}$ V^{-1}, $B' = -0.681 \pm 0.034 \times 10^{-8}$ $V^{-1}K^{-2}$, and $C' = 11530 \pm 770 \times 10^{-8}$ $V^{-1}K$. A better fit was found when Θ^* was left as a variable parameter; the coefficients were then: $\Theta^* = 17.4 \pm 0.4K$, $A' = -0.433 \pm 0.081 \times 10^{-8}V^{-1}$, $B' = -0.957 \pm 0.045 \times 10^{-8}$ VK^{-2}, and $C' = 4070 \pm 250 \times 10^{-8}$ $V^{-1}K$. This fit is indicated by the solid curve in Fig. 4-13.

Fig. 4-14 compares measured G with G^* calculated by $G^* = S/L_0T$. A divergence occurs when T > 1K, this implies the temperature-dependence of L (see section 1.1) for K at T>1K. In order to see the form of L(T) more clearly, we plot $L(T)/L_0$ versus T in Fig. 4-15. The values of $L(T)/L_0$ were obtained from

$$G^*/G = (S/L_0T)/(S/L(T)T) = L(T)/L_0.$$

In Fig. 4-15, one can see $L(T) \approx L_0$ only for T < 1K. From about 1K up to about 4K, L(T) decreases with increasing temperature. Each value of $L(T)/L_0$ in Fig. 4-15 was checked by the Wiedemann-Franz Law as follows.
Since,

$$\dot{Q} = \kappa A \Delta T/\ell, \quad R = \rho\ell/A, \quad \text{and} \quad \kappa\rho/T = L(T) \quad \text{(section 1.1)};$$
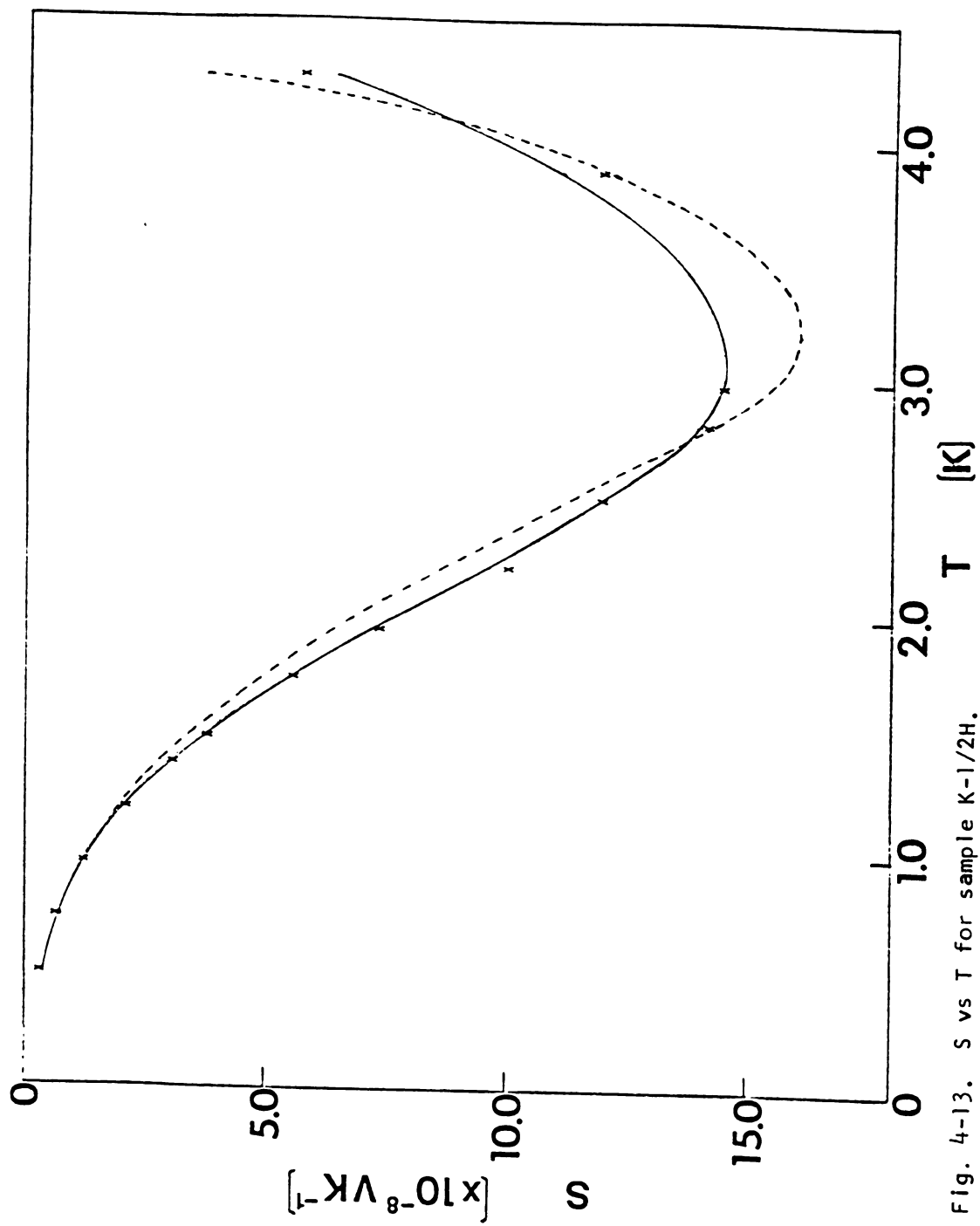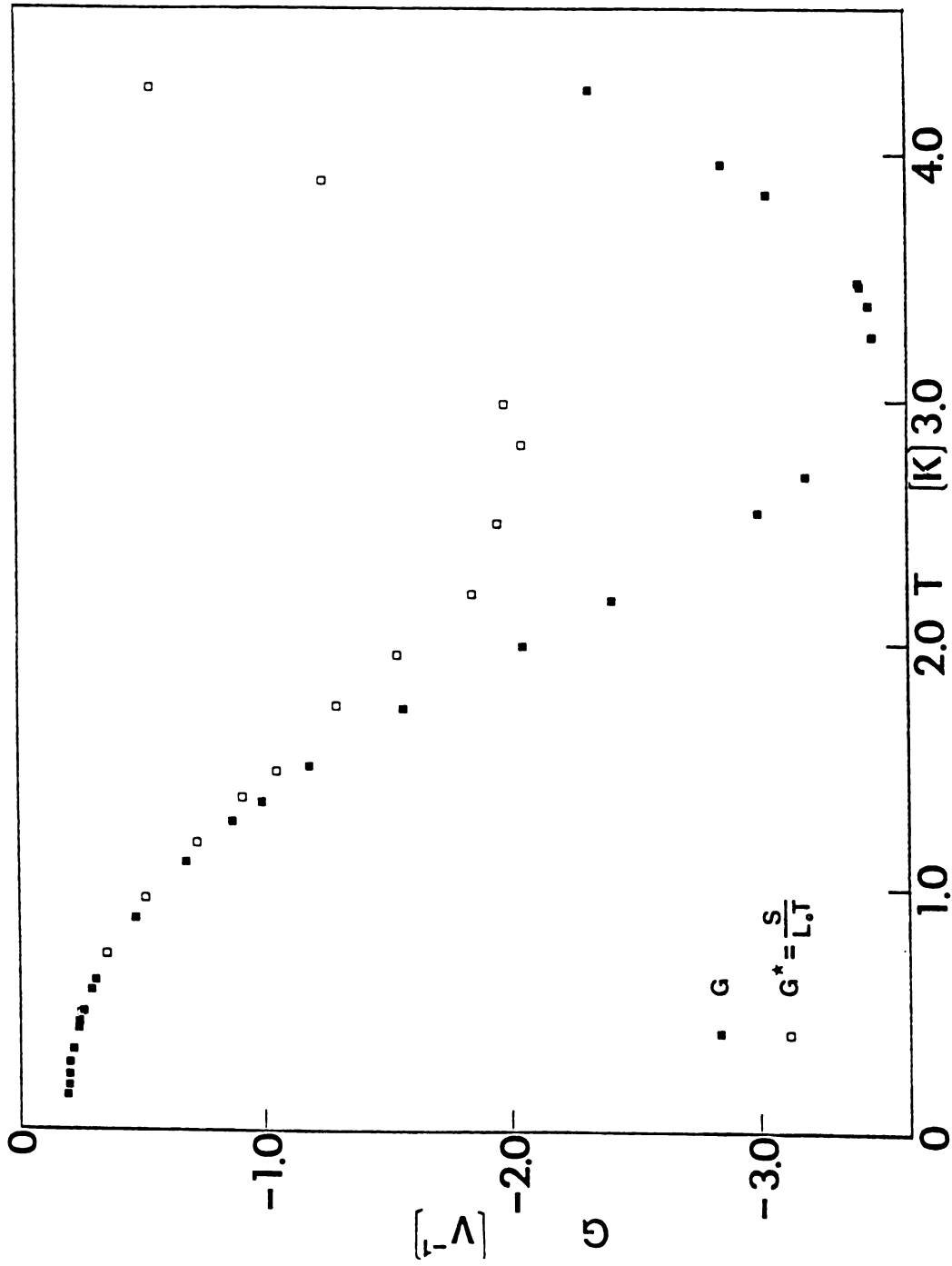
Fig. 4-13. S vs T for sample K-1/2H.

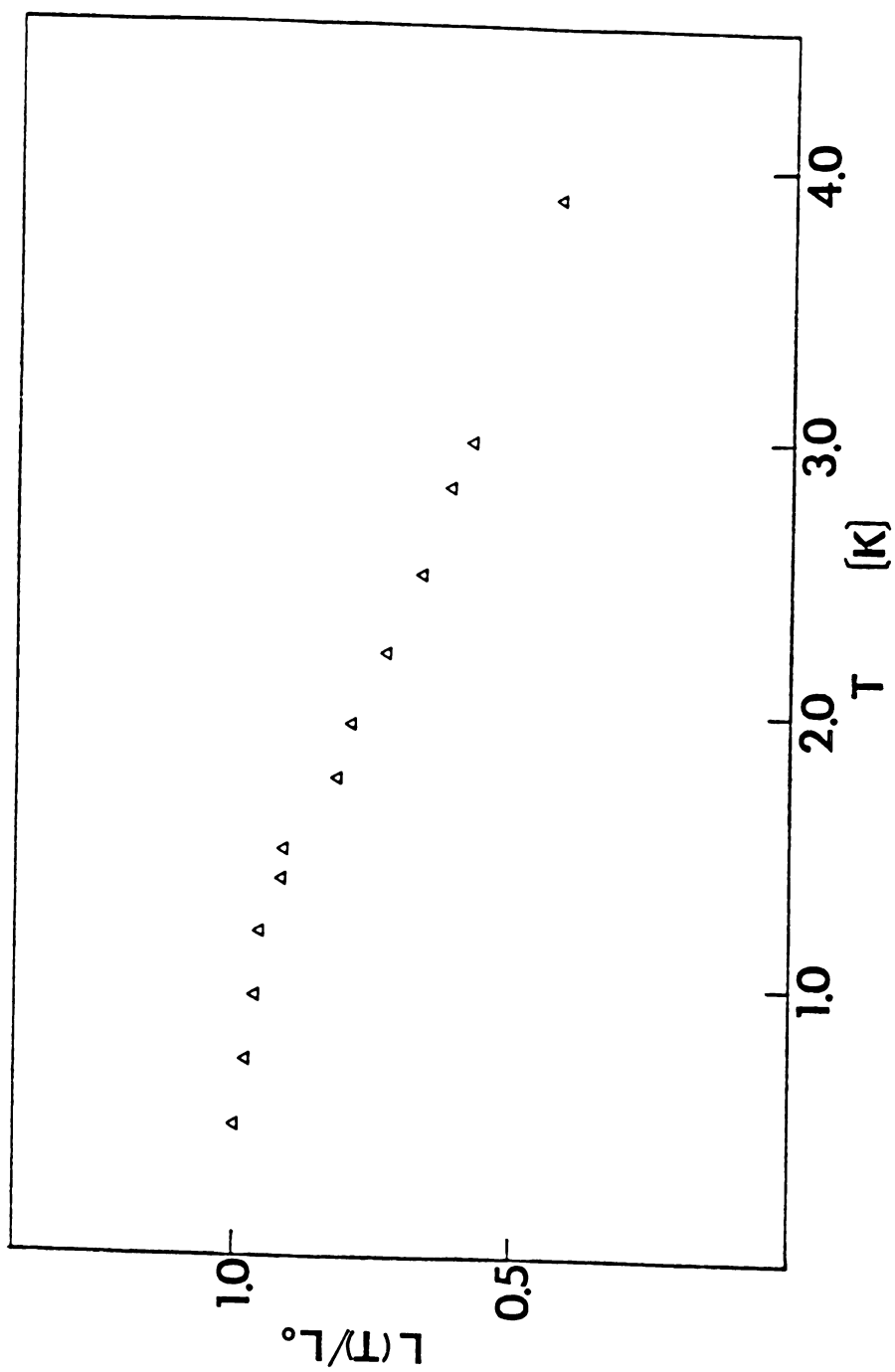Fig. 4-14. G and G*(= S/L$_o$T) vs T for sample K-1/2H.

Fig. 4-15. L(T)/L$_o$ vs T for sample K-l/2H.

so,

$$\dot{Q}R/T\Delta TL_O = \kappa\rho/TL_O = L(T)/L_O,$$

where $\dot{Q}$ can be calculated by $\dot{Q} = R_G I_G^2$ as mentioned above.
Table 4-6 compares two sets of values of $L(T)/L_O$, calculated
from G*/G and from the Wiedemann-Franz Law. One can see
these two sets of $L(T)/L_O$ are very close to each other.

4.3 NOMINAL SINGLE-CRYSTAL K SAMPLE

4.3.1 The Resistivity

As mentioned above, in an attempt to get a longer mean-
free-path of electron-impurity scattering, so as to see
whether the size-effect could be observed in a thicker
sample, we tried to make and measure a "nominal" single-
crystal K sample with d = 1.5 mm: sample K-S. The word
"nominal" is used here because, since only one X-ray spot on
the sample was tested, the verification of the whole sample
as a single crystal was not established (section 3.4).
Sample K-S had one of the lowest ρ_O's and one of the largest
RRR's for K in this study (ρ_O = 0.92 nΩcm, RRR = 6150) (the
details of its characteristics are given in Table 3-5).
However, the mean-free-path of K-S was not much longer than
the previous ones; l_{ei} = 0.5 mm was obtained from Eqn.
(4-1), still much smaller than d (d = 1.5 mm). As expected,
no clear size-effects were seen in this sample.

Fig. 4-16 shows a plot of $d\rho/dT$ versus T. The data at
around T = 0.7 K look a little low, but not low enough to

Table 4-6. $L(T)/L_o$ values calculated from G*/G and from
Wiedemann-Franz Law for sample K-1/2H

T(K)	$L(T)/L_o$ from G*/G	$L(T)/L_o$ from W-F Law
0.482	1.00	1.00
0.714	0.98	0.98
0.948	0.96	0.96
1.182	0.95	0.94
1.368	0.91	0.91
1.483	0.91	0.89
1.741	0.81	0.81
1.941	0.76	0.78
2.201	0.76	0.75
2.490	0.67	0.66
2.808	0.62	0.61
2.977	0.58	0.56
3.874	0.42	0.40
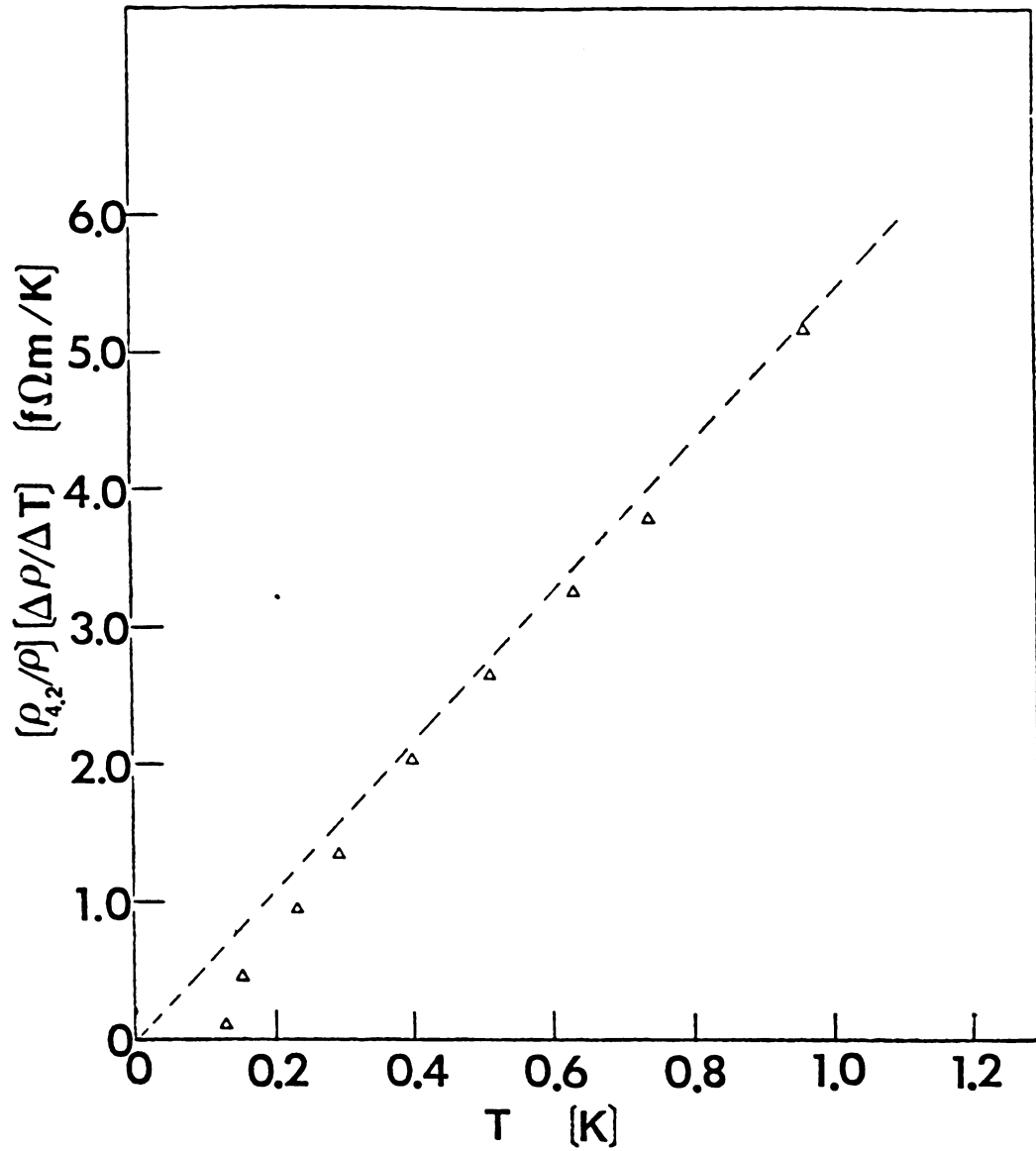
Fig. 4-16. $(P(4.2K)/P)(\Delta P/\Delta T)$ vs T for the nominal single crystal
K sample.

show clear evidence of size-effects; while the data at T <
0.2 K show a clear turn down. In order to see the anomalous
turn down, $d\rho/TdT$ is plotted versus T in Fig. 4-17. It is
clearly seen in Fig. 4-17 that the anomalous turn down
occurs when T < 0.3 K. This anomalous turn down is
completely different from the size-effects described above.
In section 4.4 we will see similar turn-downs for K samples
encased in polyethylene tubes. Further discussion of this
turn-down will be given in section 4.4.

4.3.2   The Thermoelectric Ratio G

G measurements were made for sample K-S from about 4.2K
down to about 70 mK. Fig. 4-18 shows a plot of G versus T
for samples K-S ($\triangle$) and, for comparison, K-H6a (x) which was
plotted in Fig. 4-3). These two sets of data almost overlap
each other for T > 1.5 K. For T < 1.5 K, the data of sample
K-S stay slightly less negative than K-H6a, a result
consistent with the Gorter-Nordheim rule (Eqn. 2-41) (see
section 4.2.2).

4.4   HIGH-PURITY K SAMPLES IN CONTACT WITH PLASTICS OR OIL

4.4.1   The Resistivity

As mentioned in section 1.2.1, van Kempen et al. (ref.
14) and Greenfield et al. (ref. 18) measured ρ of high-
purity K samples inside polyethylene tubes down to about 1K.
The details of the results from these two groups are given
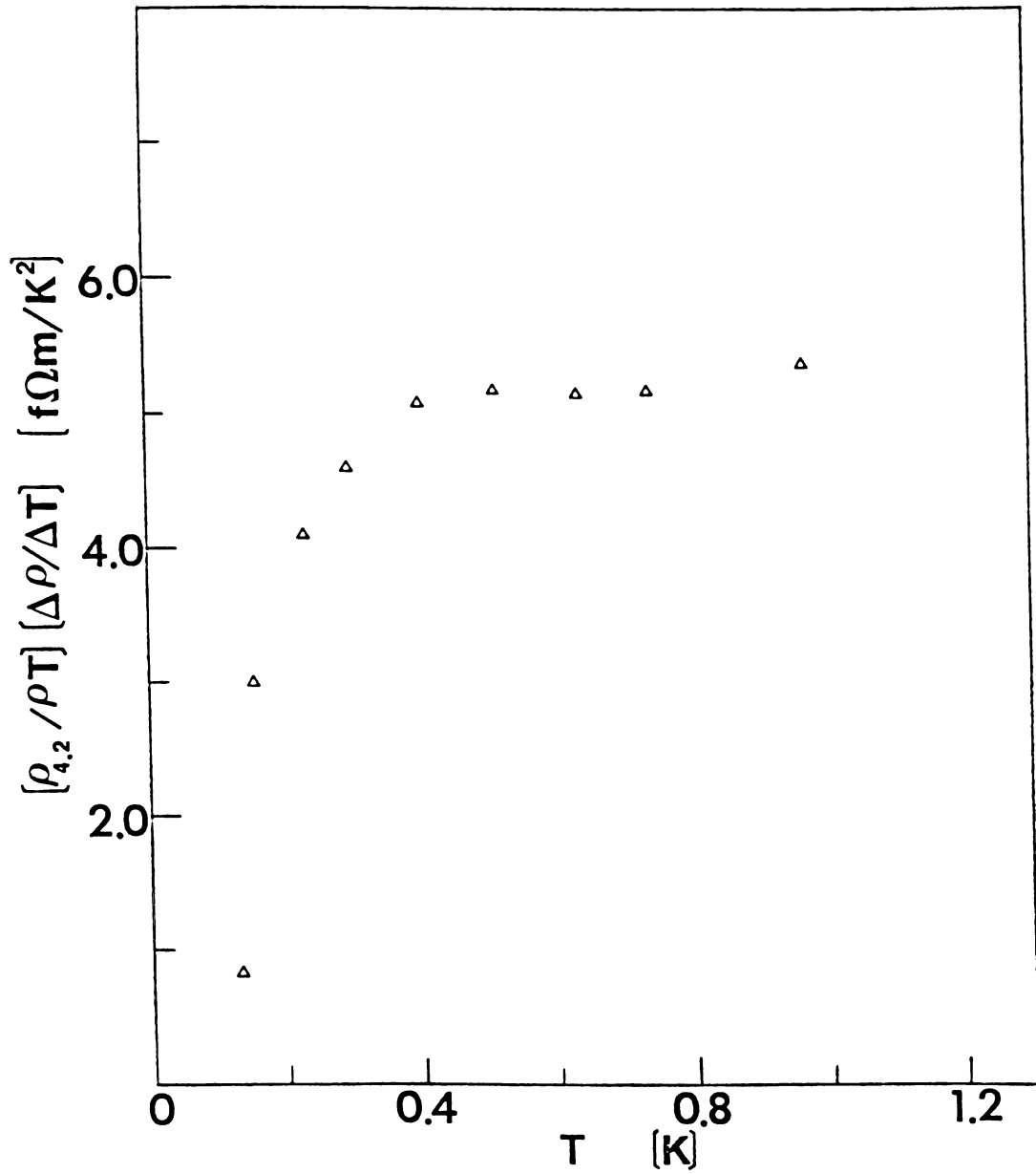in section 1.2.1. To investigate further the variations in

Fig. 4-17. $(\rho(4.2K)/\rho T)(\Delta\rho/\Delta T)$ vs T for the nominal single crystal K sample.
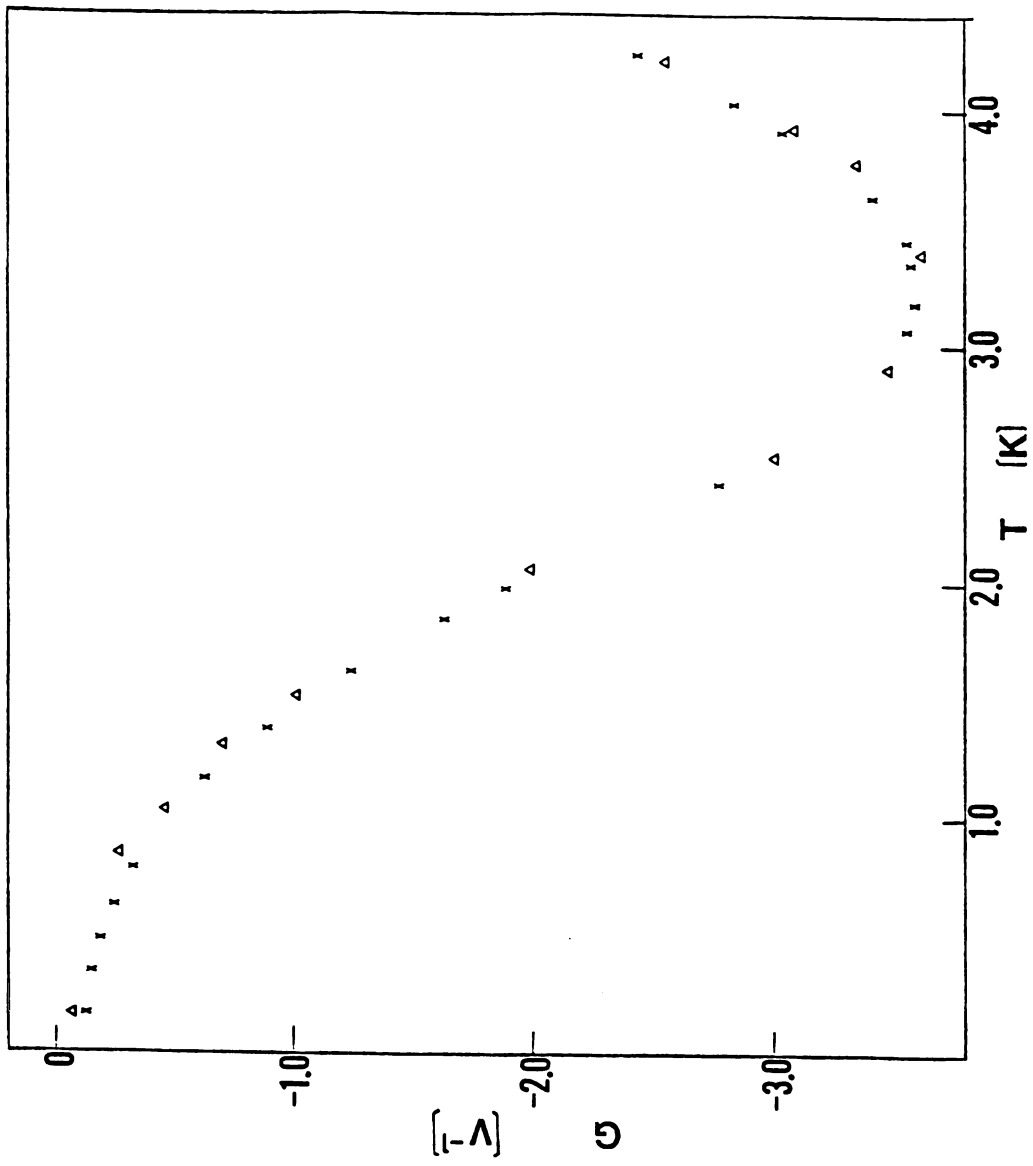
Fig. 4-18. G vs T for the nominal single crystal K sample.

magnitude of the T^2 coefficient reported by both of them, we measured four pure K samples clad in polyethylene tubes down to 0.07K. To test for annealing effects, each sample was measured several times, with intervening anneals for varying periods of time at room temperature under Ar gas, He gas, or partial vacuum. Sample K-PH1 was in a 1.6 mm dia polyethylene tube and was measured 5 times under He gas and partial vacuum. After the second measuring run it was taken out of the sample can. It was remounted just before the third run with a new bare K sample as the reference. Sample K-PH2 was in a 0.9 mm dia polyethylene tube and measured 4 times under He gas with a reference K sample inside a 1.5 mm dia teflon tube. After the third run, one of its connections broke and the sample can was opened and the sample repaired. It was remounted just before the fourth run using the same reference sample. Samples K-PA1 and K-PA2 were in 0.9 mm dia and 1.6 mm dia polyethylene tubes respectively, and were measured concurrently 5 times under Ar gas. To test for the rolling effect reported by Greenfield et al. (ref. 18), both of these samples were taken out of the sample can after the third run, rolled, left at room temperature for about 20 hours, and then remounted just before the fourth run. After the fourth run, both samples were again taken out of the sample can, and later remounted for the fifth run. The details of the preparation of these samples are given in section 3.4. The details of the characteristics of each sample in each measurement are given in Table 3-5.

Fig. 4-19 and Fig. 4-20, in different scales, show a normalized $d\rho/TdT$ (ref. 59) plotted versus T for five runs of sample K-PH1. Similarly, Fig. 4-21 and Fig. 4-22 for four runs of sample K-PH2; Fig. 4-23 and Fig. 4-24 for five runs of sample K-PA1; and Fig. 4-25 and Fig 4-26 for five runs of sample K-PA2. For comparison, the data of sample K-S plotted in Fig. 4-17 were added in Fig. 4-19; and the data of samples 2a, 2b, 2c from van Kempen et al., which were also measured under He gas, are added in Fig. 4-21. At T > 1.1K our data in Fig. 4-21 are consistent with the data for samples 2a and 2b of van Kempen et al., which had ρ_o's comparable to ours. Sample 2c of van Kempen et al. had a lower ρ_o, and its data stay well below our data (see Fig. 4-21). The dashed curve in each of these figures shows, for comparison, typical behavior of a free-hanging, bare, high-purity, thick K sample (section 4.1.1). At T < 1K, the data presented in these figures, including the data of sample K-S, which was melted in clean paraffin oil during its growth, exhibit similar deviations from the dashed curve. For samples encased in polyethylene tubes, sample annealing at room temperature significantly brings both the normalized value of $d\rho/TdT$ and ρ_o down until $d\rho/TdT$ becomes negative and large. To fully develop the negative deviation requires about 10 days of annealing. The temperature at which $d\rho/dT$ crosses zero corresponds to a resistivity minimum, which in the fully developed samples occurs between 0.3 and 0.5K. When first cooled and measured, the samples appeared to have
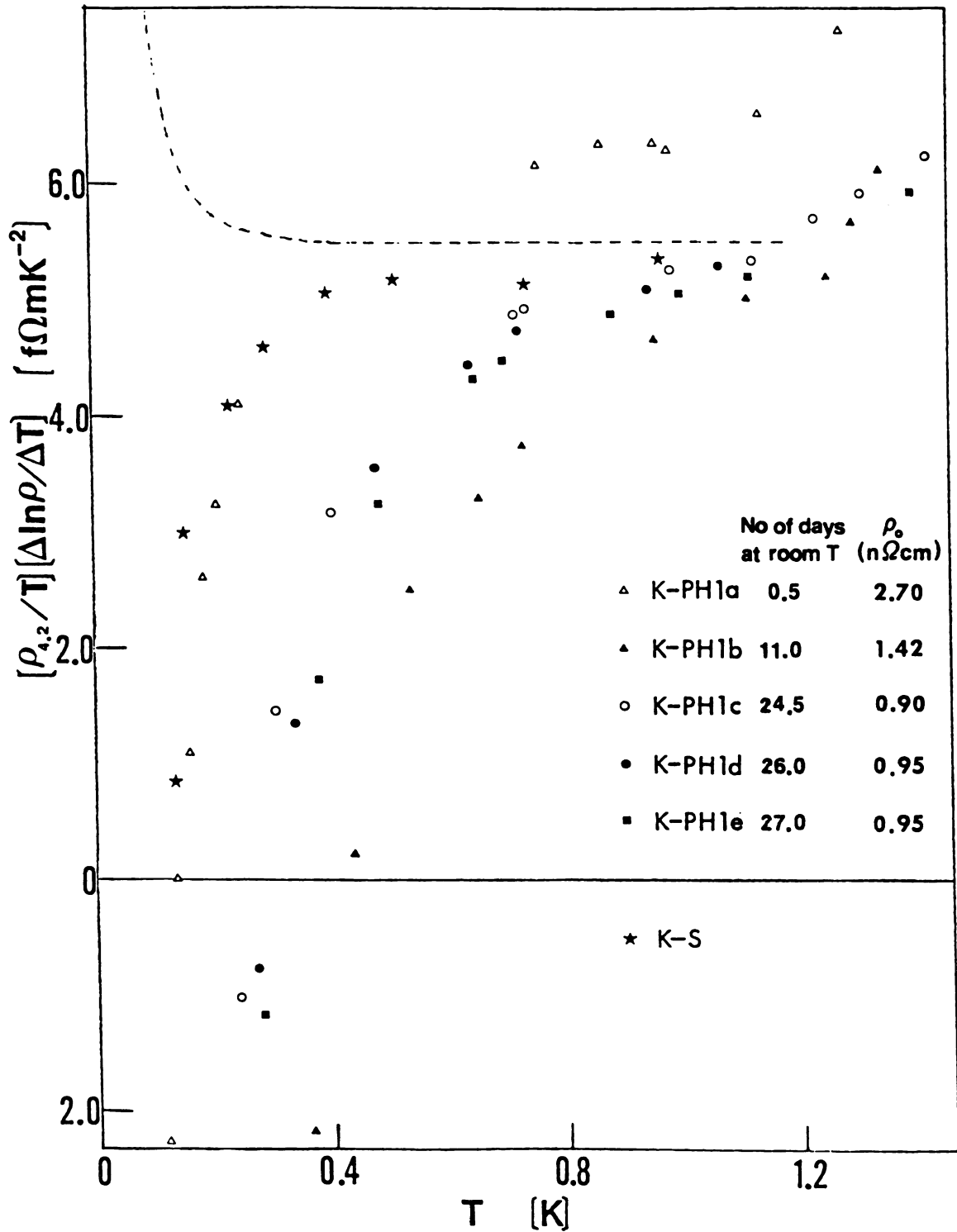
Fig. 4-19. $(\rho(4.2K)/T)(\Delta\ln\rho/\Delta T)$ vs T for sample K-S and five runs of sample K-PH1.

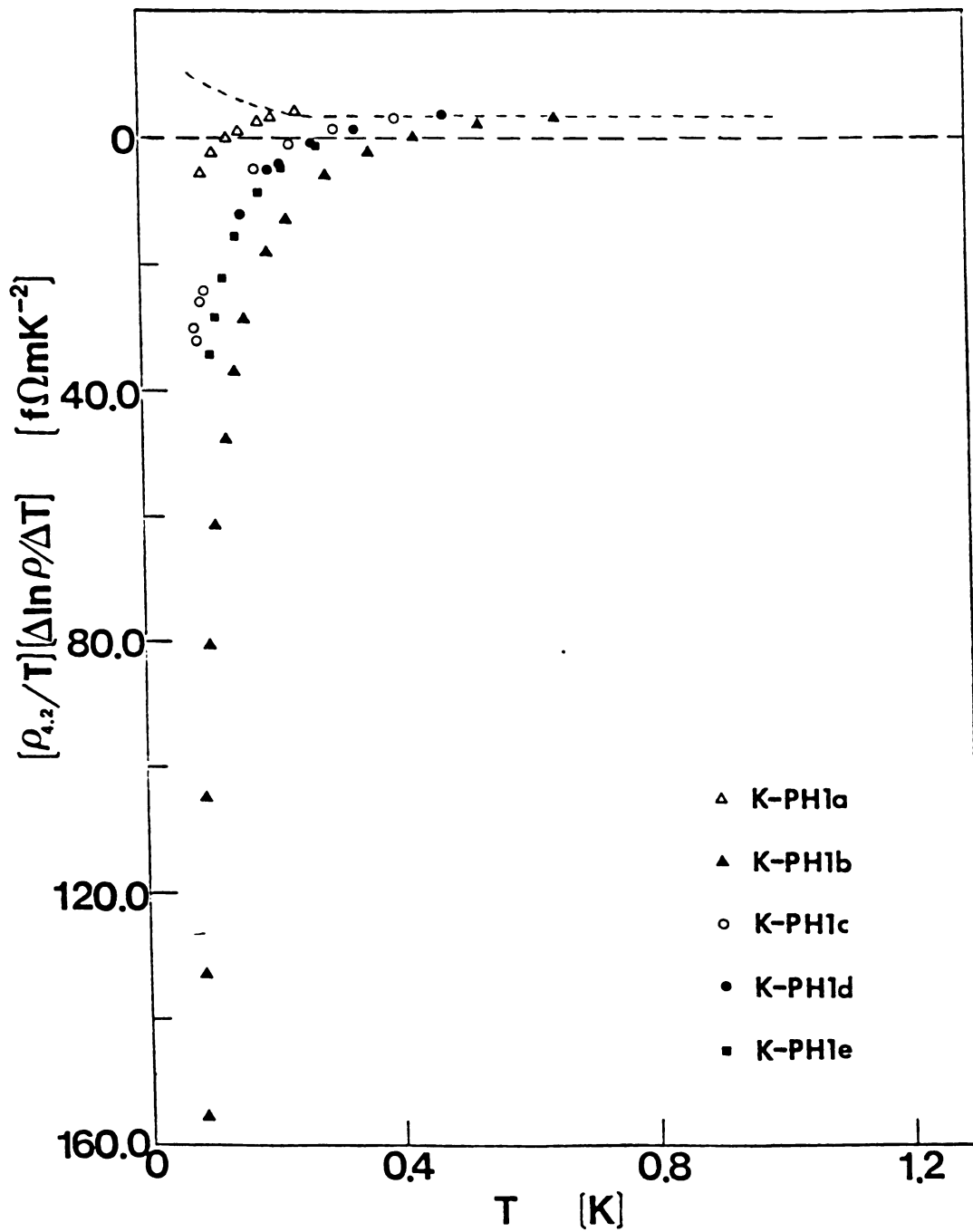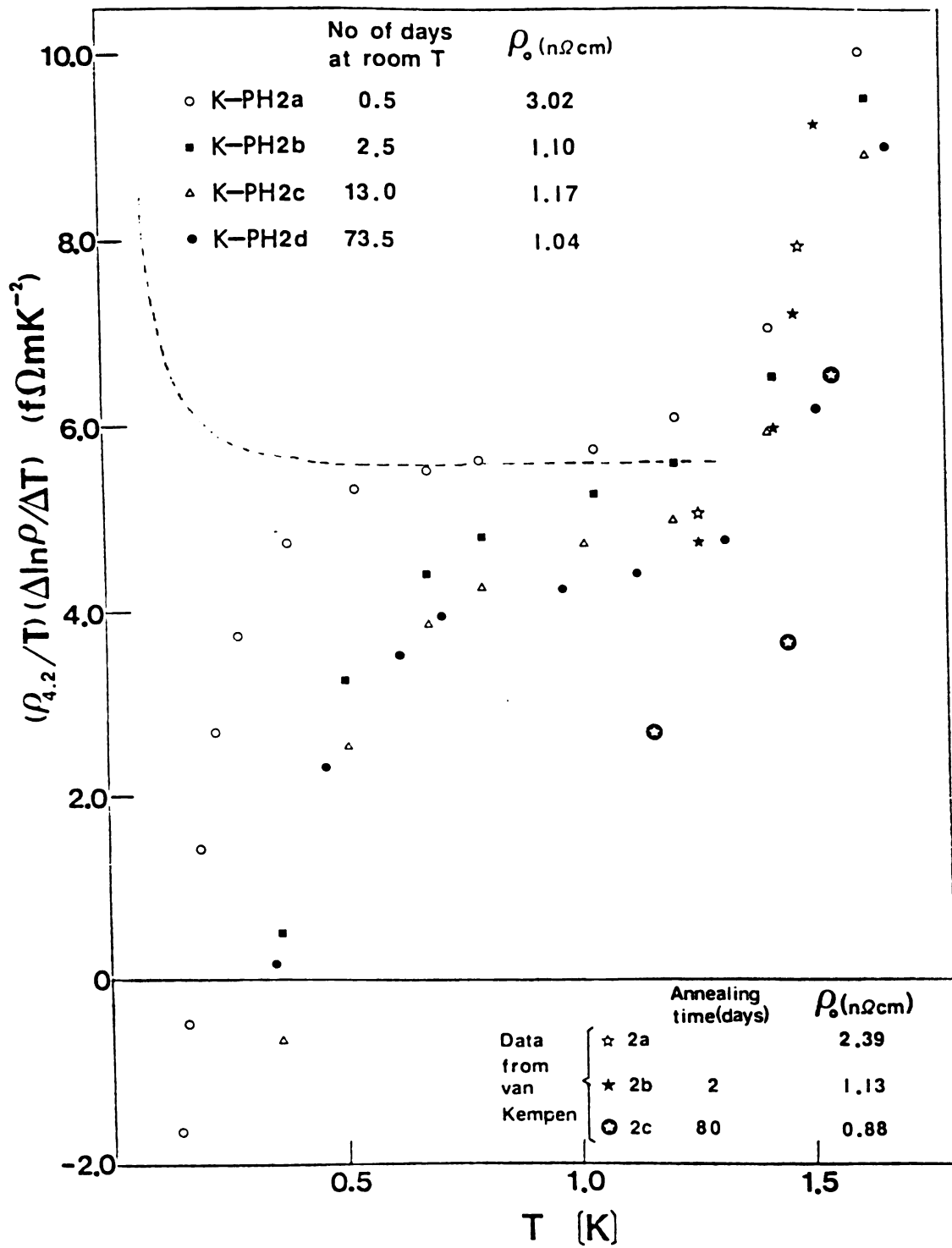Fig. 4-20. A version of Fig. 4-19 to larger scale.

Fig. 4-21. $(P(4.2K)/T)(\Delta\ln P/\Delta T)$ vs T for four runs of sample K-PH2. For comparison, the data of samples 2a, 2b, and 2c of van Kempen et al. are indicated.
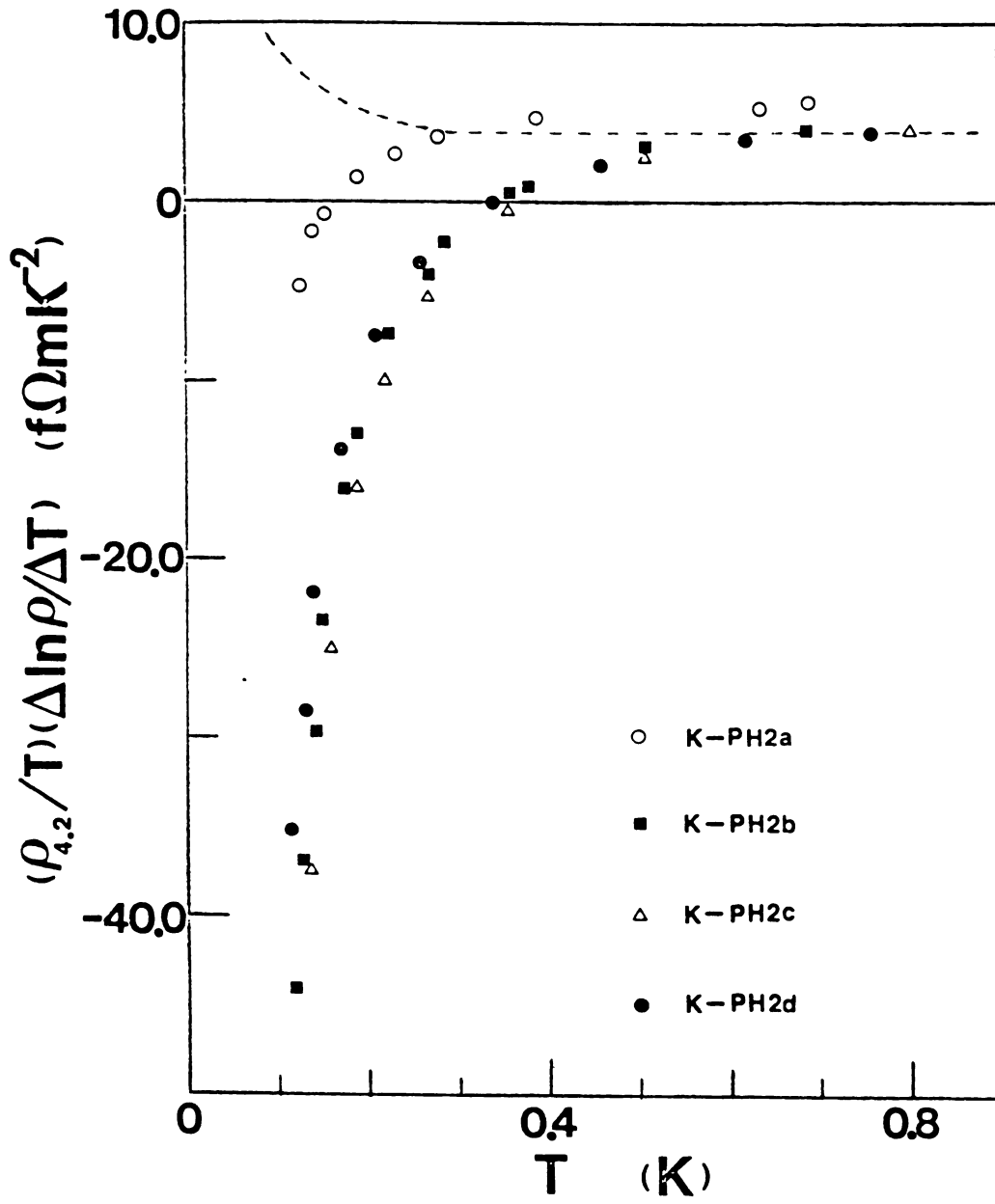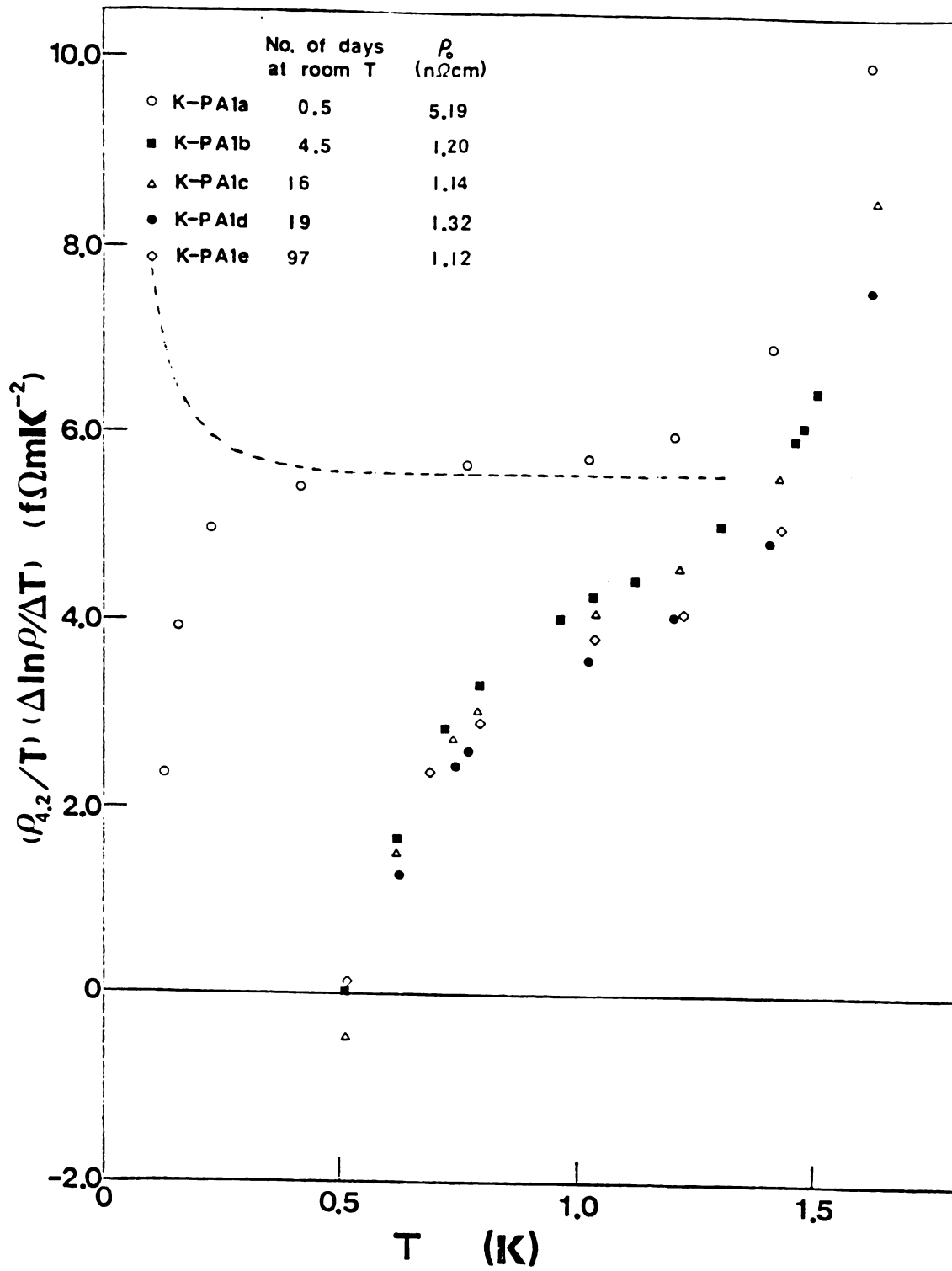
Fig. 4-22. A version of Fig. 4-21 to larger scale.

Fig. 4-23. $(P(4.2K)/T)(\Delta \ln P/\Delta T)$ vs T for five runs of sample K-PA1.

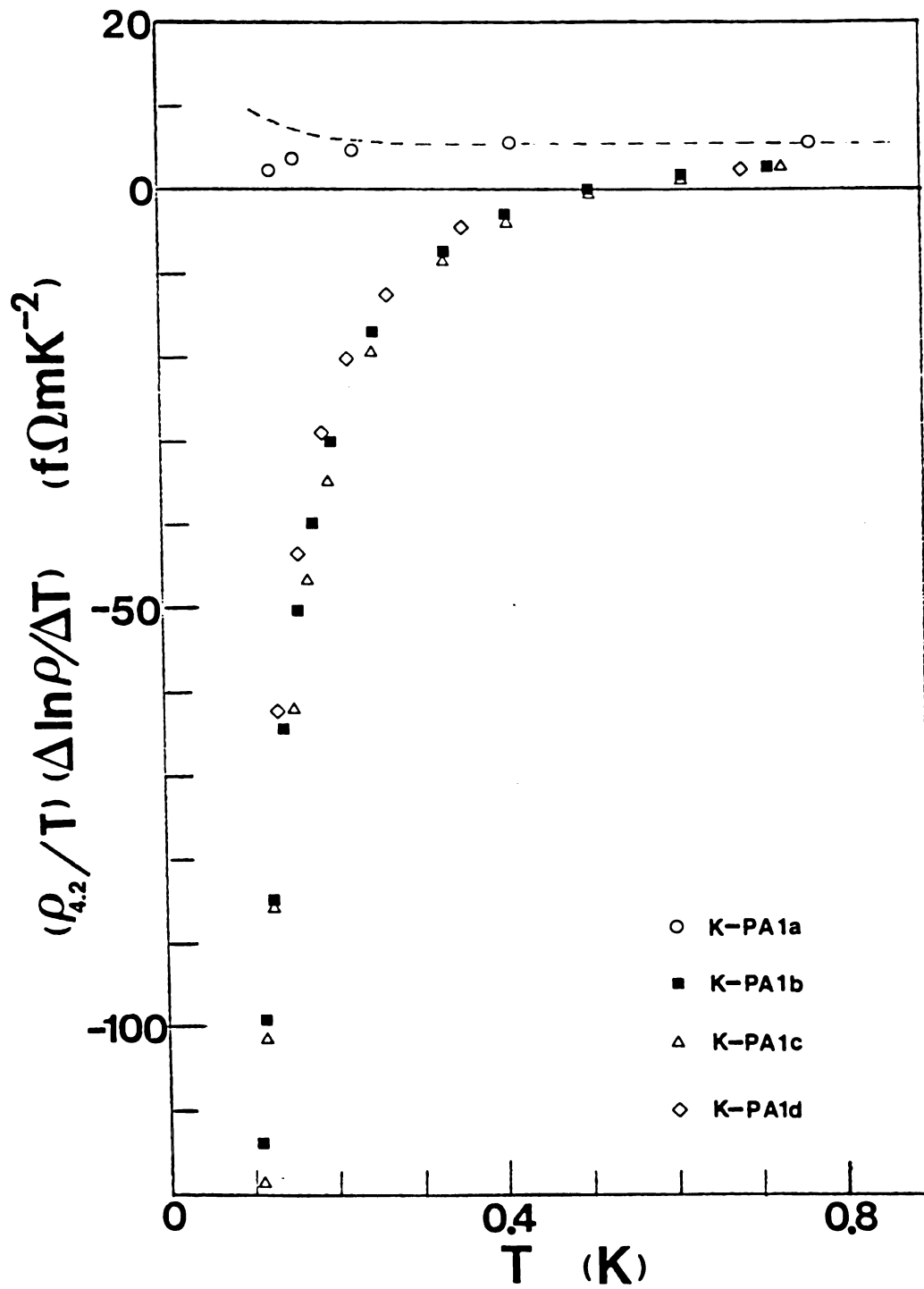Fig. 4-24. A version of Fig. 4-23 to a larger scale.

159
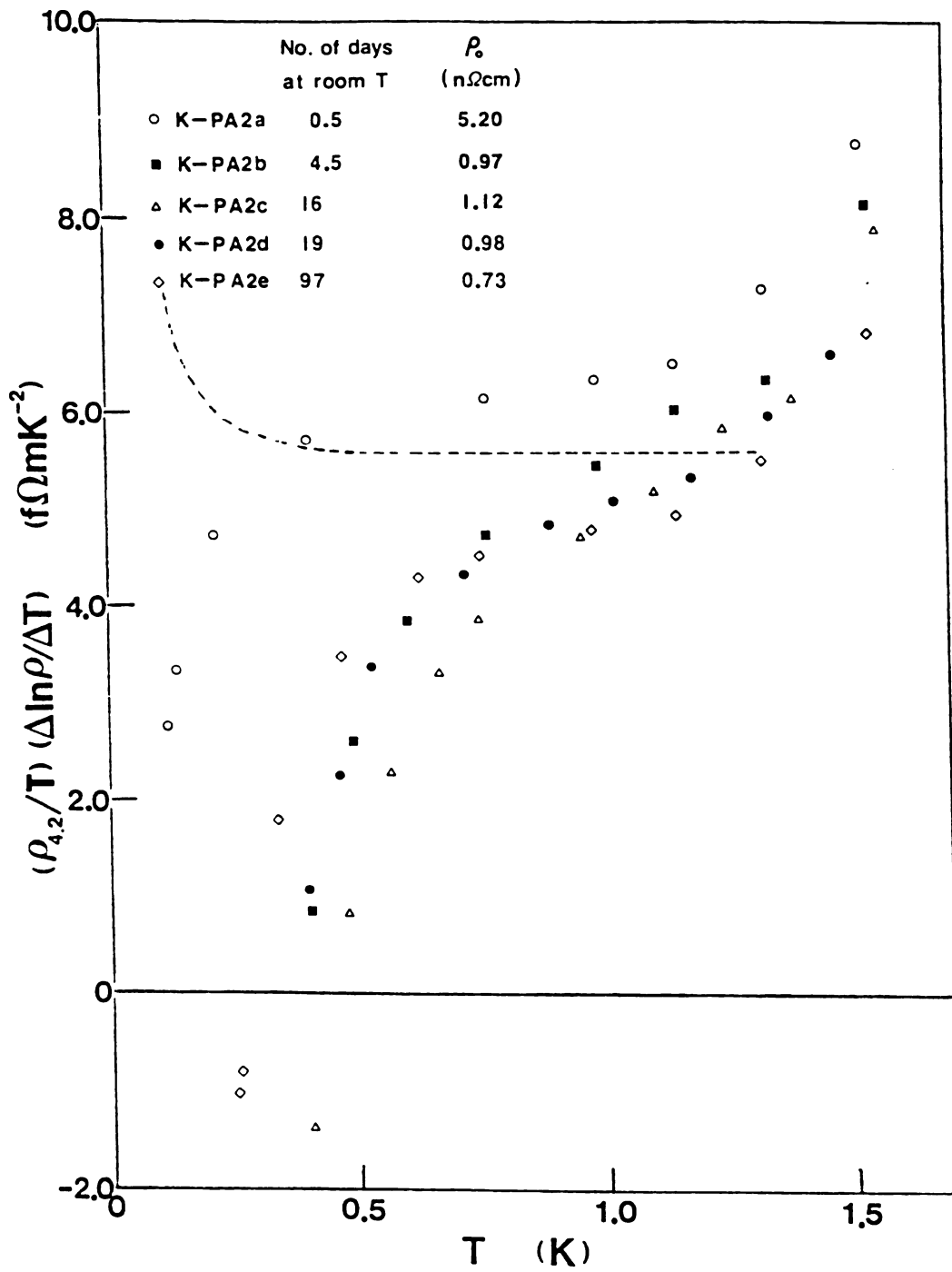

Fig. 4-25. $(P(4.2K)/T)(\Delta\ln P/\Delta T)$ vs T for five runs of sample K-PA2.
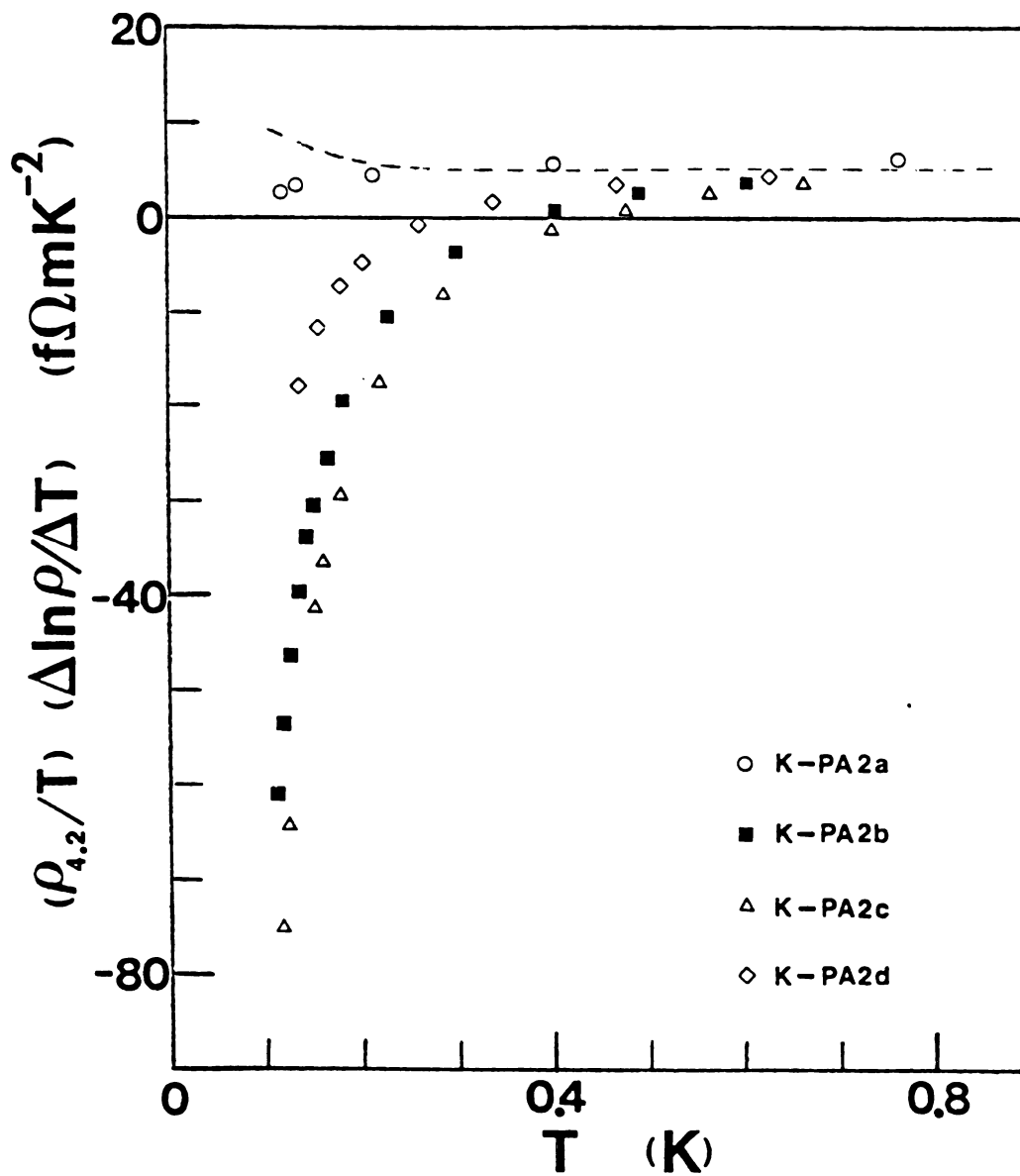
Fig. 4-26. A version of Fig. 4-25 to a larger scale.

a rather large concentration of impurities or defects, as indicated by the relatively large value of ρ_0. About 3 days of room temperature annealing seemed adequate to bring ρ_0 down to its normal value for free-hanging, bare, thick K samples. For reasons not yet clear, sample disturbance during sample remounting at room temperature seemed to bring $d\rho/TdT$ up, particularly for data at low temperature end, but did not affect ρ_0 significantly. The effect of sample rolling was not simple. For K-PAl, after rolling, ρ_0 increased, but $d\rho/TdT$ did not change significantly; while for K-PA2, ρ_0 did not change significantly, but $d\rho/TdT$ increased.

For a possible Kondo effect, the electrical resistivity at low enough temperature is expected to have the form $\rho = \rho_0 + AT^2 - B\ln T$ (section 2.2.7). Thus, $d\rho/TdT = 2A - BT^{-2}$. In this case, a plot of $d\rho/TdT$ versus T^{-2} should be a straight line of negative slope $-B$ and with an intercept of $2A$ at $T^{-2} = 0$. Figures 4-27, 4-28, and 4-29 show plots of $d\rho/TdT$ versus T^{-2} for samples K-PH1 and K-PH2, K-PA1 and K-PA2 respectively. All the data in these figures are well fitted by $d\rho/TdT = 2A-BT^{-2}$, as indicated by the broken lines. It is also clearly seen in these figures that sample annealing at room temperature enhances the effect (brings the magnitude of coefficient B up) while sample disturbance appears to weaken the effect (brings the magnitude of B down). This can also be seen in Table 4-7.
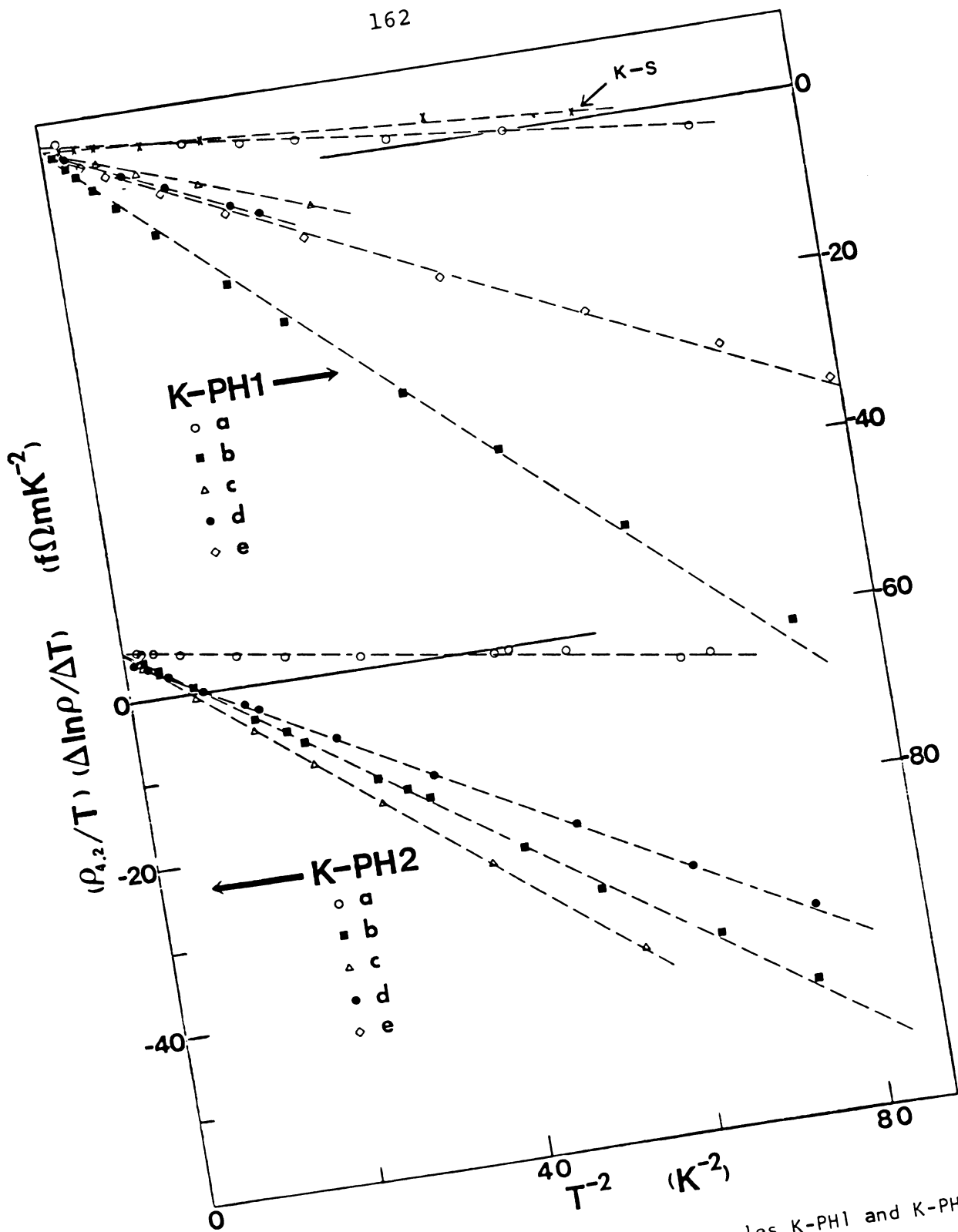
Fig. 4-27. $(\rho(4.2K)/T)(\Delta \ln \rho / \Delta T)$ vs T^{-2} for samples K-PH1 and K-PH2.

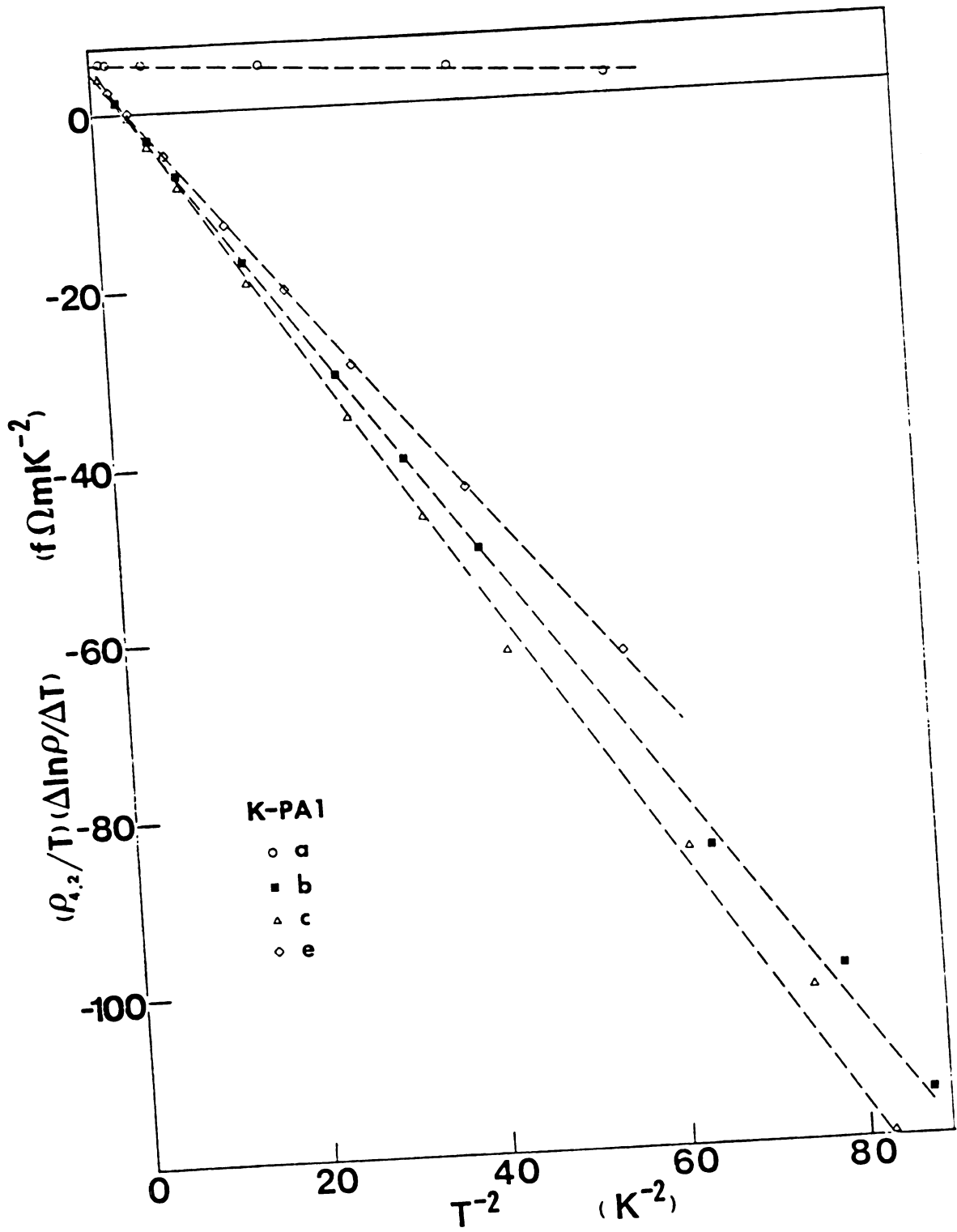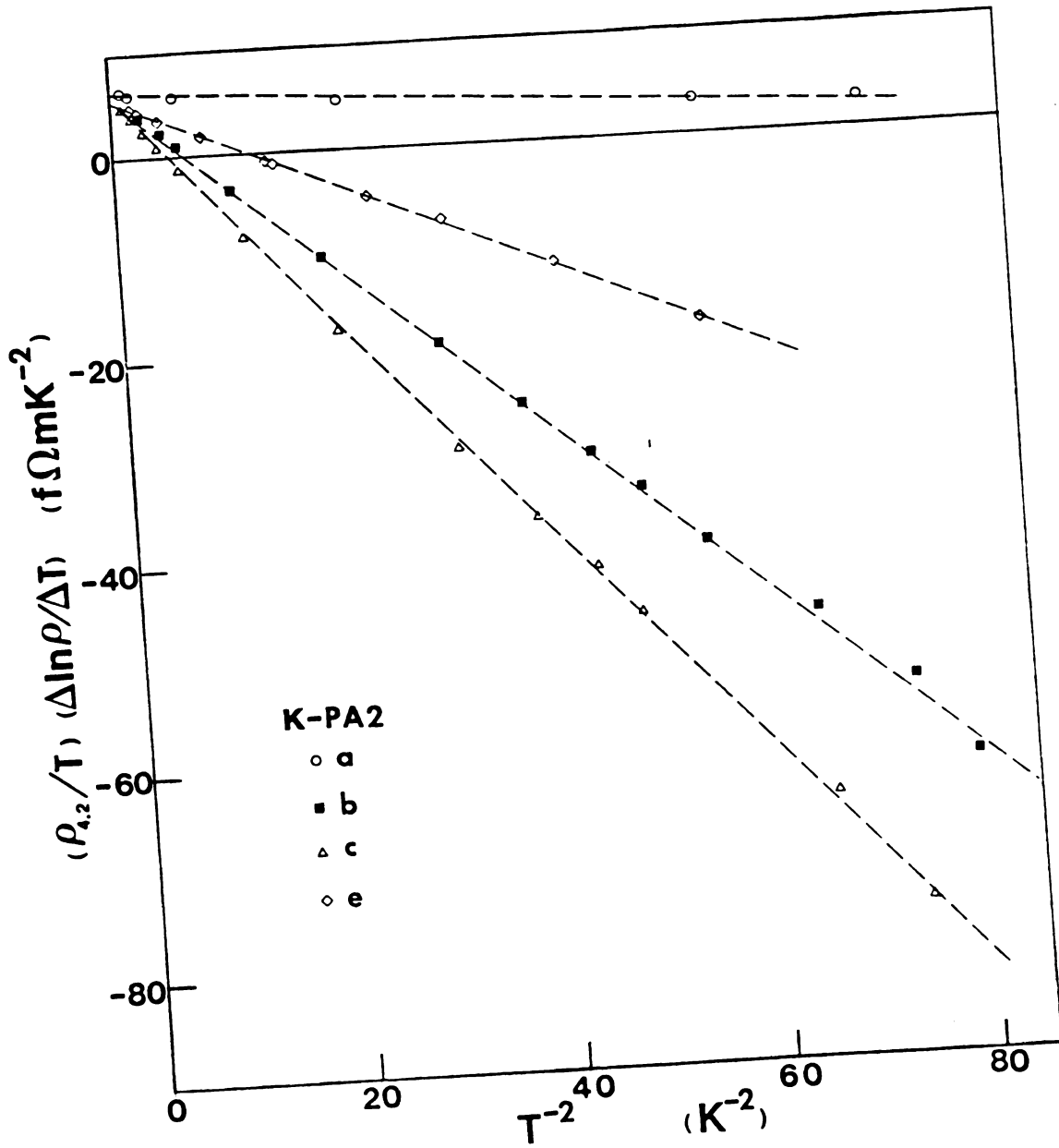Fig. 4-28. $(\rho(4.2K)/T)(\Delta\ln\rho/\Delta T)$ vs T^{-2} for sample K-PA1.

Fig. 4-29. $(\rho(4.2K)/T)(\Delta\ln\rho/\Delta T)$ vs T^{-2} for sample K-PA2.

Table 4-7. The coefficient B from fits to the ρ data of K samples encased in polyethylene tubes

Sample	Gas	d (mm)	No. of days at room T	After sample disturbance	ρ_o (nΩcm)	B (fΩcm)
K-PH1a	10 μHg He	1.6	0.5	Yes	2.97	0.14
K-PH1b	10 μHg He	1.6	11.0	No	1.68	0.90
K-PH1c	He atm.	1.6	24.5	Yes	1.18	0.32
K-PH1d	10 μHg He	1.6	26.0	No	1.20	0.47
K-PH1e	100 μHg He	1.6	27.0	No	1.20	0.47
K-PH2a	He atm.	0.9	0.5	Yes	3.02	0.16
K-PH2b	He atm.	0.9	2.5	No	1.10	0.72
K-PH2c	He atm.	0.9	13.0	No	1.17	0.87
K-PH2d	He atm.	0.9	73.5	Yes	1.04	0.55
K-PA1a	Ar atm.	0.9	0.5	Yes	5.19	0.06
K-PA1b	Ar atm.	0.9	4.5	No	1.20	1.39
K-PA1c	Ar atm.	0.9	16.0	No	1.14	1.50
K-PA1d	Ar atm.	0.9	19.0	Yes	1.32	—
K-PA1e	Ar atm.	0.9	97.0	Yes	1.12	1.23
K-PA2a	Ar atm.	1.6	0.5	Yes	5.20	0.05
K-PA2b	Ar atm.	1.6	4.5	No	0.97	0.83
K-PA2c	Ar atm.	1.6	16.0	No	1.12	1.08
K-PA2d	Ar atm.	1.6	19.0	Yes	0.98	—
K-PA2e	Ar atm.	1.6	97.0	Yes	0.73	0.27

To test whether the effect described above only occurs for samples in contact with polyethylene and samples melted in clean paraffin oil, we measured samples encased in a teflon tube (K-TH1) under He gas, a sample in contact with Kel-F pieces (K-KA) under Ar gas, and a sample coated by cold clean paraffin oil (K-0) under Ar gas. No similar effect was found in any of these three cases. To test whether there is some kind of impurity continuously diffusing from the polyethylene tube into the K sample and causing the "turn down" effect, we measured a bare sample (K-PPA) with d = 1.5 mm and with potential leads encased in polyethylene tubes which were left in room temperature for 1.5 days before the sample was cooled down under Ar gas. No effect was found here either.

Figure 4-30 shows a plot of $d\rho/TdT$ versus T for these last four samples. Sample K-TH1 was measured 4 times concurrently with sample K-PH2 described above. The details of the characteristics of each sample in each run are given in Table 3-5. The data of samples K-KA, K-PPA, and K-0 are similar to those of bare, free-hanging, thick samples. The data of K-TH1a (the first run of sample K-TH1 with d = 1.5 mm and large ρ_0) stay more positive than those of bare thick samples. When the annealing time at room temperature increased, the residual resistivity ρ_0 dropped, and the values of $d\rho/TdT$ shifted downward with maximum shift at temperature around 1K, so that the data no longer formed a horizontal straight line. Since the smallest ρ_0 of sample
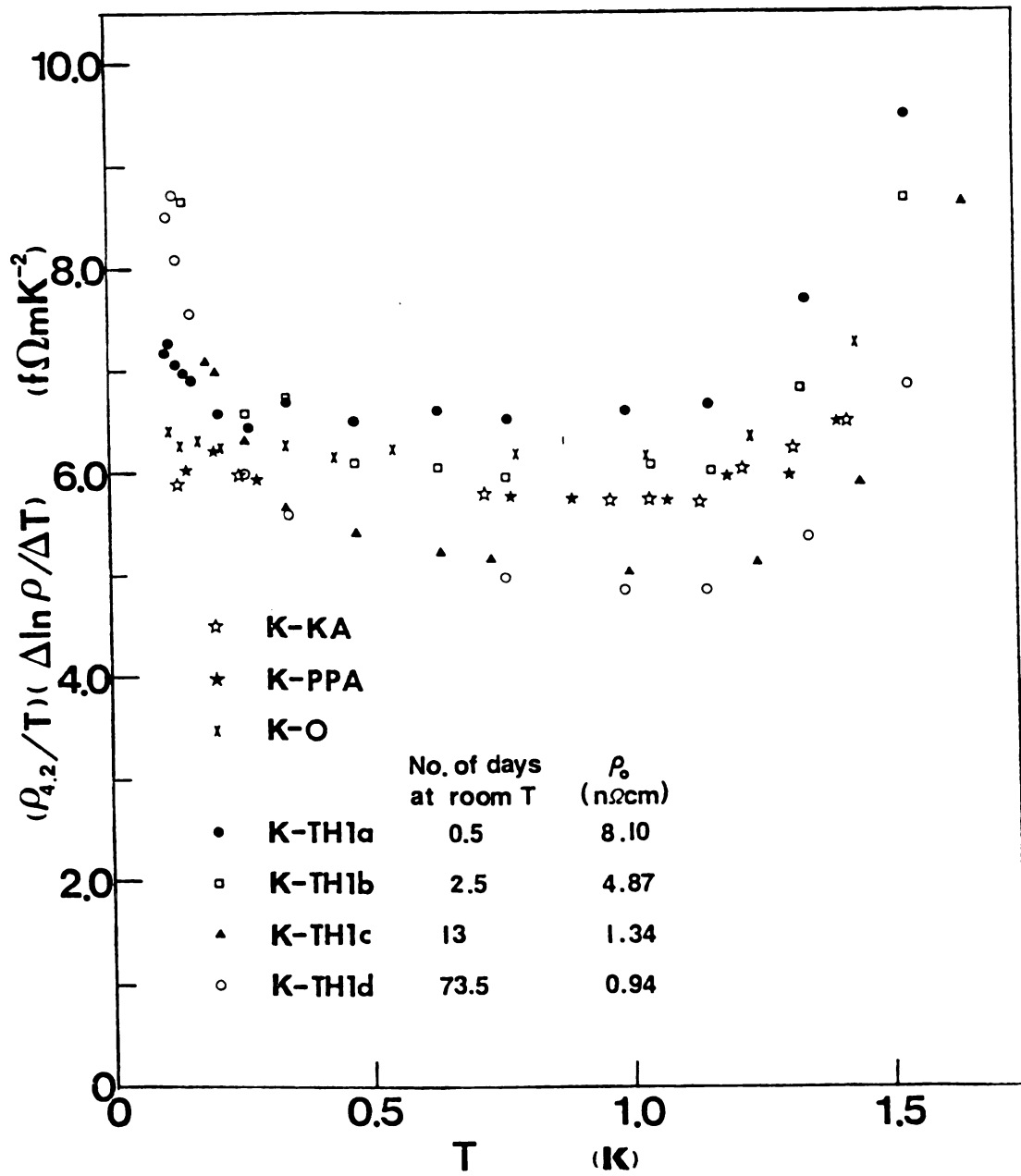
Fig. 4-30. $(P(4.2K)/T)(\Delta \ln P/\Delta T)$ vs T for K samples in contact with other plastics.

K-TH1 was 0.94 nΩcm, which yields an electron mean free path 0.26 mm (Eqn. 4-1) much smaller than the diameter of 1.5 mm, it seems unlikely that the deviation from horizontal line behavior is due to a size effect similar to that seen in the bare thin K samples. The reasons for the deviation from the horizontal straight line are not yet clear.

Further experiments recently done in our lab (ref. 68) showed that application of an average magnetic field of 0.1T longitudinally to polyethylene encapsulated samples shifts the resistance minimum to much lower temperatures. Thus, these samples seem to be exhibiting a Kondo effect due to a magnetic impurity which has an effective magnetic moment equal to or greater than one Bohr magneton. Identification of this magnetic impurity is still in progress. It seems to be a product of the reaction between potassium and hydrocarbons.

4.4.2   The Thermoelectric Ratio G

G measurements were made for each sample above, in each run, from about 4.2 K down to about 70 mk. Fig. 4-31 shows a plot of G versus T for five runs of sample K-PH1; Fig. 4-32 for four runs of sample K-PH2; Fig. 4-33 for four runs of samples K-PA1 and K-PA2. For comparison, the data of a free hanging bare thick sample (K-H6a) shown in Fig. 4-3 are also shown as a broken line in each figure above.

For the samples which have been annealed for only 0.5 days, the plots have the same form as the broken line; the deviations from the broken line, more negative at low
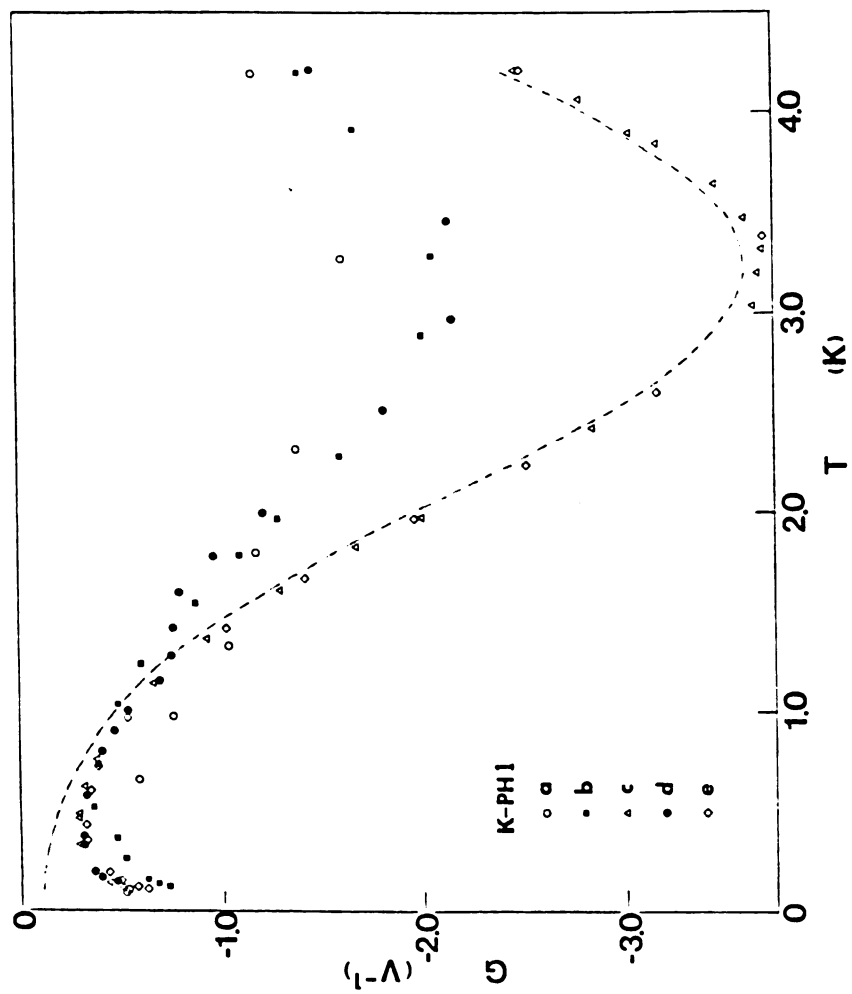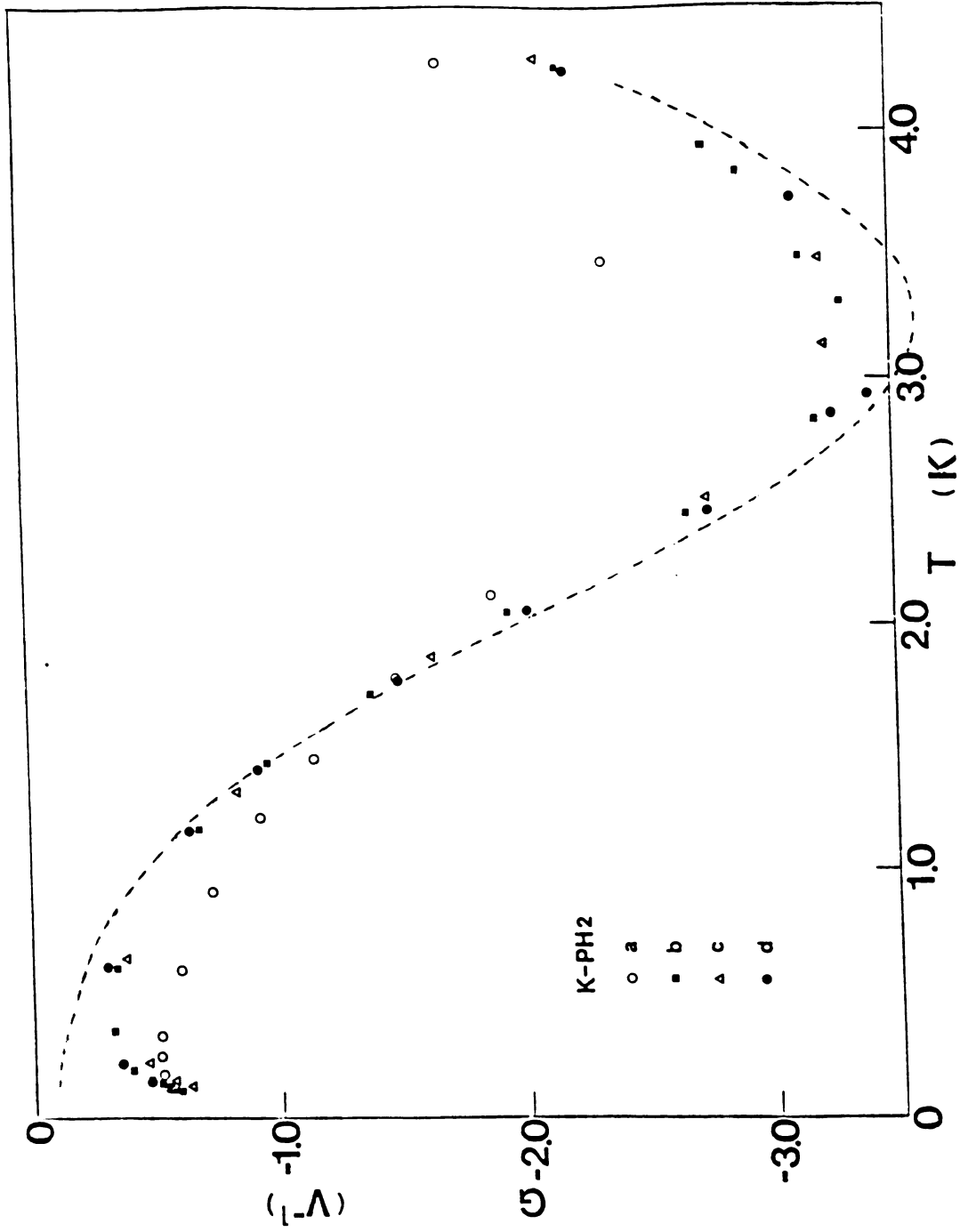
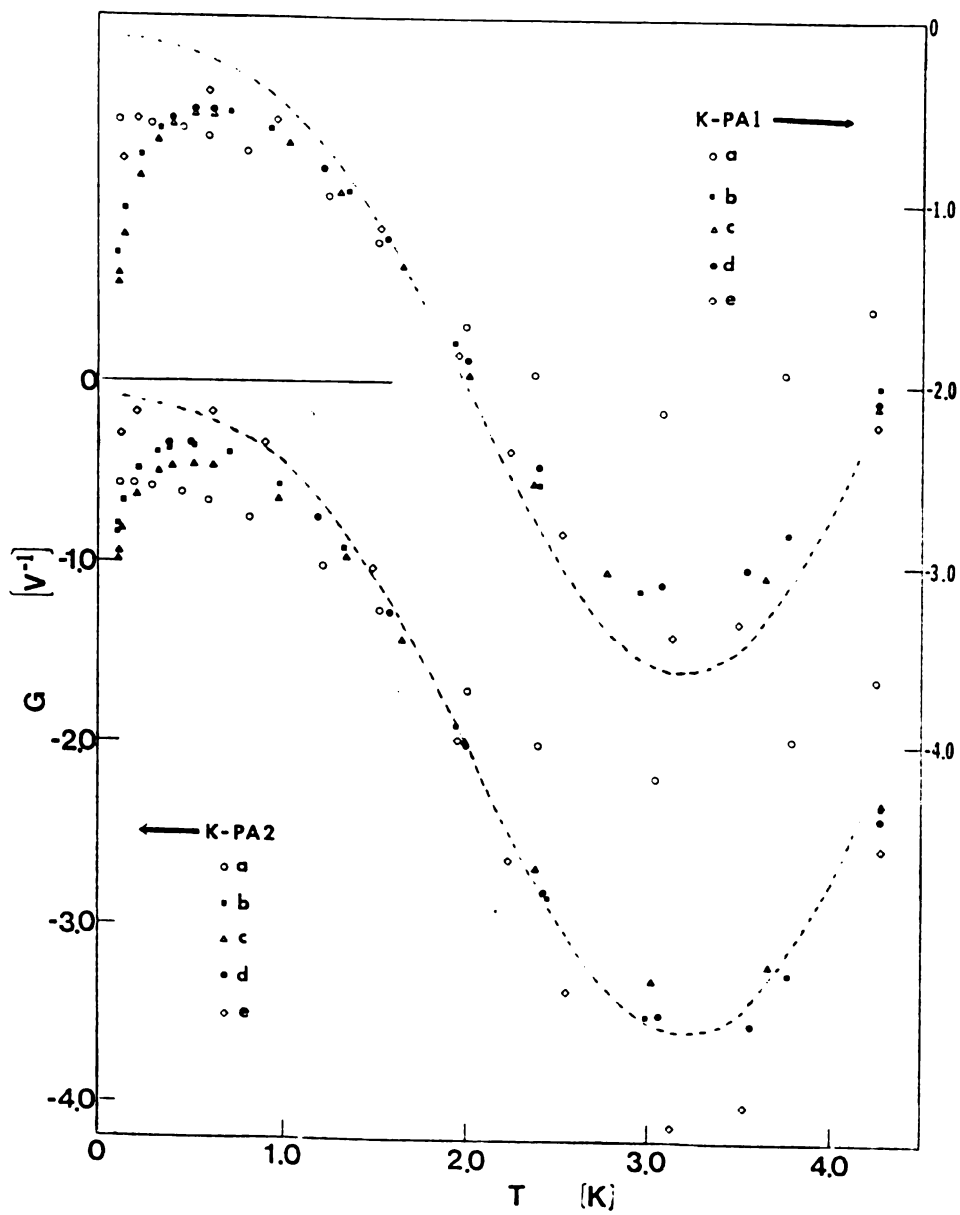Fig. 4-31. G vs T for sample K-PH1.

Fig. 4-32. G vs T for sample K-PH2.

Fig. 4-33. G vs T for samples K-PA1 and K-PA2.

temperature end and less negative at high temperature end, [i.e., with smaller magnitudes of G_o, B*, and C* (see section 4.2.2)], can be ascribed to a high level of impurities (see section 4.2.2 for details), as suggested by the large value of ρ_o.

Above 1K, further annealing causes the data in Figs. 4-31, 4-32, and 4-33 to follow more closely the broken line, but below 1K they exhibit significant negative deviations which increase when the values of B obtained from Figs. 4-27, 4-28, and 4-29, increase. A Kondo effect can produce such negative anomalies in G. Below 1K, our data can be well fitted by $G = G_o + B*T^2 + D*/T$, where the D*/T term is what is generally expected for a Kondo effect. Fig. 4-34 shows the data below 1K for two selected runs of each sample, the solid curves in this figure indicate the fits. The values of parameters G_o, B*, and D* obtained from computer fittings are given in Table 4-8.

The small bumps at T ≈ 1.5K in the plots of samples K-PH1a and K-PH1d in Fig. 4-31 are similar to the ones for their reference samples: K-H5a and K-H6b, discussed in detail in section 4.1.2.

The plot of G for samples K-KA, K-PPA, K-0, and four runs of sample K-TH1 are very similar to those of free-hanging, bare, thick samples. They are not provided in this thesis.
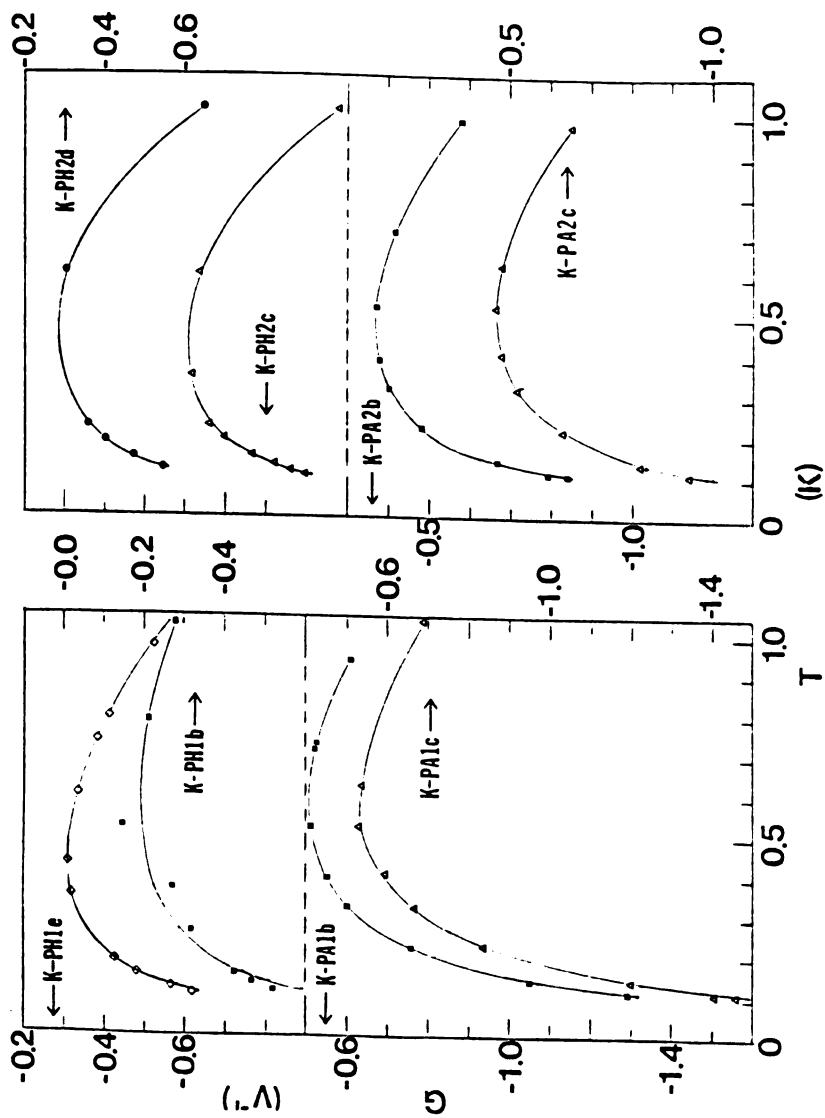
Fig. 4-34. G vs T for samples K-PH1, K-PH2, K-PA1, and K-PA2 with fitting curves at temperature below about 1K.

Table 4-8. The coefficients from fits to the G data of K samples encased in polyethylene tubes

Sample	$G(V^{-1})$	$B*(V^{-1}K^{-2})$	$D*(V^{-1}K)$
K-PH1b	-0.228 ± 0.056	-0.166 ± 0.058	-0.065 ± 0.014
K-PH1e	-0.116 ± 0.007	-0.364 ± 0.010	-0.055 ± 0.002
K-PH2c	-0.115 ± 0.006	-0.379 ± 0.006	-0.052 ± 0.001
K-PH2d	-0.060 ± 0.013	-0.393 ± 0.011	-0.061 ± 0.003
K-PA1b	-0.177 ± 0.009	-0.333 ± 0.010	-0.126 ± 0.003
K-PA1c	-0.157 ± 0.019	-0.358 ± 0.017	-0.149 ± 0.006
K-PA2b	-0.125 ± 0.010	-0.380 ± 0.011	-0.075 ± 0.003
K-PA2c	-0.192 ± 0.011	-0.379 ± 0.013	-0.089 ± 0.003

4.5 K-Rb ALLOY SAMPLES

In 1980 C. W. Lee et al. from our lab (ref. 8,23) found that $\rho = \rho_0 + AT^2 + A_i\rho_0 T^2$ for K-Rb below 1K (see section 1.2.1 for details). Assuming $G = G_0 + G_g^N + G_g^U$, they also found that phonon drag terms (G_g^N and G_g^U) are quenched in K-Rb more and more as the impurity concentration increases and that G_0 is positive and roughly obeys the Gorter-Nordheim rule $G_0 = G_i + \rho_p/\rho_0 (G_p - G_i)$ (see section 1.2.2 for details)

In this study we have improved the absolute accuracy of our temperature scale, and also our measurement precision by nearly an order of magnitude, so that we can now detect changes in $\rho(T)$ of ~2 parts in 10^8. These improved conditions allow more detailed examination of the form of $\rho(T)$ and $G(T)$ in K-Rb alloys. Moreover, using improved glovebox facilities, including an accurate, built-in weighing scale, the atomic percentage of Rb impurity can be determined more precisely.

Four K-Rb samples were measured in this study. Samples K-Rb1 and K-Rb2 were 0.077 at.% Rb alloys with d = 0.25 mm; samples K-Rb3 and K-Rb4 were 9.4 at.% Rb alloys with d = 3.2 mm. The details of the characteristics of these samples are given in Table 3-6.

4.5.1 The Resistivity

Fig. 4-35 shows a plot of residual resistivity (ρ_0) versus the Rb impurity concentration (c) for samples K-Rb1, K-Rb4, and two samples of M. L. Haerle (with 0.38 and 1.3 at.%Rb respectively). The stars indicate the two data
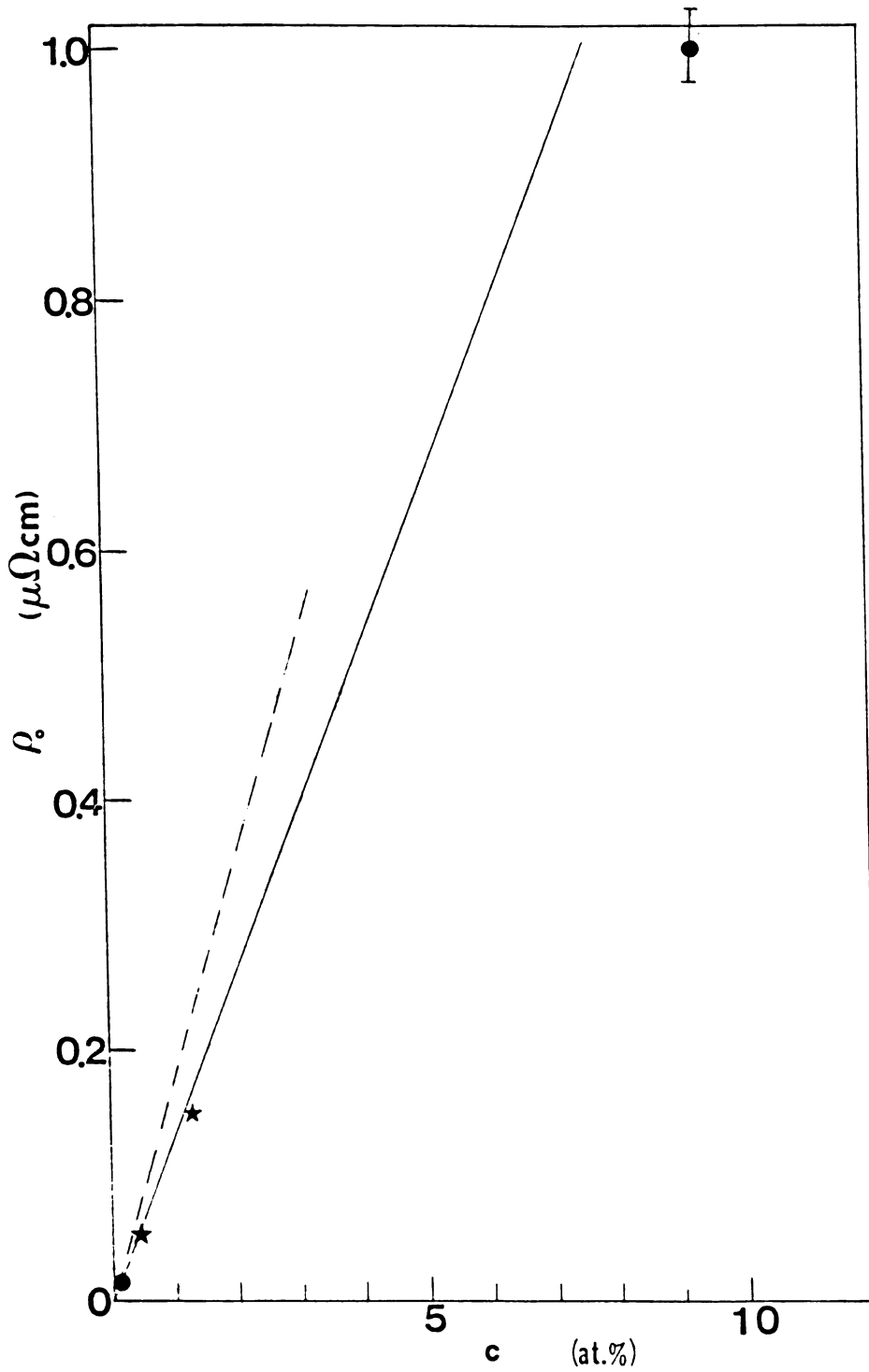
Fig. 4-35. ρ_O vs c for K-Rb samples.

points from M. L. Haerle; the solid straight line indicates the best literature value of ρ_0 per atomic percent Rb impurity (= 0.13 $\mu\Omega$cm/at%) (ref. 67); the dashed line indicates the value of ρ_0 per atomic percent Rb impurity obtained by C. W. Lee in 1980 (ref. 8,23). It is clear in Fig. 4-35 that: (a) the value of ρ_0 per atomic percent Rb impurity for our new dilute K-Rb alloy samples (including the two samples of M. L. Haerle) is now in closer agreement with the best literature value than what C. W. Lee previously obtained. (b) For our 9.4 at% samples, the value of ρ_0 per atomic percent Rb impurity departs from the solid straight line. This departure might partly be due to the finite concentration effects which yield $\rho_0 = \alpha(1-c)c$ in the simplest model. Only for dilute alloy the impurity concentration c is very small, so $(1-c) \approx 1$, and thus $\rho_0 = \alpha c$, yielding a straight line with a slope of α in a plot of ρ_0 vs c; for c = 9.4 at.% as in our case, $(1-c) = 0.91$, if α = 0.13 $\mu\Omega$cm/at% as given above, then $\alpha' = \alpha(1-c) = 0.12$ $\mu\Omega$ cm/at% should be the effective value of ρ_0 per percent Rb impurity. Actually, the value deduced from Fig. 4-35, would be 0.11 $\mu\Omega$cm/at%.

Fig. 4-36 shows a plot of normalized $d\rho/dT$ (ref. 59) versus T for sample K-Rb1 (with 0.77 at.% Rb) and two samples of M. L. Haerle (described above). The broken line indicates typical data for a free-hanging, bare, high-purity, thick K sample. The small turn up on the broken line occurs for T < 0.3K, which we tentatively associated
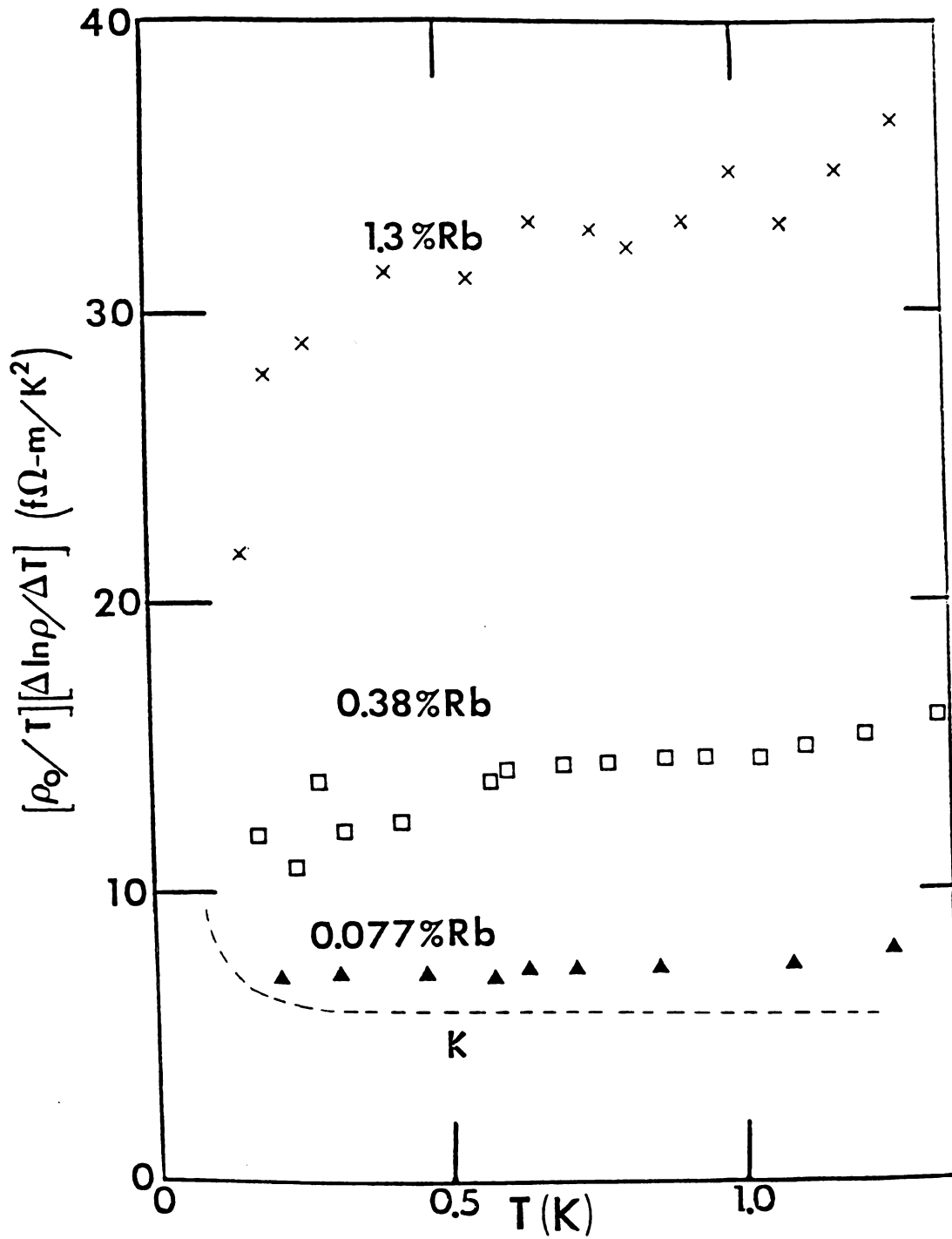
Fig. 4-36. $(\rho(4.2K)/T)(\Delta\ln\rho/\Delta T)$ vs T for dilute K-Rb alloy samples.

with residual dislocations (see section 4.1.1). In contrast, in the K-Rb alloys there is a low temperature turn-down which becomes progressively more apparent as the Rb concentration increases. This turn-down is very obvious for the 9.4 at.% samples, samples K-Rb3 and K-Rb4 shown in Fig. 4-37.

The coefficient (A) of the T^2 term was deduced from the data in the region close to a horizontal straight line in Figs. 4-36 and 4-37. We tried to fit A by $A = A_o + A_i \rho_o$ (see section 2.2.8). $A_o = 0.24 \pm 0.04$ pΩcm/K^2 is obtained, consistent with the one for thick pure K samples (see section 4.1.1), and $A_i \approx 11 \pm 2 \times 10^{-6}$K^{-2} is obtained for all of our four K-Rb samples. This value of A_i is slightly larger than $A_i \approx 8.5 \times 10^{-6}$K^{-2} obtained by C. W. Lee, and closer to the theoretical values of 13.7×10^{-6}K^{-2} from P. L. Taylor (ref. 24) and 12.5×10^{-6} from Kus and D. W. Taylor (ref. 25).

In order to intercompare the ρ_o dependence of dρ/dT for all of the dilute alloys, we have normalized the data for each sample shown in Fig. 4-36 to the data for sample K-Rb3 by multiplying by ρ_{K-Rb3}(4.2K)/ρ(4.2K) and then displacing each curve vertically to bring it into near coincidence with sample K-Rb3. Although the scatter in the data for the more dilute alloys is large, it is clear that the curves now roughly match. This means that the turn down is approximately proportional to ρ_o. Such a dependence is quite different from the ρ_o^3 and $\rho_o^{5/2}$ expected from either
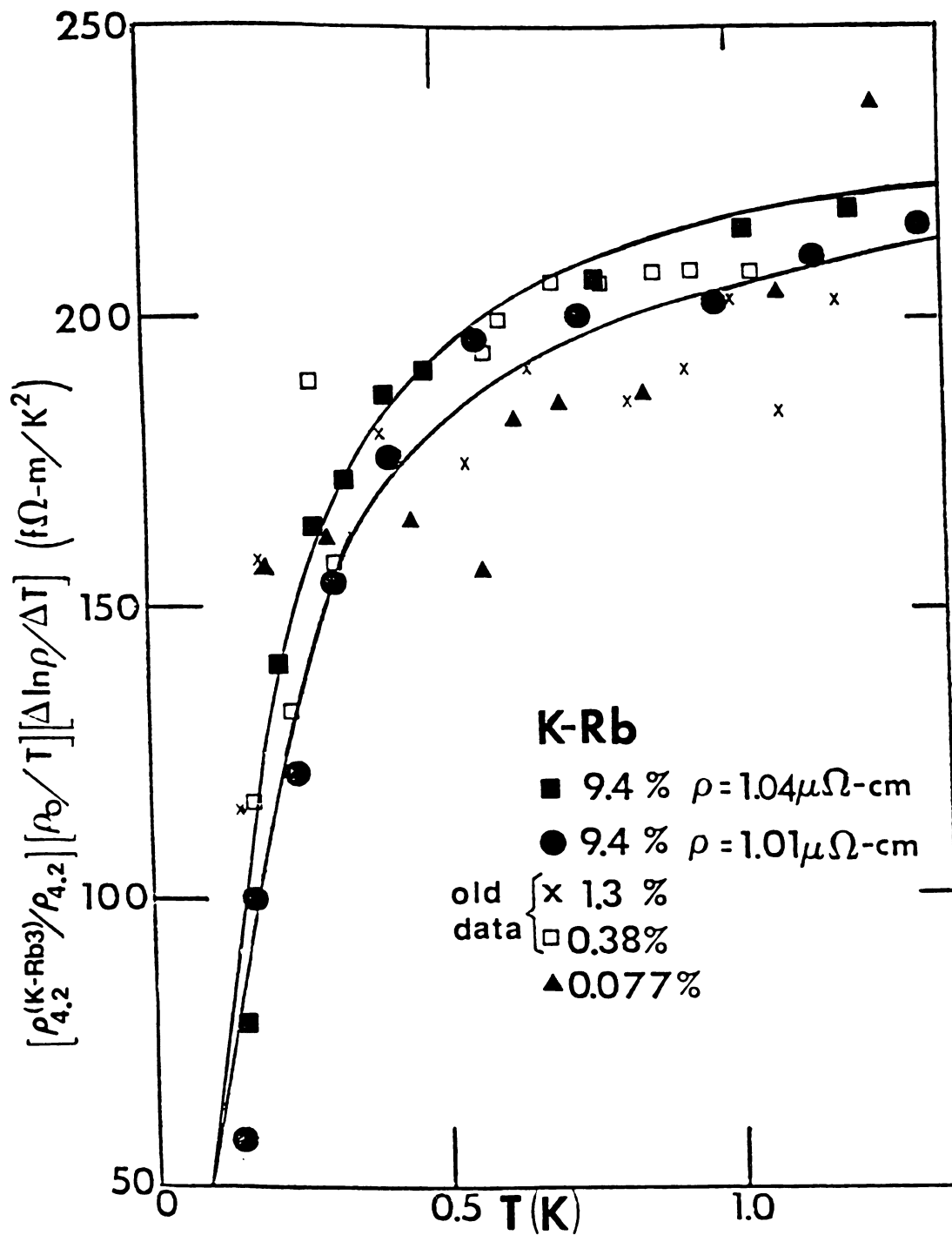
Fig. 4-37. Normalized $\Delta\rho/\Delta T$ vs T for K-Rb alloy samples.

localization or electron-electron interaction effects (see section 2.2.9).

We tried to fit the data by $\rho = \rho_o + A'T^2 + f(T)$ with various different functions $f(T)$. The best fit, shown as solid curves in Fig. 4-38, contains $f(T) = -CT$. Such a term would be expected from localization (see section 2.2.9). This fit is better than one with $f(T) = -DT^{1/2}$, which would be expected for electron interactions (see seciton 2.2.9), or $f(T) = -B\ln T$, which would be expected for a Kondo effect (see section 2.2.7), but the scatter in the data is such that neither of these two alternatives can be completely ruled out. Fig. 4-38 shows the data of samples K-Rb3 and K-Rb4 in plots of normalized $d\rho/TdT$ versus T^{-1}, $T^{-3/2}$, and T^{-2}, with these three alternative fits in the forms as: $d\rho/TdT = 2A - C/T$, $d\rho/TdT = 2A - D/2T^{3/2}$, and $d\rho/TdT = 2A - B/T^2$. The coefficients deduced from Fig. 4-38 are $C = 2.2 \pm 0.4$ pΩcmK^{-1}, $D = 2.0 \pm 0.5$ pΩcmK$^{-1/2}$, $B = 0.3 \pm 0.1$ pΩcm for sample K-Rb3, and $C = 2.3 \pm 0.8$ pΩcmK^{-1}, $D = 2.3 \pm 1.2$ pΩcmK$^{-1/2}$, $B = 0.5 \pm 0.3$ pΩcm for sample K-Rb4.

Comparing the magnitudes of our anomalies with predictions for localization or interaction effects, we found that the measured anomalies for 9.4 at% samples are about one order of magnitude larger than predicted for the interaction effects and two to three orders of magnitude larger than predicted for localization effects. The calculations are as follows:
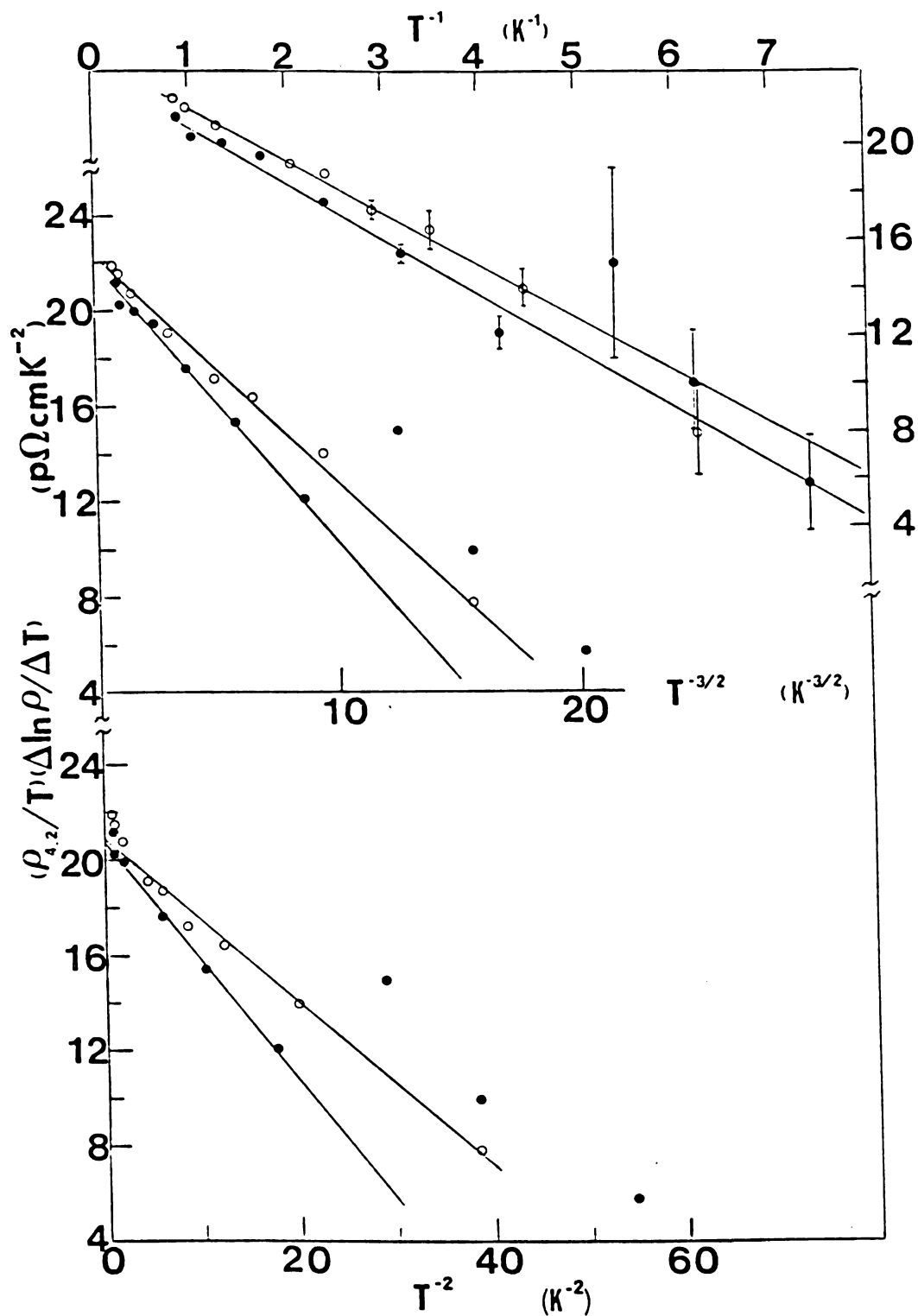
Fig. 4-38. Three different trial fittings for $(\rho(4.2K)/T)(\Delta\ln\rho/\Delta T)$ of two K-9.4at.%Rb alloy samples.

According to Kaveh and Mott (ref. 69), the conductivity contribution of electron-electron correlation effects in disordered metals is:

$$\sigma_{int}(T) = f(x) \frac{e}{\pi^2 \hbar} \frac{1}{L_{int}(T)}$$

where $L_{int}(T) = (\hbar D^*/kT)^{1/2}$ with $D^* = (1/3)V_F l_e$, and $f(x)$ is typically of the order of 0.5 in high-resistivity metallic glasses. Using $V_F = 0.9 \times 10^8$ cm/s for K, and $l_e \approx 2 \times 10^{-5}$ cm calculated from Eqn. 4-1 for our samples with $\rho_0 \approx 1~\mu\Omega$cm, we got $D^* \approx 6 \times 10^2$ cm^2/s, then $\sigma(T) = (0.2~\Omega^{-1}$cm^{-1}K$^{-1/2})T^{1/2}$. Since the resistivity contribution $\Delta\rho = -\rho_0^2\sigma(T) = -DT^{1/2}$, so $D = \rho_0^2 (0.2~\Omega^{-1}$cm^{-1}K$^{-1/2}) = 0.2~p\Omega$cmK$^{-1/2}$ for our samples with $\rho_0 = 1~\mu\Omega$cm. This calculated value of D is one order of magnitude smaller than our measured value of about 2 pΩcm/K$^{1/2}$.

According to Howson (ref. 56), the conductivity contribution of localization for high-resistivity metallic glasses has the form

$$\sigma(T) = \frac{1}{\pi^2} \frac{e}{\hbar} \frac{1}{L_i(T)} \qquad \text{with } L_i^2(T) = (1/2)l_e l_i$$

In our case $l_e = 2 \times 10^{-5}$ cm as above and $l_i = mV_F/ne^2 A_i \rho_0 T^2$ with $A_i \approx 10^{-5}$ K^{-2} (see section 2.2.8), thus $\sigma(T) \approx 0.005~(\Omega$cmK$)^{-1}$ T. Since the resistivity contribution $\Delta\rho = -\rho_0^2 \sigma(T) = -CT$, $C = \rho_0^2 (0.005(\Omega$cmK$)^{-1}) \approx 0.005~p\Omega$cmK^{-1} for our samples with $\rho_0 = 1\mu\Omega$cm. This calculated value of C is

two to three orders smaller than our measured value of about 2 $p\Omega cmK^{-1}$.

Considering the higher than linear power dependence on ρ_0 predicted for electron correlation or localization effects, the discrepancy will be even larger for the more dilute alloys.

A Kondo effect could be proportional to ρ_0, but we did not see any marked anomalies (e.g., see section 4.4.2) in the G's of our samples, such as normally occur in Kondo systems. Also, experiments more recently done in our lab (ref. 68) showed that the turn-down of $d\rho/dT$ at low temperature end for K-Rb dirty alloy was not affected by a magnetic field of 0.2T; thus it cannot be a Kondo effect.

In 1983 Cochrane and Strom-Olsen (ref. 70) used recent scaling theories of the metal-insulator transition, (which take account of both localization and electron-electron interactions), to analyze the low temperature resistivity of their Y-Al metallic glass samples and several other representative alloy systems. They argued that at finite temperature the scaling theories lead to a conductivity: $\sigma(T) = \sigma(0) (1 + T^{1/2}/\Delta)$. They also claimed that they found the correlation gap $\Delta \sim \rho^{-2}$, leading to a contribution to the conductivity: $\Delta\sigma(T) \simeq 6T^{1/2} (\Omega cm)^{-1}$.

Since the resistivity contribution $\Delta\rho = -\rho_0^2 \Delta\sigma(T)$, thus $\Delta\rho \approx -6\rho_0^2 T^{1/2}$. In our case, $\rho_0 \simeq 1 \mu\Omega cm$, this gives us a coefficient $D \approx 6$ $p\Omega cmK^{-1/2}$, which is of the same order as

our measured value of $D \simeq 2$ pΩcmK$^{-1/2}$. Again, however, the ρ_0 dependence of our data is not as predicted.

4.5.2 The Thermoelectric Ratio G

G measurements were made for samples K-Rb1, K-Rb2, K-Rb3, and K-Rb4 from about 4.2K down to about 0.1K. Fig. 4-39 shows a plot of G versus T for these samples. For comparison, data of two samples from M. L. Haerle et al., (with 0.38 at.% Rb and 1.3 at.% Rb), are plotted in the same figure.

The data of each pair of our samples with the same concentration of Rb impurity almost overlap each other over the whole temperature range. The data of samples K-Rb1 and K-Rb2 with 0.077 at.% Rb are well fitted by a solid curve of $G = G_0 + B*T^2 + (C*/T) \exp(-23/T)$ with $G_0 > 0$ in Fig. 4-39. The coefficients obtained from a computer fitting are: $G_0 = 0.353 \pm 0.051$ V^{-1}, $A* = -0.205 \pm 0.014$ V^{-1}K^{-2}, $B* = 2570 \pm 270$ V^{-1}K.

Some other results for G_0 and phonon drag terms can be seen in Fig. 4-39. For G_0: (1) The value is positive for each sample. (2) The magnitude increases with increasing ρ_0, and seems to have a limit of about 0.5 V^{-1}. For phonon drag terms (both normal and Umklapp): (1) They are quenched more and more as the impurity concentration increases, i.e., the magnitudes of these two terms decreases and thus the G data below 1 K are more positive and the data above 3K turn up more slowly with increasing temperature. (2) the G data
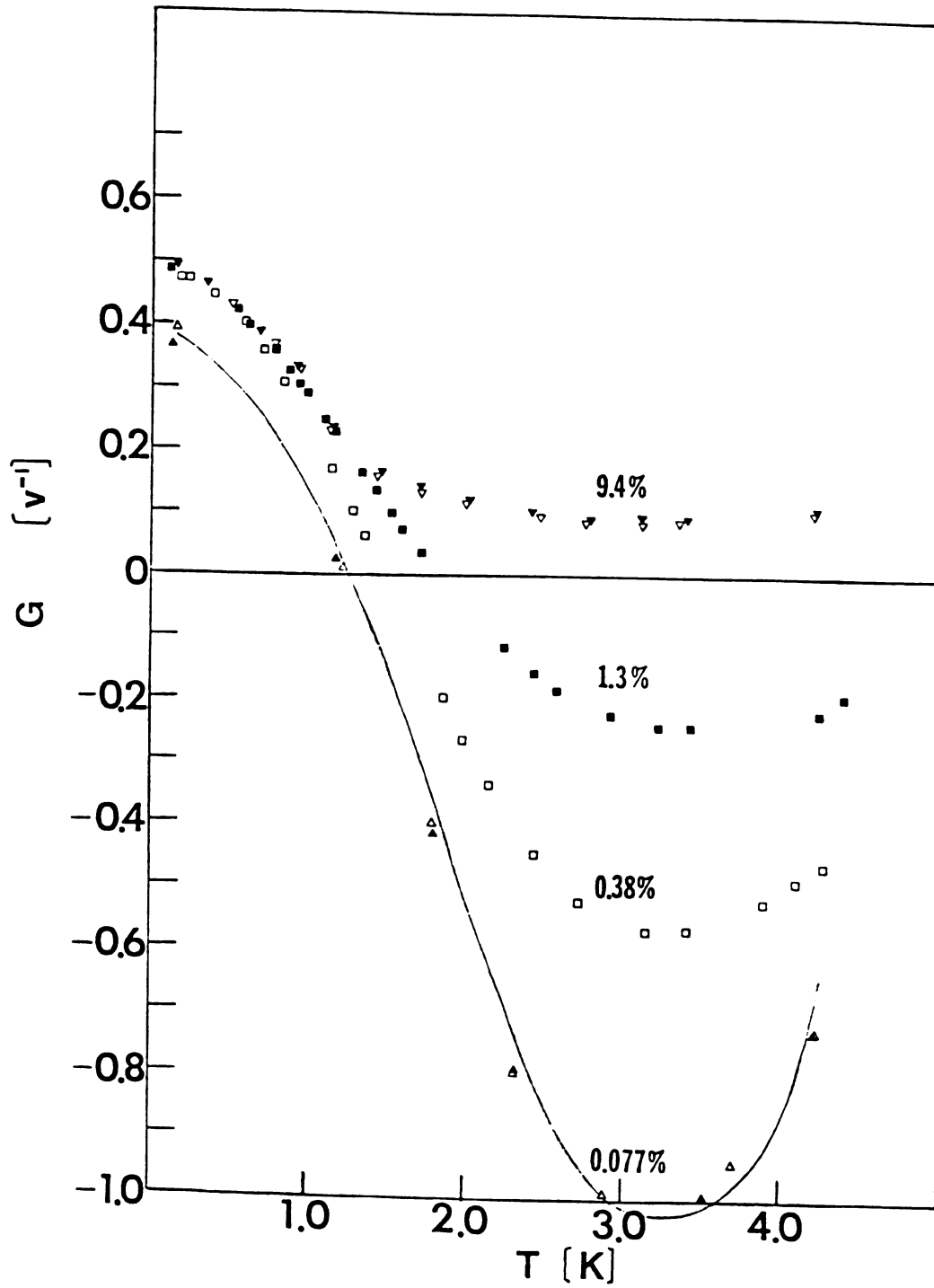
Fig. 4-39. G vs T for K-Rb samples.

of K-Rb3 and K-Rb4 with 9.4 at.% Rb can no longer be well fitted by $G = G_O + A*T^2 + (B*/T) \exp(-\theta*/T)$.

4.6 FREE HANGING, BARE, THICK, HIGH-PURITY Na, Li, AND Rb SAMPLES

According to the standard theory of $\rho(T)$ of high-purity metals (see section 2.1), when the temperature is low enough, electron-electron scattering should dominate $\rho(T)$, yielding $\rho(T) \propto T^2$. Approximate T^2 behavior of $\rho(T)$ has been reported for K (ref. 14,18,19), Na (ref. 18), and Li (ref. 20) in the vicinity of 1K. This variation has been attributed to electron-electron scattering.

If electron-electron scattering were the only source of $\rho(T)$ at very low temperatures, then the T^2 variation of $\rho(T)$ should persist to the lowest temperatures studied. For our thick high-purity K samples, $\rho(T)$ varied closely as T^2 only from 1.2K down to 0.3K; below 0.3K significant deviations from T^2 behavior occurred (see section 4.1.1).

In order to see whether there are, as in K, anomalous deviations in Na, Li, and Rb, from T^2 behavior of ρ at low temperatures, we measured four freely hanging, bare, thick, high-purity samples of each of these metals from 4.2K down to about 0.1K. G measurements were made for each sample, concurrently with ρ. The details of the characteristics of these samples, are given in Tables 3-2, 3-3, and 3-4.

4.6.1 The Resistivity

Fig. 4-40 shows a plot of $(\rho_0/\rho T)$ $(d\rho/dT)$ versus T from 3.6K to 0.1K for four thick (d - 1.00 mm) Na samples from two different sources (see Table 3-4). The two dotted lines indicate, for comparison, the T^2 coefficients reported by Levy et al. (ref. 18). The lowest temperature they reached was 1.1K. Each set of their data followed a horizontal straight line from 1.1K to 2.1K, above which the data turned upward due to electron-phonon scattering. The open circles indicate data for our sample Na-H3 with RRR = R(295K)/R(0K) 4700. The data follow approximately a horizontal straight line from 1.2K to 1.9K with a nominal T^2 coefficient (A $\approx$ 0.175 pΩcm/K^2) slightly smaller than those of Levy et al. Above 1.9K the data turn up, as did those of Levy et al., as electron-phonon scattering becomes more important. Below 1.2K, the data also turn up, as in the case of K. A few solid circles indicate data of sample Na-H4, the twin of Na-H3. The open and filled triangles indicate data of samples Na-H1 and Na-H2 with RRR $\simeq$ 400. These samples behave qualitatively like samples Na-H3 and Na-H4, but with larger apparent T^2 coefficients (A $\approx$ 0.215 pΩcm/K^2), and smaller turn-ups at the lowest temperatures.

The observed variations in the nominal T^2 coefficients of the different Na samples shown in Fig. 4-40, as well as the lack of a large temperature range over which a simple T^2 dependence is observed, mean that considerable uncertainty remains concerning the magnitude of the "intrinsic"
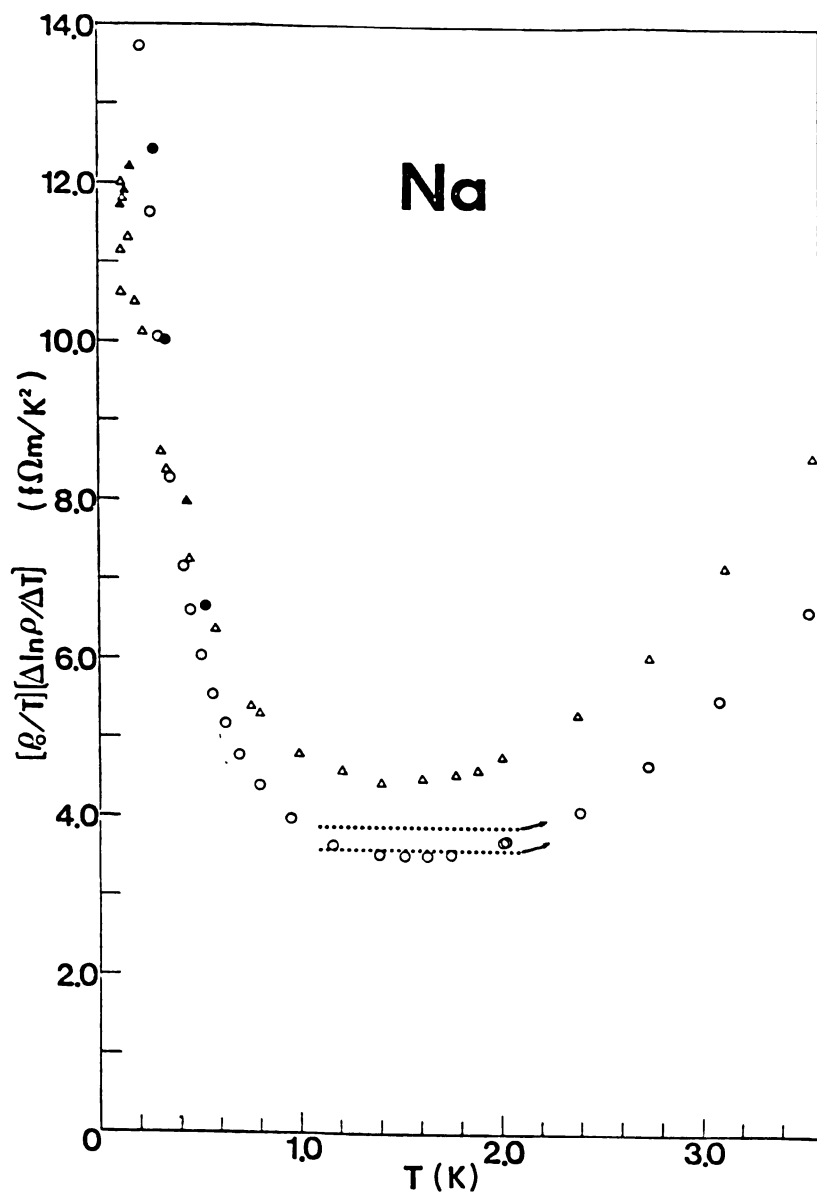
Fig. 4-40. $(\rho_o/T)(\Delta\ln\rho/\Delta T)$ vs T for free hanging, bare, thick, high-purity Na samples.

electron-electron scattering contribution to the resistivity
in Na.

Fig. 4-41 shows a plot of $(\rho_{4.2K}/\rho)$ $(d\rho/TdT)$ versus T
from 2.8K down to 0.07K for several Li and Rb samples and,
for comparison, for typical K samples of diameter 1.5 and
3 mm.

For Li, two samples were initially measured (Li-Hla:▲
and Li-H2a:▼) and then remeasured after nine days at room
temperature (Li-Hlb:△ and Li-H2b:▽). For all four sets of
measurements, the data are consistent with a horizontal
straight line from 4.2K (the highest temperature measured)
down to about 1.6K, below which the data rise anomalously
above the extension of the horizontal line. Our data are
the same to within experimental uncertainty for all four
sets of measurements and are also in good agreement with the
data of Sinvani et al. (ref. 27) in the region of overlap
above 1.2K. The horizontal dashed line in Fig. 4-41 indi-
cates the T^2 coefficient (A ≈ 3.0 pΩcm/K^2) reported by
Sinvani et al. The high Debye temperature of Li (Θ_D(Li)≈
330K) (ref. 69) ensures that electron-phonon scattering is
negligible below 4.2K, the highest temperature measured in
the present experiments.

In contrast, for Rb, which has a very low Debye
temperature (Θ_D(Rb) ≈ 65K) (ref. 70), electron-phonon
scattering remains important down to about 0.5K, below which
we see anomalous behavior. All three samples measured (Rb-
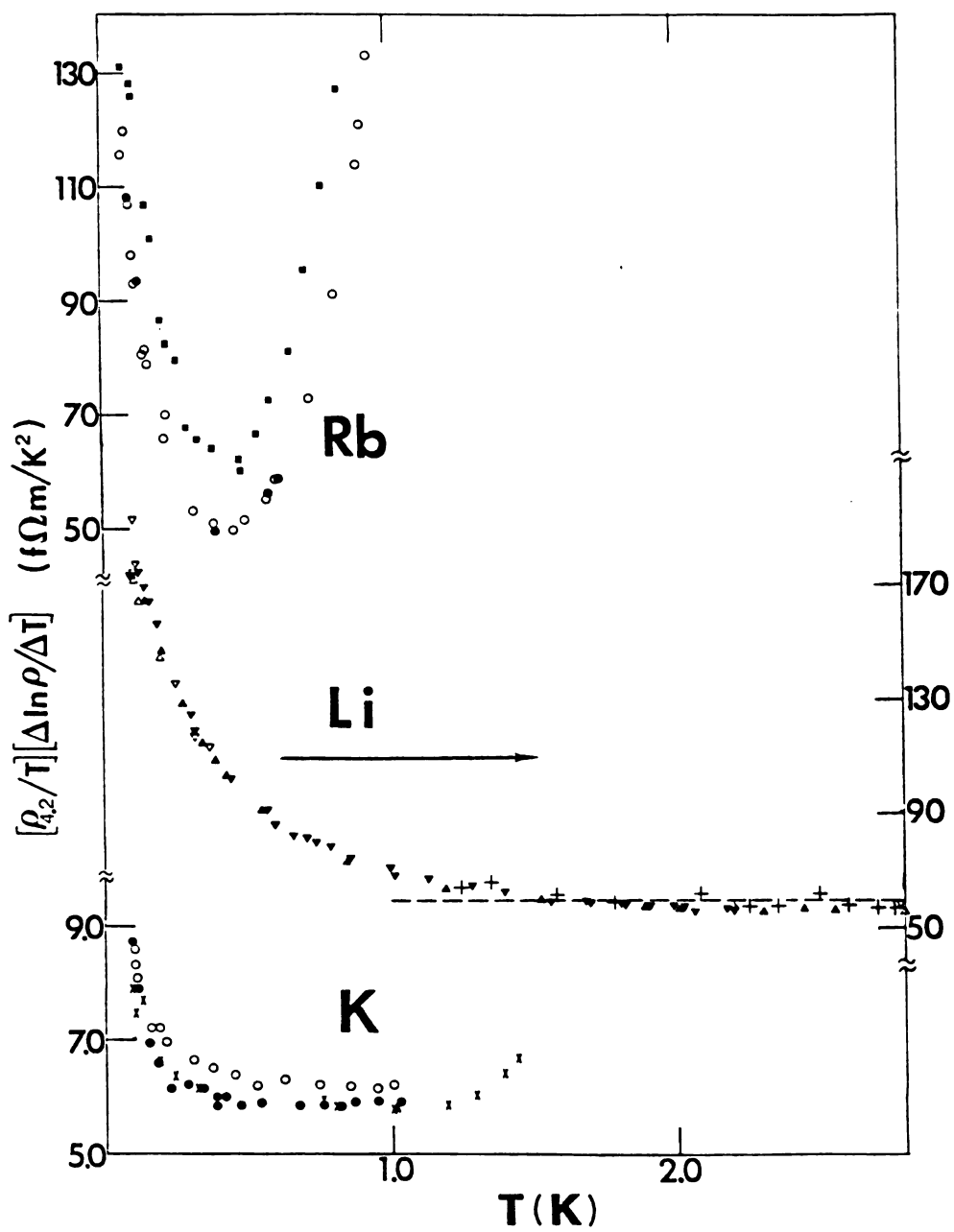H2:■, Rb-V1:●, and Rb-V2:o) show qualitatively similar

Fig. 4-41. $(\rho(4.2K)/T)(\Delta\ln\rho/\Delta T)$ vs T for Rb, Li, and K samples.

behavior, with no temperature range over which a T^2 variation is dominant.

For K, included for comparison, the data are horizontal from about 1.2K down to about 0.3K, as described in section 4.1.1, below which they rise anomalously above the extension of the horizontal line. No measurements were made on sample K-4A (●) of C. W. Lee (with d = 3.0 mm) and our sample K-Hla (o) (with d = 1.5 mm) between 1.1K and 2.8K, but measurements on our sample K-H6a (x) and some other samples (see Fig. 4-1) have established that at about 1.2K the data begin to rise rapidly above the horizontal line with increasing temperature as electron-phonon scattering becomes important. The Debye temperature of K ($\Theta_D \approx 114K$) (ref. 71) is in between those for Na and Rb, which is consistent with electron-phonon scattering becoming important in K at about 1.2K.

The standard theory of $\rho(T)$ provides no explanation for the very low temperature anomalies in Fig. 4-40 and Fig. 4-41. One possible explanation involves low energy excitations associated with residual defects, such as dislocations, which can scatter electrons inelastically (see section 2.2.2).

As noted in section 1.2.1, in their studies of deformed K, M. L. Haerle et al. (ref. 22) reported that the low temperature resistivity of the deformed samples was found to be fit reasonably well by adding to a T^2 variation a model of inelastic electron scattering due to dislocation

vibration (see section 2.2.2). In this model, a single-frequency local-phonon mode of frequency ρ_o is associated with each dislocation and yields a resistivity contribution of $\rho = (C/4T) \sinh (\hbar\omega_o/2kT)$ (section 2.2.2). Another mechanism of inelastic electron scattering can be due to additional bound states for electrons with energy slightly larger than the Fermi energy existing near the cores of dislocations. This model yields a resistivity contribution of $\rho = \alpha(1 + \beta\exp(\epsilon/kT))^{-1}$ (section 2.2.2). These two models yield maxima in both $(1/T)$ $(d\rho/dT)$ and $d\rho/dT$, with the maximum occurring at higher temperatures in the latter case. A maximum in $d\rho/dT$ was found in deformed K at about 0.2K (ref. 22).

Fig. 4-42 shows a plot of $(\rho_{4.2K}/\rho)$ $(d\rho/dT)$ vs T from 0.1K to 1.4K for the Na, Li, Rb, and for comparison for K samples shown in Figs. 4-40 and 4-41.

The K data shown in Fig. 4-42 do not display a maximum even in $d\rho/dT$. It is not yet clear whether this anomaly in undeformed K is due to residual effects of incidental plastic deformation during cooling, in part because this anomaly does not extend over a sufficiently large temperature range to allow discrimination between different models fits. Also, we do not yet have a plausible mechanism for producing enough dislocations to cause such an anomaly in the undeformed K.

The undeformed Rb data shown in Fig. 4-42 shows a hint of local maxima in $d\rho/dT$ near 0.2K, but both the uncertainty
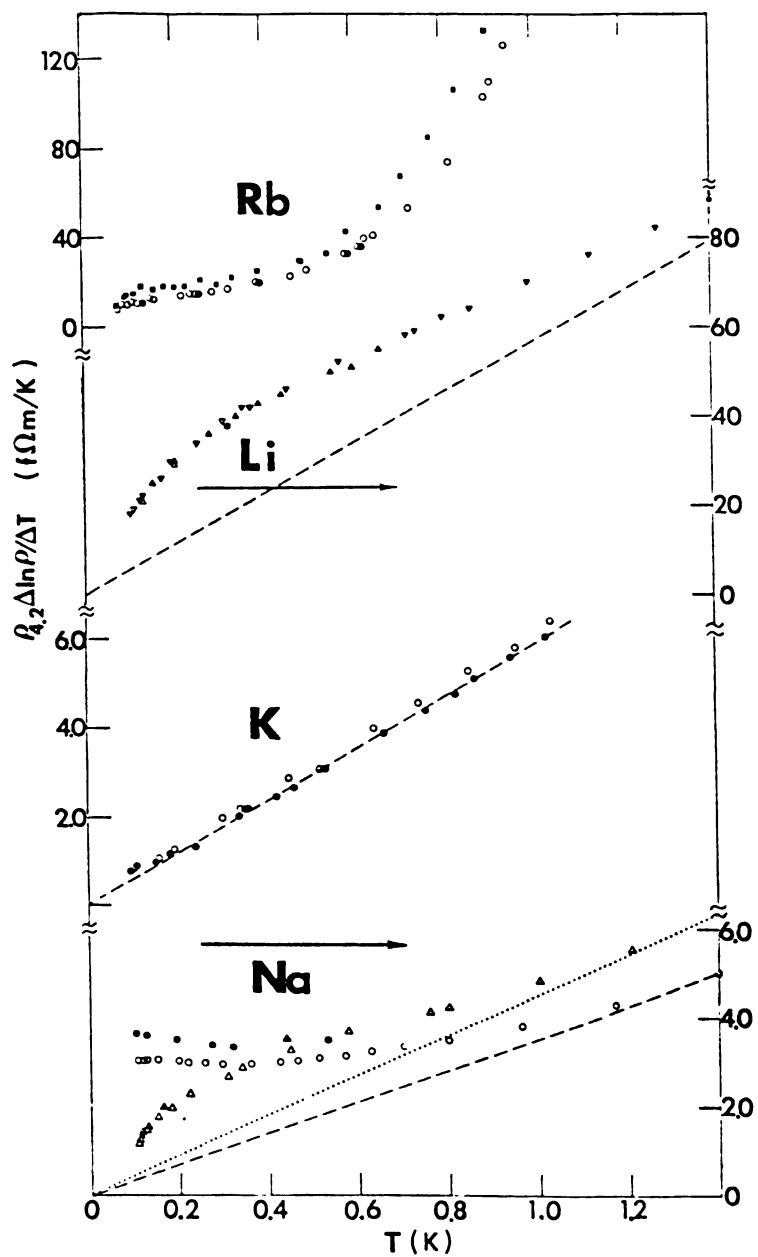
Fig. 4-42. $P(4.2K)(\Delta \ln P/\Delta T)$ vs T for Rb, Li, K, and Na samples. The data are the same as in Fig. 4-40 and Fig. 4-41. The dashed lines indicated T^2 resistivity variations inferred from all of the available data.

in the data and the large contribution of electron-phonon scattering (the very-low-temperature form of which is not known for Rb) preclude any meaningful analysis until measurements on higher purity samples are extended to still lower temperatures.

The undeformed Na data shown in Fig. 4-42 show maxima which occur at very different temperatures for Na from our two different sources.

A plausible generation mechanism for the residual defects needed to produce the observed anomalies in Na and Rb could be the martensitic transformation that Na undergoes at about 35K and Rb might undergo at about 4.2K (ref. 72).

In undeformed Li, the anomaly sets in at a high enough temperature ($\simeq 1.6$K) that a meaningful fit can be attempted, and the simple straightforward T^2 form of $\rho(T)$ above about 1.6K makes the fitting procedure highly selective between different alternatives. In addition, as recently suggested (ref. 20), the martensitic transformation that Li undergoes at about 75K provides a plausible generation mechanism for the dislocations needed to produce such an anomaly.

We tried to fit our Li data in both $d\rho/dT$ and $d\rho/TdT$ forms with several alternatives. Fig. 4-43 shows 4 different fits for the data in $d\rho/dT$ form, while Fig. 4-44 shows these fits in $d\rho/TdT$ form for our data. First we tried to fit our Li data with a T^2 term plus a single-frequency local-phonon mode term, i.e., $\rho = \rho_o + AT^2 + (C/4T)$ $\sinh^{-2}(\hbar\omega/2kT)$ (see section 2.2.2), thus,
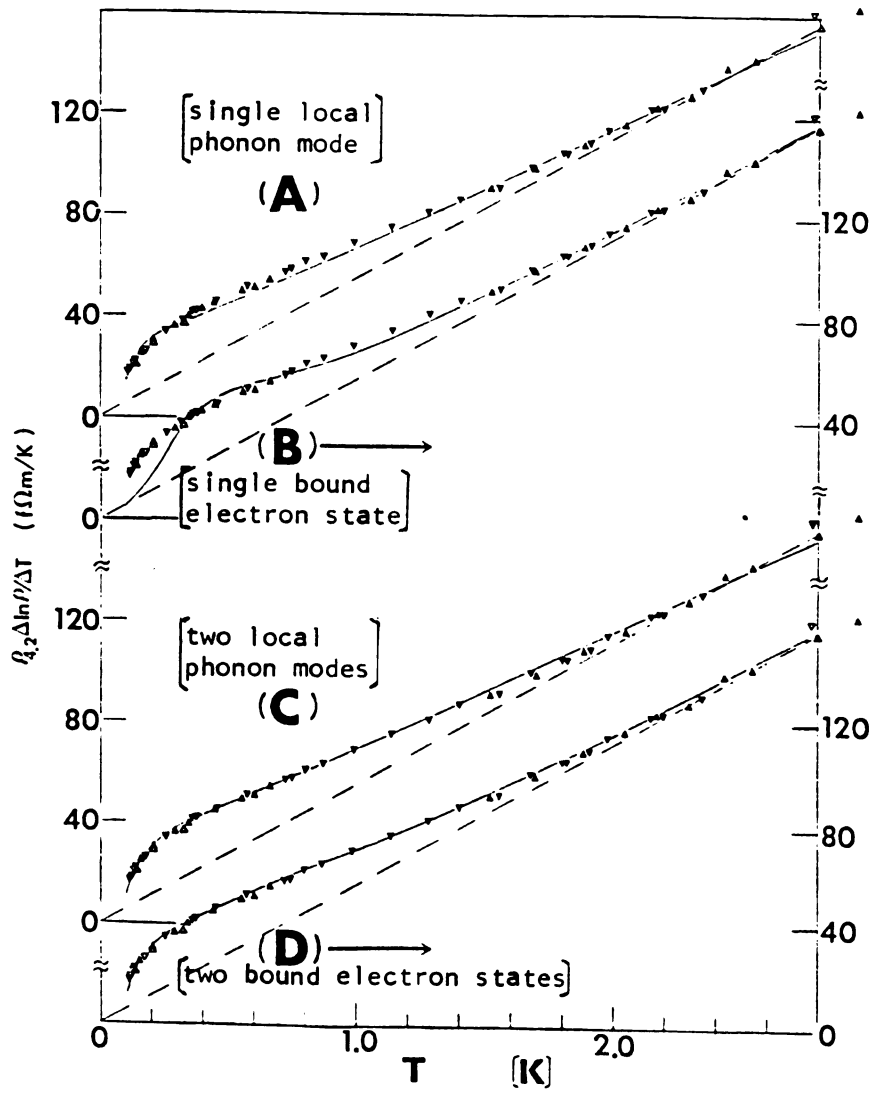
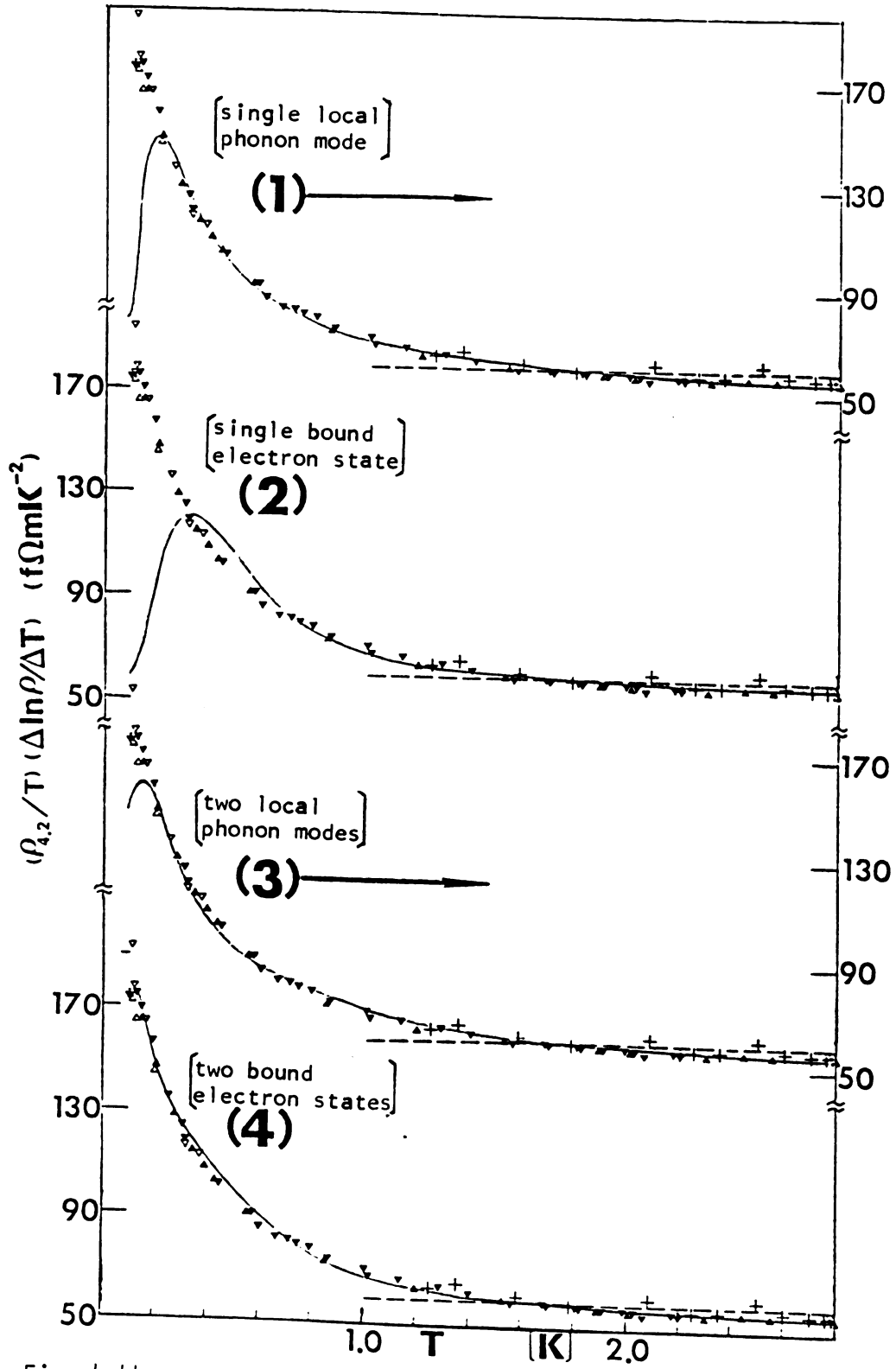Fig. 4-43. Trial fittings for $P(4.2K)\Delta\ln P/\Delta T$ of Li samples.

Fig. 4-44. Trial fittings for $(\rho(4.2K)/T)(\Delta\ln\rho/\Delta T)$ of Li samples.

$$d\rho/dT = 2AT + (C/4T^2)\sinh^{-2}(\hbar\omega/2kT) \text{ x}$$

$$((\hbar\omega/kT)\text{ ctgh}(\hbar\omega/2kT) - 1) \qquad\qquad (A)$$

and,

$$d\rho/TdT = 2A + (C/4T^3)\sinh^{-2}(\hbar\omega/2kT) \text{ x}$$

$$((\hbar\omega/kT)\text{ ctgh}(\hbar\omega/2kT) - 1) \qquad\qquad (1)$$

This model described our data reasonably well from 2.8K down to about 0.2K, see the solid curves in part (A) of Fig. 4-43 and part (1) of Fig. 4-44, below 0.2K the theoretical curves dropped off more rapidly than the data. As an alternative, we also tried a fit with a T^2 term plus a term associated with bound electron states at dislocations, i.e.,

$$\rho = \rho_0 + AT^2 + \alpha(1 + \beta\exp(E/kT))^{-1},$$

thus,

$$d\rho/dT = 2AT + (\alpha\beta E/k)\exp(E/kT)(1 + \beta\exp(E/KT))^{-2} \qquad (B)*$$

and,

$$d\rho/TdT = 2A + (\alpha\beta E/kT)\exp(E/kT)(1 + \beta\exp(E/kT))^{-2} \qquad (2)*$$

with β (the spin degeneracy of the additional level) fixed as 1, we have

$$d\rho/dT = 2AT + (\alpha E/k)\exp(E/kT)(1 + \exp(E/kT))^{-2} \qquad\qquad (B)$$

and

$$d\rho/TdT = 2A + (\alpha E/kT)\exp(E/kT)(1 + \exp(E/kT))^{-2} \qquad\qquad (2)$$

These fits shown as the solid curves in part (B) of Fig. 4-43 and part (2) of Fig. 4-44, are even worse at the lowest temperatures. The problem with both models is that at temperatures well below their maxima in $d\rho/dT$, their single exponential decay for $d\rho/dT$ is too rapid for our data. These two fits can be improved by using two local-phonon modes, or two bound electron levels, with adjustable energies and coefficients, but still fail at the lowest temperatures, as shown in parts (C) and (D) of Fig. 4-43 and parts (3) and (4) of Fig. 4-44. This improvement could mean either that we have a range of dislocation lengths in our samples, or just that we have introduced enough parameters to describe almost any smooth, peaked behavior in $d\rho/dT$. The coefficients deduced from each fit above are given in Tables 4-9 and 4-10.

The differences between the residual resistivities (measured at about 1K in this study) and 4.2K resistivities are very different for different alkali metals. As we mentioned above, this difference is about 0.28 nΩcm for potassium. For Rb, this difference is as big as about 6.2 nΩcm, since Rb has a much lower Debye temperature than K has, so the resistivity contribution of electron-phonon scattering in Rb samples at temperatures lower than 4.2K is much larger than for K samples in the same temperature range; and 1K might not be a low enough temperature for measuring the residual resistivity of Rb. On the other hand, since the Debye temperature of Na is significantly

Table 4-9. The coefficients from the local-phonon mode fits to ρ data of Li samples

Fits	A (x 10^{-13} Ωcm/K^2)	C_1 (x 10^{-13} ΩcmK)	$\hbar\omega_1/2k$ (K)	C_2 (x 10^{-13} ΩcmK)	$\hbar\omega_2/2k$ (K)
(A)	24.14 ± 0.13	6.47 ± 0.31	0.29 ± 0.06	-----	-----
(1)	23.61	14.00	0.405	-----	-----
(C)	23.23 ± 0.26	10.4 ± 7.2	1.02 ± 0.65	8.8 ± 4.0	0.33 ± 0.07
(3)	23.50 ± 0.19	10.0 ± 5.2	0.55 ± 0.27	3.2 ± 1.6	0.25 ± 0.20

Table 4-10. The coefficients from the bound electron level fits to data of Li samples

Fits	A (x 10^{-13} Ωcm/K^2)	α_1 (x 10^{-13} Ωcm)	E_1/k (K)	α_2 (x 10^{-13} Ωcm)	E_2/k (K)
(B)	27.94 ± 0.20	56.7 ± 2.4	1.10 ± 0.06	-----	-----
(2)	27.79 ± 0.11	58.0 ± 5.9	1.06 ± 0.05	-----	-----
(D)	27.42 ± 0.10	50.9 ± 1.9	1.706 ± 0.085	24.6 ± 1.8	0.536 ± 0.037
(4)	27.74 ± 0.09	50.6 ± 9.3	1.25 ± 0.20	13.8 ± 8.8	0.38 ± 0.16

higher than that of K, the resistivity contribution of electron-phonon scattering at 4.2K for Na is expected to be smaller; our results (Table 3-4) showed this contribution is less than 1% of residual resistivity. For Li, we did not measure the 1K resistivity, but the Debye temperature of Li is even higher than that of Na, so $\rho(4.2K)$ should be usable as the residual resistivity.

4.6.2 The Thermoelectric Ratio G

G measurements were made concurrently with ρ from 4.2K down to about 0.1K for all samples described in section 4.6.1.

The G data for the four Na samples are shown in Fig. 4-45. The data for samples Na-H1 and Na-H2 are similar to each other in both form and magnitude, and can be well fitted by $G = G_o + B^*T^2$, (since the Debye temperature of Na is as high as 160K, it is plausible that the Umklapp phonon drag term might be negligible below 4.2K). The lower solid curve in Fig. 4-45 indicates such a fit to sample Na-H2, and the deduced coefficients are $G_o = -0.296 \pm 0.003$ (V^{-1}) and $B^* = -0.0176 \pm 0.0004$ $(V^{-1}K^{-2})$. The data of samples Na-H3 and Na-H4, from another source, are similar in form to each other, and for reasons not yet clear, show a small turn down at the lowest temperatures. The upper solid curve in Fig. 4-45 indicates a fit of $G = G_o + B^*T^2$ for sample Na-H3. The deduced coefficients are $G_o = 0.063 \pm 0.021$ (V^{-1}) and $B^* = -0.065 \pm 0.0027$ $(V^{-1}K^{-2})$. In contrast to K samples, the Na samples with smaller ρ_os show more positive G_os.
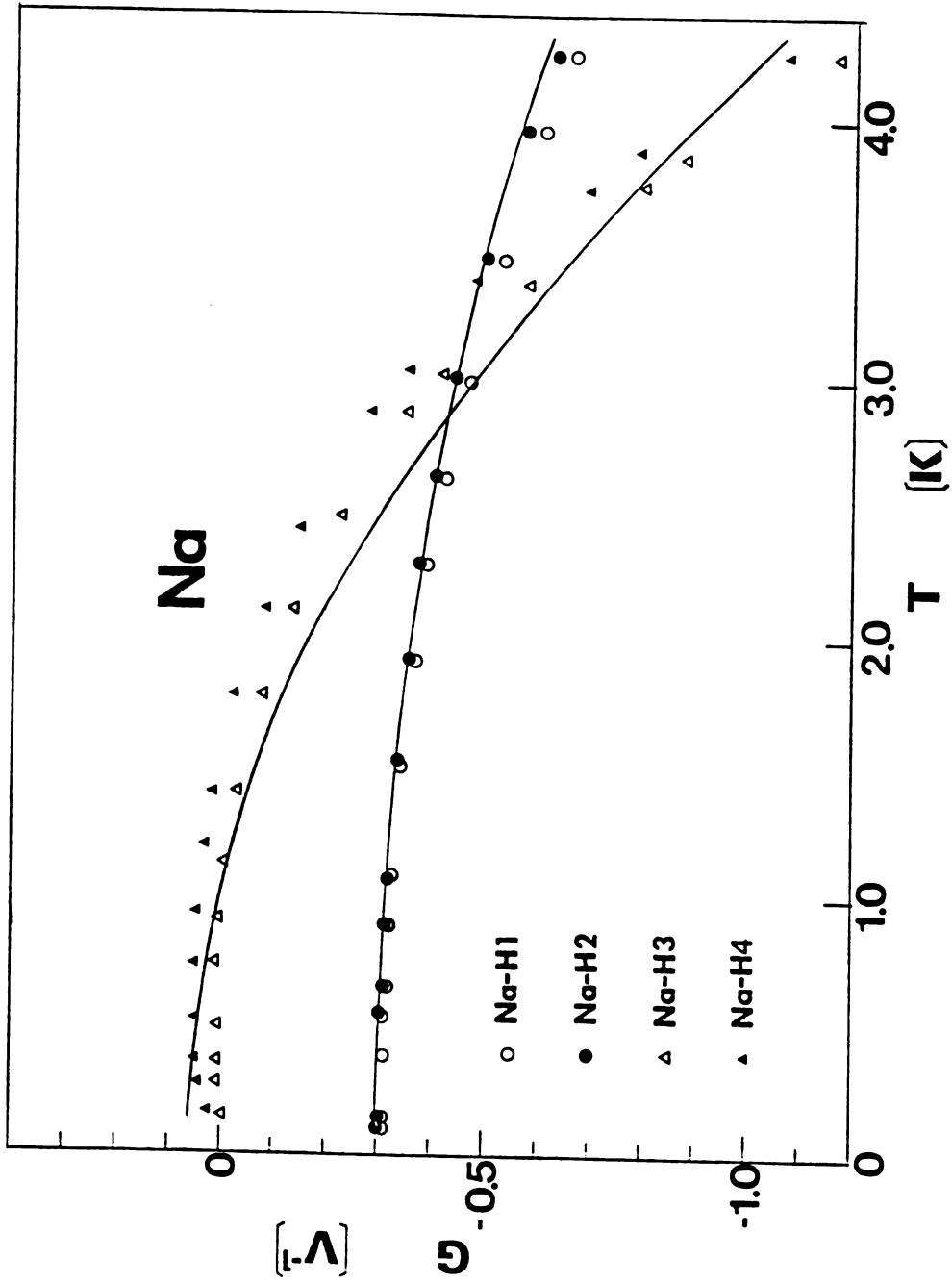
Fig. 4-45. G vs T for thick Na samples.

The G data for all four Li samples are quite similar to each other, not only in the form but also in magnitude, as shown in Fig. 4-46. Since Li has an even higher Debye temperature than Na, the G data of Li samples are also expected to be fitted by $G = G_o + B*T^2$. The solid curve in Fig. 4-46 indicates that the data of sample Li-H2b can be very well fitted by such an equation, and the deduced coefficients are $G_o = 3.7367 \pm 0.0005$ (V^{-1}) and $B* = -0.00707 \pm 0.00006$ ($V^{-1}K^{-2}$). The slight turn-up in the G data of samples Li-H1a, Li-H2a, and Li-H1b at the very lowest temperatures is not yet understood.

In the Rb samples, on the other hand, the G data show different forms from those for Na or Li. Since the Debye temperature of Rb is as low as 65K, the G contribution of Umklapp phonon drag will not be negligible even in the vicinity of 1K. The data are then expected to be fitted by

$$G = G_o + B*T^2 + C*/T \, exp(-\theta*/T).$$

The G data for all four Rb samples are shown in Fig. 4-47. The solid curve in this figure indicates that the data of Rb-H2 are almost perfectly fitted by the equation given just above. The deduced coefficients from the fit are $G_o = 1.0566 \pm 0.0025$ (V^{-1}), $B* = -0.211 \pm 0.006$ ($V^{-1}K^{-2}$), $C* = 561 \pm 32$ ($V^{-1}K$), and $\theta* = 9.71 \pm 0.12$ (K).
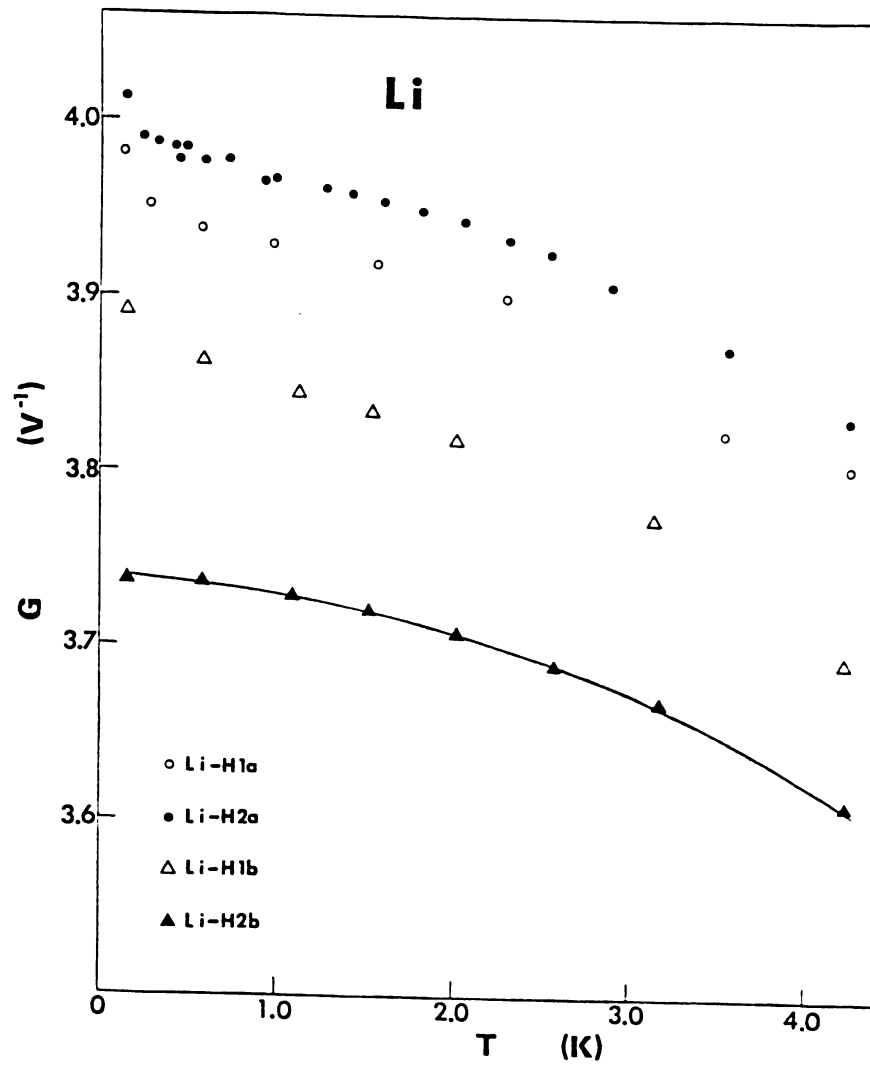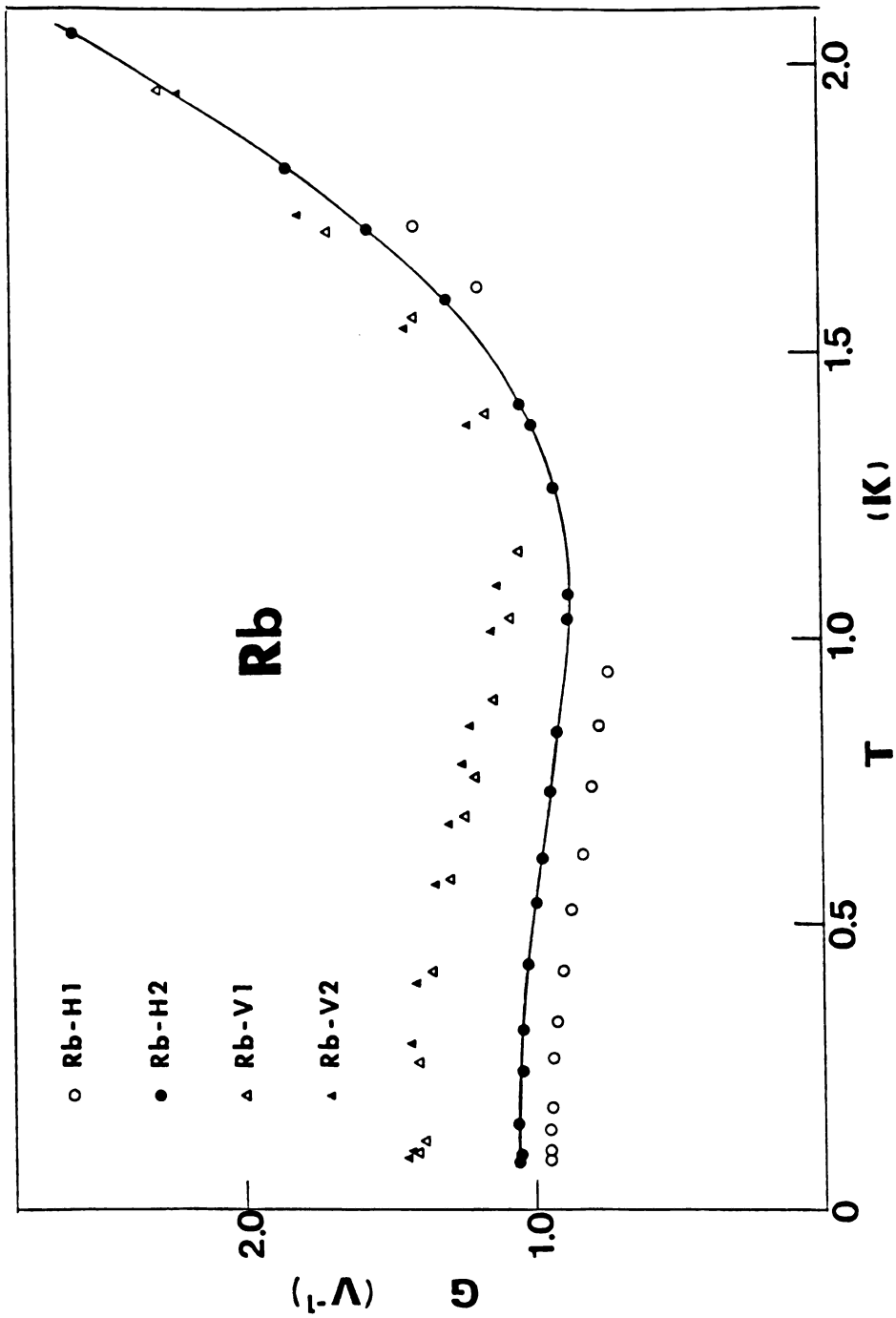
Fig. 4-46. G vs T for Li samples.

Fig. 4-47. G vs T for Rb samples.

4.7 FREE HANGING, BARE, THIN, HIGH-PURITY Na SAMPLES

In section 4.2 we described the size effects in ρ and G for free hanging, bare, thin, high-purity K samples cooled in Ar or He gas. In order to test whether similar size-effects can also be seen in pure Na, we made ρ and G measurements for six thin Na samples cooled in Ar and He gas. Samples Na-1/4A1 and Na-1/4A2 (d = 0.25 mm) were cooled in Ar gas, samples Na-1/10H1 and Na-1/10H2 (d = 0.1 mm) were cooled in He gas. The details of the characteristics of all these samples are shown in Table 3-4.

4.7.1 The Resistivity

Fig. 4-48 shows a plot of normalized ($d\rho$/TdT) versus T for these six thin Na samples from 3.6K down to about 0.1K. For comparison, the data of one thick Na sample made of Na from the same source (Na-H3 with d = 1.0 mm) are also shown in Fig. 4-48 by (x) with a solid curve through them.

The data of samples Na-1/4A1 ($\bullet$) and Na-1/4A2 (o) are quite close to the solid curve, no obvious size-effects are shown. On the other hand, data of samples Na-1/4H1 ($\not\asymp$) and Na-1/4H2 ($\bigstar$) are lower than the solid curve for T $\gtrsim$ 1K, showing a hint of the same size-effects seen in K samples. But, for reasons which are not yet understood, the data of still thinner samples, Na-1/10H1 ($\blacktriangle$) and Na-1/10H2 ($\triangle$), are a little higher than those of Na-1/4H1 and Na-1/4H2, contrary to what is expected for the size effects.

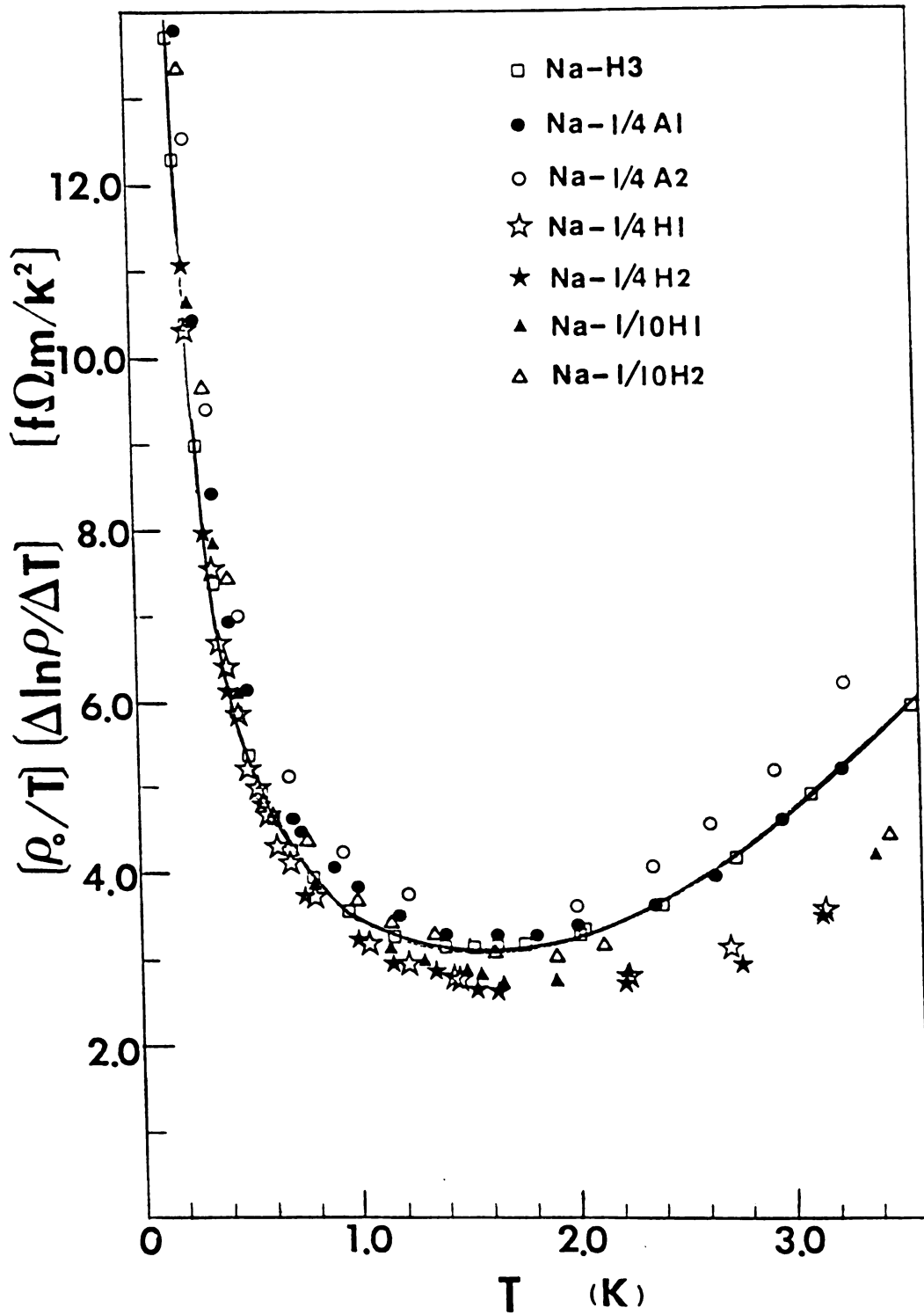To see the possible size-effects more clearly, in Fig. 4-49 we plot normalized $d\rho$/dT versus T from about 3.3K to

Fig. 4-48. $(P_o/T)(\Delta \ln P/\Delta T)$ vs T for thin Na samples.
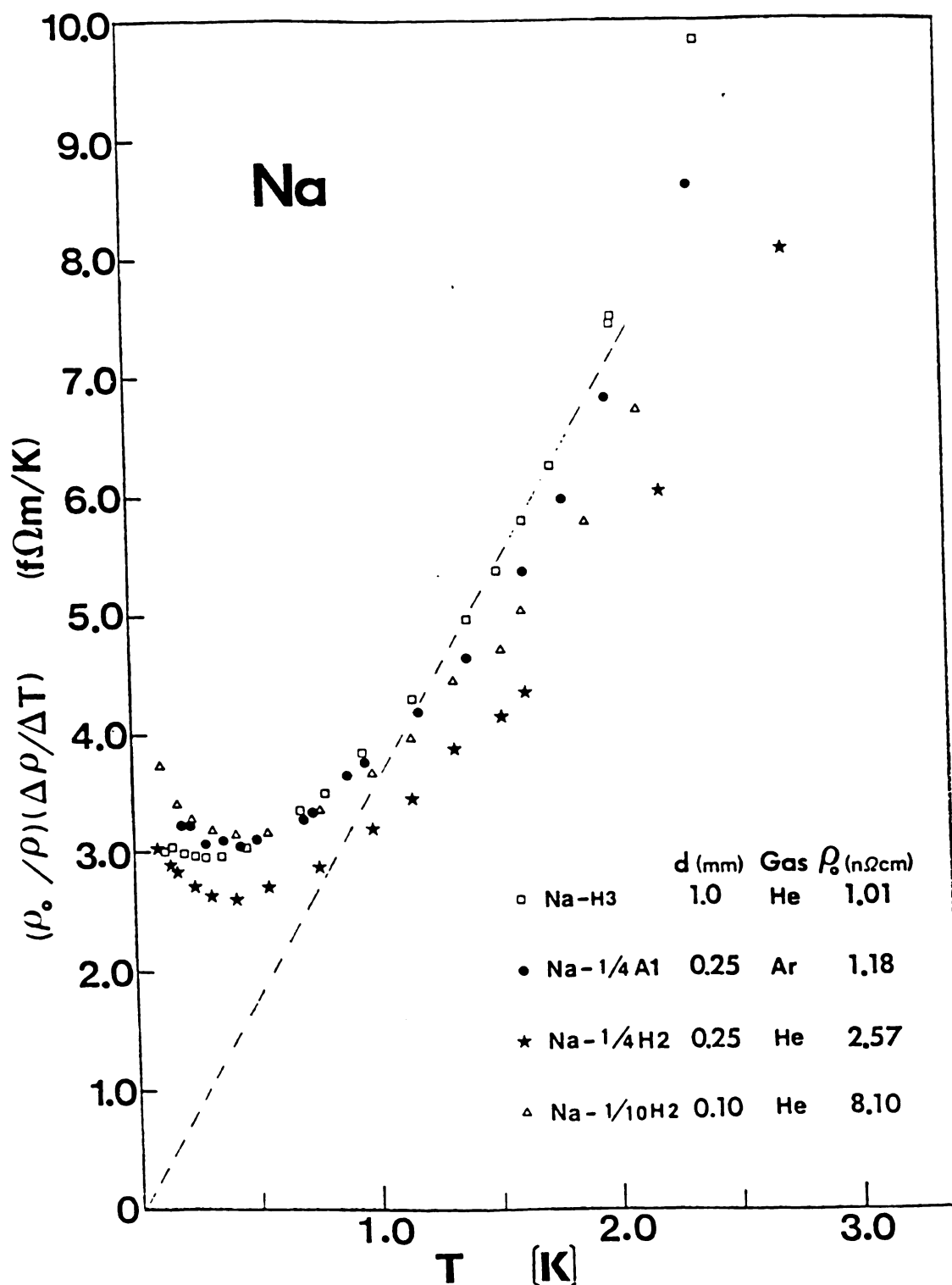
Fig. 4-49. $(P_0/P)(\Delta P/\Delta T)$ vs T for selected thin Na samples.

about 0.1K for three selected samples from above. Again, for comparison, the data of Na-H3 are indicated by open squares, and the coefficient of the nominal T^2 term is indicated by the slope of the broken line. The data of all three thin samples are lower than the broken line for temperatures between about 1K and 3.3K. According to the theory of inelastic scattering of electrons by defects and impurities, the sample with larger ρ_o is supposed to have a larger coefficient of T^2 term, but here we see contrary results. These results can be explained by electron-surface scattering effects, (i.e., size effects) (section 4.2.1). On the other hand, all six thin Na samples showed no negative $d\rho/dT$. This means that any size effects in thin Na samples are not as strong as these in thin K samples. A partial reason could be that the electron mean free-path in bulk Na samples is smaller, about 0.14 mm calculated from $l_{ei} = (1/\rho_\mu)(r_s/a_o)^2 \times 92$ Å (Eqn. (4-1); ref. 4). But this could not be the main reason, because this is only a factor of 0.65 smaller than 0.2 mm, the electron mean-free-path in bulk K samples.

4.7.2 The Thermoelectric Ratio G

G measurements were made concurrently with ρ for all six thin Na samples described in section 4.7.1 from about 4.2K down to about 0.1K.

Fig. 4-50 shows a plot of G versus T for these six samples. For comparison, the G data of sample Na-H3 (made
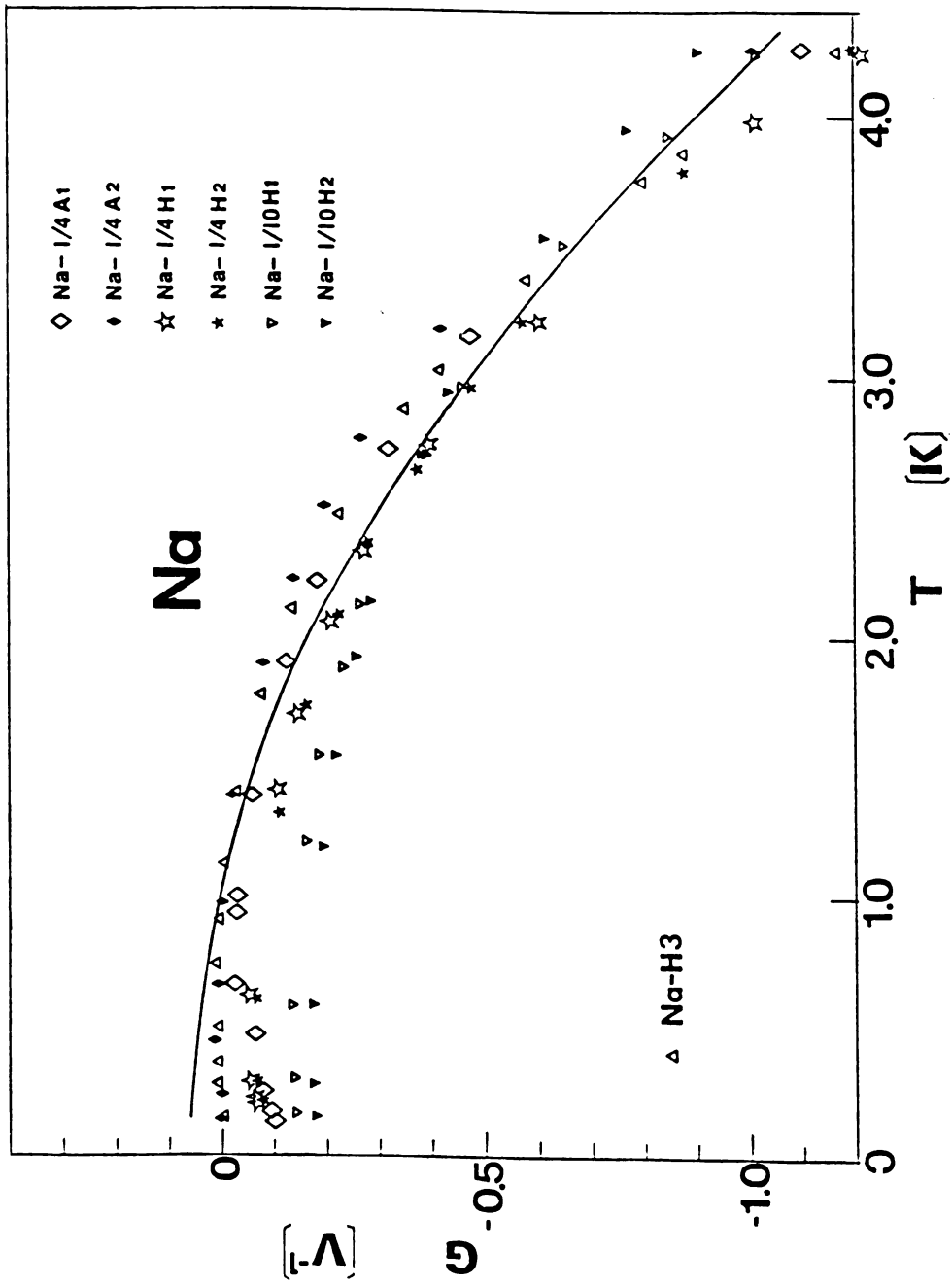
Fig. 4-50. G vs T for thin Na samples.

of Na from the same source), originally shown in Fig. 4-45 are shown again in Fig. 4-50 by means of the best-fit curve.

As in K samples (section 4.2.2), in general, the thinner Na samples show less negative G at high temperatures and more negative G at low temperatures than do the thicker samples. This means that the thinner samples have more negative G_0 and less negative B*. The possible explanations of this are given in section 4.2.2.

4.8 Na SAMPLES ENCASED IN POLYETHYLENE TUBES

In section 4.4 we described likely Kondo effects in ρ and G for K samples encased in polyethylene tubes. In order to test whether Kondo effects can also be found in Na in contact with polyethylene, we measured ρ and G for two Na samples encased in 1.6 mm dia polyethylene tubes under Ar gas (Na-PA1 and Na-PA2). To test for annealing effects, each sample was measured twice, allowing it to anneal for two different periods. The details of the characteristics of each sample in each measurement are given in Table 3-7.

4.8.1 The Resistivity

Fig. 4-51 shows a plot of normalized dρ/TdT versus T for Na-PA1a, Na-PA2a, Na-PA1b, and Na-PA2b from 3.6K down to about 0.1K. For comparison, data of sample Na-H3 are indicated by open circles in Fig. 4-51. All data of these four samples almost overlap each other and overlap the ones of Na-H3 for temperature lower than 2.2K, no Kondo-effect-like turn down (see section 4.4) have been seen in Fig. 4-51. In
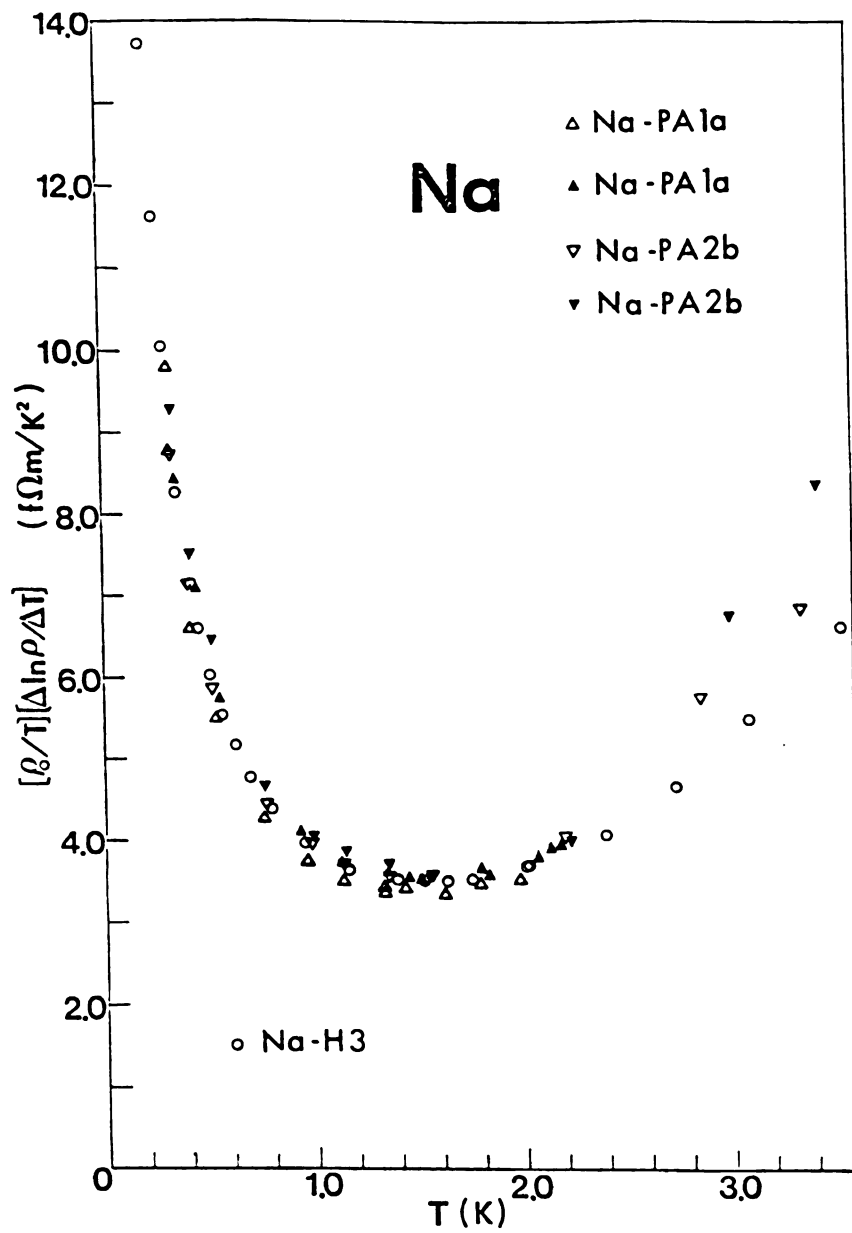
Fig. 4-51. $(P_o/T)(\Delta\ln P/\Delta T)$ vs T for Na samples encased in polyethylene tubes.

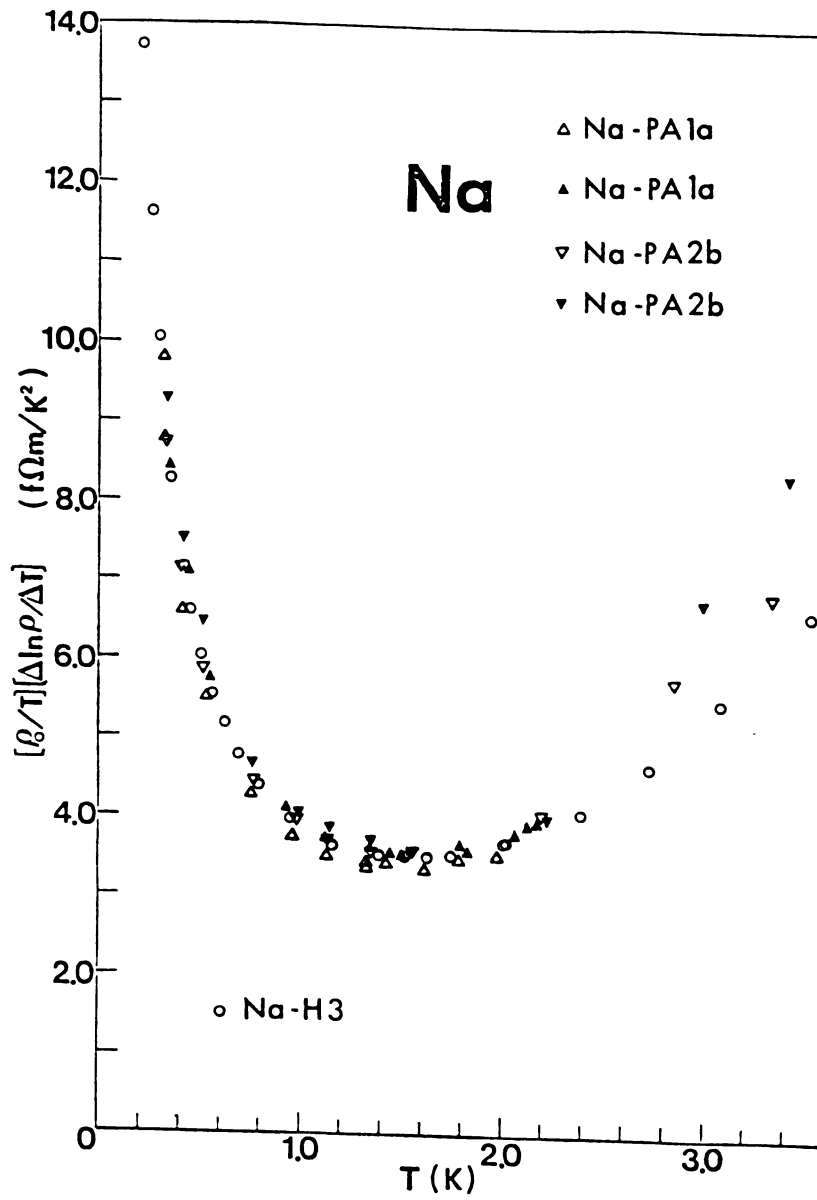Fig. 4-51. $(\rho_o/T)(\Delta\ln\rho/\Delta T)$ vs T for Na samples encased in polyethylene tubes.

order to see the data at the low temperature end more clear-
ly, we plot $d\rho/dT$ versus T in Fig. 4-52 for samples Na-PAla
and Na-PAlb. For comparison, data of samples Na-H1 and Na-
H3, originally shown in Fig. 4-42, are also shown n Fig. 4-
52. Data of sample Na-PAla in Fig. 4-52 show a clear turn-
down at temperatures lower than 0.3K, giving a hint of a
Kondo-like effect. But for reasons not yet clear, data of
the same sample annealed for a longer period show, unex-
pectedly, a low temperature turn-up.

4.8.2   The Thermoelectric Ratio G

The plots of G versus T for samples Na-PAla, Na-PA2a,
Na-PAlb, and Na-PA2b are quite similar to the ones of free-
hanging, bare, thick, pure Na samples and no negative
anomalies at low temperatures were seen. These plots are
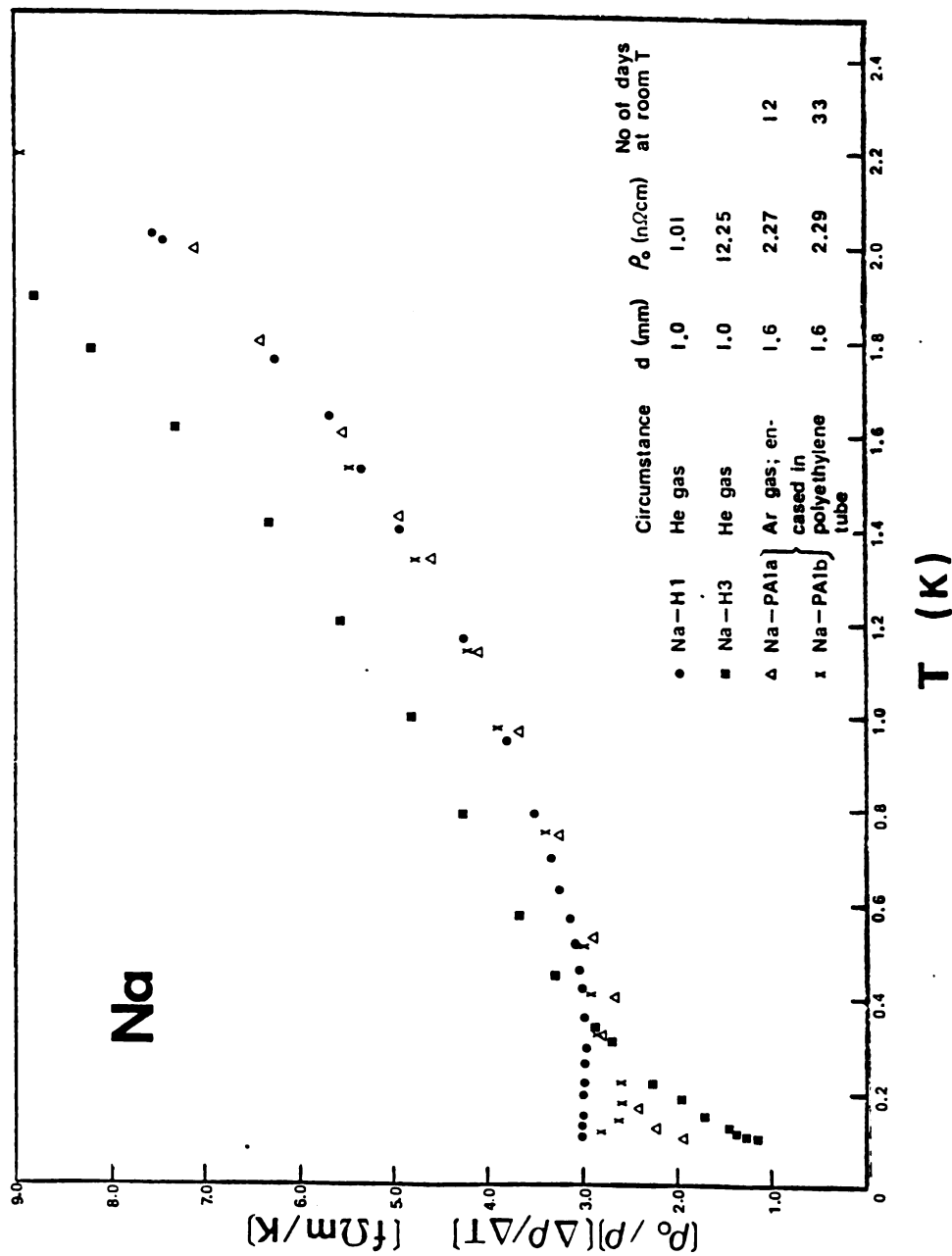not given in this dissertation.

Fig. 4-52. $\rho_0 \Delta \ln \rho / \Delta T$ vs. T for Na samples encased in polyethylene tubes.

CHAPTER 5

Summary and Conclusions

The general outline of this present thesis work is described in section 1.3. The conclusions of this study are as follows:

1) For free hanging, bare, thick, high-purity K samples cooled in Ar, He, or partial vacuum, with improved techniques we found that a) the temperature-dependent electrical resistivity $\rho(T)$ varied closely as AT^2 from 1.2K to 0.2-0.4K (for different samples), with A varying from 0.19 to 0.24 pΩcm/K^2 for samples under different circumstances; b) below 0.2-0.4K, all the samples showed an anomalous turn-up in a plot of $d\rho/TdT$ versus T; c) the thermoelectric ratio G of these samples could be well fitted by the theoretical formula $G = G_0 + B^*T^2 + (C^*/T)Exp(-\theta^*/T)$. These conclusions agree well with what C. W. Lee et al. found for thick pure K samples cooled in Ar gas. With an improved sample can and other techniques, we believe that our G data have higher accuracy than C. W. Lee's data. We have $G_0 = -0.075 \pm 0.015$ V^{-1}, $B^* = -0.484 \pm 0.005$ V^{-1}K^{-2}, and $C^* = 6200 \pm 140$ V^{-1}K, with θ^* fixed as 23K.

2) For free hanging, bare, thin, high-purity K samples cooled in He gas we found that the data of normalized $d\rho/dT$

displayed a clear pattern of unusual behavior which is
consistent with that reported by Rowlands et al. in the
temperature and diameter regions of overlap, but more com-
plex in form. $d\rho/dT$ even became negative in the vicinity of
1K for the thinnest samples whose diameters were comparable
to or smaller than electron mean free path (~0.2 mm). The
more complex behavior of our data rules out both the simple
$T^{3/2}$ form for $\rho(T)$ that Rowlands et al. originally proposed,
and all previously published explanations for the data of
Rowlands et al. The only model we know, which might explain
the negative $d\rho/dT$ we observed, is an interaction between
surface scattering and normal electron-electron scattering
as first proposed by Gurzhi and then calculated by a Monte
Carlo method by Black. However, the data are not in a
regime where a closed form expression for ρ has been de-
rived. We therefore tried various trial fits to our data.
The best fit was obtained as: $(\rho(4.2K)/\rho)\,(d\rho/dT) = 2A'T -$
$55T^{4/3}/\sqrt{d/1\text{ mm}}$, where A' ranged from 0.59 to 0.70 pΩcm/K^2
for samples with different diameters. For reasons not yet
clear, similar samples cooled in Ar gas or partial vacuum
tended to behave like data for samples in He of larger
diameter and to show greater variability for fixed sample
diameter. We also found expected size effects in the resi-
dual resistivity ρ_0. $\rho_0 = \rho_\infty + c/d$ was obtained for samples
with d$\geq$0.16 mm, where c $\simeq$ (3.4 ± 0.5) x 10^{11} Ωcm^2 was com-
parable to the best literatue value (c = 2.9 x 10^{-11} Ωcm^2).
For reasons not yet clear, the ρ_0's of our thinnest samples

($d \leq 0.1$ mm) showed a lot of scatter, with most of the ρ_O's much larger than expected.

All G data for these samples could still be well fitted by G = G_O + B*T^2 + (C*/T)Exp(-θ*/T) with θ fixed as 23K, but the thinner samples show larger magnitudes of negative G_O, smaller magnitudes of negative B*, and smaller magnitudes of C*. This behavior could be explained by the Gorter-Nordheim rule plus a surface scattering effect on phonon drag. Further investigations on size-effects, including making thin samples under vacuum and measuring thin film samples etc. are in progress in our lab.

The only S data taken on a 0.5 mm dia K sample, indicate that L(T) = L_O, i.e., S = L_OGT, is approximately valid only at T $\leq$ 1K for potassium.

3) For pure potassium samples prepared and cooled in contact with hydrocarbons, such as encased in polyethylene tubes or melted in clean paraffin oil, a Kondo-type effect was seen in both ρ and G measurements. The data of ρ can be well fitted by ρ = ρ_O + AT^2 - BlnT where the -BlnT term is the Kondo effect term. The data for G show a negative anomaly below 1K. The data below 1K can be well fitted by G = G_O + B*T^2 + D*/T, where D*/T term is attributed to the Kondo effect. A stronger Kondo effect was seen: (a) in K samples encased in polyethylene tubes compared to one melted in paraffin oil, (b) in samples encased in thinner polyethylene tubes compared to ones encased in thicker tubes, and (c) in samples encased in polyethylene tubes and held at

room temperature for a long period compared to those held for only a short period. K samples in contact with non-hydrocarbon plastics such as teflon or Kel-F showed no Kondo effect in either ρ or G. An average magnetic field of 0.1T applied longitudinally to polyethylene encapsulated samples shifted the resistance minimum to much lower temperatures. Thus, these samples seem to be exhibiting a Kondo effect due to magnetic impurities. The magnetic impurities seem to be a product of the reaction between potassium and hydro-carbons. Further investigation attempting to identify the magnetic impurities is in progress in our lab. In addition to increasing the size of the Kondo-type effect, sample annealing at room temperature also brought both ρ_0 and A down, as also observed by van Kempen et al. ρ_0 changed by a factor of about 3, consistent with the results of van Kempen et al. However, the change in A was only about 30%, much less than the factor of 3.6 reported by van Kempen et al.

4) For K-Rb alloy samples, a plot of ρ_0 vs c shows that the value of ρ_0 per atomic percent Rb impurity is in close agreement with the best literature value of 0.13 $\mu\Omega$cm/at% for our dilute alloy samples. Plots of normalized $d\rho/TdT$ vs T showed that (a) each set of data follow a horizontal straight line roughly from about 0.5K to about 1.2K, yielding $\rho = \rho_0 + A'T^2$. Here A' can be well fitted by $A' = A_0 + A_i\rho_0$, with A_0 found to be 0.24 $\pm$ 0.04 pΩcm/K^2 for an electron-electron scattering contribution, and A_i found to be 11 x 10^{-6} K^{-2} close to the theoretical values of

13.7 x 10^{-6} K^{-2} from P. L. Taylor and 12.5 x 10^{-6} K^{-2} from Kus and D. W. Taylor for inelastic electron-impurity scattering contribution; (b) a low temperature turn-down became progressively more apparent as the Rb concentration increased. The reasons for this turn-down are not yet clear, but our data can be fairly well fitted by adding to $\rho = \rho_o + A'T^2$ an additional term having any one of the alternative forms - CT, $-DT^{1/2}$, or -BlnT. The -CT term would be expected from the localization effect; the $-DT^{1/2}$ term from the electron-electron interaction effects; the -BlnT term from the Kondo effect. However, our turn-down is approximately proportional to ρ_o, not proportional to ρ_o^3 or $\rho_o^{5/2}$ as expected for localization or electron-electron interaction effects. And, the G measurements and further measurements under a magnetic field of 0.2T did not show any behavior such as normally occurs in Kondo systems. Moreover, for the 9.4 at.% samples, the calculated value of C from localization effects is two to three orders of magnitude smaller than the deduced value of C from our data, and the calculated value of D from electron-electron interaction effects is one order of magnitude smaller than the deduced value from our data. Considering the higher than linear power dependence on ρ_o predicted for electron-electron interaction or localization effects, the discrepancy will be even larger for the more dilute alloys.

We also found that the G data of dilute K-Rb alloy samples could still be well fitted by G = G_o + B^*T^2 +

$(C^*/T)\text{Exp}(-\theta^*/T)$, where G_0 is positive and increases with increasing ρ_0 to a limit of about 0.5 V^{-1}, and the magnitude of both B* and C* decrease with increasing ρ_0, (i.e., the two phonon drag terms are quenched more and more as the impurity concentration increases). These variations in G_0, B*, and C* can be explained by the Gorter-Nordheim rule plus an impurity scattering effect on phonon drag. Measurements on still more concentrated K-Rb alloys and a search for a similar anomaly in K-C_s alloy samples are planned.

5) For free-hanging, bare, thick, high-purity Na, Li, and Rb samples we made ρ and G measurements from 4.2K down to 0.07K. A T^2 dependence was found for Li from 1.6K to at least 4.2K (the highest temperature in the measurements) and, perhaps, for Na from 1.2K to 1.9K. No T^2 dependence of ρ was found for Rb. We found anomalous turn-ups at low temperatures in a plot of $d\rho/TdT$ vs T, as seen in K samples, for all Li, Na, and Rb samples. The turn-up is largest in Li and smallest in Na. Above 0.2K, the data of ρ for Li can be fairly well fitted by adding to a T^2 variation a model of inelastic electron scattering due to local phonon mode of dislocation vibration or due to bound electron states associated with dislocations. Below 0.2K the theoretical curves dropped off more rapidly than the data. The fits can be improved by using two local phonon modes, or two bound electron levels, with adjustable energies and coefficients, but still failed at the lowest temperatures.

We also found the G data of Na, Li, and Rb to be well fitted by the theoretical form $G = G_o + B*T^2 + (C*/T) \times Exp(-\theta*/T)$. For Na and Li, which have relatively high Debye temperatures, the third term due to Umklapp phonon drag was found to be negligible. Because different metals have different Debye temperatures, and thus electron-phonon scattering would die off at different temperatures, the differences between $\rho(4.2K)$ and ρ_o (measured at about 1K) were found to be very different for Rb, K, Na, and Li. We found this difference to be about 6.2 nΩcm for Rb; about 0.28 nΩcm for K, (consistent with what van Kempen et al. found); and less than 0.01 nΩcm for Na. For Na and Li, 4.2K is low enough for measuring the residual resistivity ρ_o. On the other hand, for Rb, 1K might not be quite low enough for measuring ρ_o accurately.

6) For thin Na samples we found possible size effects in both ρ and G, which, if they really exist, are much less strong than the ones in K samples. No negative $d\rho/dT$ was found in thin Na samples.

For Na samples encased in polyethylene tubes, no obvious Kondo effect was found in ρ or in G.

LIST OF REFERENCES

1. A. W. Overhauser, Adv. in Phys., 27, 343 (1978).

2. J. M. Ziman, Electrons and Phonons, Oxford University Press, London, 1960.

3. M. Kaveh, C. R. Leavens, and N. Wiser, J. Phys. F: Metal Phys., 9, 71 (1979).

4. Ashcroft/Mermin, Solid State Physics, Holt, Rinehart and Winston Press, 1976.

5. D. K. C. MacDonald, W. B. Pearson, and I. M. Templeton, Proc. R. Soc. A, 248, 107 (1958).

6. D. K. C. MacDonald, W. B. Pearson, and I. M. Templeton, Proc. R. Soc. A, 256, 334 (1960).

7. A. M. Guenault and D. K. C. MacDonald, Proc. R. Soc. A, 264, 41 (1961); Ibid., 274, 154 (1963).

8. C. W. Lee, Ph.D. Thesis, Michigan State University, 1980.

9. D. K. C. MacDonald, G. K. White, and S. B. Woods, Proc. R. Soc. A, 235, 358 (1956).

10. G. G. Natale and I. Rudnick, Phys. Rev. 167, 687 (1968).

11. J. C. Garland and R. Bowers, Phys. Kondens Materie, 9, 36 (1969).

12. J. W. Ekin and B. W. Maxfield, Phys. Rev. B4, 4215 (1971).

13. D. Gugan, Proc. R. Soc. (London) A, 325, 223 (1971).

14. H. van Kempen, J. S. Lass, J. H. J. M. Ribot, and P. Wyder, Phys. Rev. Letters, 37, 1574 (1976). H. van Kempen, J. H. J. M. Ribot, and P. Wyder, J. Phys. F 11.

15. M. Kaveh and N. Wiser, J. Phys. F: Metal Physics, 10, L37 (1980).

222

16. J. A. Rowlands, C. Duvvury and S. B. Woods, Phys. Rev. Letters, 40, 1201 (1978).

17. M. F. Bishop and A. W. Overhauser, Phys. Rev. Letters, 42, 1776 (1979).

18. B. Levy, M. Sinvani, and A. J. Greenfield, Phys. Rev. Latters, 43, 1822 (1979).

19. C. W. Lee, M. L. Haerle, V. Heinen, J. Bass, W. P. Pratt, Jr., J. A. Rowlands, and P. A. Schroeder, Phys. Rev. B, 25, 1411 (1982).

20. A. H. MacDonald and D. J. W. Geldart, J. Phys. F 10, 677 (1980); A. H. MacDonald, R. Taylor and D. J. W. Geldart, Phys. Rev. B23, 2718 (1981).

21. W. E. Lawrence and J. W. Wilkins, Phys. Rev. B, 7, 2317 (1973).

22. M. L. Haerle, Ph.D. thesis, Michigan State University, 1983; M. L. Haerle, W. P. Pratt Jr., and P. A. Schroeder, J. Phys. F 13 (1983) L243.

23. C. W. Lee, W. P. Pratt, Jr., J. A. Rowlands, and P. A. Schroeder, Phys. Rev., 45, 1708 (1980).

24. P. L. Taylor, Proc. Phys. Soc., 80, 755 (1962); Proc. R. Soc. A275, 209 (1963); Phys. Rev. A135, 1333 (1964).

25. F. W. Kus and D. W. Taylor, J. Phys. F10, 1495 (1980).

26. G. Krill, Solid State Communications, Vol. 9, 1065, 1971.

27. M. Sinvani, A. J. Greenfield, M. Danino, M. kaveh and N. Wiser, J. Phys. F11 (1983) L73.

28. F. Bloch, Z. Phys., 59, 208 (1930).

29. R. A. Brown, Can. J. of Phys., 60, 766 (1982).

30. V. F. Grantmakher and G. I. Kulesko, Sov. Phys. JETP, 40, 1158 (1975).

31. P. Fulda and I. Peschel, Adv. in Phys., 21, 1 (1972).

32. S. G. O'Hara and A. C. Anderson, Phys. Rev. B, 10, 574 (1974); Ibid, B, 9, 3730 (1974).

33. M. L. Bonack and A. W. Overhauser; Phys. Rev. B, 18 6454 (1978).

34. M. F. Bishop and A. W. Overhauser, Phys. Rev. B, 23, 3638 (1981); Ibid., 18, 2447 (1978).

35. M. Knudsen, Ann. Phys. (Leipzig) 28, 75 (1909).

36. Saul Dushman, Scientific Foundation of Vacuum Technique (Wiley, New York, 1962), 2nd ed.

37. R. W. Whitworth, Proc. Roy. Soc. London, Ser., A246, 390 (1958).

38. J. E. Black, Phys. Rev., B21, 3279 (1980).

39. Carl A. Kukkonen and Henrik Smith, Phys. Rev., B8, 4601 (1973).

40. N. H. March and S. B. Woods, Solid State Communications, 49, 993 (1984).

41. R. B. Dingle, Proc. R. Soc., 201, 545 (1950).

42. J. R. Sambles, K. C. Elson and T. W. Preist, J. Phys. F12, 1169 (1981).

43. J. R. Sambles, Private Communication.

44. R. I. Boughton and J. E. Neighbor, J. Low Temp. Phys. 7, 241 (1972).

45. R. N. Gurzhi, Zh. Eksp. Teor. Fiz., 44, 771 (1963) [Sov. Phys. JETP 17, 541 (1963)]; Sov. Phys. JETP, 20, 953 (1965).

46. J. Kondo, Prog. Theoret. Phys., 32, 37 (1964); Solid State Physics, vol. 23, F. Seitz and D. Tumbull, eds., Academic Press, New York, 1969, p. 183.

47. C. M. Hurd, Electrons in Metals, John Wiley & Sons Press, New York, (1975).

48. S. Koshino, Prog. Theor. Phys., 24, 484 (1960); Ibid., 24, 1049 (1960); Ibid., 30, 415 (1963).

49. K. Froböse and J. Jäckle, Proceedings of EPS Study Conference, C-14, 1977.

50. A. G. Aronov and B. L. Altshuler, 1978 Zh. Eksp. Teor. Phys. Pis. Red. 27 700; B. L. Atshuler, 1978 Zh. Eksp. Teor. Phys. 75, 1331.

51. V. N. Fleurov, P. S. Kondratenko and A. N. Kozlov, J. Phys. F 10, 1953 (1980).

52. D. J. Thouless, Phys. Rep. 13C, 93 (1974).

53. F. J. Wegner, Z. Phys. 25, 327 (1976).

54. H. G. Schuster, Z. Phys. 31, 99 (1978).

55. E. Abrahams, P. W. Anderson, D. C. Licciardello, and T. V. Ramakrishnan, Phys. Rev. Lett. 42, 673 (1979).

56. M. A. Howson, J. Phys. F 14 (1984), L25.

57. J. M. Ziman, Phil. Mag., 4, 371 (1959).

58. M. Bailyn, Phil. Mag., 5, 1059 (1960).

59. W. P. Pratt, Jr., Can. J. Phys., 60, 703 (1982).

60. D. Edmunds, W. P. Pratt, Jr., and J. A. Rowlands, Rev. Sci. Inst., 51, 1516 (1980).

61. J. L. Imes, Ph.D. Thesis, Michigan State University, 1974.

62. G. L. Neiheisel, Ph.D. Thesis, Michigan State University, 1975.

63. National Bureau of Standard, Washington, D.C.

64. Professor P. A. Schroeder, Michigan State University.

65. J. Bass, Adv. Phys. 21, 431 (1972).

66. S. B. Woods, private communication.

67. J. Bass, In Landolt-Bornstein Tables, New Series III/15a.

68. W. P. Pratt, Jr., et al. (unpublished).

69. M. Kaveh and N. F. Mott, J. Phys. C: Solid State Commun. 33 527, 1981.

70. R. W. Cochrane and J. O. Storm-Olsen, Phys. Rev. B, 29 1088, 1984.

71. D. K. C. MacDonald, Handb. Phys., 14, 137 (1956).

72. I. M. Templeton, J. Phys., F12, L121 (1982).